Defining Mechanisms of Protective Antibody Responses Induced by Vaccines against Blood-Stage *Plasmodium vivax* Malaria

A thesis submitted in fulfilment of the requirements

for the degree of Doctor of Philosophy

Mimi M. Hou

Oriel College

Department of Paediatrics, University of Oxford

August 2025

Word count ~40,000 (main text)

Defining Mechanisms of Protective Antibody Responses Induced by Vaccines against Blood-Stage *Plasmodium vivax* Malaria

By Mimi Hou

Abstract

Plasmodium vivax is the most common cause of malaria outside of Africa and the most geographically widespread. An effective vaccine against *P. vivax* would greatly aid malaria eliminations efforts worldwide. The leading vaccine candidates against blood-stage infection target the interaction between *P. vivax* Duffy-binding protein (PvDBP) and Duffy antigen receptor for chemokines (DARC) on red blood cells, an essential interaction required for parasite invasion. A protein/adjuvant vaccine targeting region II of PvDBP (PvDBPII) partially inhibited parasite growth in controlled human malaria infection studies. The degree of parasite growth inhibition correlated with vaccine-induced antibody responses, but the underlying mechanisms are poorly defined. The aim of this Thesis was to isolate and characterise the human antibody response to PvDBPII vaccination. A panel of over 150 IgG monoclonal antibodies (mAbs) against PvDBPII were isolated from human vaccinees. The mAbs were grouped into five epitope binning communities, which showed distinct binding and functional characteristics. Two epitope communities contained mAbs that bind subdomain 2 of PvDBPII and some inhibited binding of PvDBPII to DARC. In contrast, mAbs from all five epitope communities showed parasite growth inhibition activity (GIA) *in vitro*, including three communities that bind subdomain 3 of PvDBPII. The most potent growth-inhibitory mAbs in the panel were strain-specific, but mostly strain-transcending mAbs were found in one community that binds in subdomain 3. Testing combinations of different mAbs for functional interactions showed that mAbs from different epitope communities were predominantly antagonistic in GIA. This information on the breadth and mechanism of function of human antibodies induced by PvDBPII will help inform the rational design of future PvDBPII-based vaccines. In addition, engineering of mAbs by fusion of a DARC peptide to the Fc region identified an engineered mAb that exceeded the potency of all wild-type anti-PvDBPII mAbs and could be a candidate for further clinical development.

Acknowledgements

First of all, and most importantly, I would like to thank my supervisors Simon Draper and Angela Minassian. Thank you both for giving me the opportunity to undertake this DPhil in your group. Simon, I have really enjoyed my time in the lab and have learned a lot from this group that does great science and in such a collaborative and supportive environment. Angela, thanks for keeping me involved in all the exciting clinical trials, for your belief in me and putting me forwards for so many opportunities throughout my time working for the group.

From the lab, I would like to thank Martino Bardelli for the lab supervision at the start of my DPhil; Francesca Donellan for taking over that role after Martino left and for the thesis reviewing; Doris Quinkert and Cassie Rigby for all their support with parasite cultures and Carolyn Nielsen, Lloyd King, Kirsty McHugh, Anna Huhn, Amy Boyd and Phebe Ekregbesi who have been involved with various aspects of this project. Thanks also to Barney, Sarah, Hannah, Dimitra, Lana and Mariola for their general help around the lab and to my fellow students Ana, Anika and Wendy for being such great lab mates.

I would also like to thank our collaborators Prof Robert Moon (London School of Hygiene and Tropical Medicine) and Prof Chetan Chitnis (Institut Pasteur, Paris).

Finally, thanks to my family, especially to my parents for always being there for me.

Contents

List of Figures

List of Tables

List of Abbreviations

ACKR1	Atypical chemokine receptor 1
AMA1	Apical membrane antigen 1
BIA	Binding inhibition activity
BIAb	Binding inhibitory antibodies
CDR	Complementarity-determining region
ChAd	Chimpanzee adenovirus serotype 63
CHMI	Controlled Human Malaria Infection
CNV	Copy number variants
CSS	Cysteine-rich, small, secreted
CyRPA	Cysteine Rich Protective Antigen
DARC	Duffy antigen receptor for chemokines
DARC-Fc	$DARC_{1-60}$ ectodomain fused to Fc region
DTT	Dithiothreitol
ELISA	Enzyme-linked immunosorbance assay
Fab	Fragment antigen-binding
Fc	Fragment crystallisable
FRG KO huHep	$Fah^{-/-}Rag2^{-/-}IL2rg^{-/-}$ mice transplanted with human hepatocytes
FRGN KO	FRG mice backcrossed with non-obese diabetic mice
G6PD	Glucose-6-phosphate dehydrogenase
GIA	Growth inhibition activity
HEK	Human Embryonic Kidney
HT-SPR	High-throughput surface plasmon resonance
HIS-HEry	Human Immune System Human Erythrocyte mouse model

hTPST-2	human sulfotransferase
IgG	Immunoglobulin G
ipTM	Interface predicted template modeling
mAb	Monoclonal antibody
LDH	Lactate dehydrogenase
LSHTM	The London School of Hygiene & Tropical Medicine
MES	2-(N-morphplino)ethanesulfonic acid
MVA	Modified vaccinia virus Ankara
NAI	Naturally-acquired immunity
NBPXa	Normocyte binding protein Xa
NHP	Non-human primate
OD	Optical density
PBS	Phosphate buffered saline
PCR	Polymerase chain reaction
PBMC	Peripheral blood mononuclear cell
PkDBP	*P. knowlesi* Duffy-binding protein
PTRAMP	*Plasmodium* thrombospondin-related apical merozoite protein
PvCSP	*P. vivax* circumsporozoite protein
PvDBP	*P. vivax* Duffy-binding protein
PvDBPII	*P. vivax* Duffy-binding protein region II
PvEBP	*P. vivax* erythrocyte binding protein
PvMSP1	*P. vivax* merozoite surface protein 1
PvRBP	*P. vivax* reticulocyte-binding protein
RBC	Red blood cell
RH5	Reticulocyte-binding protein homolog 5

RIPR	RH5 interacting protein
RT	Room temperature
RT-PCR	Reverse transcription polymerase chain reaction
SalI	Salvador I
SD	Subdomain
SEC	Size exclusion chromatography
SHM	Somatic hypermutation
TBS	Tris-buffered saline
TBST	Tris-buffered saline with 0.01% Tween-20
TfR1	Transferrin receptor 1
V_H	Variable region heavy chain
V_L	Variable region light chain

1 Introduction

1.1 *Plasmodium* vivax malaria

1.1.1 *P. vivax* epidemiology

Malaria remains a major global health problem with an estimated 263 million cases occurring in 2023 (1). The number of malaria cases has steadily increased since 2020, in part due to disruption to healthcare provisions during the COVID-19 pandemic. However, encouragingly the number of malaria deaths has decreased during this time to an estimated 597,000 in 2023 (1). Four species of *Plasmodium* parasites are considered true human parasites as they use humans as their natural intermediate host: *P. falciparum*, *P. vivax*, *P. malariae* and *P. ovale* (2). In addition, *P. knowlesi* which infects macaque monkeys can also infect humans (3). Out of these species, *P. falciparum* causes the majority of malaria cases and deaths, with the greatest burden of disease in Africa. *P. vivax* is the second most common cause of malaria and accounted for an estimated 9 million malaria cases worldwide in 2023 (1). *P. vivax* is the most geographically widespread and causes between 30-70% of malaria cases in the Pacific islands, Asia and Americas (**Figure 1.1**) (4). *P. vivax* was previously thought to be absent from Sub-Saharan Africa due to the high prevalence of the Duffy negative blood group. Duffy negative red blood cells (RBCs) do not express the Duffy antigen receptor for chemokines (DARC), the essential receptor for *P. vivax* invasion of RBCs (5). However, there is increasing evidence that *P. vivax* is found across all malaria-endemic regions of the African continent and that its prevalence has likely been greatly underestimated (6). Malaria control measures have been focussed on *P. falciparum* but are less effective against *P. vivax* due to differences in parasite biology. In areas where these parasites are co-endemic, as malaria control measures have reduced *P. falciparum* infections, the proportion of malaria due to *P. vivax* has increased (7).

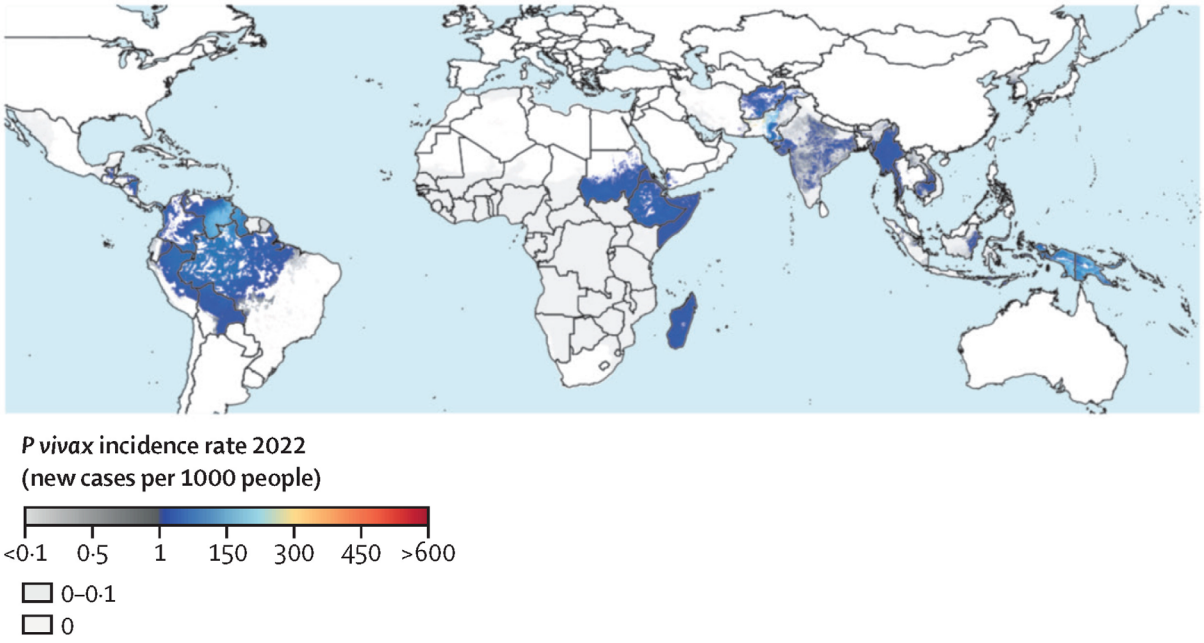

Figure 1.1 Global incidence of *P. vivax*. Map showing the incidence rate of *P. vivax*, number of cases per 1000 people per year for the year 2022, taken from (8).

P. vivax was previously thought of as the benign malaria, in contrast to *P. falciparum*. This notion has been increasingly challenged over recent years, and it has been shown that *P. vivax* is able to cause severe malaria and contributes to significant morbidity and mortality worldwide (9–12). Similar to *P. falciparum*, *P. vivax* infection is also associated with poor outcomes in pregnancy for both the mother and fetus (13–15).

These issues highlight the need for the development of new control measures that specifically target *P. vivax*. A vaccine targeting the blood-stage of infection, which causes clinical disease, has the advantage of reducing parasitaemia and disease severity even if only partially effective. The feasibility of developing an effective blood-stage vaccine is also supported by observations that naturally-acquired immunity (NAI) primarily targets the blood-stage (16). Although NAI to malaria never leads to sterile protection, after repeated exposure over time individuals are protected from or tolerised to clinical disease and are able to control parasitaemia (16).

1.1.2 *P. vivax* biology and life cycle

P. vivax has a similar life cycle to other *Plasmodium* species that infect humans and requires two hosts: the female *Anopheles* mosquito and humans (**Figure 1.2**). When an infected *Anopheles* mosquito takes a blood meal, sporozoites are injected from the mosquito salivary glands into the skin of the human (17). The motile sporozoites then migrate from the skin into blood vessels and infect hepatocytes in the liver. In the hepatocyte, each sporozoite develops over 7 to 10 days into mature schizonts, which then rupture and release merozoites into the bloodstream (18). Once released into blood, the merozoites infect RBCs, where they asexually replicate, producing more merozoites that are released into blood. These blood-stage parasites are the cause of clinical disease. A small proportion of merozoites differentiate into sexual-stage gametocytes, which are ingested by an *Anopheles* mosquito during a blood meal. The gametocytes complete the sexual-stage of replication within the mosquito midgut, resulting in the formation of new sporozoites, which migrate to the mosquito salivary gland and perpetuate the life cycle when injected into a new human host.

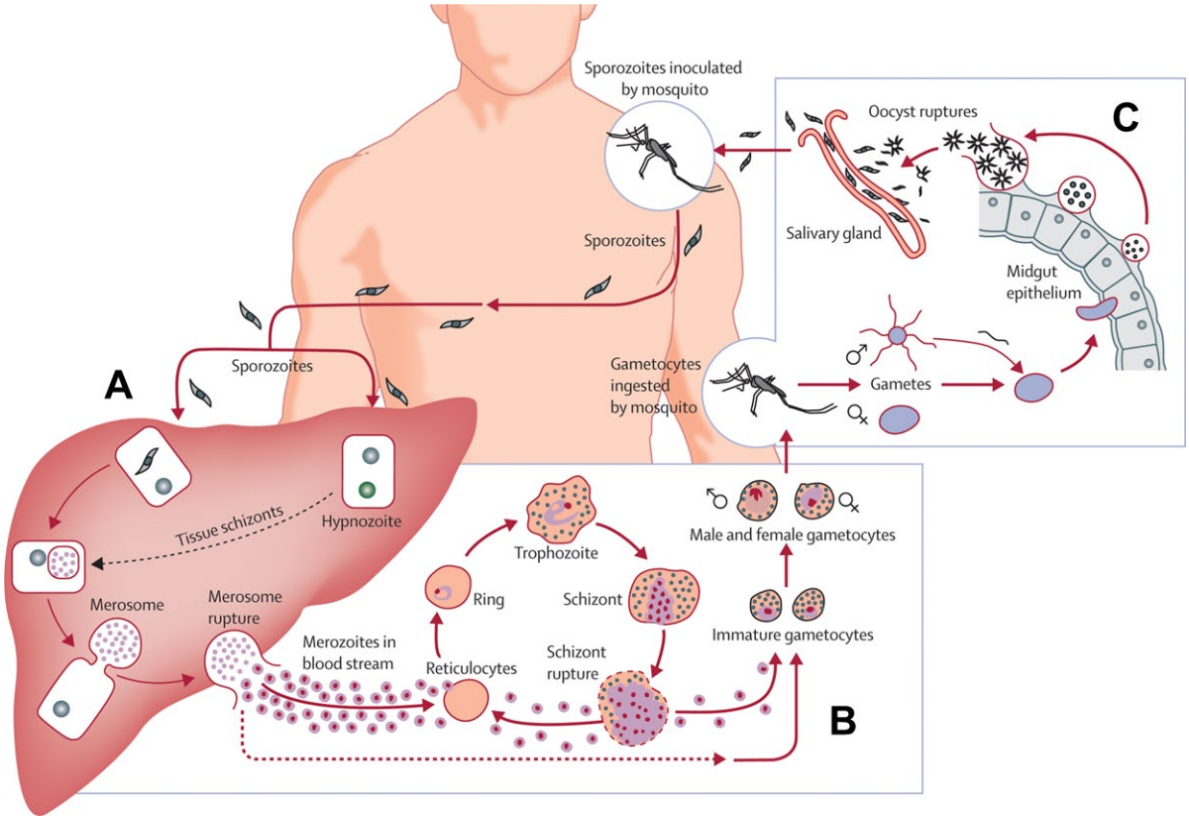

Figure 1.2 *P. vivax* life cycle. The life cycle is commonly divided into three main stages: the pre-erythrocytic or liver-stage **(A)**, blood-stage **(B)** and transmission-stage **(C)**. Reproduced from (17), with permission from Elsevier.

P. vivax has important differences in its biology and life cycle compared to *P. falciparum*, which contribute to the difficulty in its control. Firstly, a proportion of *P. vivax* sporozoites that infect hepatocytes become dormant hypnozoites, which persist in the liver and can become activated weeks to months later to cause a relapse of the blood-stage infection (19,20). There are no diagnostic tests for hypnozoites and antimalarial drugs including artemisinins and chloroquine are only effective against blood-stage parasites. Radical cure of *P. vivax* requires additional treatment to clear hypnozoites, but only two drugs are available that kill hypnozoites: primaquine and, more recently, tafenoquine (21). Neither of these 8-aminoquinoline drugs can be used in people with severe glucose-6-phosphate dehydrogenase (G6PD) deficiency, because they cause severe haemolysis in these individuals (22). G6PD deficiency is an X-linked enzyme deficiency that is relatively common in some populations

living in *P. vivax* endemic areas, but testing is not always accessible (23). To reduce the risk of drug induced haemolysis, many countries use a lower dose of primaquine given over 14 days, however this longer treatment is associated with poor adherence leading to lower effectiveness.

Secondly, unlike *P. falciparum* which invades mature erythrocytes, *P. vivax* has a tropism for reticulocytes (24,25). Reticulocytes arise from the bone marrow, or other haematopoietic tissues, and comprise only a small percentage of peripheral RBCs before rapidly maturing. This likely explains the low peripheral parasitaemia observed in *P. vivax* compared to *P. falciparum*, which can result in difficulty diagnosing *P. vivax*, particularly with rapid diagnostic tests which have lower sensitivity at low levels of parasitaemia (26). More recently, it has become apparent that a large proportion of *P. vivax* blood-stage parasite biomass accumulates outside of the peripheral circulation, particularly in the spleen but also the bone marrow (27–31). This is likely due the physiological accumulation of reticulocytes within the spleen, thereby creating a niche for *P. vivax* replication.

The reticulocyte tropism of *P. vivax* has also hampered studies of parasite biology as it has not been possible to establish long-term *in vitro* cultures of blood-stage *P. vivax*, as has been done for *P. falciparum* (32). This has limited the study of *P. vivax* to facilities in endemic countries that have access to fresh parasites from infected patients. There are also few small animal models that replicate *P. vivax*-human biology and studies have primarily used non-human primates which can be infected with *P. vivax* or the closely related *Plasmodium* species *P. cynomolgi* and *P. knowlesi* (33). The primary hosts of *P. knowlesi* and *P. cynomolgi* are macaques, but both *Plasmodium* species are also able to zoonotically infect humans (3,34). To circumvent the difficulties with establishing long-term cultures of *P. vivax*, advances have been made in adapting *P. knowlesi* to grow in human RBCs to allow *in vitro* testing of blood-stage interventions (35).

Lastly, gametocytes development during the blood-stage of infection is significantly quicker in *P. vivax* compared to *P. falciparum*, taking only 2 to 3 days (36). An individual can therefore transmit *P. vivax* before they develop clinical symptoms and seek medical treatment (37). This means that malaria control measures focussing on early diagnosis and treatment have less impact on transmission of *P. vivax* compared to *P. falciparum*.

1.1.3 Red blood cell invasion

Studies of RBC invasion by *P. knowlesi* and *P. falciparum* have shown that parasite invasion of RBCs occurs quickly and is completed in around 30 seconds (38,39). Upon initial contact of merozoites with a RBC, merozoites undergo gliding motility across the RBC membrane and frequently dissociate (40). This is then followed by stable adhesion to and deformation of the RBC membrane. The merozoite re-orientates itself so its apical end comes into direct contact with the RBC membrane and a tight junction forms. The apical end of the merozoite is located at the wider end of the merozoite, not the narrow end as previously thought, with a protrusion that contains the apical complex becoming more pronounced during RBC invasion (40). Tight junction formation is mediated by adhesins which are released from micronemes and rhoptries within the merozoite. A parasitophorous vacuole forms around the merozoite during its entry into the RBC. Once the merozoite has completely entered the RBC, the parasitophorous vacuole seals around the merozoite and pinches off from the RBC membrane, resulting in the merozoite residing in the parasitophorous vacuole within the RBC.

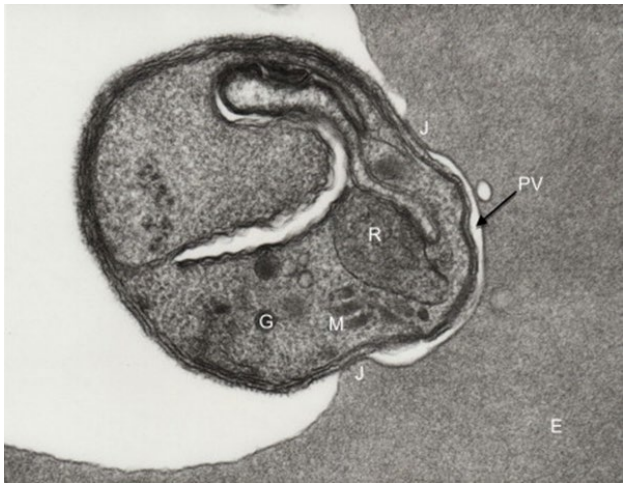

Figure 1.3 *Plasmodium knowlesi* invasion of RBC. A *P. knowlesi* merozoite at the start of invasion of a *Macaca mulatta* RBC. The apical end of the merozoite has orientated towards the erythrocyte (E) membrane. Micronemes (M) and rhoptry (R) within the merozoite release their contents. A tight junction (J) forms between the merozoite and RBC membrane and moves across the merozoite surface. Invagination of the RBC membrane around the merozoite forms a parasitophorous vacuole (PV). The merozoite moves into the PV, which seals around it, releasing the parasite into the RBC cytoplasm. Image from (41), with permission from Elsevier.

The interaction between parasite invasion ligands and their specific RBC surface receptors, which mediate the apical attachment of the merozoite to a RBC, have been the focus of studies as potential targets for a blood-stage vaccine. For *P. vivax*, the interaction between its Duffy-binding protein (PvDBP), which is released from micronemes, and the receptor DARC on RBC appears to be essential for formation of the tight junction during RBC invasion (42).

Other parasite ligands in addition to PvDBP are also involved in invasion of RBCs and recent research has focussed on identifying reticulocyte-specific ligands. *P. vivax* has two families of reticulocyte-binding proteins, PvRBP1 and PvRBP2, and for some of these proteins their corresponding receptor and involvement in RBC invasion have been identified (43). PvRBP1a binds to reticulocytes, but does not appear to be essential for invasion (44). PvRBP2a binds to CD98 on reticulocytes and was shown to be involved in RBC invasion, but may not be an essential interaction (45). PvRBP2b has been shown to bind to the transferrin receptor 1 (TfR1 or CD71) on reticulocytes and antibodies that target this interaction were shown to inhibit invasion of *P. vivax* isolates from Brazil and Thailand in *ex*

vivo invasion assays (46). However, a recent study on *P. vivax* isolates from Cambodia showed that the interaction between PvRBP2b and CD71 was not essential for reticulocyte invasion (47). This suggests that there is variation in invasion pathways used by different *P. vivax* strains and there is likely redundancy amongst the multiple reticulocyte-binding proteins (48). There are also other proteins such as erythrocyte binding protein (PvEBP), a paralog of PvDBP that binds to CD1 on RBCs, which may also be involved in RBC invasion (49,50). However so far, the only essential interaction identified for *P. vivax* invasion of RBCs remains the one between PvDBP and DARC.

P. knowlesi invasion of human RBCs also requires binding of DARC to a DBP protein - PkDBPα (51). PkDBPα and PvDBP are structurally similar and share around 70% amino acid identity. Blocking of the interaction between PkDBPα and DARC prevents merozoite fusion to the RBC membrane and apical reorientation of the merozoite (52). In addition to PkDBPα, *P. knowlesi* has two paralogs of DBP, PkDBPβ and PkDBPγ, which share high amino acid identity to PkDBPα (53) but bind to a different receptor that is not found on human RBCs (54). In addition to PkDBPα, *P. knowlesi* has a reticulocyte binding like protein, normocyte binding protein Xa (NBPXa), which is also essential for merozoite invasion of human RBCs (55).

1.2 *P. vivax* Duffy-binding protein

Between the 1920s until 1940s, when penicillin was discovered, fever deliberately induced by malaria was used in the treatment of neurosyphilis (56). It was observed during malariotherapy that people of African origin were refractory to infection with *P. vivax*, the main *Plasmodium* species used in malariotherapy. The reason for this resistance to infection was discovered in the 1970s, when it was observed that a lack of the Duffy blood group

antigen on RBCs, a phenotype that is predominantly found in populations of West and Sub-Saharan Africa, was associated with protection from induced *P. vivax* infection (5). Due to the inability to culture *P. vivax*, *in vitro* studies were conducted in *P. knowlesi* and showed that Duffy negative RBCs were resistant to invasion by merozoites (51). This led to the hypothesis that DARC is an essential ligand required by *P. vivax* and *P. knowlesi* to invade human RBCs. The corresponding ligand on the parasite was first identified in *P. knowlesi* (57), followed by the identification of the ortholog in *P. vivax* (58) and was named Duffy-binding protein. The receptor binding domain of PvDBP was found to be contained within region II of PvDBP (PvDBPII) (59) and this domain has been the main focus of blood-stage vaccine development in *P. vivax*.

The *PvDBP* gene encodes a protein of 1070 amino acids with a molecular weight of 140 kDa. PvDBP shares homology with other erythrocyte-binding antigens found in other *Plasmodium* species and consists of a signal sequence at the N-terminus, extracellular domains I to VI, a transmembrane domain and a short cytoplasmic tail which corresponds to region VII, at the C-terminus (**Figure 1.4**) (60). The receptor binding domain is found within region II, which spans D194 to T521 (61), numbered in PvDBP Salvador I (SalI) sequence (62). Region II is further subdivided into three subdomains. Region II is cysteine rich, containing 12 conserved cysteines that form disulphide bonds, which stabilise each subdomain.

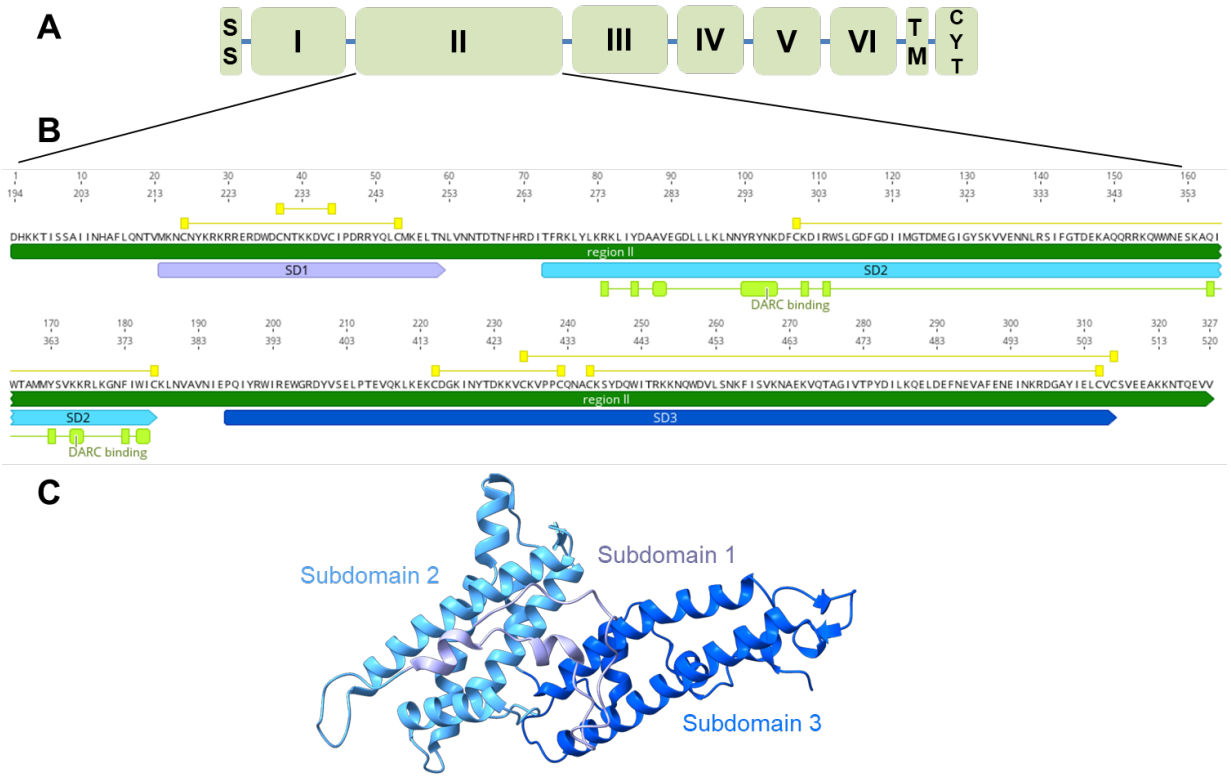

Figure 1.4 PvDBP structure. **(A)** PvDBP consists of regions I to VI, with a signal sequence (SS) at the N-terminus and transmembrane domain (TM) and cytoplasmic domain (CYT) at the C-terminus. **(B)** Sequence of PvDBP region II labelled with the three subdomains (SD1, SD2 and SD3). Disulphide bridges are shown in yellow. DARC binding site labelled in light green (from (63)). **(C)** The structure of PvDBPII (pdb_00008a44) (63), showing the three subdomains.

PvDBP is polymorphic, particularly in region II, except the highly conserved cysteine residues (64–67). The majority of polymorphisms within PvDBPII are found in subdomain 2 (SD2), surrounding (but not within) the DARC binding site, whilst residues directly involved in DARC binding are well conserved (68). In one study of global *P. vivax* isolates, 31 polymorphic residues in PvDBPII occurred in at least 0.5% of isolates and some polymorphisms were found at frequencies of 50% or more, with the highest frequency found at residue D338 (69). Certain polymorphisms are often found together, for example N372K, W392R and I458K; this set of polymorphisms have been shown to result in loss of inhibition by antibodies to PvDBP (70). This indicates that the polymorphisms within PvDBP are likely a mechanism of escape from host immune responses. The high polymorphism within PvDBPII means that vaccines based on a single strain may only induce strain-specific

responses. Development of a strain-transcending vaccine that is effective against different strains found worldwide may require strategies to focus the immune response to target conserved residues within PvDBPII.

In addition to polymorphisms, *PvDBP* gene amplification has been found in isolates from different regions. *PvDBP* copy number ranged from one to five copies in isolates from diverse regions in Southeast Asia, South America and Africa and high copy number variants (CNV) were commonly observed in some studies (71–73). Phylogenetic analyses indicate that high CNVs evolved from isolates with a single copy of *PvDBP* independently at different times and in different locations (72). The different gene copies of *PvDBP* in a single isolate shared identical gene sequences, which suggests that gene duplications occurred recently. *PvDBP* gene amplification may be an adaptation by the parasite to overcome host immune responses targeting PvDBP; in support of this, one study has shown that parasites with higher *PvDBP* copy number are less susceptible to invasion-inhibitory mAbs *in vitro* (74). *PvDBP* gene amplification may also aid RBC invasion in Duffy-negative individuals, although high CNVs are commonly found in areas where Duffy-negativity is rare (71).

1.2.1 Duffy Antigen Receptor for Chemokines

The Duffy blood group antigen is encoded by the atypical chemokine receptor 1 (*ACKR1*, or *FY*) gene, which is expressed on erythroid and endothelial cells and adipocytes (75). DARC is a transmembrane glycoprotein, with a 60-amino acid N-terminal extracellular domain, seven transmembrane domains and an intracellular domain, which lacks the G-protein signalling domain found in classical chemokine receptors (**Figure 1.5**). DARC is able to bind the widest variety of both CC and CXC chemokines of all chemokine receptors. It functions to transport and present chemokines and regulate chemokine concentrations by acting as a

chemokine reservoir and has physiological roles in angiogenesis and chemotaxis. DARC was first discovered in 1950 as a minor RBC antigen that was the cause of a haemolytic transfusion reaction in a patient who had previously received multiple blood transfusions (76). Subsequently, its importance in determining susceptibility to *P. vivax* infection renewed interest in DARC.

The *FY* gene has two co-dominant alleles *Fy*A* and *Fy*B*, which differ by a single nucleotide polymorphism, resulting in glycine in Fya versus aspartic acid in Fyb at residue 42. These give rise to the Fy(a+b−), Fy(a−b+) and Fy(a+b+) Duffy blood group phenotypes. The Duffy negative Fy(a−b−) phenotype is the result of a homozygous single nucleotide mutation in the promoter region of the *Fy*B* allele that silences expression of the *Fy*B* gene in erythroid cells, but not in endothelial cells (known as $Fy*B^{ES}$ erythroid silent allele) (77–79). Other less common mutations in the *FY* gene include those that reduce expression of *Fy*A* or *Fy*B* and mutations that silence *Fy*A* expression on erythroid cells (80). *Fy*B* is the ancestral form of DARC and is most common in European populations, whilst *Fy*A* is now the most prevalent allele in modern humans, with the highest frequency in Asia (79). $Fy*B^{ES}$ is near fixation in western and central African populations, but almost absent in European or Asian populations.

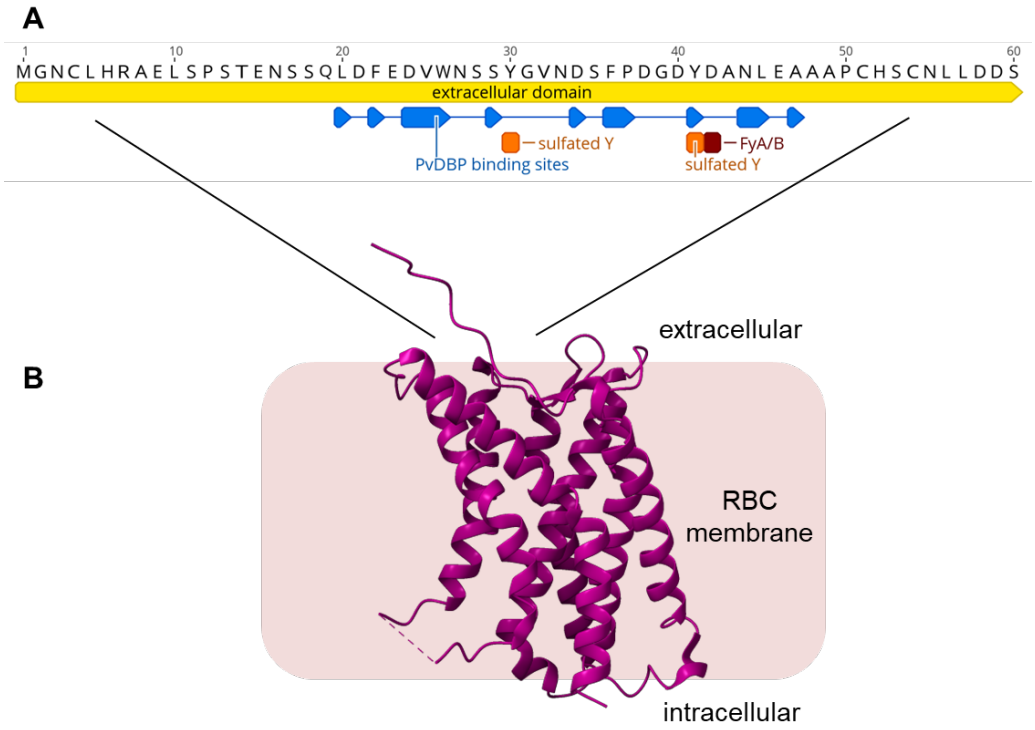

Figure 1.5 Structure of DARC. DARC consists of an extracellular domain, seven transmembrane domains and an intracellular domain. **(A)** Sequence of N-terminal extracellular domain of DARC. Residue 42 is an aspartic acid in FyB and a glycine in FyA. Binding site of PvDBP shown in blue (from (63)). Sulfated tyrosines, which are required for PvDBP binding are labelled in orange. **(B)** Structure of DARC showing the seven transmembrane domains (pdb_00008jps). The proximal end of the N-terminal domain was not resolved.

In erythroid cells, DARC expression is highest in progenitor nucleated erythroid cells found in the bone marrow and declines as erythrocytes mature (81). DARC expression in erythroid cells in the bone marrow has been shown to regulate haematopoietic stem cell development (82). In mice, a lack of DARC expression in erythroid cell progenitors in the bone marrow combined with expression of DARC on endothelial cells in venules, resulted in neutrophils with a distinct phenotype that readily egressed from the circulation resulting in neutropenia (82). This mechanism likely explains the neutropenia that is observed in Duffy-negative individuals, in whom DARC expression is absent from erythroid cells but expressed in endothelial cells (83).

The dogma of complete protection of Duffy-negative individuals from *P. vivax* infection has been challenged over the last 15 years. There are now numerous reports of *P. vivax* infection in Duffy-negative individuals throughout Africa (6) and evidence of transmission of *P. vivax* in populations that are almost completely Duffy-negative (84). However, studies in *P. vivax* endemic areas with populations that have different Duffy phenotypes show that Duffy-negativity does confer substantial resistance to *P. vivax* infection. For example, a study in Ethiopia found that *P. vivax* infection was up to 20 times less common and symptomatic disease was up to 50 times less common in Duffy-negative compared to Duffy-positive individuals (85). Parasitaemia in Duffy-negative individuals is significantly lower than in Duffy-positive individuals, often below levels detectable by microscopy (86). Without more widespread use of molecular diagnostic tests that are species specific, the prevalence of *P. vivax* in Africa will be likely be greatly underestimated. Infection of Duffy-negative individuals by *P. vivax* suggests that the parasite is either using alternative ligands for RBC invasion or that Duffy-negativity does not entirely abolish DARC expression on RBCs. Support for the latter comes from two recent studies, which showed that DARC is transiently expressed on genotypically "Duffy-negative" RBCs, but at lower levels than in Duffy-positive RBCs (87,88). DARC expression was highest in erythroid precursors in the bone marrow compared to peripheral mature RBCs (88). This suggests that the bone marrow and other haematopoietic tissues could be a major reservoir of *P. vivax* infection and that peripheral parasitaemia significantly underestimates the total parasite biomass present (27,28). The low number of DARC expressing erythroid cells and their restriction to sites of erythropoiesis in Duffy-negative individuals would explain the very low peripheral parasitaemia that is often observed in these individuals. When erythroid precursors from genotypically Duffy-negative individuals were co-cultured with *P. vivax* merozoites, only erythroid precursors expressing DARC were invaded by the parasites, suggesting that

invasion of genotypically Duffy-negative erythroid cells still requires interaction of PvDBP with DARC (87).

Apart from the *Fy*B*^{ES} allele providing resistance to *P. vivax* infection, studies have also compared the effects of *Fy*A* and *Fy*B*. Some cohort studies have found that the *Fy*A* is protective and associated with a lower risk of developing clinical *P. vivax* disease (89–91). PvDBPII binding was also observed to be lower to Fya compared to Fyb (90). However in another study Fya was associated with a higher frequency of *P. vivax* infection (92) and genetic studies are also inconclusive as to whether *Fy*A* is under positive selection or not (93).

1.2.2 PvDBP-DARC binding

PvDBPII binds to the N-terminal ectodomain of DARC to mediate invasion of merozoites into RBCs (94,95) (**Figure 1.6**). Initial structural studies of PvDBPII and the 60-mer ectodomain of DARC have suggested a step-wise binding event, whereby the binding of DARC to PvDBPII induces dimerisation of PvDBPII to form a heterotrimer, which then binds a second DARC to form a heterotetramer (96). In this model, the DARC binding site and PvDBPII dimerisation sites were mapped to SD2 of PvDBPII. However, in these structural studies only residues 19 to 30 of DARC could be resolved and the DARC fragment used, which was produced in *E coli*, was not sulfated. Previous studies have shown that tyrosine residues 30 and 41 within the DARC ectodomain are sulfated when recombinantly expressed in a human cell line and that sulfation of tyrosine 41 was essential for binding of PvDBPII to DARC (97,98). Mutagenesis studies have also previously identified additional residues on PvDBPII, to those noted in the structural studies, which are involved in PvDBPII-DARC binding, which correspond to the dimer interface (98,99). In more recent structural

studies using sulfated DARC ectodomain produced in human cells, DARC residues 19 to 47 could be resolved and were shown to bind around a protrusion on the PvDBPII surface (63). The study confirmed that sulfation of tyrosine 30 and 41 was required for binding of DARC to PvDBPII and that tyrosine 41 contributed most to binding affinity. Dimerisation of PvDBPII was not observed in this study and it remains unclear if dimerisation occurs *in vivo* under physiological conditions.

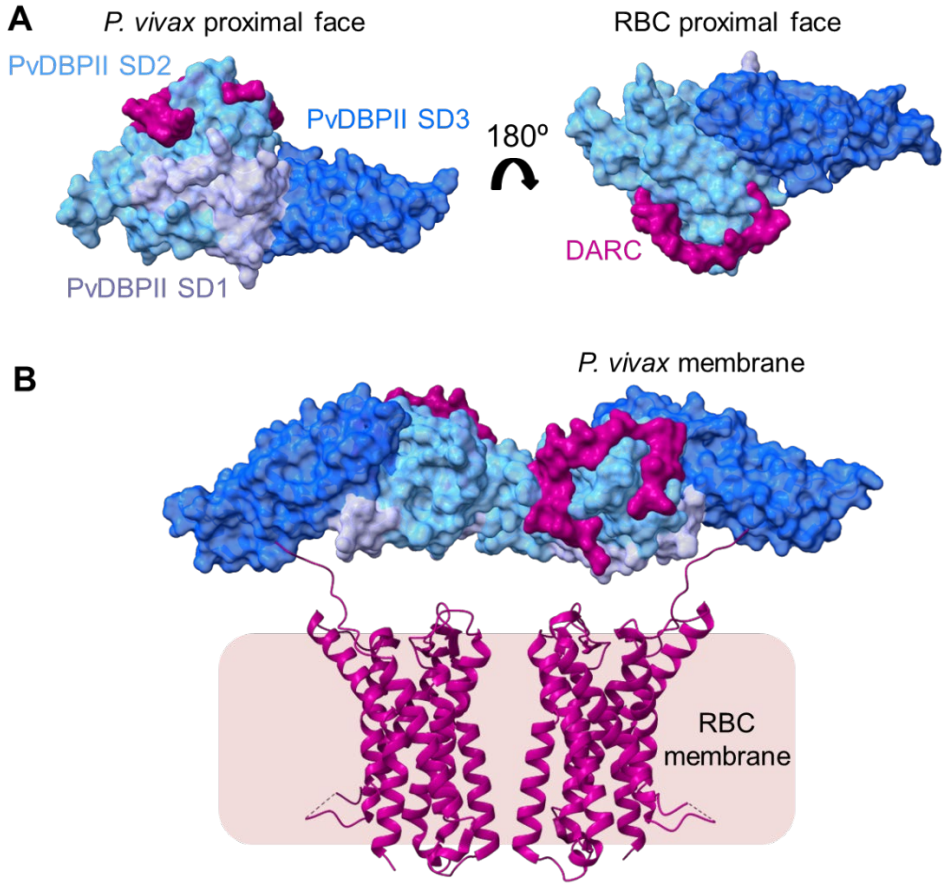

Figure 1.6 PvDBPII binding to DARC. The three subdomains (SD1-3) of PvDBPII are coloured in lilac, cyan and blue; DARC is coloured in magenta. **(A)** Structure of PvDBPII binding to $DARC_{19\text{-}47}$ (pdb_00008a44) (63). **(B)** Model of PvDBPII-DARC binding as proposed by Batchelor *et al.* (62). Initial binding of PvDBPII to DARC is followed by receptor-induced dimerisation of PvDBPII to form a heterotrimer. This brings a second PvDBPII molecule close to a second DARC ectodomain and a second binding event creates a heterotetramer as shown. Structure of PvDBPII binding to $DARC_{19\text{-}47}$ (pdb_00008a44) superimposed onto structure of dimer of PvDBPII (pdb_00004nuv). Structure of transmembrane domains of DARC shown (pdb_00008jps).

The structure of full length DARC has recently been elucidated, in complex with the chemokine CCL7 (100). CCL7 bound the distal part of the N-terminal domain and made contacts with transmembrane domains 6 and 7 and the third extracellular loop of DARC. The proximal part of the N-terminal domain of DARC, which is involved in PvDBP binding, was not resolved in this structure so the interaction between full-length PvDBP and DARC remains to be determined. Given that the interaction between PvDBP and DARC appears to be essential for invasion of *P. vivax* into RBCs, understanding fully the interaction between PvDBP and DARC could reveal new targets for naturally-acquired or vaccine-induced immunity that could effectively inhibit this interaction.

1.3 Naturally-acquired immunity to *P. vivax*

NAI to malaria develops following repeated exposure to infection over years (101). NAI encompasses reduction in clinical symptoms and control of parasite growth, resulting in mild or asymptomatic disease and low parasitaemia (102). The quality and longevity of this response is highly variable between individuals and depends on factors including host immunity and age, parasite species and strains and malaria transmission intensity (16). In high transmission areas, NAI to *P. vivax* develops within the first few years of life (103). Continuous exposure to infection is required to maintain NAI and if infection ceases, NAI can rapidly wane.

The mechanisms of NAI and correlates of protection to malaria are not known. NAI appears to primarily target the blood-stage of infection, although immunity to other parasite life-stages does develop. NAI is predominantly antibody-mediated as evidenced by experiments showing that passive transfer of serum from humans with NAI can protect naïve recipients

from clinical malaria or reduce disease severity and parasitaemia (104). Few studies have been conducted on *P. vivax* to look for correlates of protection and these have previously focussed on a small number of antigens including PvDBP and *P. vivax* merozoite surface protein 1 (PvMSP1). Although many antigen targets likely contribute to development of NAI to *P. vivax*, development of immunity targeting the essential interaction for parasite invasion between PvDBP and DARC is likely an effective and important contributor to NAI.

Naturally-acquired antibodies to PvDBP develop in individuals living in endemic areas and generally increase with age and exposure (105,106). Antibody responses to PvDBP are variable and can be short-lived, strain-specific (107) and have low binding inhibition activity (108). A small proportion of people develop high levels of strain transcending binding inhibitory antibodies (BIAb) suggesting that conserved epitopes are present in PvDBP which can elicit broadly neutralising antibodies (108). The relatively low immunogenicity of PvDBP may be due to the short time that the antigen is exposed to the immune system during merozoite invasion. High levels of antibodies with high affinity and avidity are likely required to effectively inhibit parasite invasion and this may be more readily achieved through vaccination than natural exposure.

Naturally-acquired polyclonal anti-PvDBPII antibodies are able to inhibit recombinant PvDBPII binding to DARC and parasite invasion into RBCs *in vitro* (109). Studies have also looked at associations of anti-PvDBP antibodies and *P. vivax* infection and disease. Higher total anti-PvDBPII antibodies have been associated with lower risk of clinical *P. vivax* disease in some studies (110), but not others (106). When focussing on BIAbs, higher binding inhibition was associated with lower parasitaemia, which could also explain the association seen with protection from infection diagnosed by microscopy but not protection from infection diagnosed by PCR (107,108). Higher BIAbs have also been associated with delay in time to next *P. vivax* disease (106). However, in another study, BIAbs showed no

significant association with risk of infection (110). BIAbs target the conserved DARC binding site so should afford strain-transcending immunity. In studies testing binding inhibitory activity against different variants, high BIAbs were mostly strain-transcending and remained at a stable level over time (106,108). In contrast, antibodies to other regions of PvDBPII may not be neutralising or may target polymorphic regions making them strain-specific. Binding inhibition is commonly measured using recombinant PvDBPII and nDARC-Fc fusion protein in an enzyme-linked immunosorbance assay (ELISA). This may not represent all mechanisms of neutralising activity of antibodies and may underestimate the parasite invasion inhibition activity of antibodies which could act through mechanisms other than direct DARC binding blockade. This may explain the weak correlations observed between *P. vivax* disease and BIAbs in some studies.

1.4 Monoclonal antibodies to PvDBPII

Studies on antibodies against PvDBP aim to identify highly potent antibodies that are effective at inhibiting invasion of diverse *P. vivax* allelic variants. This information could be used to guide vaccine design to target conserved, neutralising epitopes within PvDBP and avoid eliciting responses to immunogenic but non-neutralising epitopes. To date, small panels of monoclonal antibodies (mAbs) have been isolated from vaccinated animals and vaccinated and naturally-infected humans.

A panel of 10 anti-PvDBPII mAbs were isolated from vaccinated mice and tested for PvDBP binding and DARC binding inhibition against a number of different PvDBPII variants (111). The ability of mAbs to inhibit PvDBPII binding to RBCs was determined using an assay that measures the binding of COS7 cells expressing PvDBPII to RBCs. Subsequent studies used a variety of methods including X-ray crystallography, hydrogen–deuterium exchange mass

spectrometry, mutational screening and phage display expression library to elucidate the epitopes of inhibitory mAbs. The four most inhibitory mAbs (3C9, 2D10, 2C6 and 2H2) all bind within subdomain 3 (SD3), a well conserved area within PvDBPII (112,113). These epitopes are located distant from the DARC-binding domain and putative PvDBPII dimerisation domain found in SD2 and their mechanism of action is unclear. The epitope of a non-inhibitory murine mAb 3D10 was also determined and found to be a partially linear epitope within subdomain 1 (SD1) (**Figure 1.7**) (113).

In addition to these murine mAbs, a number of human mAbs have been isolated from naturally-infected individuals. The first human anti-PvDBPII mAbs were isolated from *P. vivax* infected patients in Korea (114). The three mAbs produced were all able to block binding of RBCs to PvDBPII expressed on COS7 cells, but neither their effect on parasite invasion nor epitopes were determined. In a study by Carias *et al.*, adults with a history of *P. vivax* infection were screened to identify those with serum that had high binding inhibition of recombinant PvDBPII to DARC-Fc fusion protein in an ELISA-based assay (115). From three individuals with the highest binding inhibitory serum, a total of 13 mAbs from different B cell clonal groups were then produced and characterised. All except one of these mAbs inhibited PvDBPII-DARC binding *in vitro* and 11 of the mAbs recognised overlapping epitopes within SD2. The epitopes of two mAbs, 053054 and 092996, were later determined and found to bind overlapping epitopes within SD2, corresponding to the primary DARC binding site and PvDBPII dimerisation site (116). Some of the mAbs were tested in *P. vivax ex vivo* invasion assays and all mAbs which were tested had similar potency against different *P. vivax* isolates, inhibiting invasion by around 40-50% at 100 µg/mL.

Human mAbs have also been isolated from malaria naïve adults vaccinated with viral-vectored PvDBPII vaccines in a Phase 1 trial (117). Ten mAbs were isolated from two vaccinees and were tested for binding characteristics and parasite growth inhibition activity

(GIA) (118). Recombinant PvDBPII-DARC binding inhibition was assessed by an ELISA-based assay. Parasite GIA was assessed using transgenic *P. knowlesi* parasites expressing PvDBP (119) and using different isolates of *P. vivax* in an *ex vivo* assay. The hierarchy of potency of growth inhibition for the panel of mAbs was the same in the *P. vivax ex vivo* assay as with the transgenic *P. knowlesi* parasite, suggesting that the transgenic *P. knowlesi* parasite GIA assay is a valid surrogate assay for *P. vivax* invasion inhibition. One mAb, DB9, was broadly inhibitory and showed potent growth inhibition across 10 out of 11 *P. vivax* isolates tested. The epitope of DB9 was determined by X-ray crystallography and found to bind within SD3. A number of antibodies with parasite GIA have now been found to bind to SD3, which does not contain the primary receptor binding site. The mechanism(s) of parasite growth inhibition of these SD3-targeting antibodies is not clear. Possible hypotheses include that these antibodies may sterically prevent PvDBP approaching the RBC membrane, or that there may be an, as yet, unidentified secondary binding event which involves SD3. Of note, the binding inhibition activity of mAbs did not always correlate with GIA indicating that the ELISA-based binding inhibition assay may not capture all mechanisms of parasite GIA by antibodies. For example, mAbs DB1 and DB10 which have overlapping epitopes, did not inhibit PvDBPII-DARC binding in the ELISA-based assay, but were the most potent mAbs in parasite invasion inhibition assays, although both mAbs were strain-specific. The epitope of DB1 has since been determined to be in a polymorphic site in SD2, in the putative PvDBPII dimerisation site, but distant from the DARC binding site (63). Its mechanism of action could be through blockade of PvDBP dimerisation if this does occur *in vivo*; or the dimerisation site could be involved in the binding of full-length PvDBP to DARC, which is not detected by the recombinant ELISA-based assay as this uses only PvDBPII and not the full-length protein .

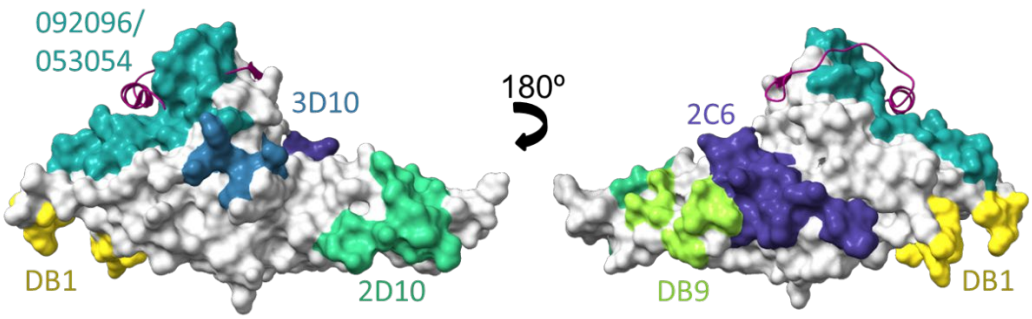

Figure 1.7 Epitopes of mAbs on PvDBPII. Epitopes of mAbs mapped onto structure of PvDBPII (white) binding to $DARC_{19-47}$ (magenta) (pdb_00008a44) (63). Murine mAb 2C6 inhibited RBC binding, whilst 3D10 was non-inhibitory (112). Human naturally-acquired mAbs 092096 and 054054 have overlapping epitopes and inhibited DARC binding (116). Vaccine-induced mAbs DB1 and DB9 both showed parasite growth inhibition activity (63,118).

To date, studies on human mAbs have been limited to small panels and may not be fully representative of the clones induced by natural infection or vaccination. Information from further studies to identify the most functional antibody isotype, subclass and epitopes, as well as determining if any synergy or antagonism occurs between combinations of antibodies, could be used to rationally improve PvDBP vaccine designs.

1.5 Vaccines against *P. vivax*

The Malaria Vaccine Technology Roadmap was updated in 2013 and expanded the strategic goals to include the need to target *P. vivax* for vaccine development in addition to *P. falciparum* (120). However, *P. vivax* vaccine development still lags behind that for *P. falciparum,* and few vaccine candidates against *P. vivax* are progressing through clinical development. This is in part due to the lack of long-term *in vitro* culture system for *P. vivax* and limited animal models. The most clinically advanced candidate vaccines targeting the pre-erythrocytic stages are based on radiation-attenuated sporozoites or the *P. vivax*

circumsporozoite protein (PvCSP). The most clinically advanced vaccines targeting the blood-stage utilise PvDBPII. More recently, vaccines against the transmission-stage have also entered clinical trials.

Two subunit *P. vivax* vaccines targeting PvCSP have progressed to clinical studies. VMP001 (vivax malaria protein 1) is a chimeric PvCSP-based subunit protein vaccine adjuvanted with AS01, which was tested in a Phase 1/2a trial for efficacy by Controlled Human Malaria Infection (CHMI) (121). The vaccine did not induce sterile protection in any participant but there was a small, yet significant, delay in time to patent parasitaemia in 59% of vaccinees compared to unvaccinated controls. Another PvCSP-based vaccine which was comprised of a synthetic peptide CS derivative, adjuvanted with Montanide ISA 51, has also been tested in a Phase 2a trial with CHMI in both malaria-naïve and semi-immune adults (122). Overall, there was no statistically significant difference in frequency of infection between unvaccinated controls and vaccinees following CHMI.

Radiation-attenuated sporozoites delivered by mosquito bite were first used as a vaccination on two volunteers in the 1970s who showed sterile protection upon CHMI (123). Radiation-attenuated sporozoites were then not tested again until a recent study conducted in Colombia (124). In this study, vaccination comprised of bites from irradiated, *P. vivax*-infected mosquitoes delivered a total of 7 times, at intervals of around 9 weeks. Out of the 12 Duffy blood group positive participants who received irradiated sporozoites, 5 showed sterile protection. The large number of irradiated sporozoites required, the challenges in producing *P. vivax* sporozoites and inability to cryopreserve purified sporozoites limits this approach as a vaccination strategy that could be used in the field.

The first transmission-blocking vaccine candidate to enter clinical testing is Pvs25, a surface protein on *P. vivax* ookinetes. The vaccine was first tested with the adjuvant Alhydrogel and

showed relatively low immunogenicity (125), but up to 30% transmission blocking activity was seen in direct membrane feeding assays using sera from vaccinees with the highest antibody responses. To try to improve the immunogenicity, Pvs25 was then tested adjuvanted with Montanide ISA 51, but severe adverse reactions to this formulation seen during dose escalation resulted in vaccinations being halted in the trial (126). Recently a new vaccine targeting Pvs25, Pvs25-IMX313 adjuvanted with Matrix-M, has been tested in a Phase 1 trial in the UK (NCT05270265). Pvs25-IMX313 is a protein-nanoparticle in which Pvs25 is fused to the IMX313 oligodimerisation domain. Results from this trial are awaited. A new transmission blocking antigen target has also recently entered clinical trials. Pvs230D1-EPA is a recombinant protein vaccine based on Pvs230, which is expressed on the surface of gametocytes, and is being tested in a study conducted in the USA (NCT05913973).

Development of an effective vaccine against malaria will likely require a combination of different antigens from one life-cycle stage or from different life-cycle stages to achieve high efficacy against malaria disease and reduce malaria transmission. A pre-erythrocytic vaccine, even if only partially effective, theoretically has the potential to substantially reduce transmission of *P. vivax* by preventing formation of hypnozoites and subsequent relapses (127). However, if a pre-erythrocytic vaccine fails to induce sterile immunity, the individual can go on to develop malaria disease in the blood-stage. Transmission-blocking vaccines do not provide protection from malaria disease for the individual but instead aim to induce immunity that inhibits transmission of the parasite in mosquitoes and therefore reduce transmission of malaria at a population level. A blood-stage vaccine fills the gap by targeting the disease-causing stage of the parasite lifecycle and even if only partially effective, it may confer some protection by reducing parasitaemia and disease severity and could also reduce transmission.

1.5.1 Vaccines targeting PvDBPII

PvDBPII is the leading vaccine candidate against blood-stage *P. vivax* malaria. In pre-clinical studies in small animal models and non-human primates, PvDBPII-based vaccines induced antibodies that blocked PvDBPII-DARC binding (128–131). In a study in *Aotus* monkeys, animals vaccinated with PvDBPII in Freund's adjuvant, had longer pre-patent period and lower parasitaemia following *P. vivax* malaria challenge (130). However, animals that received PvDBPII in Montanide ISA720 had lower antibody responses and showed no efficacy following malaria challenge.

The first clinical study of PvDBPII-based vaccines tested chimpanzee adenovirus serotype 63 (ChAd63) and modified vaccinia virus Ankara (MVA) viral vectored PvDBPII (SalI strain) vaccines (117). This study, VAC051, was conducted in Oxford between 2013 to 2014 and showed that a heterologous prime-boost regimen with ChAd63 prime, followed by MVA boost 8 weeks later was the most immunogenic and induced antibodies that inhibited binding of vaccine homologous and heterologous variants of recombinant PvDBPII to DARC.

A recombinant protein vaccine PvDBPII (SalI strain) adjuvanted with glucopyranosyl lipid adjuvant-stable emulsion has also been developed and was tested in a Phase 1 trial in India (132). The study showed that the highest dose of 50 μg PvDBPII elicited the highest and most persistent antibody response and that the antibodies induced were able to inhibit binding of different allelic variants of PvDBPII to DARC *in vitro*.

Both the viral vectored and protein/adjuvant PvDBPII vaccines were then taken forward for testing of efficacy by CHMI in two trials, VAC071 and VAC079, which ran in parallel in Oxford between 2019 and 2022 (133). The trials showed that the protein PvDBPII vaccine with Matrix-M adjuvant (Novavax) given in a delayed dosing regimen (doses given at 0, 1 and 14 months) was able to reduce parasite growth in the blood by an average of 50%

compared to unvaccinated controls during CHMI. PvDBPII/Matrix-M given in a monthly dosing regimen (doses given at 0, 1 and 2 months) and the ChAd63/MVA PvDBPII vaccines both induced lower anti-PvDBPII antibody titres and did not significantly inhibit parasite growth. In these studies, the magnitude of anti-PvDBPII antibody and PvDBPII-DARC BIAb titres were correlated with the degree of parasite growth inhibition observed during CHMI. The *in vitro* parasite GIA, tested against transgenic *P. knowlesi* parasites expressing PvDBP, also correlated with *in vivo* parasite growth. The CHMI was conducted with a *P. vivax* clone (PvW1), which originated from Thailand (134), that is heterologous to the vaccine strain (SalI), indicating that the antibodies induced by vaccination were able to recognise conserved epitopes within diverse variants of PvDBP. These studies provided the first evidence in humans that vaccination against PvDBPII can induce parasite growth inhibiting immunity. However, the degree of parasite growth inhibition achieved was insufficient to ultimately prevent (and only delayed) malaria diagnosis in malaria-naïve UK adults and improvements in efficacy will thus likely be needed to achieve clinical significance in the field.

1.5.2 Blood-stage vaccines against *P. falciparum*

Recent advances with vaccines targeting *P. falciparum* reticulocyte-binding protein homolog 5 (RH5) have shown for the first time that significant clinical efficacy can be achieved with a blood-stage malaria vaccine. In a Phase 2 trial of the RH5.1 protein vaccine with Matrix-M adjuvant, the delayed dosing regimen (0, 1, 5 months) showed an efficacy of 55% against clinical malaria in African children over a 6-month follow-up (135). RH5 is a well conserved merozoite protein that forms an essential interaction with basigin (CD147) on RBCs to mediate parasite invasion (136). In *P. falciparum* merozoites RH5 forms a complex, termed the PCRCR complex, with five other proteins which are all required for RBC invasion: Cysteine Rich Protective Antigen (CyRPA), RH5 interacting protein (RIPR), *Plasmodium*

thrombospondin-related apical merozoite protein (PTRAMP), and cysteine-rich, small, secreted (CSS) (137,138). There are no RH5 orthologs in *P. vivax* but orthologs of RIPR, PTRAMP and CSS are found across all *Plasmodium* species (139). It has recently been hypothesised that these three proteins form a conserved complex across *Plasmodium* species that is involved in merozoite invasion into RBCs by binding to other, species-specific RBC-binding proteins, although these have yet to be identified for *P. vivax* (140).

To study the human vaccine-induced antibody response to *P. falciparum* RH5 in more detail, the Draper group have recently conducted a study isolating and characterising a large panel of >200 mAbs from vaccinees who received the RH5.1 vaccine (141). Single cell sorting was used to isolate RH5-specific B cells, from which recombinant mAbs were made and the biophysical and functional properties of the mAbs were then tested. This study provided an in-depth analysis of the antigenic landscape of RH5 and found that epitope specificity, antibody association rate and functional interactions between mAbs determined the potency of parasite growth inhibition. In this Thesis, a similar approach was taken to assess the leading blood-stage *P. vivax* vaccine candidate PvDBPII and greatly expand upon the small panel of anti-PvDBPII mAbs isolated in previous studies.

1.6 Thesis outline

P. vivax is an important cause of malaria in humans, but research on *P. vivax* lags behind that for *P. falciparum*. The prevalence of *P. vivax* is likely greatly underestimated in Africa, as it has become apparent that Duffy-negativity does not offer complete protection from *P. vivax* infection as previously thought. The low parasitaemia in Duffy-negative individuals with *P. vivax* infections also means that diagnosis can be missed by microscopy or rapid diagnostic tests. Malaria control measures are bringing down the burden of *P. falciparum* on the

continent, but because they are less effective against *P. vivax* compared to *P. falciparum*, the proportion of malaria caused by *P. vivax* is expected to increase. The development of a *P. vivax* vaccine would therefore greatly aid malaria elimination efforts worldwide.

The leading *P. vivax* vaccine candidate targeting the blood-stage of infection is PvDBPII. Two vaccine formulations targeting PvDBPII have been tested for efficacy by CHMI by our group in Oxford. We showed that the protein/adjuvant vaccine, given with a delayed third dose, was partially effective and able to inhibit parasite growth by around 50% during CHMI. We also showed that vaccine-induced immunity was predominantly associated with antibody-mediated responses. Whilst this was the first time that *P. vivax* blood-stage vaccines were found to show any efficacy in humans, the trials also showed that improvements in vaccine efficacy are required. The availability of these trial samples, especially from the group who showed partial efficacy, offered an opportunity to study the antibody response to vaccination in molecular detail and expand upon the small panel of mAbs isolated in previous studies.

This thesis describes the discovery and characterisation of a large panel of novel vaccine-induced human mAbs against PvDBPII. Single cell sorting was used to isolate antigen-specific B cells from vaccinees and mAbs were produced recombinantly and characterised using a variety of *in vitro* assays to determine their binding properties and functional activity.

Chapter 3 describes the isolation and production of the panel of >100 mAbs and initial characterisation of their binding properties, including determining epitope communities, binding kinetics and analysis of native antibody sequences. Chapter 4 describes the functional activity of the mAbs, in terms of their receptor binding inhibition activity and *in vitro* GIA against transgenic *P. knowlesi* parasites expressing vaccine homologous and heterologous PvDBPII variants. Chapter 5 describes the assessment of the functional interaction of mAbs

and the inhibitory activity of engineered mAbs, two approaches trialled to improve mAb potency and breadth of GIA.

The aims of the Thesis were to isolate a large panel of anti-PvDBPII mAbs from vaccinated humans, determine the epitope specificities and antibody characteristics that elicit the most potent and strain-transcending parasite growth inhibition and provide insights to guide rational design of next generation vaccines and prophylactic antibodies targeting PvDBPII.

2 Materials and Methods

Buffers, media, plasmid maps and oligomer primers are listed in the appendix.

2.1 Clinical trial samples and cell sorting

Antigen probes were produced by Martino Bardelli and Kirsty McHugh. B-cell sorting and isolation were performed by Carolyn Nielsen and Lawrence Wang.

Blood samples were collected from malaria naïve participants in a Phase 1/2a clinical trial (VAC079), which tested the protein vaccine PvDBPII with Matrix-M adjuvant (133). Volunteers received three doses of the vaccine at 0, 1 and 14 months. Cryopreserved peripheral blood mononuclear cell (PBMC) samples used for mAb isolation were taken at one week after the third vaccination. PBMC were enriched for B cells and then single cell sorted for antigen-specific memory B cells using the following panel: single, live, CD19+, CD27+CD38- or CD27-CD38- or CD27-CD38+, IgD-, IgM- and PvDBPII probe++. Single B cells were sorted into 96-well plates containing lysis buffer and stored at -80 °C.

PvDBPII-specific B cells were identified from pooled PBMC samples from 5 volunteers from the VAC079 trial using the Beacon Optofluidic System and these mAbs were produced by L. Wang.

mAb isolation and production from the VAC071 clinical trial were performed by Alexiou Vasiliki and M. Bardelli. VAC071 was a Phase 1/2a clinical trial, which tested ChAd63 and MVA viral-vectored PvDBPII vaccines (133). Cryopreserved PBMC samples taken at 1 week after the second vaccination (given at 8 weeks after the first vaccination) were used to isolate SD3-specific B cells. PBMC enriched for B cells were single cell sorted for antigen-specific memory B cells using the following panel: single, live, CD19+, IgG+, SD3 probe++.

2.2 Amplification of antibody variable regions

Reverse transcription polymerase chain reaction (RT-PCR) was performed to reverse transcribe RNA of each single sorted B cell into cDNA, followed by two nested PCRs (PCR1 and PCR2) to amplify the Vγ, Vκ and Vλ sequences of the B cell receptor. cDNA from the RT-PCR step was amplified in PCR1 using a mix of forward and reverse primers to amplify the Vγ sequences in one reaction and Vκ and Vλ sequences in a separate PCR reaction. In PCR2, nested primers were used to amplify the Vγ and Vκ and Vλ sequences from the corresponding PCR1 products. PCR2 products were run on 1% agarose gels and visualised.

PCR products from a single B cell in which both the Vγ and a corresponding Vκ or Vλ PCR2 product were successfully amplified were sent for Sanger sequencing (Eurofins).

PCR reaction mixtures and thermal cycler conditions are listed below.

Component	**Volume (µL)**
RNAse out	0.5
5X FS Buffer	5
DTT	1.25
Random Hexamer (150 ng/µL)	1
dNTP (10 mM)	2
SuperScriptIV RT enzyme	0.375

Table 2.1. RT-PCR reaction mixture

Temp	**Time**
50°C	5 min
42°C	10 min
23°C	10 min
50°C	10 min
80°C	10 min
4°C	hold

Table 2.2. RT-PCR thermal cycler settings

Components	**Vγ PCR1 Volume (µL)**	**Vκ and Vλ PCR1 Volume (µL)**
cDNA	3	3
10X PCR buffer	2.5	2.5
dNTP (10mM)	0.5	0.5
$MgCl_2$ (25µM)	0.25	0.25
carrier RNA (1mg/mL)	0.25	0.25
VH-Ext Fwd Mix (5µM each)	2.5	
VH-Ext Rev (25µM)	0.5	
VK-Ext Mix (5mM each)		2.5
VL-Ext Mix (5mM each)		2.5
IGKCrev-Ext (25mM)		0.5
IGLCrev-Ext (25mM)		0.5
HotStarTaq Plus DNA polymerase	0.25	0.25
H_2O	15.25	12.25

Table 2.3. PCR1 reaction mixture for Vγ and Vκ and Vλ

Temp	**Time**
95°C	5 min
95°C	30 s
step 2	30 s
72°C	45 s
go to step 2	50 cycles
72°C	7 min
10°C	Hold

Table 2.4. PCR1 thermal cycler settings for Vγ, Vκ and Vλ.

Step 2: Start at 67°C, go down 0.5°C for 24 cycles until reach 55°C (25 cycles for first phase), continue for another 25 cycles.

Components	**Vγ PCR2 Volume (µL)**	**Vκ and Vλ PCR2 Volume (µL)**
Ext PCR1 product	1.5	1.5
10X PCR buffer	2.5	2.5
dNTP (10mM)	0.5	0.5
$MgCl_2$ (25µM)	0.25	0.25
carrier RNA (1mg/mL)	0.25	0.25
VH-Int Fwd Mix (5mM each)	2.5	

VH-Int Rev (25mM)	0.5	
VK-Int Mix (5mM each)		2.5
VL-Int Mix (5mM each)		2.5
IGKCrev-Int (25mM)		0.5
IGLCrev-Int (25mM)		0.5
HotStarTaq Plus DNA Polymerase	0.25	0.25
H_2O	16.75	13.75

Table 2.5. PCR2 reaction mixture for Vγ and Vκ and Vλ (using HotStarTaq Plus DNA Polymerase).

Temp	**Time**
95°C	5 min
95°C	30 s
step 2	30 s
72°C	45 s
go to step 2	50 cycles
72°C	7 min
10°C	Hold

Table 2.6. PCR2 thermal cycler settings for Vγ, Vκ and Vλ.

Step 2: Start at 72°C, go down 0.5°C for 22 cycles until reach 61°C (23 cycles for first phase), continue for another 27 cycles.

2.3 Antibody gene sequence analysis

Sequencing chromatograms were visualised and checked for quality. B cells from which the Vγ and corresponding Vκ or Vλ variable regions were successfully sequenced were selected. Variable region sequences were sent to Twist Bioscience for gene synthesis, cloning into corresponding AbVec expression plasmids expressing human IgG1 Fc region, and transformation of *Escherichia coli*.

Multiple sequence alignments were carried out with Geneious Prime version 2025.1 (Biomatters) and unique VH and VL sequences were sent for cloning. Phylogenetic trees

were built in Geneious Prime using Neighbour-Joining. Antibody gene sequences were analysed using IMGT/V-Quest for gene usage, complementarity-determining region (CDR3) length and mutation count (142).

2.4 Molecular analyses and AlphaFold predictions

Molecular graphics and analyses were performed using UCSF ChimeraX, developed by the Resource for Biocomputing, Visualization, and Informatics at the University of California, San Francisco, with support from National Institutes of Health (143).

AlphaFold Server running AlphaFold3 model (144) was used to predict the structure of a complex of three protein sequences: PvDBPII and the heavy and light chain variable region of each antibody. The interface predicted template modelling (ipTM) score is a measure of the accuracy of the predicted positions of each protein in the complex. An ipTM score of ≥ 0.7 was used as the cut-off for an accurate prediction. UCSF Chimera X matchmaker tool was used to superimpose predicted AlphaFold structures onto published structures of mAbs bound to PvDBPII.

2.5 Plasmid production

LB growth media containing 100 μg/mL carbenicillin was seeded with bacterial glycerol stocks and grown at 37°C overnight in a shaking incubator. QIAGEN Plasmid Mini, Midi or Maxi kits were used to extract DNA plasmids as per manufacturer's instructions. Plasmid DNA were eluted into water and concentrations were measured using a Nanodrop spectrophotometer.

2.6 Expression of recombinant mAbs

Matched heavy and light chain plasmids were co-transfected into Expi293F cells using the ExpiFectamine 293 Transfection Kit (Thermo Fisher Scientific). Cells were incubated in a shaking incubator at 37°C, 180-225rpm and 8% CO_2 and harvested 6 days after transfection. Cell cultures were centrifuged, the supernatant was filtered through a sterile filter and purified using HiTrap Protein G, Protein A or Fibro Prism A columns (Cytiva) on an ÄKTA Pure FPLC system and eluted in glycine. Antibodies were buffer exchanged into Tris-buffered saline (TBS) or parasite culture media and concentrated using Amicon Centrifugal Filters (Millipore). Antibody concentrations were measured using a Nanodrop spectrophotometer.

2.7 Fab production

2.7.1 Subcloning into Fab expression vector

VH gene sequences were cloned into in-house Fragment antigen-binding (Fab) AbVec expression plasmid with histidine tag. IgG1 γ heavy chain expression plasmid and Fab expression plasmids were digested using AgeI-HF and SalI-HF restriction enzymes (NEB) and incubated at 37°C for 1 h.

	Vector reaction (µL)	Insert reaction (µL)
H_2O	15.5	15.5
10X rCutSmart Buffer	2	2
DNA	1 (= 2µg)	1 (= 1µg)
AgeI-HF	0.75	0.75
SalI-HF	0.75	0.75

Table 2.7. Fab digestion reactions.

For the vector reaction only, Quick CIP was added to the digestion reaction and incubated at 37°C for a further 10 min. Digestion reactions were run on 1% agarose gel and digested vector and inserts were excised and gel extracted using Qiagen QiaQuick Gel Extraction kits. Ligation reactions were carried out using Quick ligation kit (NEB) with a 3:1 to 10:1 molar ratio of insert:vector and incubated at room temperature (RT) for 5-10 min. Transformation of 5-alpha Competent *E. coli* (C2987, NEB) was carried out with 5 µL of ligation reaction per 40 µL of *E. coli*, using the following heat shock protocol: incubated on ice for 30 min, at 42°C for 30 s, on ice for 5 min. 250 µl of SOC was added and placed at 37°C for 60 min, then plated out onto ampicillin agar plates and incubate overnight at 37°C. The next day, individual colonies were picked and grown in LB media with carbenicillin overnight. DNA was then purified and sent for sequencing to confirm presence of insert.

2.7.2 Expression and purification of Fab

Matched Fab and light chain plasmids were co-transfected into Expi293F cells using the ExpiFectamine 293 Transfection Kit (Thermo Fisher Scientific) and cells were harvested 6 days after transfection. Supernatant was sterile filtered and purified using HisTrap Excel 5mL column (Cytiva) and eluted in 250mM imidazole. The eluate was then run on a Superdex 200 Increase 10/300 GL column (Cytiva) into TBS.

2.8 Engineered mAb production

Wild-type mAbs were modified by fusion of a 35-mer DARC$_{8\text{-}42}$ peptide to the C-terminus of the Fc region with a GGGG linker. The following eDB-mAbs were produced by me: eDB59, 95, 103, 144, 165, 171, 176, 178, 202 and e092096-DARC35. The remainder of the eDB-mAbs were produced by Martino Bardelli.

2.8.1 Subcloning into eDB-DARC35 expression vector

VH gene sequences were cloned into in-house eDB-DARC35 AbVec Vγ expression plasmid. The IgG1 γ heavy chain expression plasmid, for the desired insert, and eDB1-DARC35 expression plasmid, used as the vector, were digested using AgeI-HF and SalI-HF restriction enzymes (NEB). Cloning was performed using the same method as for subcloning into Fab expression vector.

2.8.2 Expression and purification of eDB mAbs

Matched eDB AbVec Vγ and light chain plasmids were co-transfected with human sulfotransferase plasmid (hTPST-2, Addgene) in a 2.5:2.5:1 ratio, into Expi293F cells using the ExpiFectamine 293 Transfection Kit (Thermo Fisher Scientific). Cells were harvested 6 days after transfection and purification was carried out as for mAb production.

2.9 Recombinant PvDBPII protein production

2.9.1 Subcloning PvDBPII allelic variants

DNA sequences of PvDBPII P, W1 and AH allelic variants, codon optimised for mammalian expression, were synthesised by GeneArt and used for cloning into in-house mono-Fc PvDBPII Bap C-tag expression vector. Digestion reactions were performed using BamHI-HF and KpnI-HF restriction enzymes (NEB) and incubated for 37°C for 1 h.

	Vector reaction (µL)	Insert reaction (µL)
H_2O	14	14.5
10X rCutSmart Buffer	2	2
DNA	2.5 (= 2µg)	2 (= 1µg)
BamHI-HF	0.75	0.75
KpnI-HF	0.75	0.75

Table 2.8. PvDBPII variants digestion reactions.

For the vector reaction Quick CIP was added to the digestion reaction. Digestion reactions were run on 1% agarose gel and digested vector and inserts were excised and gel extracted. Ligation reactions were carried out using Quick ligation kit (NEB) with a 3:1 molar ratio of insert:vector and incubated at RT for 5-10 min. Transformation of 5-alpha competent *E. coli* (C2987, NEB) was carried out using the same protocol as used for cloning of Fabs, except *E. coli* were cultured in presence of kanamycin.

2.9.2 Expression and purification of PvDBPII protein allelic variants

Plasmids with monomeric-Fc and C-tag expressing each PvDBPII variant were transfected into Expi293F cells using the ExpiFectamine 293 Transfection Kit (Thermo Fisher Scientific). Cells were harvested 4 days after transfection and supernatant was sterile filtered. Purification was carried out using a 10 mL C-tag column, eluting in 2M $MgCl_2$/20mM Tris, followed by purification using a HiLoad 16/600 Superdex 200 pg column, eluting in TBS. TEV cleavage was then carried out to cleave PvDBPII from monomeric-Fc. TEV protease was mixed with the protein in a 1:5 wt/wt protease:protein ratio and incubated overnight at 4°C on a roller mixer. The next day, the sample was centrifuged at 3000 xg for 20 min to remove aggregates and the supernatant was purified again using a C-tag column, followed by size exclusion chromatography (SEC) on a HiLoad 16/600 Superdex 200 pg column into TBS. Fractions collected from the final SEC were analysed by SDS-PAGE (**2.11**) and those judged to contain monomeric PvDBPII protein were pooled. Purified protein was measured using a Nanodrop spectrophotometer and stored at -80°C.

2.10 Recombinant nDARC-Fc protein production

2.10.1 nDARC-Fc expression vector cloning

Recombinant N-terminal DARC fused to monomeric-Fc including the hinge region was produced by adapting methods described previously (145,146). DNA encoding the first 60 N-terminal amino acids of DARC FyB allele, with a C51A mutation, was synthesised by GeneArt. In-Fusion Snap Assembly (Takara Bio) was used to clone this into in-house AbVec human IgG1 γ heavy chain vector retaining the hinge and Fc region. The γ heavy chain vector and DARC insert were linearised by PCR.

Component	**µL**
Vector/insert DNA 5ng	1
2X Phusion PCR mastermix	12.5
Vector/insert forward primer 0.5µM	1.25
Vector/insert reverse primer 0.5µM	1.25
H_2O	9

Table 2.9. PCR reaction to linearise DNA for nDARC-Fc cloning.

Temp	**Time vector reaction**	**Time insert reaction**
98°C	30 s	30 s
98°C	5 s	5 s
61 - 66.8°C	30 s	30 s
72°C	2m 30 s	3 s
	35 cycles	35 cycles
72°C	10 min	10 min
10°C	hold	hold

Table 2.10. Linearsing PCR thermal cycler settings for nDARC-Fc cloning.

PCR reactions were run on 1% agarose gel, bands were excised and gel extracted. In-Fusion cloning reaction was set up with an insert:vector ratio of 2:1, incubated for 15 min at 50°C, then placed on ice.

Reaction component	**Cloning reaction**

Purified PCR fragment (10-200ng)	13 ng (0.4µL)
Linearised vector (50–200 ng)	187 ng (6µL of 66.8°C vector)
5X In-Fusion Snap Assembly Master Mix	2 µL
H_2O	to 10 µL (1.6µL)

Table 2.11. In-Fusion cloning reaction for nDARC-Fc.

Transformation of 5-alpha competent *E. coli* (C2987, NEB) was carried out using the same protocol as used for cloning of Fabs.

2.10.2 Expression and purification of nDARC-Fc

nDARC-Fc plasmid was co-transfected with human sulfotransferase plasmid (hTPST-2, Addgene) in a 5:1 ratio. hTPST-2 was used to promote sulfation of the tyrosines in DARC, which is essential for PvDBPII binding. Transfection was carried out in Expi293F cells using the ExpiFectamine 293 Transfection Kit (Thermo Fisher Scientific) and cells were harvested 3 to 5 days after transfection. Supernatant was sterile filtered and purified using HiTrap Protein A 5mL column (Cytiva) and eluted in glycine. Analytical SEC was carried out on a Superdex 200 Increase 10/300 GL column (Cytiva).

2.11 SDS-PAGE

NuPAGE 4-12% Bis-Tris Midi gels (Invitrogen) were used for SDS-PAGE of recombinant proteins. Gels were run at 200V in 2-(N-morphplino)ethanesulfonic acid (MES) running buffer. Protein samples were boiled at 100°C for 10 min, with and without reducing agent. Samples were mixed with Laemmli loading buffer (Bio-Rad) before being loaded into the gel. Gels were stained overnight using Quick Coomassie stain, and then de-stained in water.

2.12 Enzyme-linked immunosorbent assay (ELISA)

Nunc MaxiSorp 96-well ELISA plates (Thermo Fisher) were coated with 50 µL per well of 2 µg/mL PvDBPII, denatured PvDBPII (heated to 100°C for 15 min in the presence of reducing agent dithiothreitol) or SD3 protein, diluted in phosphate buffered saline (PBS) and incubated overnight at 4°C. Plates were washed 6 times with PBS/0.05% Tween and blocked with 100 µL Starting Block T20 or Casein (Thermo Fisher) for 1 h at RT. Plates were washed. 50 µL each mAb diluted to 5 µg/mL in blocking buffer was added to each well in triplicates and incubated at RT for 2 h. Plates were washed and 50 µL alkaline phosphate-conjugated goat anti-human IgG antibody (Merck) diluted 1:1000 in blocking buffer was added to each well and incubated for 1 h at RT. Plates were washed and 100 µL per well of development buffer was added and incubated for about 15 min at RT in the dark. Optical density (OD) was measured at 405 nm using a microplate absorbance reader (BioTek).

2.13 PvDBPII-DARC binding inhibition activity assay

The ability of mAb to inhibit binding of PvDBPII to nDARC-Fc was assessed using an ELISA-based assay, which was adapted from Shakri *et al.* (145).

Nunc MaxiSorp 96-well ELISA plates (Thermo Fisher) were coated with 50 µL per well of 1 µg/mL nDARC-Fc protein, diluted in PBS and incubated overnight at 4°C. Plates were washed 6 times with PBS/0.05 % Tween and blocked with 100 µL Casein (Thermo Fisher) for 2 h at RT. 5 µg/mL mAb was mixed with 25 ng/mL PvDBPII diluted in PBS and incubated for 30 min at RT. Plates were washed and 50 µL of the pre-incubated mAb/PvDBPII mix was added to each well in triplicate and incubated at RT for 1 h. Plates were washed and 50 µL anti-PvDBPII rabbit sera diluted to 1:1000 in PBS was added for 1 h. Plates were washed and 50 µL alkaline phosphate-conjugated anti-rabbit IgG antibody

(Merck) diluted 1:2000 in TBS was added to each well and incubated for 1 h at RT. Plates were developed as for standard ELISA. Wells containing only PBS were used as blanks and these OD values were subtracted from all test values. The average OD of wells containing PvDBPII only and no mAb were used as negative controls representing no binding inhibition. Binding inhibition activity (BIA) was calculated as:

% BIA = 100% - (OD_{405} value of test mAb/OD_{405} value of negative control) x 100

Those mAbs which showed high BIA or had conflicting results were tested in 5-fold dilution series starting at 5 μg/mL.

2.14 Carterra epitope binning

High-throughput surface plasmon resonance (HT-SPR) was used to perform epitope binning of the full mAb panel on a Carterra LSA instrument by Anna Huhn. Binning was performed in a classical sandwich format using a HC30M chip (Carterra). The HC30M chip was primed with 25 mM MES 150 mM NaCl buffer and conditioned with 1 min injections of 50 mM NaOH, 1 M NaCl and 10 mM glycine (pH 2.0). The chip was then activated with a 1:1:1 mixture of 25 mM MES, 100 mM sulfo-N-hydroxysuccinimide, and 400 mM 1-ethyl-3-(3-dimethylaminopropyl) carbodiimide hydrochloride. 30 μg/mL of each mAb in 10 mM acetate (pH 5.0) was coupled to the chip surface. The chip surface was then quenched with 0.5 M ethanolamide and washed with 10 mM glycine (pH 2.0). 50 nM PvDBPII protein was injected over the chip for 4 min, followed by 30 μg/mL of the sandwiching mAb for 4 min, both diluted in Tris-buffered saline with 0.01% Tween-20 (TBST). Regeneration was performed with 10 mM glycine (pH 2.0) using three 30 s regeneration cycles followed by a stabilisation for 1 min. Data were analysed using Epitope Software (Carterra).

2.15 Carterra mAb binding kinetics

High-throughput SPR mAb binding kinetics measurements were performed on a Carterra LSA instrument using a HC30M chip by Anna Huhn. The chip was primed and conditioned as for the epitope binning experiment. mAbs at 1 μg/mL in TBST were coupled to the surface. A nine-point three-fold dilution series of PvDBPII in TBST, from 100 nM to 46 pM, was sequentially injected over the chip. Injection times for each phase were as follows: antigen injection 5 min (association phase), TBST 20 min (dissociation phase), 10 mM glycine (pH 2.0) (regeneration phase) using three 30 s injections. Kinetics Software (Carterra) was used to analyse the non-regenerative kinetics data using the Langmuir 1:1 model to calculate association rate constant (k_a), dissociation rate constant (k_d) and equilibrium dissociation constant (K_D). Data were double referenced before model fitting. Binding kinetics were not able to be calculated for mAbs that did not conform to the Langmuir 1:1 model, which was defined as residual standard deviation >7% of the calculated Rmax.

2.16 Growth inhibition activity (GIA) assays

GIA assays were performed using a transgenic *P. knowlesi* parasite line (*P. knowlesi* PvDBP^{OR}ΔβΔγ) provided by Prof Robert Moon at the London School of Hygiene and Tropical Medicine (LSHTM). In the PvDBP SalI transgenic parasite line, the *PvDBP SalI* allele transgene replaced the native *PkDBPα* gene, *PkDBPβ* was lost and *PkDBPγ* was deleted (119). Two additional PvDBPII variant parasite lines were used in GIA, which express the PvDBPII P and W1 variants. These variant strains were generated in two steps: first *PkDBPα* was replaced by *PvDBP SalI* and *PkDBPβ* was lost (but *PkDBPγ* remained); then region II of *PvDBP SalI* was replaced with the *PvDBPII P* or *W1* variant. In addition to

the transgenic *P. knowlesi* parasites, the parental *P. knowlesi* A1H1 strain was also used to test mAbs in GIA assays.

Parasites were maintained in O+ RBCs at 0.3% to 5 % parasitaemia at 2% haematocrit in parasite culture medium at 37°C and gas mixture of 5% O_2, 5% CO_2 and 90% N_2.

Cultures of *P. knowlesi* parasites were synchronised to late trophozoite/schizont stage by magnetic separation using MACS LD column (Miltenyi Biotec). Synchronised late-stage parasites were mixed with test antibodies and uninfected RBCs to a final parasitaemia of 0.75% and haematocrit of 2% in a final volume of 40 µL per well in 96-well plates. mAb were tested at a single concentration of 0.5 mg/mL. Human mAb DB9 (118) was used as a positive control antibody at 800 µg/mL, 125 µg/mL and 40 µg/mL (corresponding to EC_{70}, EC_{50} and EC_{30} of DB9 respectively) and EBL040, a human mAb against Ebola (147), was used as a negative control antibody. Plates were incubated for about 27 h, equivalent to one parasite life cycle, after which parasitaemia was measured by determining parasite lactate dehydrogenase (LDH) activity. Infected RBCs were washed and resuspended in PBS, LDH substrate was added and absorbance was measured at 650 nm when OD reached 0.4 to 0.6 in the negative control wells containing only media and infected RBCs. Wells used as blanks contained EDTA and RBCs representing uninfected RBCs and the average OD of the blank wells was subtracted from all test samples. Each mAb was tested in triplicate and median % GIA calculated. % GIA was calculated as:

% GIA = 100% - (OD_{650} of test mAb - OD_{650} uninfected RBC)/(OD_{650} infected RBC – OD_{650} uninfected RBC) x 100

The average OD of blank wells representing uninfected RBCs is subtracted from all test samples and from negative controls of infected RBCs. If the OD of the blank wells is greater than the OD of the test mAb, then the calculated % GIA for the test mAb will be >100%.

2.16.1 Dilution curves GIA

Those mAbs which had a % GIA similar or greater than DB9 control at 0.5 mg/mL were tested in dilution series starting from 2 mg/mL. Non-linear regression using a four-parameter dose response curve was fitted to % GIA against log_{10} transformed mAb concentration and used to interpolate the concentrations of the mAb which gave 30, 50 and 80% GIA (EC_{30}, EC_{50} and EC_{80}). Geometric mean of EC_{50} values were calculated for replicate runs.

2.16.2 Synergy GIA

One representative mAb with high GIA and another mAb with no or low GIA from each epitope community was selected to test in pairwise combination in the GIA assay to assess for synergistic or antagonistic activity. Each mAb was tested in isolation and pre-mixed in pairwise combination in the same assay. For testing at single concentration, growth inhibitory mAbs were tested at their EC_{50} concentration and non-inhibitory mAbs were tested at 0.25 or 0.5 mg/mL. For dilution curves the starting concentration of each mAb was 0.25 mg/mL (total starting concentration of a pair of mAbs was 0.5 mg/mL).

The expected additive GIA of the pairwise combination of mAb was calculated from the measured GIA of each mAb run alone using Bliss additivity (141,148):

$$GIA_{Bliss} = GIA_A + GIA_B - GIA_A \times GIA_B$$

2.17 Statistical analysis

GraphPad Prism 10 (GraphPad Software Inc.) was used to plot all GIA data and fit non-linear regression curves to estimate GIA EC_{50} values.

R version 4.5.1 and R Studio were used to perform other statistical analyses and plot graphs. Statistical comparisons were performed using non-parametric tests. Spearman's rank correlation was used to assess correlation between numerical variables. Kruskal-Wallis test with Dunn's multiple comparison post-test was used to compared multiple groups. Wilcoxon rank sum test was used to compare two groups. Reported p values are two-tailed with $p > 0.05$ not considered significant. The following R packages were used: circlize (149), DescTools, ggbreak (150), ggpubr (151), hablar, janitor, jsonlite (152), patchwork (153) and tidyverse (154).

3 Isolation and characterisation of binding of PvDBPII-specific mAbs

3.1 Authorship statement

Antigen probes for B cell sorting were produced by Kirsty McHugh and Martino Bardelli. B cell sorting was performed by Carolyn Nielsen and Lawrence Wang. Recombinant SD3 protein was produced by Martino Bardelli and Lloyd King. All 22 mAbs from the VAC071 study were isolated by Vasiliki Alexiou and Martino Bardelli. 21 mAbs from the VAC079 study were isolated by Lawrence Wang, Martino Bardelli and Dylan Mac Lochlainn. Epitope binning and kinetic experiments on the Carterra LSA platform were performed with supervision from Kirsty McHugh and Anna Huhn.

3.2 Introduction

Characterising the human antibody response to the leading *P. vivax* blood-stage vaccine candidate PvDBPII by isolation of mAbs could help determine the type of antibodies induced by vaccination and elucidate the mechanism(s) of action of antibodies that inhibit parasite

invasion of red bloods cells. This information could then be used in the redesign of future vaccines to direct the immune response to induce more potent antibodies. Identification of a potent mAb could also lead to its development as a therapeutic agent.

Previous studies of mAbs against PvDBP have been limited to small panels targeting region II, which were isolated from vaccinated mice and humans or from naturally-infected humans (112,116,118). PvDBPII generally induces a weak and transient antibody response following natural infection and therefore PvDBPII-specific antibodies are relatively rare in naturally-infected humans (105). In contrast, the peak PvDBPII antibody concentration induced by vaccinations in the latest clinical trials were high, increasing the chance of obtaining a large panel of PvDBPII-specific human mAbs (133).

The first panel of human vaccine-induced mAbs were isolated from the Phase 1a study of viral-vectored PvDBPII vaccines (ChAd63 and MVA vectors) conducted by the Draper group (118). This small panel of 10 mAbs included a SD3-binding mAb named DB9, that was found to inhibit parasite growth *in vitro* against a broad range of *P. vivax* isolates.

Following on from this Phase 1a study, our group completed two further Phase 1/2a trials testing PvDBPII-based vaccines for efficacy by CHMI (133). The VAC071 study (NCT04009096) tested the viral-vectored vaccines and the VAC079 study (NCT04201431) tested a recombinant PvDBPII protein/adjuvant vaccine (**Figure 3.1**). The availability of these clinical trial samples afforded a unique opportunity to greatly expand the panel of human vaccine-induced PvDBPII-specific mAbs for characterisation. The studies showed that the protein vaccine given in a delayed third dose regimen induced the highest antibody response and reduced parasite growth by about 50% during CHMI. Given that the best response was observed in this study group, samples from participants who received the delayed third dose regimen were selected for mAb isolation.

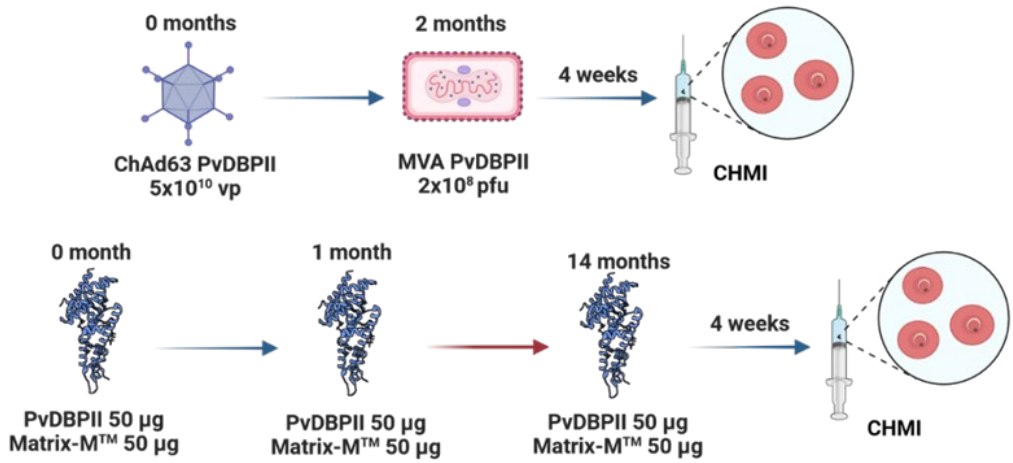

Figure 3.1 PvDBPII vaccination regimens. Viral-vectored and protein/adjuvant PvDBPII vaccination regimens from which samples were used for mAb isolation.

Single cell cloning was used as the method for mAb isolation because it is a relatively high throughput antibody discovery method and has the advantage of preserving the cognate heavy and light chain pairing (141). The single cell cloning method used in this Thesis consists of sorting antigen-specific B cells, amplifying the variable antibody genes, followed by cloning into human IgG1 vectors and production of recombinant IgG mAbs (**Figure 3.2**).

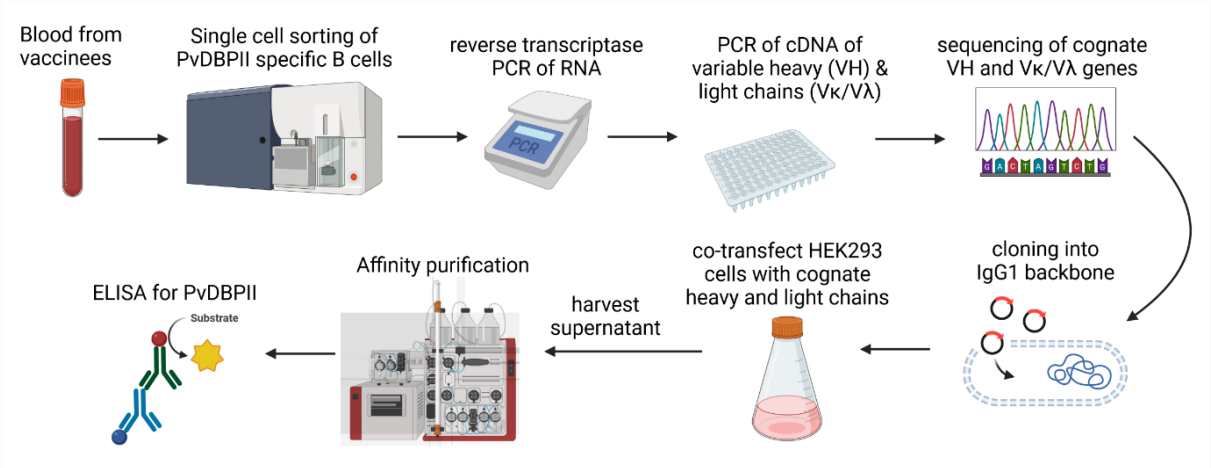

Figure 3.2 Overview of methods used for mAb isolation and production.

In addition to mAbs isolated from the VAC079 study, samples from two participants in the VAC071 study were previously used to isolate a small panel of 22 SD3-specific mAbs. The

rational for using a SD3 probe for B cell sorting was to isolate more DB9-like broadly inhibitory mAbs (118).

The first section of this Chapter describes the isolation and production of mAbs from the protein/adjuvant PvDBPII vaccine study (VAC079) that I performed. The remainder of this Thesis describes the analysis and characterisation of the full panel of PvDBPII-specific vaccine-induced human mAbs, which includes the sentinel mAbs DB1 to DB10 isolated from the Phase 1a viral-vectored PvDBPII vaccines (118) and the SD3-specific mAbs isolated from the VAC071 study. The second part of this Chapter details the antibody gene sequence analysis and binding characteristics of the full panel of 175 PvDBPII-specific mAbs.

3.3 Production of mAbs induced by PvDBPII protein/adjuvant vaccines

Blood samples from participants in the VAC079 study who received three doses of 50 μg PvDBPII protein vaccine with 50 μg Matrix-M adjuvant at 0, 1 and 14 months were used for mAb isolation. PBMC samples taken at 7 days after the third vaccination from 5 volunteers were used to sort single antigen-specific memory B cells using PvDBPII probes. Between 41 to 192 PvDBPII-specific B cells were sorted from each participant into lysis buffer and cryopreserved.

Variable region heavy chain (V_H) and light chain (V_L) gene amplification was performed from single sorted B cells using RT-PCR to amplify all RNA, followed by two nested PCR steps to amplify V_H and V_L genes separately. PCR efficiency was around 60% overall and was generally higher for V_L than for V_H genes (**Figure 3.3**).

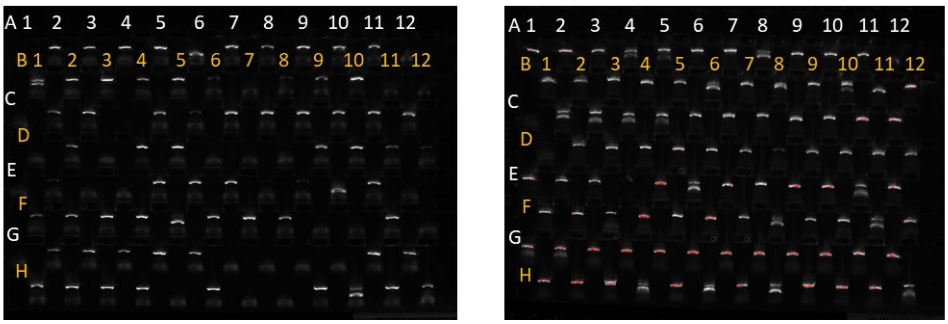

Figure 3.3 PCR amplification of V_H and V_L genes. PCR2 products from volunteer 5 shown as example. Each lane represents a PCR product from a single B cell, run on 1% agarose gel. Left panel shows V_H genes, right panel shows corresponding V_L genes. Number and letters indicate wells in 96-well plate.

PCR2 products of successfully amplified, paired V_H and V_L genes from a single B cell were sent for sequencing. Good quality sequences for both V_H and V_L genes were obtained for about half of the B cells. No sequences were recovered from one plate from participant 8, which could be due to an error in the RT-PCR step of that plate.

190 pairs of cognate V_H and V_L gene sequences were sent to Twist Bioscience for cloning into IgG1 expression plasmids. Plasmids were co-transfected into HEK293 cells, supernatant was harvested after 6 days, mAbs were affinity purified, and antigen-specificity was tested by ELISA. 121 mAbs bound PvDBPII on ELISA. The efficiency of each step of the mAb production process is summarised below (**Table 3.1**). The PCR amplification and sequencing steps were the least efficient steps.

Volunteer	No of sorted B cells	PCR: both V_H & V_L +ve	Sequencing success	Transfection success	PvDBPII +ve ELISA
3	41	8	3	3	3
5	96	69	48	48	33
6	192	124	67	66	38
7	77	54	36	36	16
8	192	123	36	35	30
Total	598	378	190	188	120
% of sorted B cells		63%	32%	31%	20%

Table 3.1 Efficiency of mAb production from sorted B cells.

3.4 Full panel of PvDBPII-specific mAbs

In addition to the 121 mAbs produced by me, vaccine-induced human PvDBPII-specific mAbs were previously produced by others in the Draper group using different methods as summarised below (**Table 3.2**). Ten sentinel mAbs were isolated from plasmablasts from the VAC051 study, which was a Phase 1a study of the ChAd63 and MVA viral vectored PvDBPII vaccines (117); 22 mAbs were previously isolated from memory B cells from 2 participants in the Phase 1/2a study (VAC071) of the same viral-vectored PvDBPII vaccines; 8 mAbs from the VAC079 study were isolated from memory B cells sorted using a Beacon Optifluids system from pooled PBMC samples from 5 participants (and it is not possible to determine which individual these mAbs were derived from). A panel of N=173 vaccine-induced PvDBPII-specific human mAbs, including the 10 sentinel mAbs DB1 to 10 (for which structures have been published for DB1 and DB9 (63,118)), were characterised in the remainder of this Thesis. I also included two published mAbs for which structural epitope information is known – 2D10 (derived from a vaccinated mouse (112)) and 092096 (derived from a naturally-infected human (116)); making N=175 in total analysed.

Vaccine	Trial	Antigen-specific B cell sort	Total no of mAb	Volunteer ID	No of mAb	Timepoint
Viral vectored	VAC051	None	10	9	9	V2+7
				10	1	V2+7
	VAC071	SD3	22	1	13	V2+14
				2	9	V2+14
Protein	VAC079	PvDBPII	141	3	3	V3+7
				4	4	V3+14
				5	33	V3+7
				6	38	V3+7, V3+14
				7	25	V3+7, V3+14
				8	30	V3+7
		PvDBPII (Beacon)		NA	8	V3+7

Table 3.2 Full panel of human vaccine-induced anti-PvDBPII mAbs. Plasmablasts were single cell sorted without antigen-specific probes on VAC051 samples. Memory B-cells were sorted using SD3 probes on VAC071 samples and using PvDBPII probes on VAC079 samples. Timepoint indicates number of days after second (V2) or third vaccination (V3).

3.5 Binding characteristics of mAb panel

3.5.1 Binding to denatured PvDBPII

Binding of the full panel of mAbs to heat-denatured PvDBPII was tested by ELISA to assess if any mAbs bound to linear epitopes. Heat-denatured PvDBPII showed reduced binding compared to native PvDBPII for all mAbs tested and no mAb bound strongly to denatured PvDBPII (**Figure 3.4**). This suggests that all mAbs bind at least largely confirmational epitopes.

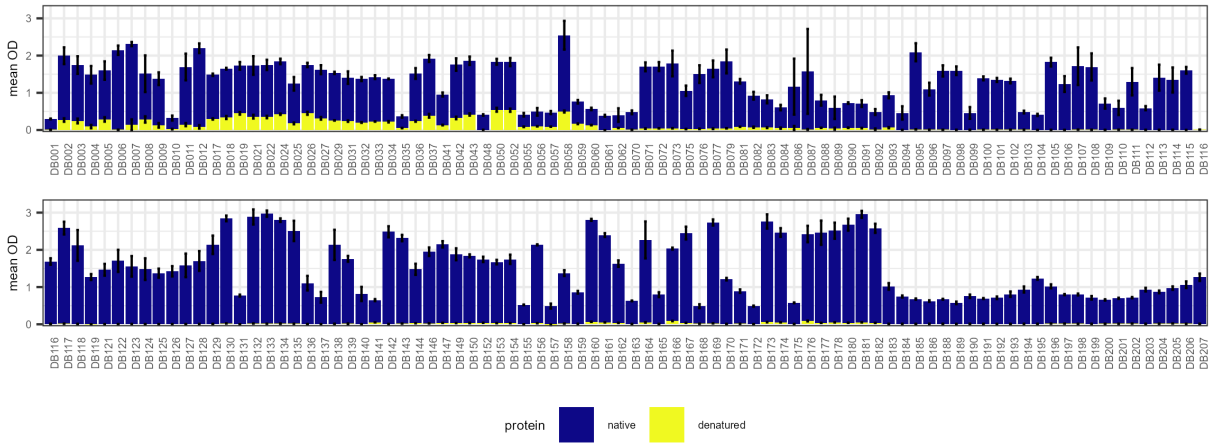

Figure 3.4 Binding of mAbs to native and denatured PvDBPII. Denatured PvDBPII was boiled in presence of reducing agent. mAbs were tested in triplicates, bars represent mean OD_{405} and error bars show standard deviation.

3.5.2 Binding to SD3

To determine the epitope binding to subdomains of PvDBPII, binding of mAbs to SD3, the subdomain that can be recombinantly expressed, was tested by ELISA. Out of 141 mAbs isolated from the VAC079 study using a PvDBPII probe for cell sorting, 94 mAbs (67%) bound SD3. All mAbs which were isolated from the VAC071 study were sorted using a SD3-probe and these mAbs bound SD3 on ELISA.

3.6 Epitope binning

To further delineate the epitopes of the full panel of anti-PvDBPII mAbs, epitope binning was performed to group the mAbs into communities that compete for binding to the antigen. This was done by testing the panel of mAbs for pairwise competitive binding using HT-SPR on a Carterra-LSA platform. In this assay each mAb is covalently arrayed on the sensor surface as the ligand. In each cycle, PvDBPII is injected, followed by injection of a second test mAb as the analyte. The surface is then regenerated to leave only the ligand mAb on the

sensor. If the second analyte mAb does not bind to the PvDBPII that is bound to the ligand mAb on the chip, then this mAb pair compete for binding.

All 175 anti-PvDBPII mAbs were tested, including the 10 sentinel human vaccine-induced mAbs, DB1-10, and the two published mAbs, 2D10 and 092096, which have known epitopes. Those mAbs which showed low binding to PvDBPII or did not self-compete when tested as either the ligand or analyte were excluded from the analysis. In total, 15/175 mAbs were excluded as both ligand and analyte so could not be included in the epitope binning analysis (community not determined [ND]). The remaining 160 mAbs were sorted into epitope communities using the Carterra Epitope software. This used the normalised response unit for each mAb pair to classify pairs as competing or not competing for binding to PvDBPII. The panel of mAbs were then sorted into a heatmap and hierarchical clustering used to plot a dendrogram which groups mAbs with similar competitive binding interactions (**Figure 3.5**). A cutoff height was set to classify mAbs into epitope communities, which can be visualised in a network plot (**Figure 3.6**). The panel of mAbs were clustered into 5 epitope communities: community 1 (N=63), community 2 (N=26), community 3 (N=27), community 4 (N=23) and community 5 (N=21). The largest epitope community was community 1 and similar numbers of mAbs were from each of the other epitope communities 2 to 5.

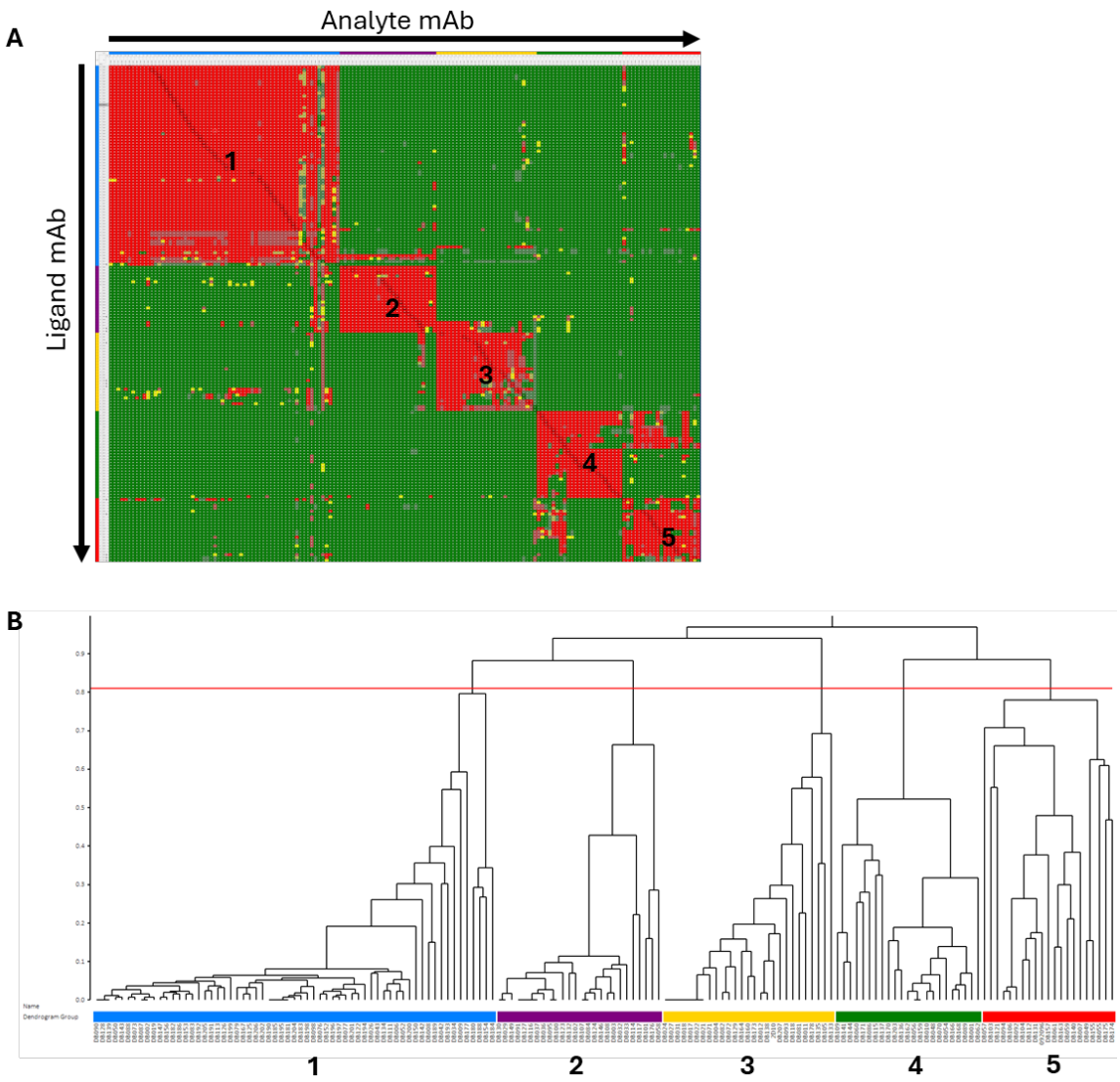

Figure 3.5 Epitope binning of anti-PvDBPII mAbs. **(A)** Epitope binning heatmap showing competition interactions between pairs of mAbs as ligands (y axis) and analytes (x axis). Red indicates competition between mAb pairs, green indicates no competition and yellow indicates intermediate weak competition. **(B)** Epitope binning dendrogram showing epitope communities of mAbs as determined by their pairwise competitive binding interactions. Epitope communities were assigned a number, which correspond to the same epitope communities in a network plot.

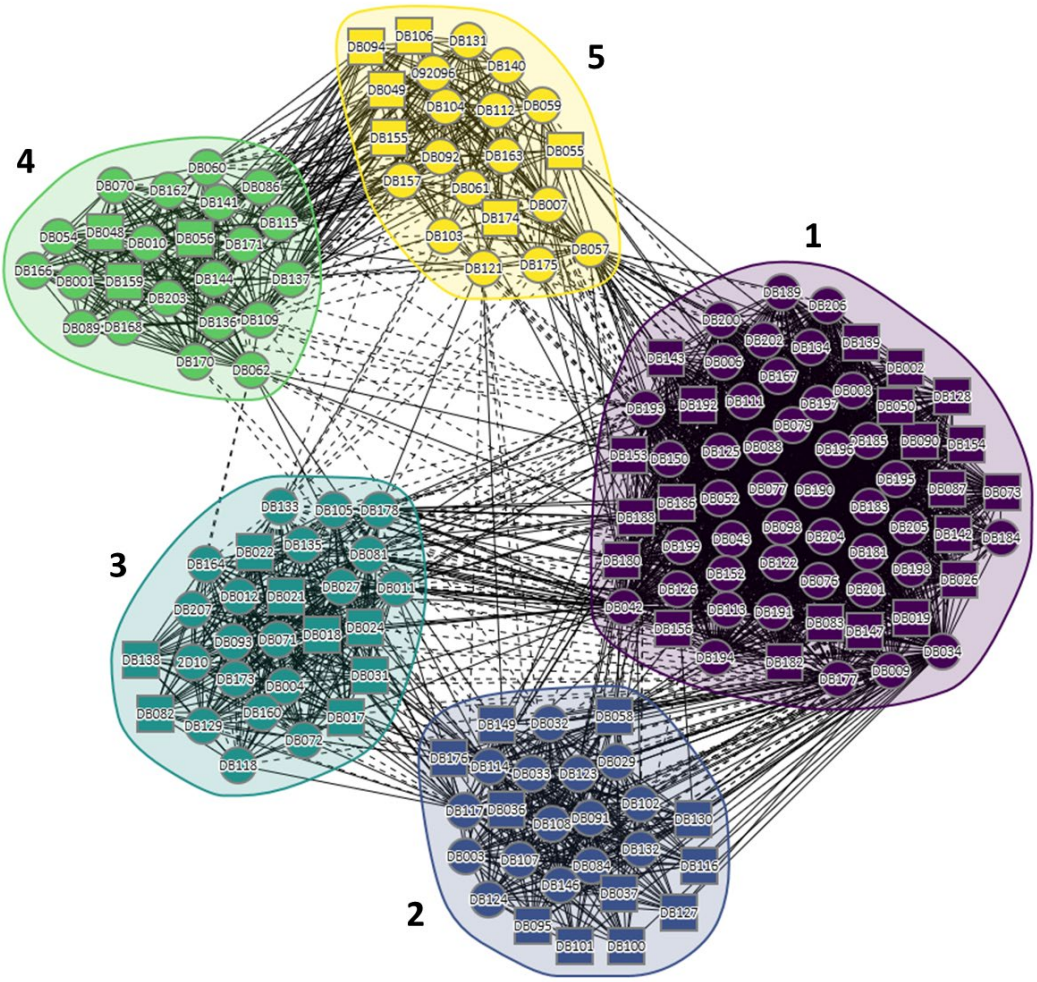

Figure 3.6 Anti-PvDBPII mAb epitope binning network plot. Network plot showing pairwise competitive binding relationship between anti-PvDBPII mAbs. Communities are defined by colour and numbers, individual mAbs are shown as nodes. Square nodes indicate mAbs that were excluded as either a ligand or an analyte. Solid lines between nodes represent bidirectional competition, dashed lines indicate unidirectional competition.

Structural epitope information is available for mAbs in the following epitope communities: DB9 in community 1 (binds in SD3); 2D10 in community 3 (binds in SD3); DB1 in community 4 (binds in SD2); and 092096 in community 5 (binds in SD2). Structural epitope information was not available for any community 2 mAbs. Results from the SD3 binding ELISA was overlaid onto the community network plot and showed that mAbs in communities 1 to 3 bind SD3 (**Figure 3.7**). From structural epitope information available for sentinel mAbs, we can conclude that mAbs in communities 4 and 5 bind in SD2.

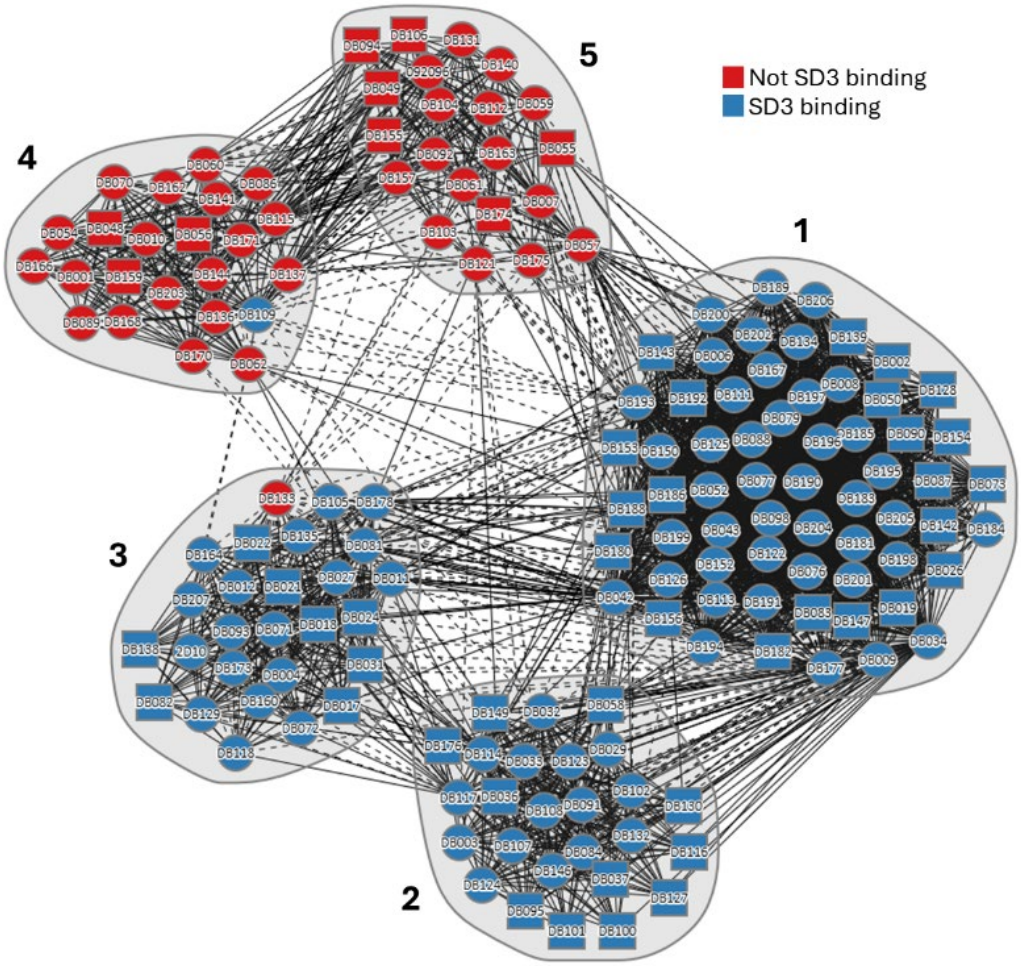

Figure 3.7 Community network overlaid with SD3 binding. Epitope communities network plot overlaid with SD3 binding activity as assessed by ELISA. Communities 1 to 3 contain SD3 binding mAbs. Communities 4 and 5 contain mAbs that bind SD2.

The number of mAbs in each epitope community which were isolated from a single volunteer varied between volunteers and in some volunteers one epitope community dominated (**Figure 3.8**). All mAbs were isolated with a SD3 antigen probe from volunteers 1 and 2, so these mAbs were in communities 1 to 3. For volunteers who received the protein vaccine, mAbs were isolated with a PvDBPII antigen probe. mAbs isolated from volunteers 5 and 6 were from all 5 epitope communities. In contrast, in volunteer 7 there was a predominance of SD2 binding mAbs and in volunteer 8 the majority of mAbs were from community 1.

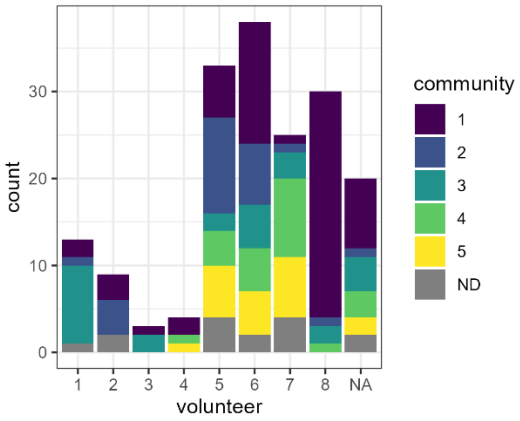

Figure 3.8 Epitope communities of mAbs by volunteer. Number of mAbs isolated from each volunteer, coloured by epitope community; ND = not determined.

3.7 Antibody gene sequence analysis

3.7.1 Antibody subclass

B cells used for mAb isolation were sorted for IgG. The original IgG subclass of B cells isolated from the VAC079 study could be determined from their BCR gene sequences. Antibodies isolated from other studies used different PCR protocol and primers, which did not amplify enough length of the constant region to allow determination of antibody subclass. Out of the 136 antibodies isolated from the VAC079 study, 124 were IgG1 (91%), 6 were IgG3, 5 were IgG2 and 1 was IgG4. Nonetheless, for this study recombinant mAbs were all made in IgG1 expression vectors.

3.7.2 Antibody variable gene sequences

The variable heavy and light chain gene sequences of each antibody were annotated using International ImMunoGeneTics information system V-quest (IMGT-VQUEST) (**Appendix 7.3**). Gene usage across the whole panel of human vaccine-induced antibodies (N=173) was diverse, with 5 heavy chain and 9 light chain gene families used. The most commonly used heavy chain gene families were IGHV1, 3 and 4, each used by about 30% of antibodies. The

most common light chain gene family was IGKV1 used by about 30% of antibodies in the panel. A total of 30 different combinations of gene family pairings were observed, with the most common pairing IGHV1/IGKV1 used by 18 out of 173 antibodies (**Figure 3.9A**).

Individual gene usage across the panel of antibodies was also diverse. The most common heavy chain gene was IGHV4-59, used by 29 antibodies and the most common light chain gene was IGKV4-1, used by 23 antibodies (**Figure 3.9B**). Both the IGHV4-59 and IGKV4-1 genes were associated with antibodies from epitope community 1 (**Figure 3.9C-D**). There were 125 different gene pairings, with 96 mAbs using unique gene combinations. The most common V gene pairing was IGHV4-59/IGKV4-1, which was used by 11 antibodies isolated from 4 different individuals (**Figure 3.9E**) and was associated with community 1. The second most common gene pairing, IGHV3-30-3/IGLV2-14, was used by 7 antibodies, which were all isolated from the same volunteer who received the viral-vectored vaccine, and all were from epitope community 3 (**Figure 3.9F**). Six of these antibodies (DB11, DB17, DB18, DB21, DB31 and DB25) had similar CDR3 sequences (≥75% similarity) suggesting these are a clonally-related group of antibodies.

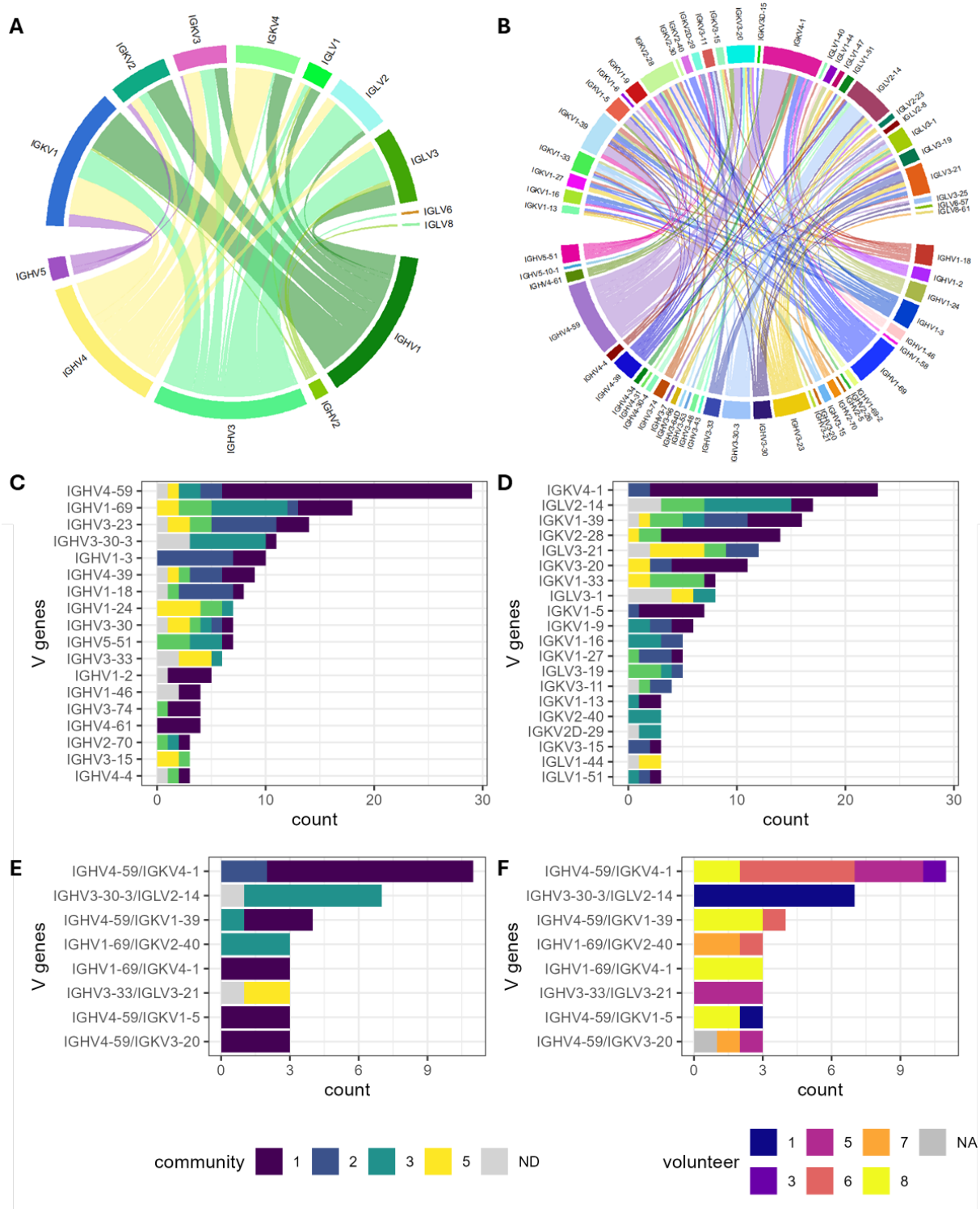

Figure 3.9 Antibody V gene usage. **(A-B)** Chord plots showing pairings of **(A)** immunoglobulin heavy chain variable (IGHV) and light chain kappa/lambda variable (IGKV/IGLV) gene families and **(B)** genes used by antibodies. Chord width is proportional to the number of antibodies that use that pairing. (C-D) Most common V genes used by 3 or more antibodies coloured by epitope community for **(C)** heavy chain V genes and **(D)** light chain V genes. **(E-F)** Gene pairings used by 3 or more antibodies, coloured by **(E)** epitope community and **(F)** by volunteer; ND = community not determined.

Somatic hypermutation (SHM) in the variable heavy chain ranged from 0.3% to 13.9%, with a median of 5%. SHM did not differ by epitope community (Kruskal-Wallis test, $p = 0.2$) (**Figure 3.10A**). SHM was significantly higher in antibodies isolated from those who received the protein vaccine with a delayed third dose compared to those that received the viral-vectored vaccine (Wilcoxon rank sum test, $p < 0.001$) (**Figure 3.10B**). The length of the CDR3 of the heavy chain ranged from 10 to 28 amino acids, with a median of 17. There were no significant differences in CDR3 length by epitope community or vaccine group (**Figure 3.10C-D**).

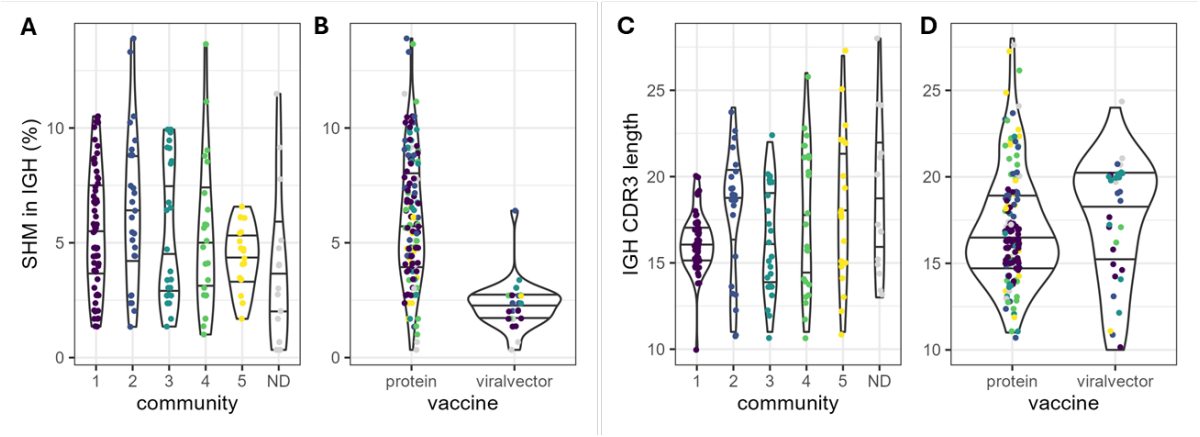

Figure 3.10 Antibody SHM and CDR3 length. Percentage SHM in IGHV gene is shown by **(A)** epitope community and **(B)** vaccine group, comparing those that received the protein/adjuvant vaccine with a delayed third dose with the viral-vectored vaccine. CDR3 length of IGHV gene in number of amino acids is shown by **(C)** epitope community and **(D)** vaccine group. Individual antibodies are shown with median and interquartile range and coloured by epitope community; ND = community not determined.

3.8 Binding to PvDBPII allelic variants

PvDBP is highly polymorphic with most polymorphisms found within PvDBPII, in particular within SD2. The PvDBPII-specific mAbs were induced by vaccination with the SalI strain sequence of PvDBPII. Given the polymorphic nature of PvDBPII, it is important to test if the vaccine-induced mAbs are strain-specific and only bind to the SalI strain antigen sequence. I therefore selected three PvDBPII variants - AH, P and W1 variants, and tested the binding of mAbs to these variants (**Figure 3.11**). The W1 variant was selected as it was the *P. vivax*

strain used for CHMI in the clinical trials and contains 10 polymorphisms including an insertion at position 430 (134). The other two variants, AH and P, were selected to cover the majority of other common polymorphisms, which are not found in the W1 variant (**Table 3.3**). These three PvDBPII variants were produced as recombinant proteins and binding of the mAbs was tested by ELISA.

Figure 3.11 PvDBPII sequence alignment. Protein sequence alignment of PvDBPII variants SalI, AH, P and W1. Polymorphisms compared to PvDBPII SalI sequence are highlighted.

AA position	261	263	288	326	330	339	340	341	345	353	359	372	374	379	392	430	458
SalI	F	R	L	K	N	D	E	K	R	S	T	N	I	L	W	-	I
W1	L	S	.	.	.	G	K	N	H	T	R	.	.	I	.	L	.
P	.	S	F	.	D	G	K	N	H	.	.	K	.	I	R	.	K
AH	.	S	.	E	.	G	.	Q	.	.	.	K	.	I	R	.	K
frequency (%)	4	26	16	25	8	77	28	35	58	6	10	42	9	56	46	1	48

Table 3.3 Table of polymorphisms in PvDBPII variants. Amino acid (AA) position within PvDBP indicated in top row. Frequency of polymorphisms found at each position, in 1358 protein sequences from global *P. vivax* isolates, are taken from (69).

Out of 173 mAbs, 124 mAbs (72%) were able to bind to all three variants (**Figure 3.12**). 15 mAbs lost binding to all three variants, 13 mAbs lost binding to W1 only and 18 mAbs lost binding to both AH and P variants. Most mAbs showed the same pattern of binding to the AH

and P variants, with only 9 mAbs showing loss of binding to only one but not the other of these two variants.

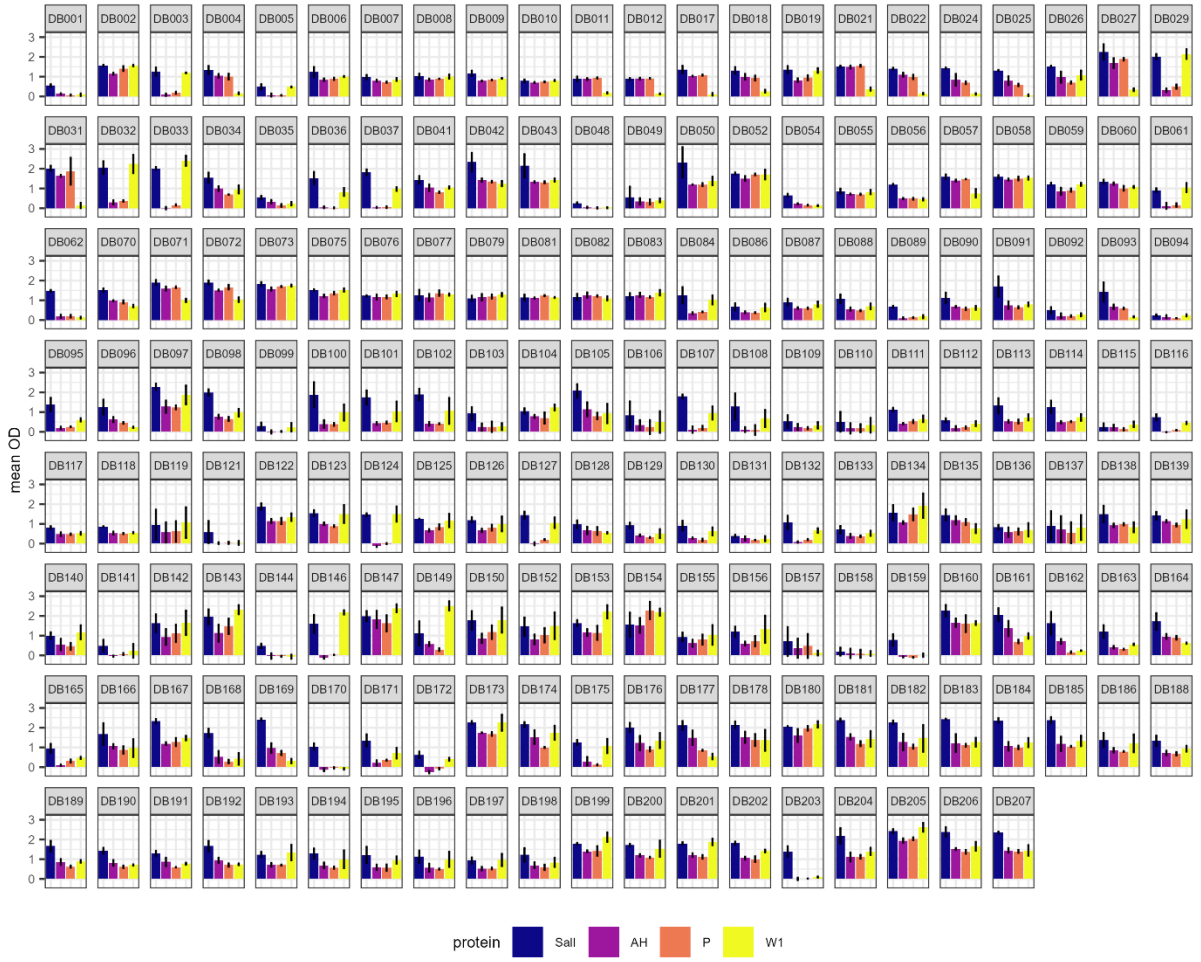

Figure 3.12 Binding of mAbs to PvDBPII variants. mAbs were tested in triplicates, bars represent mean OD_{405} and error bars show standard deviation. OD>0.3 was used to designate a mAb as binding.

3.9 Antibody binding kinetics

3.9.1 Binding to PvDBPII SalI

The binding kinetics of the panel of mAbs to PvDBPII was measured using HT-SPR on the Carterra-LSA platform (**Appendix 7.4**). Out of the 175 mAbs, binding kinetics could not be determined for 28 mAbs due to low binding of the mAbs to PvDBPII. Iso-affinity plot of the mAb association (k_a) and dissociation (k_d) rates showed a wide range of affinity constants (**Figure 3.13**). The equilibrium dissociation constant ($K_D = k_d / k_a$) ranged from

approximately 1 pM to 10 nM, with a median of 20 pM. 61 out of 147 mAbs with binding kinetics data had k_d rates slower than 1 x 10^{-5} s^{-1}, the lower limit of the experimental conditions used. The k_a rates of mAbs ranged from 1 x 10^5 to 1 x 10^7 $M^{-1}s^{-1}$.

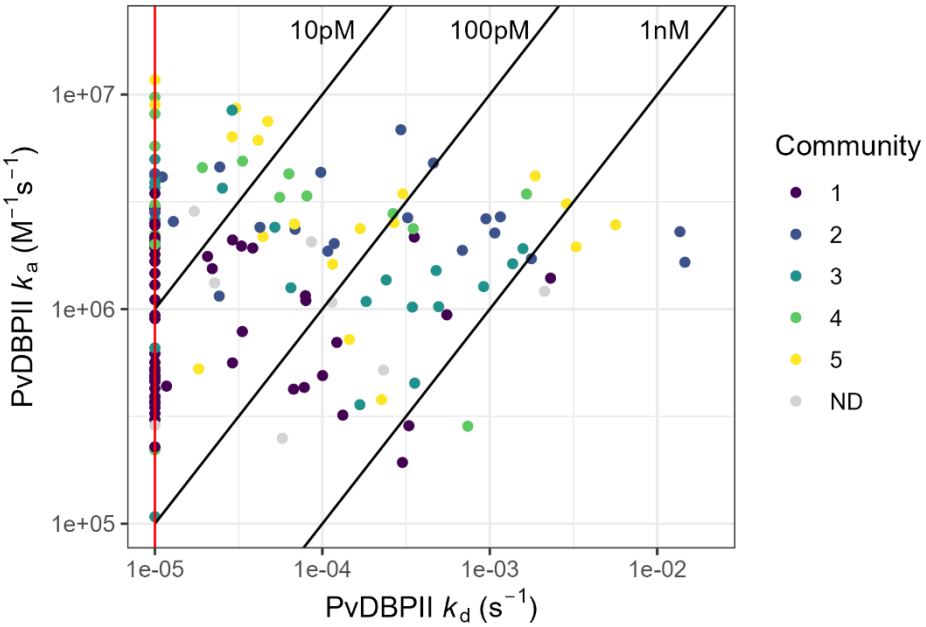

Figure 3.13 Iso-affinity plot of kinetic rate constants of mAbs to PvDBPII (SalI). Diagonal lines indicate the same equilibrium dissociation constant (K_D). Red vertical line indicates the lowest limit of k_d rate in the experimental conditions used. mAbs are coloured by epitope community; ND = not determined.

Analysis of the binding kinetics of mAbs by epitope community showed that there were no significant differences in K_D between different communities (Kruskal-Wallis test, $p = 0.2$) (**Figure 3.14**).

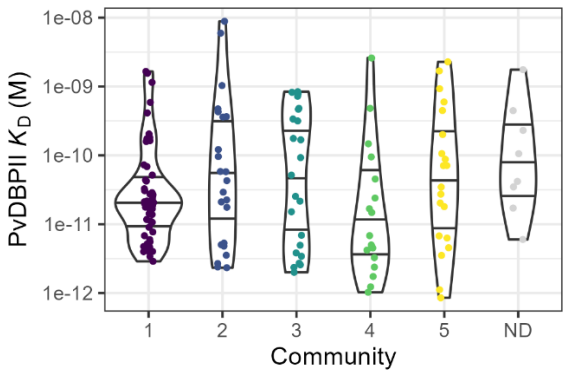

Figure 3.14 Binding affinities of mAbs to PvDBPII (SalI) by epitope community. Equilibrium dissociation constants (K_D) of mAbs by epitope community; ND = not determined. Individual antibodies are shown with median and interquartile range.

Given the differences in SHM noted between mAbs isolated from different vaccine groups, binding kinetics were also compared by vaccine group (**Figure 3.15**). This showed that mAbs from the protein vaccine delayed third dose group had significantly lower K_D constant compared to the viral-vectored vaccine group and that this difference was predominantly driven by slower k_d rate in the protein vaccinees. Correlation of SHM with kinetic parameters showed that higher SHM was associated with stronger mAb binding affinity (lower K_D constant) suggesting that the difference in binding affinities between mAbs from different vaccine groups is partly explained by differences in SHM. There was no significant correlation between CDR3 length and k_a rate, whereas shorter CDR3 length was weakly correlated with lower K_D constant and slower k_d rate.

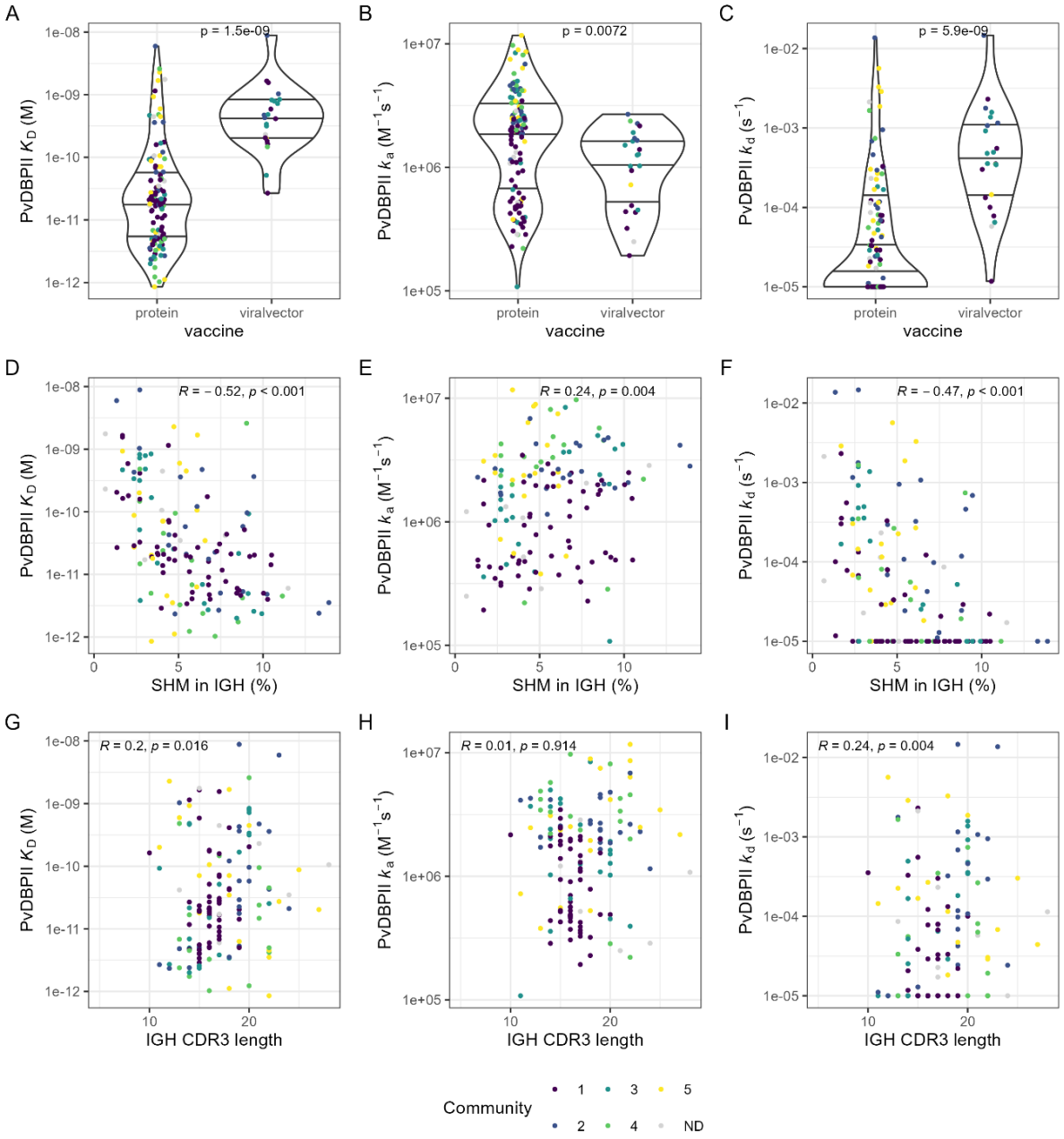

Figure 3.15 Binding affinities of mAbs to PvDBPII (SalI) by vaccine group, somatic hypermutation and CDR3 length in IGHV gene. **(A)** Equilibrium dissociation constants (K_D), **(B)** association rates (k_a) and **(C)** dissociation rates (k_d) of mAbs are shown by vaccine group, with median and interquartile range. In **(A-C)** Wilcoxon rank sum test *p* values are shown. Correlations of **(D)** K_D, **(E)** k_a and **(F)** k_d with percentage SHM of mAbs. Correlations of **(G)** K_D, **(H)** k_a and **(I)** k_d with CDR3 length in number of amino acids. In **(D-I)** Spearman's rank correlation coefficient (*R*) and *p* values are shown. MAbs are coloured by epitope community; ND = not determined.

3.9.2 Binding to PvDBPII P and W1 variants

The binding kinetics of mAbs to two PvDBPII variants W1 and P were also determined by HT-SPR to corroborate findings from the ELISA experiments (**Appendix 7.4**). Out of the

147 mAbs with binding kinetics for PvDBPII SalI, 24 mAbs lost binding to P variant only, 20 mAbs lost binding to W1 variant only and 12 mAbs did not bind to both P and W1 variants. Binding kinetics were similar between PvDBPII SalI variant and the P and W1 variant. The correlation plots show that some mAbs did not completely lose binding to the P or W1 variant but showed significantly weaker binding to the variant compared to SalI (**Figure 3.16**).

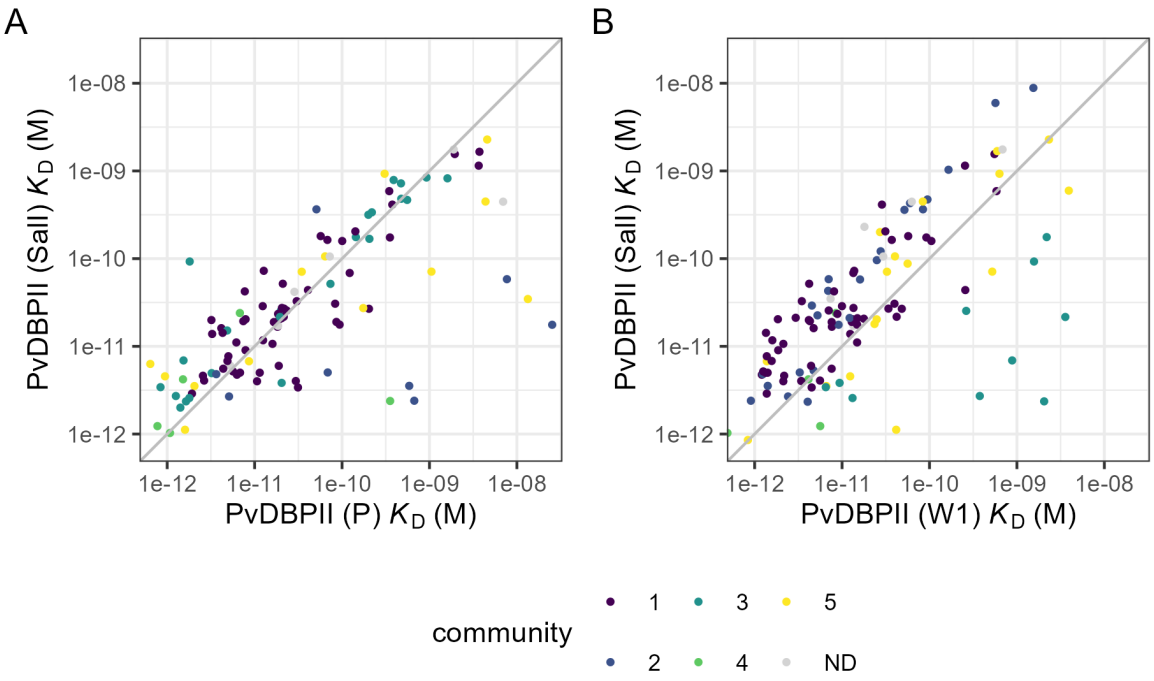

Figure 3.16 Binding affinities of mAbs to PvDBPII variants. Equilibrium dissociation constants (K_D) of mAbs binding to PvDBPII SalI compared to binding to **(A)** PvDBPII P variant and **(B)** PvDBPII W1 variant. Grey line indicates equivalent K_D.

Overall, there was good agreement between binding of mAbs to different PvDBPII variants as assessed using HT-SPR and ELISA, with 112/147 mAbs concordant in the two assays. For those mAbs that were not concordant, binding to more variants was seen on ELISA (25/147) compared to HT-SPR (6/147).

The data from the HT-SPR and ELISA experiments were combined to designate binding of mAbs to PvDBPII SalI, P and W1 variants (**Appendix 7.4**). The binding of mAbs to each

variant was then overlaid onto the epitope community network plot (**Figure 3.17**). This showed that community 1 mAbs almost all retained binding to both the P and W1 variants. Some community 2 and community 5 mAbs lost binding to the P variant, some community 3 mAbs lost binding to the W1 variant and some community 4 mAbs lost binding to both the P and W1 variants. From the location of the polymorphisms in each variant and the known epitopes of published mAbs and SD3 binding activity, we can deduce the likely epitopes of each community. Community 1 mAbs bind in the distal part of SD3 after polymorphic residue 458; community 2 bind to polymorphic residues 392 or 458; community 3 bind to polymorphic residue 430; community 4 bind to polymorphic residues 339-341 or 345; and community 5 bind to polymorphic residues 288, 330 or 372.

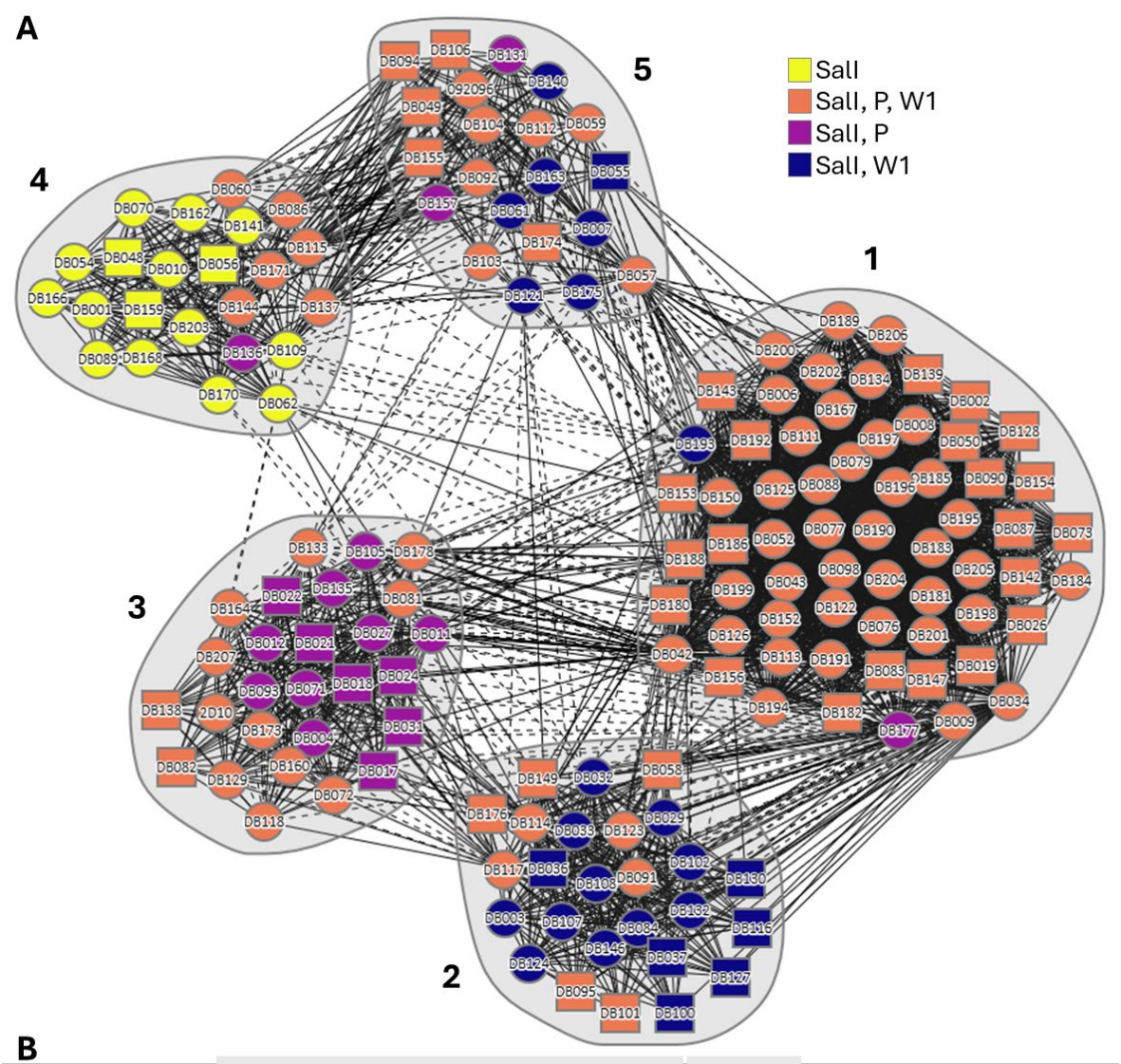

	Subdomain 2 (SD2)												SD3		
AA Position	261	263	288	330	339	340	341	345	353	359	372	379	392	430	458
PvSalI	F	R	L	N	D	E	K	R	S	T	N	L	W	-	I
PvW1	L	S	.	.	G	K	N	H	T	R	.	I	.	L	.
PvP	.	S	F	D	G	K	N	H	.	.	K	I	R	.	K

Figure 3.17 Binding of mAbs to PvDBPII variants. **(A)** Epitope community network plot overlaid with mAb binding to three PvDBPII variants SalI, P and W1 as measured by ELISA and HT-SPR. **(B)** Table shows polymorphic residues in PvDBPII W1 and P compared to SalI variant. Amino acid (AA) position in PvDBP SalI.

3.10 Predicting mAb epitopes

Structural epitope information is available for the following published mAbs from four epitope communities (**Figure 3.18**):

- community 1 – DB9 (pdb_00006r2s) (118)
- community 3 – 2D10 (pdb_00005f3j) (112)
- community 4 – DB1 (pdb_00008a44) (63)
- community 5 – 092096 (pdb_00006oao) (116)

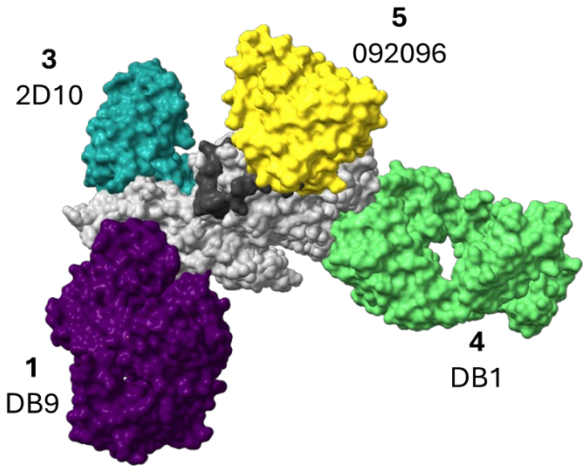

Figure 3.18 mAbs bound to PvDBPII. Composite structure showing four published antibodies DB1 (pdb_00008a44), DB9 (pdb_00006r2s), 2D10 (pdb_00005f3j) and 092096 (pdb_00006oao) bound to PvDBPII (light grey) and DARC (dark grey) (pdb_00008a44).

To try to identify the epitopes for the remaining mAbs in the panel and to corroborate potential binding sites deduced from the PvDBPII variant binding data, AlphaFold3 was used to predict the structure of PvDBPII in complex with the heavy and light chain variable regions of each mAb (155). Each prediction was run once and any predictions with low predictive accuracy where ran again until they were predicted successfully, or up to a maximum of 10 times.

63 out of 175 (36%) of Fab-PvDBPII complexes were predicted with high confidence, with an interface predicted template modeling (ipTM) score of 0.8 or higher, whilst 43 (25%) complexes fell in the grey zone with an ipTM score of between 0.6 and 0.8; finally 69 (39%) of complexes could not be predicted and had an ipTM score of below 0.6. Around half of epitope community 1 and community 2 mAbs were predicted with high confidence, whereas

a smaller proportion of mAbs from other communities were successfully predicted (**Table 3.4**).

Epitope community	No. of mAbs	No. of predictions with ipTM ≥0.8	No. of predictions with ipTM <0.6
1	63	36	10
2	26	12	10
3	27	6	12
4	23	5	14
5	21	3	13
ND	15	1	10
Totals	175	63	69

Table 3.4. Fab-PvDBPII complex predictions using AlphaFold3. Accuracy of predictions of Fab-PvDBPII complex predictions for all mAbs in panel, grouped by mAb epitope community; ND = not determined.

Accurately predicted AlphaFold3 structures were superimposed onto structures of published mAbs and the predicted binding sites of mAbs were compared to their epitope communities as determined by epitope binning. Overall, there was good agreement between predicted binding sites of structures with an ipTM score of 0.7 or higher and the experimentally determined epitope binning communities. Disagreement was only seen for three mAbs – DB81 was binned into community 3 but predicted to bind with community 4 mAbs; DB121 was binned into community 5 but predicted to bind with community 3 mAbs; and DB133 was binned into community 3 but predicted to bind with community 4 or 5 mAbs. The predicted binding sites for DB81 and DB121 do not fit with their SD3 binding ELISA so the epitope binning is more likely to be correct. DB133 did not bind SD3 on ELISA, which is more consistent with the predicted binding and suggests the epitope binning was incorrect.

Epitopes of mAbs in the predicted AlphaFold3 structures were analysed in ChimeraX and the predicted binding sites compared to sites of polymorphisms of the PvDBPII P and W1 variants (**Figure 3.19**). Epitope community 1 mAbs, like DB9, bind to the distal part of SD3 after the polymorphic residue at position 458. Epitope community 2 mAbs bind around

polymorphic residue 458 in SD3, resulting in loss of binding of some mAbs to the PvDBPII P variant. Epitope community 3 mAbs, like 2D10, bound around residue 430, where a leucine insertion in the PvDBPII W1 variant resulted in loss of binding of some mAbs. Epitope community 4 mAbs, like DB1, bind polymorphic residues 339-341 and many lost binding to both the PvDBPII P and W1 variants. Epitope community 5 mAbs, including 092096, bind around the DARC binding site. Some community 5 mAbs bind around polymorphic residue 372 and lost binding to the PvDBPII P variant. Structures were successfully predicted for three mAbs – DB119, DB158 and DB165, for which no epitope binning data were available. These mAbs were predicted by AlphaFold3 to bind overlapping epitopes in SD2 near the DARC binding site, which would fit with community 4 or 5.

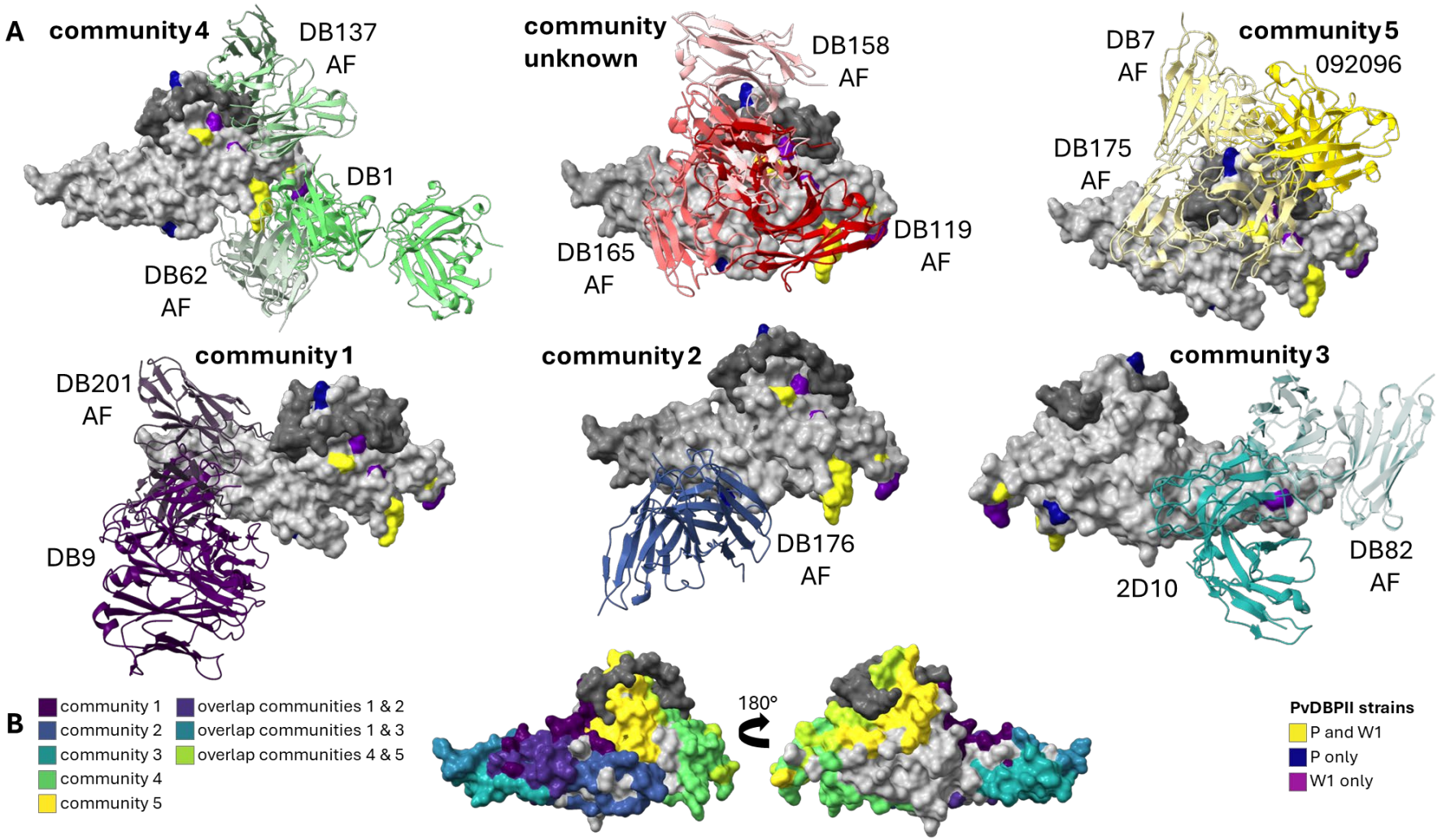

Figure 3.19 Structures of mAbs from each epitope community bound to PvDBPII. **(A)** AlphaFold3 (AF) predicted structures are aligned onto structure of PvDBPII (light grey) and DARC (dark grey) bound to published antibodies DB1 (pdb_00008a44), DB9 (pdb_00006r2s), 2D10 (pdb_00005f3j) and 092096 (pdb_00006oao). Polymorphisms in PvDBPII found in P and W1 strains compared to SalI are coloured. **(B)** Structure of PvDBPII coloured by interface residues used by mAbs from each community.

3.11 Discussion

This Chapter detailed the isolation of a large panel of human vaccine-induced mAbs against PvDBPII and the characterisation of the binding properties of these mAbs. The mAbs were isolated from two clinical trials testing different formulations of vaccines targeting PvDBPII – viral-vectored and protein/adjuvant vaccines, offering the opportunity to isolate a diverse panel of human antibody specificities.

Single-cell cloning was used for mAb isolation in this study and memory B cells were sorted with an antigen-specific probe to identify antigen-specific B cells. PvDBPII-probes were used on samples from the protein/adjuvant vaccine samples to isolate mAbs against the full vaccine construct. In contrast, mAbs isolated from the viral-vectored study were sorted with a SD3-specific probe.

The overall efficiency of isolation and production of mAbs from single-sorted B cells was around 20%. PCR amplification of variable regions and sequencing of the amplicons were the least efficient steps in mAb production. Sequencing efficiency was lowered by being unable to obtain any sequences from one 96-well plate of PCR products, probably due to incompatibility of the PCR and sequencing primers as this plate underwent RT-PCR using a different protocol.

Different antigen probes (SD3 and PvDBPII), different PCR protocols and primers and different cell sorting methods (flow cytometry and Beacon Optifluids platform) were used over time to isolate the mAbs from different vaccine groups and volunteers. Different numbers of B cells were sorted from each volunteer and there were also differences in the efficiency of mAb production from samples from different volunteers, resulting in small number of mAbs isolated from some volunteers. This makes any comparisons of characteristics of mAbs between different vaccine groups or volunteers difficult to interpret

as the mAbs isolated may not be representative of the repertoire found in each person. To study differences in antibody repertoire induced by different vaccine formulations or regimens in the future, more in-depth sequencing of antigen-specific B cells would be required to obtain a more representative pool from each comparison group. Single cell sequencing could be used to sequence the B cell receptors of antigen-specific B cells with next generation sequencing (156). This technique retains the cognate heavy and light chain pairing and in addition to greatly expanding the number of antibody sequences that can be obtained, would negate the requirement for the PCR amplification steps in the mAb isolation method used in this Thesis, which may be a source of bias.

Only IgG+ B cells were isolated in this Thesis because IgG was the predominant antigen-specific antibody subtype in the polyclonal serum (157). As recombinant mAbs were all expressed on an IgG1 backbone, isolating IgG+ B cells also meant that biologically representative clones were characterised in this study. One aim of mAb isolation in this Thesis was to identify functionally potent mAbs and these are more likely to be derived from affinity matured IgG+ memory B cells, compared to IgM+ B cells or plasma cells. As participants were malaria naïve, antigen-specific B cells were vaccine-induced and not naturally-acquired, pre-existing memory B cells. In future studies on vaccine-induced antibody repertoires, single cell sequencing could be used to study all subtypes of antibodies derived from different types of B cells and the full antibody repertoires could be compared between different vaccines and vaccination regimens.

The full panel of over 150 PvDBPII-specific mAbs were diverse and could be grouped into 5 epitope communities, with each community showing distinct binding properties. All the mAbs in the panel bind conformational epitopes in SD2 and SD3, and no mAbs appear to bind solely to SD1, which is a small subdomain. Around two-thirds of mAbs bind SD3, which indicates that SD3 may be immunodominant, as has been suggested previously (158).

However, as many mAbs in community 1, which bind in SD3, were isolated from a single volunteer, they may not be fully representative of the polyclonal response across different individuals. Determining the antibody subclasses of the mAbs in this panel showed that IgG1 was predominant, which is similar what was observed in the polyclonal serum from the trials (157). In contrast, no IgG2 was detected in the polyclonal serum, whereas in this panel 5/136 mAbs where IgG2. The proportion of κ to λ Ab light chains in the isolated mAbs were approximately 2:1, as expected of the human repertoire (159). Analysis of the antibody gene usage showed a common gene pairing (IGHV4-59/IGKV4-1) used by 11/175 antibodies, which were isolated from different individuals and were mostly from epitope community 1. This in support of functional antibodies showing 'light chain coherence', where the heavy chain determines the light chain pairing (160).

Comparison with vaccine-induced human mAbs isolated against *P. falciparum* RH5 show that the antibody binding affinities and CDR3 lengths were similar, whilst the level of SHM was slightly higher in these anti-PvDBPII mAbs (141). Similar to anti-RH5 mAbs, anti-PvDBPII mAbs isolated from the delayed booster vaccinees showed stronger binding affinities to their antigen (lower K_D). Stronger binding affinity of mAbs was predominantly driven by slower dissociation rate, rather than faster association rate. Slower dissociation rate was also strongly correlated with more SHM. The anti-PvDBPII mAbs were isolated from memory B cells, following two to three doses of vaccinations, and have likely undergone iterative cycles of affinity maturation in germinal centres, during which progressive increases in SHM result in selection of antibodies with increasing affinity to the antigen (161).

PvDBPII is highly polymorphic and the antibody response induced by the vaccines, which are both based on PvDBPII SalI variant may be strain-specific in terms of binding and/or function. It is therefore important to test the mAbs induced by the vaccines against other variant sequences of PvDBPII. In this Chapter the binding of mAbs to different variants of

PvDBPII was tested by ELISA and HT-SPR. The variants were chosen to cover the majority of common polymorphisms found in PvDBPII. The results showed that except epitope community 1, at least half of the mAbs from each of the other four epitope communities lost binding to one or both of the variants tested. This suggests that only mAbs from community 1 are potentially strain transcending (of which DB9 is the sentinel example).

Epitope binning is only able to group mAbs into communities with overlapping epitopes but does not provide any information on where the epitopes are located. Four published mAbs with known epitopes were therefore included in the epitope binning, which allowed the binding sites of 4 out of 5 epitope communities to be determined. The pattern in loss of binding of mAbs from different epitope communities to each PvDBPII variant can also be used to infer the likely epitopes of each mAb. In addition, AlphaFold3 was used to predict the binding of each mAb in the panel to PvDBPII. AlphaFold3 successfully predicted the binding of about half of the mAbs in the panel. The largest number of accurate predictions were of mAbs from epitope communities 1 and 2 but a handful of mAbs from every epitope community were successfully predicted. Comparison of the AlphaFold3 predictions to the epitope binning data showed good agreement for the majority of the mAbs. Taking the data from epitope binning, binding to PvDBPII variants, AlphaFold3 predictions and known epitopes of published mAbs, the epitope area for each community can be inferred.

Following on from determining the binding characteristics of this panel of mAbs, the next step was to test the functional activity of these mAbs, which will be covered in Chapters 4 and 5. The functional activity of mAbs from different epitope communities can then be compared and mapped to different binding sites on PvDBPII, to provide insights into possible mechanism(s) of action of mAbs in each community.

4 Functional activity of PvDBPII-specific mAbs

4.1 Authorship statement

Transgenic *Plasmodium knowlesi* parasite lines were provided by Prof Robert Moon at the LSHTM. The ELISA-based receptor binding inhibition assay was adapted from a protocol shared by Prof Chetan Chitnis, Institut Pasteur, Paris. Anti-PvDBPII rabbit serum was provided by Lloyd King. GIA assays prior to 2023, which included GIA assays testing mAbs DB1 to DB48 and one set of dilution series GIA assays for novel mAbs DB86 to DB207, were performed by Amelia Lias, Doris Quinkert and Cassandra Rigby. Otherwise, all other data were generated by me.

4.2 Introduction

Short-term culture of blood-stage *P. vivax* for *ex vivo* invasion assays enable the testing of the functional activities of mAbs. However, *P. vivax* cannot be cultured long-term *in vitro*, limiting the functional testing that can be carried out on a larger number of samples and requires access to fresh or cryopreserved *P. vivax* field isolates from infected patients. To address the need for a higher throughput *in vitro* parasite culture assay, Prof Moon's group at LSHTM have developed transgenic *Plasmodium knowlesi* parasites expressing PvDBP that have been adapted to grow in human RBCs (35).

P. knowlesi is a closely related zoonotic parasite that primarily infects macaques but can also infect humans (3). *P. knowlesi* invasion of human RBCs requires the binding of PkDBPα to DARC (51). PkDBPα is structurally similar to PvDBP, with region II of DBP sharing around 70% identity (**Figure 4.1**). In addition to PkDBPα, *P. knowlesi* has two paralogues of DBP; PkDBPβ and PkDBPγ, which share high amino acid identity to PkDBPα, but bind to a different receptor that is not found on human RBCs (53). The parental *P. knowlesi* A1H1

(PkA1H1) strain has been adapted to long-term culture in human RBCs and therefore allow *in vitro* testing of a large number of mAbs for functional activity using the GIA assay methodology (35,162). In the transgenic *P. knowlesi* parasites developed from the PkA1H1 parental strain, the *PkDBPα* gene was replaced by *PvDBP SalI* variant, *PkDBPβ* was lost and *PkDBPγ* was deleted (119). The resultant transgenic *P. knowlesi* parasites are therefore reliant on the PvDBP protein for invasion of human RBCs. In addition to the transgenic *P. knowlesi* expressing the vaccine homologous PvDBPII SalI variant, a number of transgenic *P. knowlesi* parasite lines expressing different variants of PvDBPII were made. These variant strains were generated in two steps: first *PkDBPα* was replaced by *PvDBP SalI* and *PkDBPβ* was lost (but *PkDBPγ* remained); then region II of *PvDBP SalI* was replaced with region II of a different *PvDBP* variant. These PvDBPII variant parasite lines enable the testing of the panel of mAbs against polymorphic PvDBPII variants, to determine the breadth of *in vitro* inhibitory activity.

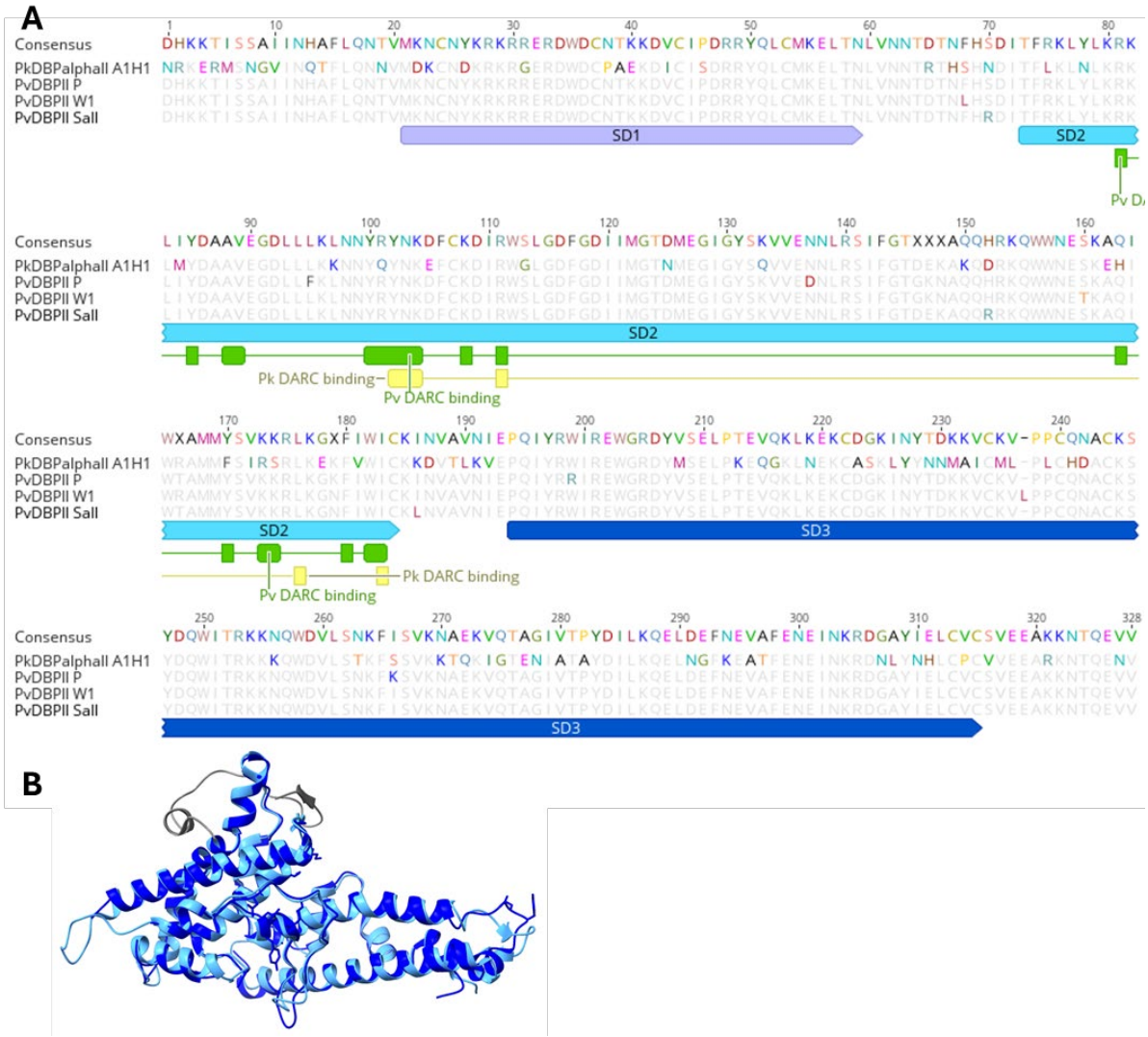

Figure 4.1 Comparison of region II of PvDBP and PkDBPα. **(A)** Protein sequence alignment of PkDBPαII A1H1 strain and PvDBPII SalI, P and W1 strains. Variant residues are coloured. Annotations showing subdomains 1-3 (SD1-3), PvDBP DARC binding site in green (from (63)) and PkDBPα DARC binding site in yellow (from (132)). **(B)** Structure of PvDBPII in light blue and DARC in grey (pdb_00008a44), superimposed onto the structure of PkDBPαII (pdb_00005x6n) in dark blue.

The *in vitro* GIA assay is well established for blood-stage *P. falciparum* and has more recently been adapted for use with *P. knowlesi* (162). In the assay, synchronised late blood-stage parasites are grown in the presence of test samples for one parasite life cycle and parasite growth is then quantified by measuring parasite LDH activity, which correlates with parasite biomass. The standard GIA assay does not include any immune cells or complement and therefore does not measure any Fc receptor mediated function (except for steric

hindrance). The *in vitro* GIA assay has been shown to correlate with *in vivo* parasite growth inhibition in *P. falciparum* $MSP1_{42}$ and RH5 vaccine studies in *Aotus* monkeys (163,164) and in a *P. knowlesi* apical membrane antigen (AMA1) vaccine study in rhesus macaques (165). Both *Aotus* studies reported that over a threshold of 60% *in vitro* GIA, the animals were protected from *P. falciparum* blood-stage malaria challenge. The transgenic *P. knowlesi* parasites have also now been used to measure *in vitro* GIA of total IgG purified from serum samples from the PvDBPII vaccine studies, from which this panel of mAbs were derived; again GIA was found to correlate with the degree of *in vivo P. vivax* parasite growth inhibition following blood-stage CHMI with PvW1 parasites (133). Together, these data indicate that the transgenic *P. knowlesi* GIA assay is a valuable *in vitro* assay for assessing the function of anti-PvDBP antibodies.

In this Chapter, the functional activity of the full anti-PvDBPII mAb panel was assessed. The ability of mAbs to inhibit DARC binding was first determined using an ELISA-based recombinant protein assay and by HT-SPR. Thereafter, the ability of mAbs to inhibit parasite growth was assessed using the GIA assay against transgenic *P. knowlesi* expressing the vaccine homologous PvDBP SalI sequence. This was followed by testing mAbs for GIA against transgenic *P. knowlesi* expressing two different vaccine heterologous PvDBPII sequences – the PvDBPII P and W1 variants. These two PvDBPII variant sequences were previously tested for binding to the panel of mAbs (**Chapters 3.8, 3.9**) and using the same variant sequences here allows comparison of GIA with the binding data. Lastly the strain-transcending mAbs were also tested against wild-type *P. knowlesi* A1H1 strain to assess for potential species-transcending GIA.

4.3 Receptor binding inhibition

Assays have been previously developed to measure the ability of antibodies to inhibit PvDBPII binding to its receptor DARC. One established assay is a sandwich ELISA-based assay and uses recombinant PvDBPII and sulfated $DARC_{1-60}$ ectodomain fused to Fc region (DARC-Fc) (145). The same recombinant PvDBPII and DARC-Fc were also used to test receptor binding inhibition activity (BIA) here using HT-SPR. The two different methods are summarised below (**Figure 4.2**). In the ELISA-based assay, an excess of the test mAb was pre-incubated with PvDBPII and then added to DARC-Fc coated on the ELISA plate. If the mAb did not inhibit DARC binding, then the PvDBPII-mAb complex could bind to DARC-Fc. The bound PvDBPII was then detected by polyclonal anti-PvDBPII rabbit sera, followed by an ALP-conjugated anti-rabbit secondary Ab; so a positive signal indicated that the mAb did not inhibit DARC binding. In the HT-SPR experiment, the mAb binning experiment set-up was used, whereby the mAb being tested was coupled to the SPR surface, then PvDBPII was injected, followed by DARC-Fc; if binding of DARC-Fc to the PvDBPII-mAb complex was seen on SPR, then this indicated that the mAb did not inhibit DARC binding.

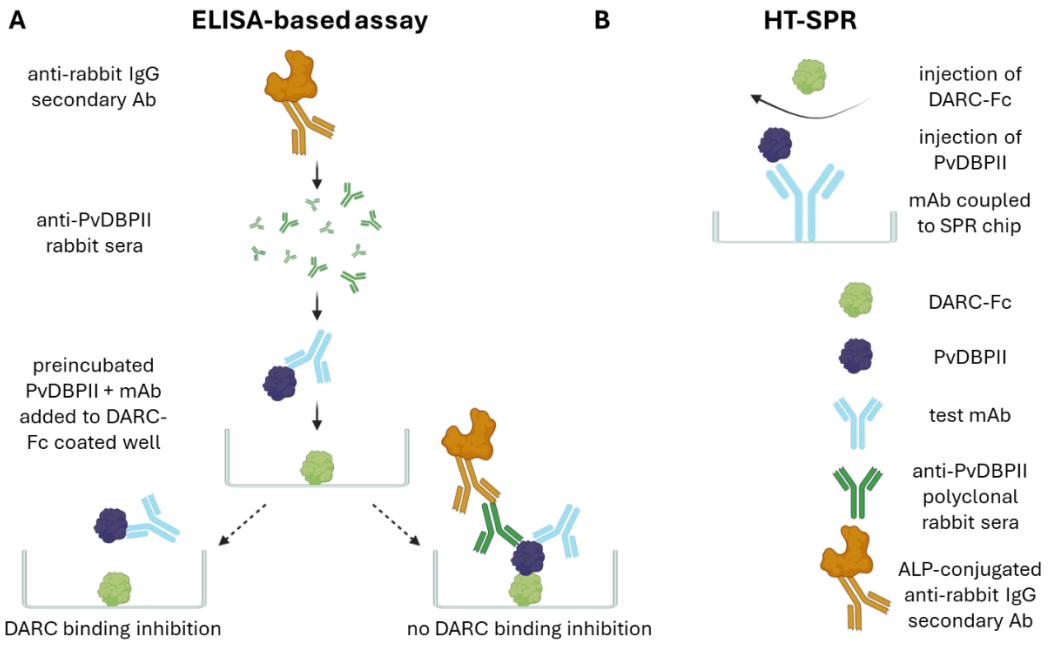

Figure 4.2 PvDBPII-DARC-Fc binding inhibition assays. Comparison of sandwich ELISA-based assay and HT-SPR to test mAbs for their ability to inhibit PvDBPII-DARC binding.

Most mAbs showed low binding inhibition in the ELISA-based assay, with the peak distribution of binding inhibition falling between 0-30% inhibition, which likely represents mAbs with no binding inhibition activity. A threshold above this of ≥40% binding inhibition was set to designate a mAb as binding inhibitory on ELISA (**Figure 4.3B**). The ELISA was then compared to the HT-SPR result to classify each mAb for PvDBPII-DARC BIA (**Appendix 7.5**). There was generally good concordance between the two methods, with 146/175 mAbs classified the same and 21/175 mAbs classified differently by ELISA compared to HT-SPR (**Figure 4.3C**). For 8 mAbs, data from HT-SPR was not available as the mAbs did not bind PvDBPII and only the ELISA results were used to classify these mAbs. All 144 mAbs that showed binding inhibition of <40% threshold on ELISA were classified as not DARC-binding inhibitors, irrespective of HT-SPR result. Out of the 31 mAbs with binding inhibition of ≥ 40% threshold on ELISA, 24 were classified as DARC-binding inhibitors, as they were in concordance with the HT-SPR result or no HT-SPR data was available. Seven mAbs which showed binding inhibition of ≥ 40% threshold on ELISA but did not prevent DARC binding to PvDBPII on HT-SPR, were assigned as 'conflicting'. The final classification of DARC-binding inhibition for each mAb was overlaid on the epitope community network plot (from **Chapter 3.6**), which showed that the majority of PvDBPII-DARC BIAbs are found in epitope community 5, with some in community 4 (**Figure 4.3A**). This is in agreement with these communities containing SD2-binding mAbs that likely bind within the receptor binding domain in PvDBPII (see **Chapter 3.6**).

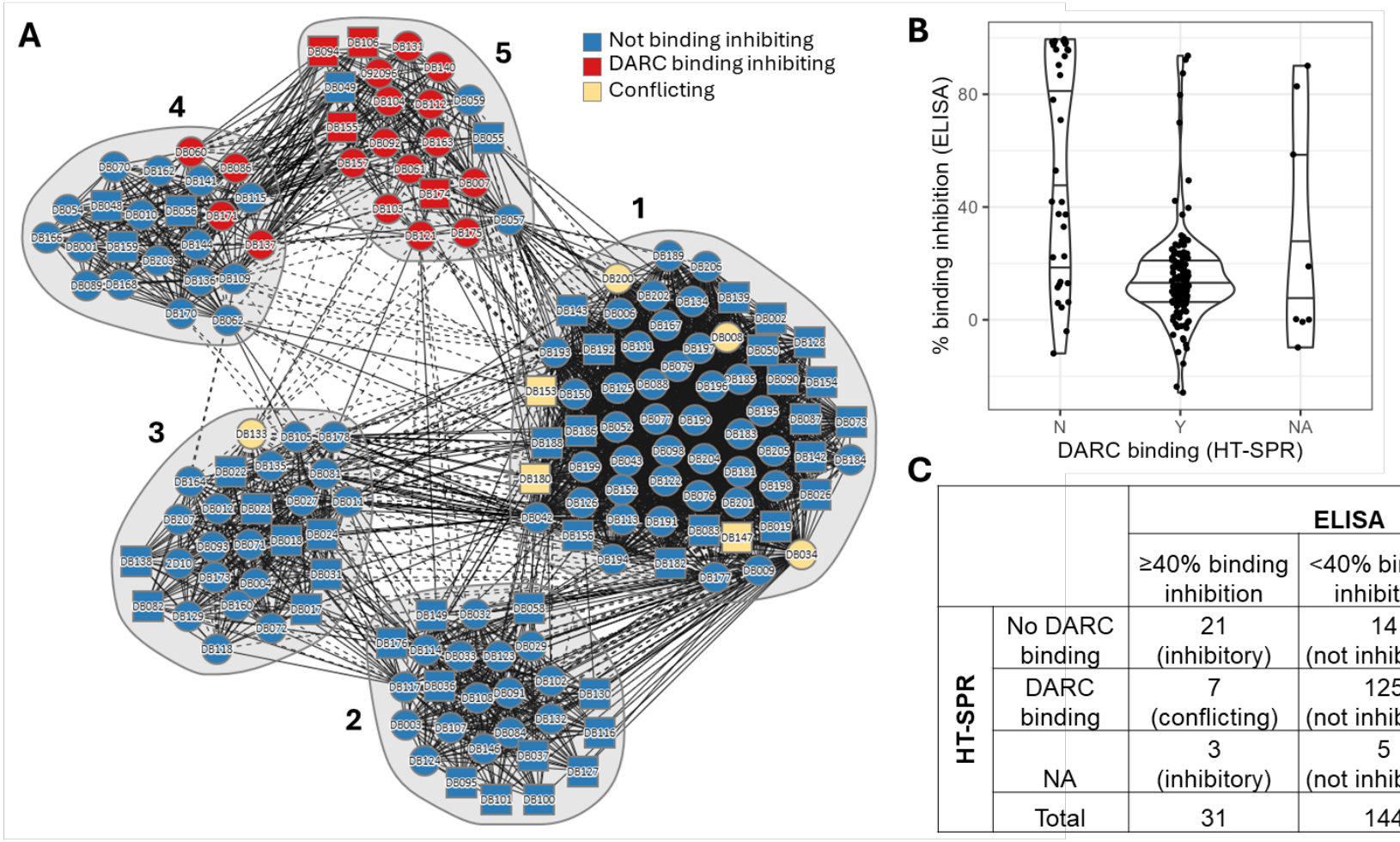

C

		ELISA		
		≥40% binding inhibition	<40% binding inhibition	Total
HT-SPR	No DARC binding	21 (inhibitory)	14 (not inhibitory)	35
	DARC binding	7 (conflicting)	125 (not inhibitory)	132
	NA	3 (inhibitory)	5 (not inhibitory)	8
	Total	31	144	175

Figure 4.3. PvDBPII-DARC binding inhibition activity of mAbs. **(A)** Epitope community network plot overlaid with PvDBPII-DARC binding inhibition activity of mAbs, as classified using both ELISA and HT-SPR result. **(B)** Comparison of binding inhibition of mAbs measured using the ELISA-based assay and HT-SPR (no DARC binding to PvDBPII indicates mAb has binding inhibition activity, DARC binding to PvDBPII indicates mAb does not have binding inhibition activity). **(C)** Table showing number of mAbs with binding inhibition activity by ELISA and HT-SPR. The final classification of PvDBPII-DARC binding inhibition activity of each group of mAbs is shown in brackets.

4.4 GIA against vaccine homologous PvDBP-expressing parasites

The GIA assay for *P. knowlesi* parasites is summarised below (**Figure 4.4**). In each assay, DB9, a broadly neutralising human vaccine-induced mAb (118), is used as a positive control and EBL040, which is an Ebola virus mAb (147), is used as a negative control. The anti-PvDBPII mAb panel was first tested against transgenic *P. knowlesi* expressing the vaccine homologous SalI strain sequence of PvDBP.

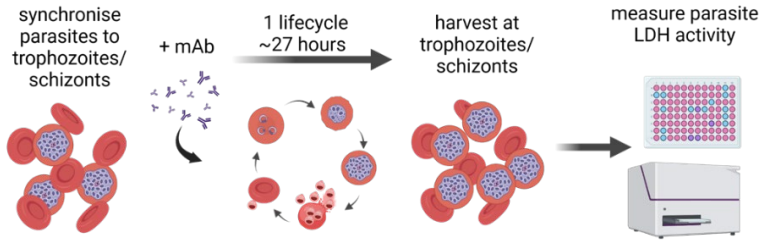

Figure 4.4. Summary of *P. knowlesi* GIA assay. Parasites are synchronised to the late trophozoite and schizont stage and incubated with test samples for the duration of one growth cycle (~27 h). The assay is then harvested and parasite growth is calculated by measuring parasite LDH activity.

The panel of mAbs were first screened at a single concentration of 0.5 mg/mL. The GIA of the test mAb was compared to the GIA of DB9 at the same concentration in the same assay to downselect mAbs to be tested further in dilution series (**Figure 4.5**). There was significant variation in GIA potency between different assay runs and so comparison of GIA potency is more reliable between samples that are run in the same assay. Initially 3 technical repeats (3 repeats within the same assay run) were conducted for each sample. However, it was observed that the variation between wells was generally much lower compared to the variation between different assay runs. In addition, a study measuring the variation in the GIA assay showed that variation from assays using RBCs from different donors was higher than the variation from conducting assays on different days with the same RBCs (166). I therefore changed to conducting a single technical replicate, but triplicate experimental

replicates for each sample using three batches of RBCs from different donors where practical, in order to improve the precision of the GIA measurements.

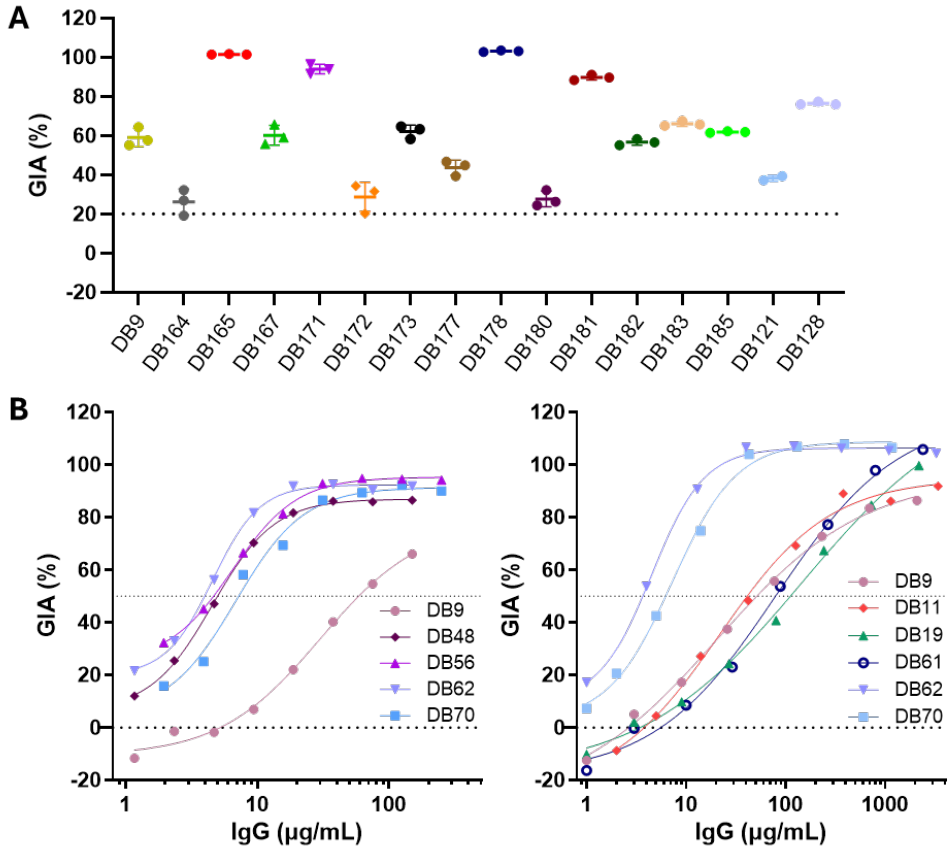

Figure 4.5. GIA against transgenic *P. knowlesi* expressing PvDBP (SalI). **(A)** Example of single concentration GIA assay. Each mAb was tested at 0.5 mg/mL and median % GIA was compared to DB9 control. GIA <20%, indicated by dotted line, was considered negative. **(B)** Example of dilution series GIA assays. A four-parameter non-linear regression curve was fitted to the dilution curves for each mAb and used to estimate GIA EC_{50} values.

Out of the 163 anti-PvDBPII mAbs in the panel only 9 mAbs (6%) were GIA negative (<20% GIA). 115 mAbs (70%) had a GIA% at 0.5 mg/mL that was similar to, or better than DB9 control, which varied between 40-60% GIA in different assays. These 115 mAbs were then tested in dilution series. A four-parameter non-linear regression model was fitted to log-transformed mAb concentration to estimate GIA EC_{30}, EC_{50} and EC_{80} values (**Figure 4.6**, **Appendix 7.6**). The dilution series were repeated in experimental replicates for the most potent mAbs, with at least three separate assays conducted for the 27 most potent mAbs in the panel.

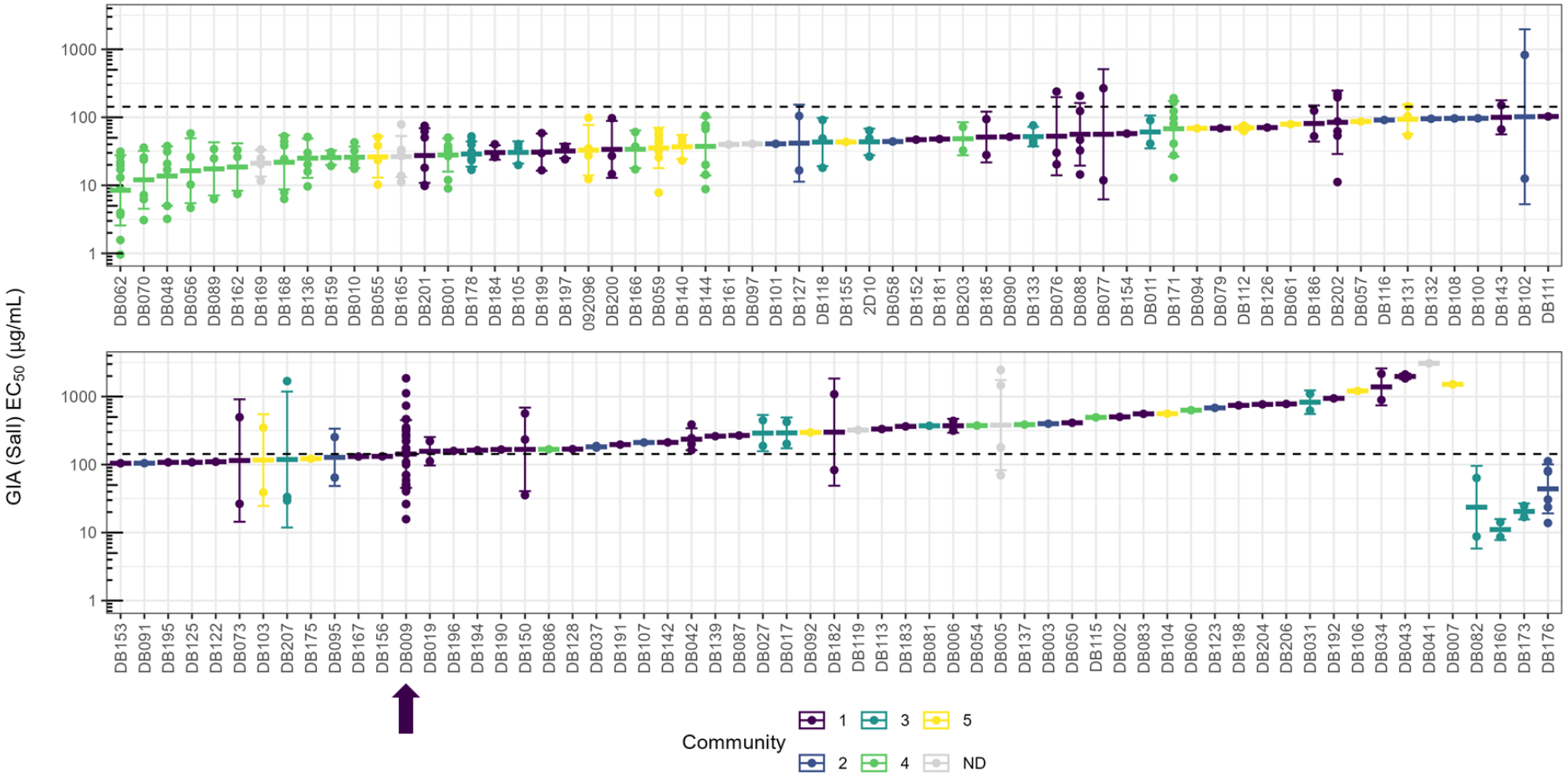

Figure 4.6. GIA potency of mAbs. The concentration of mAb required to achieve 50% GIA (GIA EC_{50}) is shown for each mAb tested in dilution series. Geometric means of biological replicates are shown with error bars indicating 1 standard deviation. mAbs are ordered by potency and coloured by epitope community; ND = community not determined. Five mAbs did not reach 50% GIA in all assays and are shown to the right of the panel. Arrow indicates DB9 control and dashed line indicates GIA EC_{50} of DB9 (143 µg/mL [95% CI 94 to 216]).

4.4.1 GIA by epitope community and binding characteristics

The most potent mAb in the panel was DB62 with a geometric mean GIA EC_{50} of 8 μg/mL (95% CI 4 to 19); this was about 18-fold more potent than DB9 (geometric mean GIA EC_{50} 143 μg/mL [95% CI 94 to 216]) (**Figure 4.6**). DB62 was consistently the most potent mAb out of any mAbs tested in the same assay. When comparing GIA potency across epitope communities, all epitope communities contained mAbs that were GIA positive (**Figure 4.7**). The top 10 most potent mAbs were found in epitope community 4, which bind SD2, and mAbs from epitope community 4 were on average more potent than mAbs from epitope communities 1 to 3, which bind SD3 (Kruskal-Wallis test with Dunn's multiple comparison, $p < 0.02$ for each pairwise comparison). There was no significant difference when comparing mAb potency by DARC binding inhibition activity, and the most potent mAbs in the panel from community 4 were not DARC binding inhibitors. SD2 binding mAbs were more potent than SD3 binding mAbs; this difference was mostly driven by the highly potent mAbs in community 4.

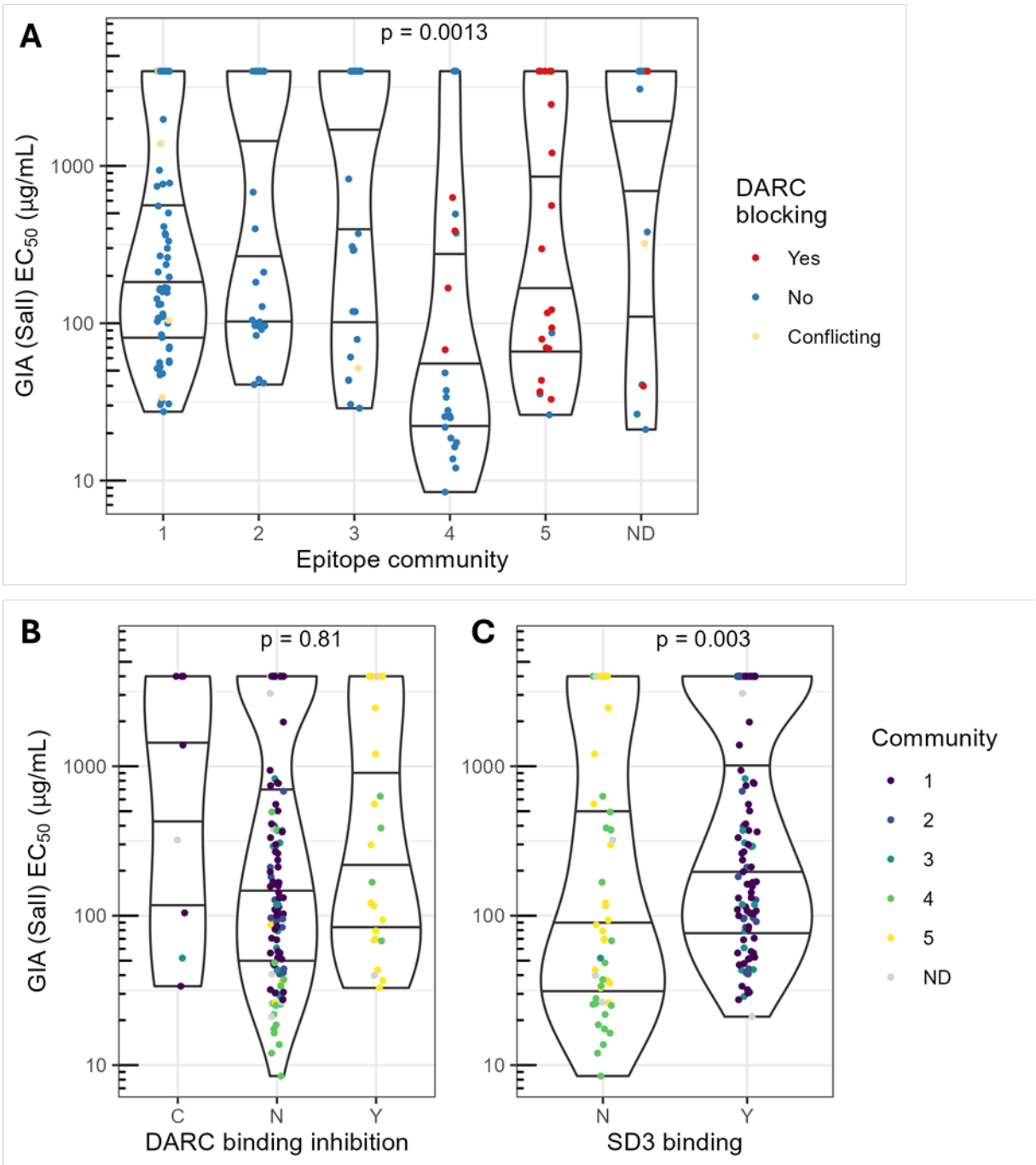

Figure 4.7. Comparison of GIA potency across groups. Geometric mean of GIA EC_{50} is shown for each mAb, with group median and quartiles. MAbs which did not reach 50% GIA at 2 mg/mL were assigned an EC_{50} of 4 mg/mL for analysis. P values of comparisons between multiple groups were calculated by Kruskal-Wallis test and between two groups by Wilcoxon rank sum test. MAbs are grouped by **(A)** epitope community and coloured by DARC binding inhibition activity as determined by ELISA and HT-SPR; **(B)** DARC-binding inhibition; **(C)** SD3 binding. In **(B-C)** mAbs are coloured by epitope community; ND = community not determined. C = conflicting, N = No, Y = Yes.

4.4.2 Correlation of GIA to mAb binding kinetics

To investigate other factors that might affect GIA potency, mAb binding kinetics were correlated with GIA EC_{50} (**Figure 4.8**). Faster antibody association (k_a) rate and smaller equilibrium dissociation constant (K_D) were correlated with higher GIA potency, whereas no correlation was seen between GIA EC_{50} and antibody dissociation (k_d) rate.

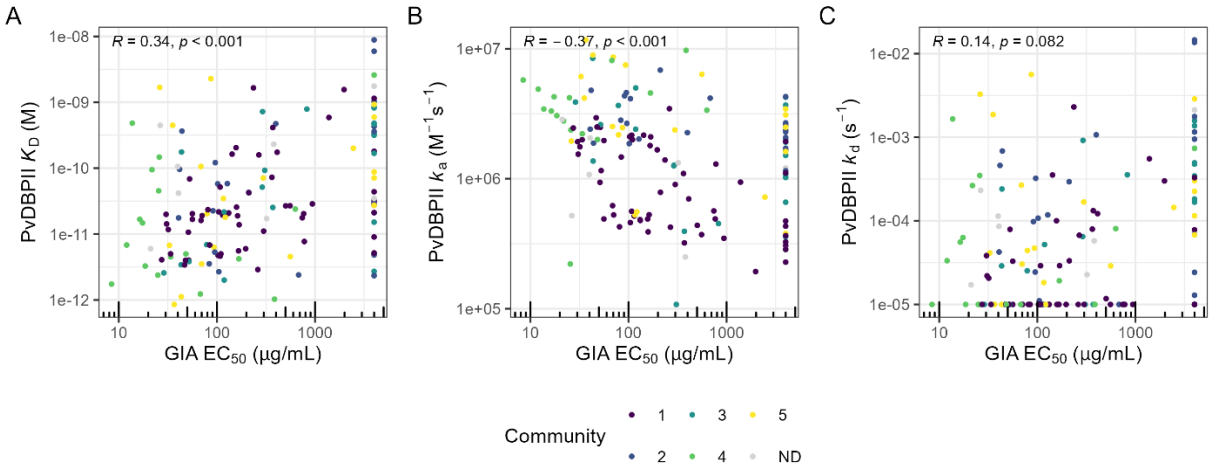

Figure 4.8. Correlation of binding kinetics to GIA potency. GIA EC_{50} was correlated with mAb **(A)** K_D, **(B)** k_a and **(C)** k_d. Spearman's rank correlation coefficient (R) and p values are shown. GIA negative mAbs were assigned a GIA EC_{50} of 4 mg/mL. mAbs are coloured by epitope community; ND = community not determined.

4.4.3 Correlation of GIA to Ab gene sequences

GIA potency was also assessed by antibody gene sequences. Lower GIA EC_{50} was correlated with higher antibody V gene somatic hypermutation (SHM) (**Figure 4.9**), which was correlated with stronger binding affinities (see **Chapter 3.9**). GIA EC_{50} was also analysed by V gene usage to assess if there were any specific heavy and light chain V gene combinations with high GIA potency, as was found in an analysis of *P. falciparum* RH5-specific mAbs (141). Analysis of GIA EC_{50} of PvDBPII-specific mAbs which use the same V gene combinations did not identify any highly potent gene pairings.

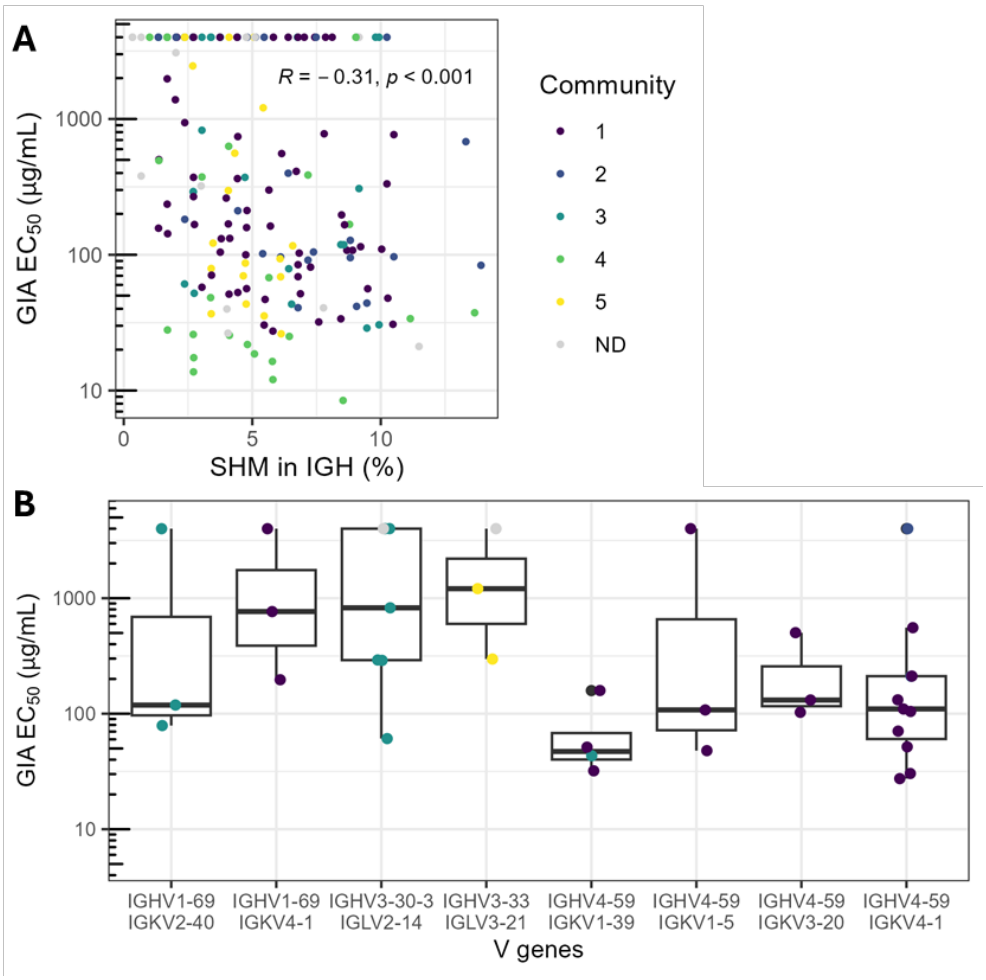

Figure 4.9. GIA potency by antibody gene sequence. **(A)** GIA EC_{50} was correlated with percentage somatic hypermutation (SHM) in IGH V genes. Spearman's rank correlation coefficient (*R*) and *p* values are shown. **(B)** GIA EC_{50} grouped by IG V gene pairs used by 3 or more mAbs in the panel. Boxplots show median and interquartile range. GIA negative mAbs were assigned a GIA EC_{50} of 4 mg/mL. mAbs are coloured by epitope community; ND = community not determined.

4.4.4 GIA by Duffy phenotype

Previous studies have suggested that different RBC Duffy positive sero-phenotypes have differing susceptibility to invasion by *P. vivax* (**Chapter 1.2.1**). Out of the two co-dominant alleles, Fyb positive RBCs have been shown in some studies to be more susceptible than Fya to *P. vivax* infection (91,92,108). DB9 was included as a control in the dilution series GIA assays and a total of 32 GIA EC_{50} values were obtained from assays using RBCs with different Duffy sero-phenotypes. Comparison of GIA EC_{50} values between the three Duffy positive sero-phenotypes showed no significant difference (Kruskal-Wallis test $p = 0.5$).

There was a large range in GIA EC_{50} values for DB9 between different assays indicating large assay to assay variation.

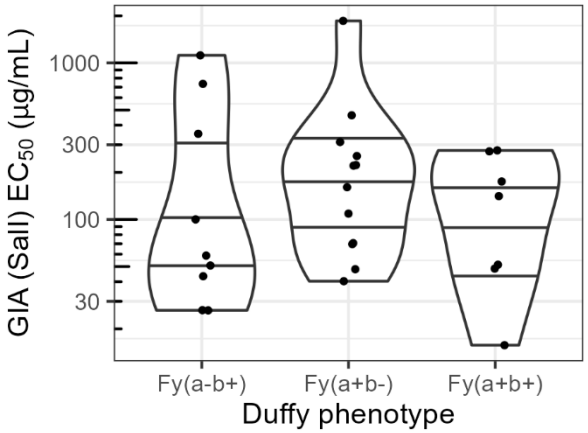

Figure 4.10. GIA EC_{50} of DB9 by Duffy sero-phenotype. Violin plots showing GIA EC_{50} of DB9, used as a positive control mAb, grouped by Duffy sero-phenotype of the RBCs used in the GIA assay, with group median and quartiles.

4.5 GIA against vaccine heterologous PvDBPII variants

The ELISA and HT-SPR experiments described in **Chapter 3.9** showed that some mAbs in the panel lost binding to vaccine heterologous PvDBPII variant sequences and may therefore also lose GIA against those variants. To assess the functional activity of the panel of mAbs against vaccine heterologous variants, they were tested in GIA assays against two different transgenic *P. knowlesi* parasites – one expressing the PvDBPII P variant and another expressing the W1 variant of *P. vivax*. The panel of mAbs were tested for binding to both of these variants as recombinant proteins in the binding assays (**Chapter 3.8, 3.9**) and the GIA results can therefore be compared to the binding results.

Those mAbs which showed similar or higher GIA potency to DB9 against the vaccine homologous PvDBPII SalI variant (**Chapter 4.4**) were downselected to test against both the P and W1 PvDBPII transgenic *P. knowlesi* parasite lines. These mAbs were tested at a single concentration of 0.5 mg/mL in the GIA assay and those mAbs which were negative (<20%

GIA) were designated as having lost GIA to the tested variant. Out of a total of 123 mAbs tested, 84 mAbs (68%) retained GIA to both PvDBPII P and W1 variants. 14 mAbs (11%) lost GIA against the PvDBPII P variant only, 12 mAbs (10%) lost GIA against the PvDBPII W1 variant only, and 13 mAbs (11%) lost GIA against both the P and W1 variants (**Appendix 7.6**).

The GIA results against the two variants were mostly in concordance with the binding data (**Figure 4.11**, **Table 4.1**). For 113/123 mAbs, GIA against the PvDBPII P and W1 variants matched the binding results to the two variants. For the 10 mAbs where GIA and binding results were discordant, 6 mAbs had retained binding to both variants but lost GIA to one of the variants and 4 mAbs had lost binding to one variant but retained GIA to both variants.

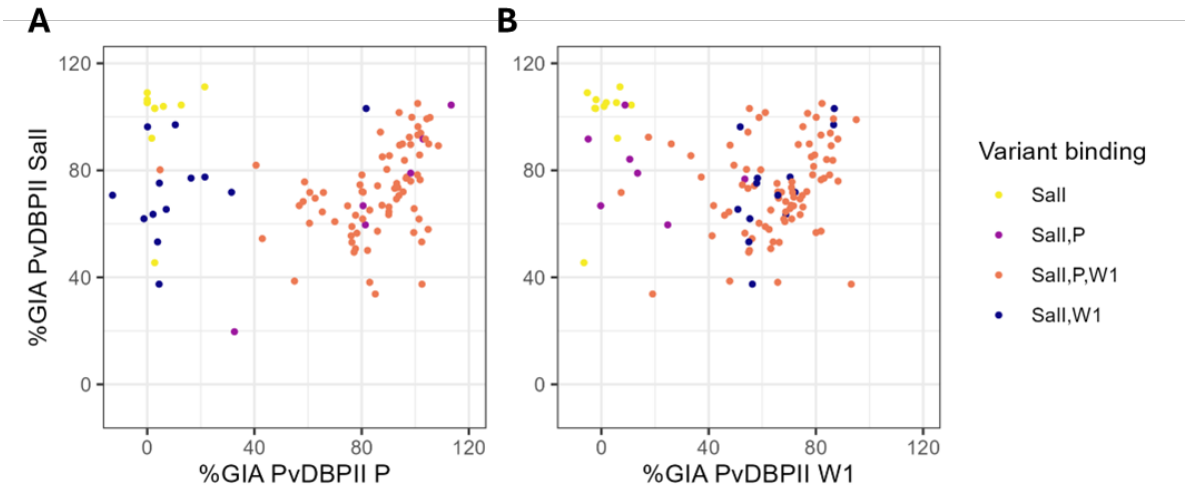

Figure 4.11. GIA against parasites expressing the vaccine-heterologous PvDBPII P and W1 variants compared to the vaccine-homologous SalI variant. % GIA of mAbs tested at 0.5 mg/mL against **(A)** PvDBPII P and **(B)** W1 variants plotted against % GIA against PvDBPII SalI. mAbs are coloured by which PvDBPII variant(s) they bind to by ELISA and HT-SPR assay.

		GIA				
		SalI	**SalI, P**	**SalI, W1**	**SalI, P, W1**	**Not tested**
binding	**SalI**	13				4
	SalI, P		7		1	14
	SalI, W1			13	3	13
	SalI, P, W1		5	1	80	21

Table 4.1. Comparison of GIA against and binding of mAbs to PvDBPII variants. Number of mAbs that bind to and retain GIA to PvDBPII SalI, P or W1 variants are shown.

A subset of the most potent mAbs which retained GIA against one or both of the PvDBPII variants were tested in dilution series, to compare potency across the different variants. 27 mAbs were tested in dilution series against P variant parasites and 18 were tested in dilution series against W1 variant parasites. Eight mAbs which retained GIA against both P and W1 variants were only tested in dilution series against P and not W1 variant (**Figure 4.12A**). The GIA EC_{50}s of the tested mAbs were mostly comparable between the three strains, except DB144 and DB178 which were less potent against the W1 variant and DB101 and DB185 were less potent against the P variant.

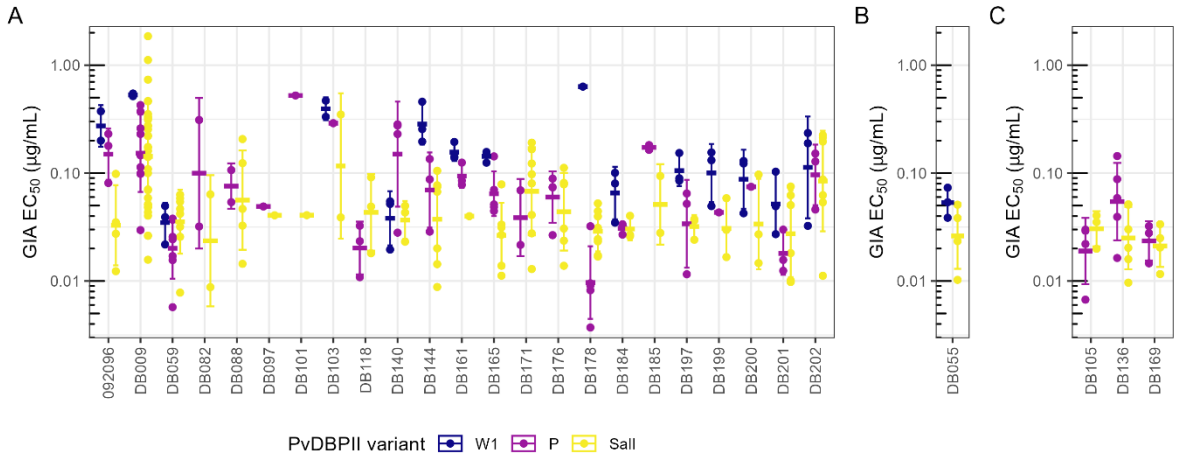

Figure 4.12. GIA EC_{50} against PvDBPII SalI, P and W1 variant-expressing parasites. Comparison of GIA EC_{50} of mAbs against PvDBPII SalI, P and W1 variants. **(A)** GIA EC_{50} of mAbs which retained GIA against both PvDBPII P and W1 variants. **(B)** GIA EC_{50} of mAbs which retained GIA against PvDBPII W1 variant only. **(C)** GIA EC_{50} of mAbs which retained GIA against PvDBPII P variant only. In **(A-C)** geometric means of biological replicates are shown with error bars indicating 1 standard deviation. mAbs are coloured by the PvDBPII variant against which they were tested.

The GIA activity of mAbs against the P and W1 variants were also overlaid onto the epitope community network plot (**Figure 4.13**). Community 1 to 3 mAbs bind in SD3, whereas community 4 and 5 mAbs bind in SD2, with community 5 mAbs containing the majority of DARC-binding inhibitory mAbs (**Chapter 3.6, 4.3**). All but one out of the 51 mAbs from community 1 which were tested retained GIA against both PvDBP P and W1 variant parasites. In contrast, epitope communities 2, 3 and 5 contained a larger proportion of mAbs

which lost GIA against one of the variants tested (11/16, 4/13 and 5/17 mAbs tested, respectively). Community 4 contained all the mAbs which lost GIA to both P and W1 variants (13/20). None of these 13 mAbs that lost GIA to both P and W1 variants inhibited DARC binding in the recombinant assays. In contrast, mAbs in communities 4 and 5 which did inhibit DARC binding, were able to retain GIA against at least one of the variants tested. Out of 23 mAbs which showed DARC binding inhibition, 12 retained GIA to both variants, 6 lost GIA to only the P or W1 variant, none lost GIA to both variants and 5 had low GIA and were not tested against the two variants. The 12 most potent mAbs in the panel, which had the lowest GIA EC_{50} against PvDBPII SalI expressing parasites, were strain-specific and lost GIA to at least one of either PvDBPII P or W1 variant parasite lines.

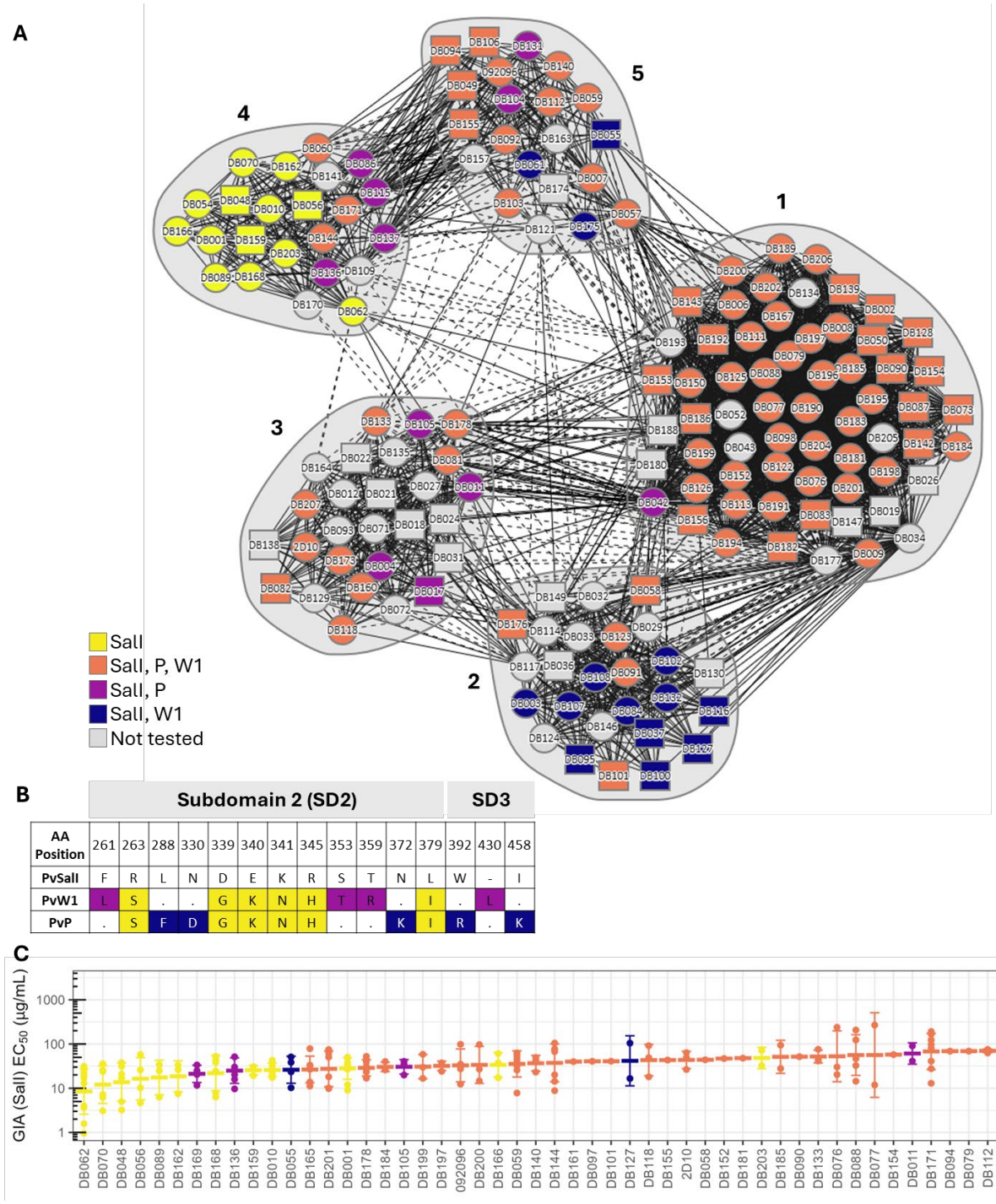

AA Position	261	263	288	330	339	340	341	345	353	359	372	379	392	430	458
PvSalI	F	R	L	N	D	E	K	R	S	T	N	L	W	-	I
PvW1	L	S	.	.	G	K	N	H	T	R	.	I	.	L	.
PvP	.	S	F	D	G	K	N	H	.	.	K	I	R	.	K

Figure 4.13. GIA against PvDBPII SalI, P and W1 variant expressing parasites. **(A)** Epitope community network plot overlaid with GIA of mAbs against three different PvDBPII variant expressing parasites. **(B)** Table shows polymorphic residues in PvDBPII W1 and P compared to SalI variant. **(C)** GIA EC_{50} of top 50 most potent mAbs against PvDBPII SalI variant. Geometric means of biological replicates are shown with error bars indicating 1 standard deviation. mAbs are coloured by which PvDBPII variants they have GIA against: yellow – SalI only; salmon – SalI, P and W1; purple – SalI and P; blue – SalI and W1; grey – not tested (due to low GIA against SalI in primary screen).

4.6 GIA against wildtype *P. knowlesi*

Both PvDBP and PkDBPα bind to DARC to enter human RBCs and there is high sequence homology in region II. Some anti-PvDBPII mAbs may therefore be cross-reactive against PkDBPα. To screen for any cross-reactive mAbs, I selected the more potent mAbs against PvDBPII SalI that also retained GIA against both PvDBPII P and W1 variants and tested them at a high single concentration of 2 mg/mL in the GIA assay against PkA1H1 strain (wild-type *P. knowlesi*). Out of the 68 mAbs tested at 2 mg/mL (nearly half the panel), the majority had no GIA (<20%), 5 mAbs showed low GIA of 20-40% and only 3 mAbs - DB112, DB133 and DB171 showed high GIA (>80%) (**Figure 4.14**). The three mAbs with high GIA were then tested in dilution curves. DB171 was more potent than DB112 and DB133 against PkA1H1. GIA EC_{50} of the three mAbs was comparable between transgenic *P. knowlesi* expressing PvDBPII SalI and PkA1H1. DB112 was binned into community 5, DB171 into community 4 and DB133 into community 3 (**Chapter 3.6**). The epitope binning for DB133 is likely incorrect as it did not bind SD3 on ELISA and in an AlphaFold3 predicted complex of DB133 and PvDBPII, DB133 bound within the DARC binding site in SD2 (**Figure 4.14**, **Chapter 3.10**). All three mAbs inhibited DARC-binding on the ELISA-based assay, suggesting that they bind the DARC binding domain within PvDBPII.

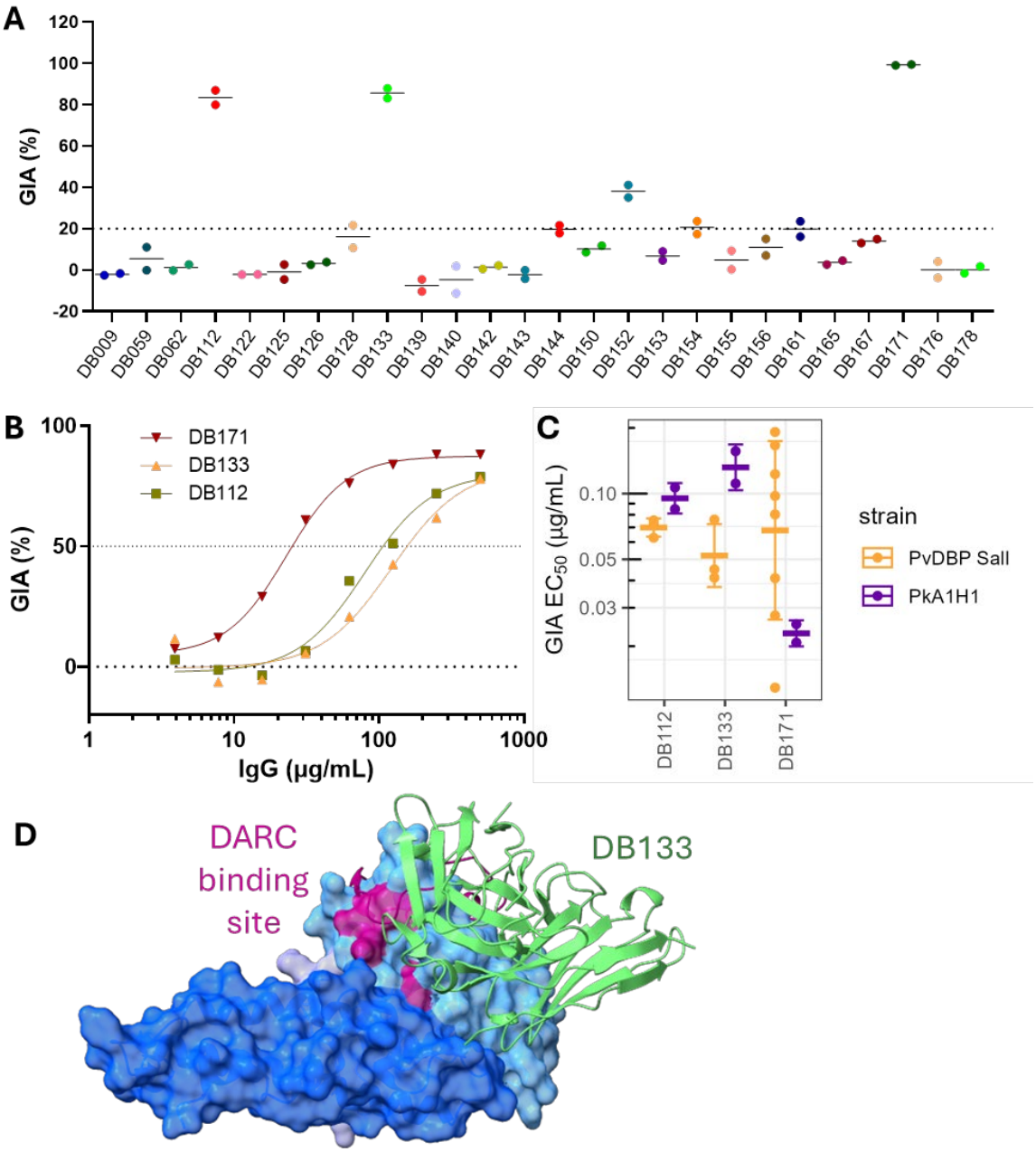

Figure 4.14. GIA of mAbs against *P. knowlesi*. **(A)** Example of single concentration GIA assay against PkA1H1 strain. Each mAb was tested at 2 mg/mL. GIA below 20%, indicated by the dotted line, was considered negative. **(B)** Example of dilution series GIA assays. A four-parameter non-linear regression curve was fitted and used to estimate GIA EC_{50} values. **(C)** Comparison of GIA EC_{50} of mAbs against PkA1H1 strain and transgenic *P. knowlesi* expressing PvDBPII SalI. Geometric means of biological replicates are shown with error bars indicating 1 standard deviation. mAbs are coloured by the parasite strain against which they were tested. **(D)** AlphaFold3 predicted structure of DB133 (in green) in complex with PvDBPII, aligned onto the structure of PvDBPII (SD2 in light blue, SD3 in dark blue) and DARC (in magenta) (pdb_00008a44). Residues Y295, N296, K297, L304 and I376 essential for DARC binding in both PvDBP and PkDBPα region II highlighted in magenta.

4.7 Discussion

In this Chapter the functional activity of the panel of anti-PvDBPII mAbs was tested, first using assays that test receptor binding inhibition, followed by parasite growth inhibition activity assays using transgenic *P. knowlesi* parasites.

4.7.1 DARC binding inhibition activity of mAbs

The ability of mAbs to inhibit binding of PvDBPII to DARC was tested using an established ELISA-based assay which uses recombinant PvDBPII and DARC-Fc proteins (145). Receptor BIA was also tested by HT-SPR using the same recombinant proteins, although the experimental set-up differed between the two assays. Results between the assays were mostly in concordance (**Chapter 4.3**). These assays showed that only a minority of mAbs, which bind in epitope communities 4 and 5, were able to inhibit PvDBPII-DARC binding. This is in concordance with previous structural studies which have shown that the DARC binding site lies within SD2 (96) and community 4 and 5 mAbs in this panel bind within SD2 (**Chapter 3.10**). The epitope of mAb 092096 (116), which is in community 5, overlaps with the DARC binding site and this mAb showed BIA when tested in both the ELISA-based assay and by HT-SPR. DB1 in community 4 was previously shown to bind within the putative PvDBP dimerisation site, but not within the DARC binding site (63) and did not show BIA in either recombinant assay. None of the mAbs in this panel in epitope communities 1, 2 and 3 showed BIA, which is in concordance with them binding in SD3 (**Chapter 3.6**), which is not involved in DARC binding.

4.7.2 Factors predictive of GIA potency of mAbs against vaccine homologous PvDBP

The full panel of mAbs was next tested for parasite GIA using transgenic *P. knowlesi* parasites expressing PvDBP with SalI strain sequence. The PvDBPII vaccines which induced these mAbs were based on the SalI strain, so these GIA assays tested for vaccine homologous inhibition. The majority of the anti-PvDBPII mAbs in the panel were GIA positive against the PvDBPII SalI parasite line and around two-thirds of mAbs showed a similar (or better) GIA potency to DB9, which was used as the positive control in these GIA assays. GIA positive mAbs were found in all epitope communities, including in communities 1 to 3, which bind SD3 and did not show DARC binding inhibition activity in the recombinant assays. The most potent mAbs in the panel were from epitope community 4, which also did not show receptor binding inhibition activity. The majority of mAbs which showed receptor BIA were GIA positive, although a small number were GIA negative at the maximum concentration tested. These results show that the recombinant binding inhibition assays are not predictive of parasite GIA. These binding inhibition assays have been used in the past as a surrogate for parasite neutralisation, often with polyclonal antibodies (106,108,167), however, these assays have likely missed antibodies with parasite GIA and underestimated the functional activity of antibodies in these studies.

The discrepancies between the binding inhibition and GIA assays could be due to a number of reasons. The binding inhibition assays used recombinant PvDBPII protein and N-terminal DARC peptide fused to a Fc scaffold. It is possible that the binding of native PvDBPII to DARC also involves other regions of the full-length PvDBP molecule and DARC. A mAb which disrupts contacts outside of PvDBPII and N-terminal DARC would not show binding inhibition in assays using these smaller regions of recombinant proteins. The recombinant protein assay may also simply not replicate all the features of the protein-protein binding event(s) at the cellular level. The transgenic *P. knowlesi* parasites express the full-length

PvDBP gene and interact with human RBCs expressing native DARC and therefore more closely resemble what is found in *P. vivax* invasion of reticulocytes *in vivo*. Another explanation for the discrepancies between the binding inhibition and GIA assays could be that mAbs inhibit parasite invasion of RBCs through mechanisms other than binding to and blocking the DARC-binding site. Antibodies are relatively large proteins and their binding to PvDBP could sterically hinder its approach to the RBC membrane and prevent its access to DARC. A similar mechanism for GIA of mAbs against a *P. falciparum* blood-stage antigen PfCyPRA has recently been proposed (137).

The binding of PvDBP and DARC might also involve other critical steps such as dimerisation of PvDBP, as has been suggested based on structural studies of PvDBPII (168). Antibodies such as DB1 in epitope community 4, which bind to the dimerisation site could mediate GIA by blocking this process but without showing BIA in assays using recombinant proteins (63). The most potent mAb in the panel was another community 4 mAb DB62, which had a GIA EC_{50} of 8 µg/mL (95% CI 4 to 19). Notably, the top 10 most potent mAbs in the panel were all from epitope community 4 and showed no BIA in the recombinant assays, but may act by inhibiting PvDBPII dimerisation. It is unclear what drives the high potency of community 4 mAbs compared to mAbs from other communities but one possible explanation could be that the epitopes of community 4 mAbs are more accessible to antibodies compared to the epitopes of other communities within native PvDBP.

Analysis of factors that predict PvDBPII SalI GIA potency across the panel of anti-PvDBPII mAbs found that faster association rate (k_a) of mAb binding to PvDBPII was correlated with higher GIA potency, whereas no correlation was seen with dissociation (k_d) rate. The importance of antibody association rate with functional potency has also been observed before for mAbs against the blood-stage *P. falciparum* antigen RH5 (141) and as well as for a mAb against respiratory syncytial virus (169). The association of faster antibody binding with

higher GIA potency is likely explained by the short time that merozoite antigens are exposed to antibodies, before they invade RBCs and are no longer accessible (170). This suggests that addition of antibodies or drugs that slow invasion of merozoites into RBCs could improve the potency of anti-PvDBPII mAbs in general (38,141).

4.7.3 Precision of *P. knowlesi* GIA assay

I observed large assay-to-assay variation in GIA measurements between different runs. Previous studies of *P. falciparum* and *P. knowlesi* GIA assays observed larger variation between independent assays compared to small variation seen between different wells in the same assay (166,171). The major contributor to assay-to-assay variation in the *P. falciparum* GIA study was from using RBCs from different donors in each assay. I therefore changed from performing technical replicates to biological/experimental replicates using different batches of RBCs and performed at least 3 biological replicates, when more accurate measurement was required to compare GIA potency across different antibodies. To compare the GIA potency of different mAbs tested across different assay runs, the GIA of a test sample could be standardised against a positive control to try to correct for the assay-to-assay variation in GIA. In these transgenic *P. knowlesi* GIA assays, DB9 was ran as a positive control in each assay run. The degree of deviation of GIA of DB9 in each assay from the median GIA of DB9 could be used to normalise the GIA of test samples, which are run in the same assay. This normalised GIA of the test sample may more accurately reflect the comparative GIA potency of different mAbs.

The large assay-to-assay variation observed in these *P. knowlesi* GIA assays could be due to factors related to the RBCs such as differences in red blood cell antigen or haemoglobin phenotypes or different age and condition of RBCs, which could affect the susceptibility of

RBCs to parasite invasion and the parasite growth efficiency within RBCs. Parasite growth could also be affected by the health of the parasites, which is not directly measured in the GIA assay. Final parasitaemia was measured in the GIA assay but this was not correlated with GIA potency.

4.7.4 GIA of mAbs against vaccine heterologous PvDBP variant parasite lines

The generation of transgenic *P. knowlesi* lines expressing vaccine heterologous variants of PvDBPII has allowed me to test the functional activity of the mAb panel against other PvDBPII variants and determine if the loss of binding seen on ELISA against specific variants corresponds to loss of invasion inhibition. Results from the GIA assay were largely in agreement with the binding data. Screening of the panel of mAbs against two variants showed that only epitope community 1 mAbs, which bind to SD3, almost all retained GIA against both variants, whereas the other communities contained mAbs that are strain specific. Community 4 mAbs contained some of the most potent mAbs in the panel but these potent mAbs lost GIA against both variants tested. These mAbs include DB1, which is known to bind the polymorphic 'DEK' epitope (position 339-341) in SD2, with D339G found in more than two thirds of global isolates of *P. vivax* (69). PvDBP vaccine candidates have been based historically on the SalI strain sequence because this was the first *P. vivax* genome sequenced (62). For future vaccine candidates, using a PvDBPII variant that incorporates globally conserved residues may induce antibodies that are more strain transcending.

The panel of mAbs was also tested against two PvDBPII variant parasite lines, P and W1, which covered many of the common polymorphisms found in PvDBPII. However, to determine if the mAbs are truly strain-transcending it will be important to test the mAbs against a greater number of PvDBPII variant parasite lines covering the full range of

polymorphisms found in different *P. vivax* strains worldwide. It would be very labour intensive and time consuming to test each mAb against a single strain of transgenic *P. knowlesi* in separate GIA assays. To increase the throughput of the GIA assay with different strains of *P. knowlesi*, Prof Moon's group at LSHTM are developing transgenic *P. knowlesi* lines expressing different PvDBPII variants with a 'barcode' genetic sequence tag to identify each variant line. This allows pools of parasites with different variants to be tested in the same GIA assay with a sequencing-based readout and should greatly expand the number of variants against which mAbs can be tested in a single assay. Testing mAbs against a much wider range of variants will improve the precision in identifying which polymorphisms result in loss of functional activity of each mAb and help determine if epitope community 1 mAbs are truly strain-transcending.

Community 1 mAbs were mostly broadly inhibitory, whereas a proportion of mAbs from epitope communities 2 to 5 lost GIA to one or both of the PvDBPII variant lines tested. However, mAbs in communities 4 and 5 which inhibited PvDBP-DARC binding in the recombinant assays were also more likely to retain GIA to both variants. These binding inhibitory mAbs may be strain-transcending if they bind the well conserved residues within the DARC binding site. Other mAbs in communities 4 and 5 that are not DARC binding inhibitors likely bind polymorphic residues near to, but outside of, the DARC binding site and they therefore lose GIA to one or both of the PvDBP variants tested.

4.7.5 GIA of mAbs against *P. knowlesi*

In addition to testing against different variants of PvDBPII, I also screened a selection of mAbs in the GIA assay with wild-type *P. knowlesi* and found 3 mAbs that retained GIA against *P. knowlesi* - DB112, DB133 and DB171. The common feature shared between these

mAbs is that they likely bind within the DARC binding site within PvDBPII. DB112 and DB171 showed receptor BIA on the ELISA-based assay and HT-SPR and are from epitope communities 5 and 4 respectively. DB133 showed BIA on the ELISA-based assay but not on HT-SPR. However, the HT-SPR results for DB133 for receptor binding inhibition and epitope binning are likely incorrect as they are not in concordance with other assay results. The SD3-binding ELISA and the AlphaFold3 predicted complex of DB133 suggest that it binds within the receptor binding domain in SD2.

There is high homology between PvDBP and PkDBPα region II and the DARC binding site in both sequences is similar (**Figure 4.1**). Previous studies have identified essential, conserved residues that are involved in DARC binding to region II in both PvDBP and PkDBPα as Y295, N296, K297, R304, L369 and I376 (132). No structural epitope information is available for any of the three cross-reactive mAbs but an AlphaFold3 predicted complex of PvDBPII with DB133 showed that its epitope overlaps residues K297 and I376 (**Figure 4.1**, **Chapter 3.10**). Other DARC-binding inhibitory mAbs which were tested against *P. knowlesi* did not show high GIA. This could be due to loss of binding of these mAbs to PkDBPα, which should next be tested by ELISA. PvDBPII-specific mAbs that bind in SD3 are also expected to lose binding to PkDBPα, as there is lower homology in SD3 than in SD2, and indeed no SD3-binding mAbs in this panel showed GIA against *P. knowlesi*. The identification of a small number of mAbs that can inhibit both *P. vivax* and *P. knowlesi* indicate that antibodies that are functional against DBP in both species can be induced and although rare, these antibodies can be relatively potent.

4.7.6 Conclusion

In this Chapter the functional activity of the panel of anti-PvDBPII mAbs was tested. DARC receptor binding inhibitory mAbs were only found in epitope communities 4 and 5, whereas

GIA positive mAbs were found in all epitope communities. This suggests that direct blocking of receptor binding is not the only mechanism of GIA. GIA positive mAbs were tested against two vaccine heterologous PvDBPII variant parasite lines, which showed that the majority of mAbs retained GIA against both variants. However, the most potent mAbs in the panel, which were from community 4, were strain-specific. Strain-transcending mAbs were also screened for GIA against wild-type *P. knowlesi*, which identified three species-transcending mAbs which inhibit PvDBPII-DARC binding. In the next Chapter, different approaches to improve mAb GIA potency and breadth were trialled.

5 Functional interactions of mAbs and engineered mAbs

5.1 Authorship statement

Transgenic *Plasmodium knowlesi* parasite lines were provided by Prof Robert Moon at LSHTM. GIA assays prior to 2022 (shown in **Figure 5.5**) were performed by Amelia Lias and Doris Quinkert. Engineered mAbs were designed by Martino Bardelli and 10 engineered mAbs were produced by him. All other data was generated by me.

5.2 Introduction

Monoclonal antibodies targeting the pre-erythrocytic stage of *P. falciparum* are in clinical development and showing promising protective efficacy in clinical trials (172–174). No mAbs against *P. vivax* have yet reached clinical testing but anti-PvDBPII mAbs could potentially be a candidate for further development. The major limitations to using a single anti-PvDBPII mAb as a prophylactic agent are the potential loss of neutralisation activity against different strains and the lower potency of strain-transcending mAbs, which would require high doses of mAbs to be administered to achieve therapeutic concentrations in humans.

One approach to potentially overcome these limitations is by combining two or more mAbs together. The functional activity of combinations of different mAbs could be either additive, antagonistic or synergistic. Additivity occurs when no functional interaction occurs between each mAb, i.e. they act independently of each other. Antagonism occurs when the combined activity of two or more mAbs is lower than the activity predicted from the sum of each individual mAb, i.e. the action of one mAb reduces the action of the other by some mechanism. Synergy occurs when the combined activity of multiple mAbs is greater than the

predicted sum of each individual mAb, i.e. the action of one mAb enhances the activity of the other and/or vice versa.

One model used to predict the functional effect of drug combinations is Bliss additivity (148). In the Bliss model of additivity, each drug is acting independently of the other drug that is present. The Bliss additivity is the joint probability of two independent events, calculated from the probability of each event acting alone. Applied to the GIA of mAbs, the predicted functional activity of a combination of two mAbs which are additive, is calculated from the observed GIA of each individual mAb using the following formula:

$$GIA_{Bliss} = GIA_A + GIA_B - GIA_A \times GIA_B$$

By comparing the observed functional activity of a combination of drugs to the predicted Bliss additivity calculated from each drug individually, the activity of the combination of drugs can be classified as additive, synergistic or antagonistic. In the first part of this Chapter, a selection of anti-PvDBPII mAbs from different epitope communities were tested in pairwise combinations in GIA assays to determine the functional interactions between mAbs.

In the second part of this Chapter, a different approach to try to improve mAb potency and increase the breadth of inhibition was tested. A selection of anti-PvDBPII mAbs with high potency from different epitope communities were selected to make engineered versions of each mAb. These engineered mAbs comprise of a 35-mer N-terminal domain DARC peptide fused to the C-terminus of the Fc region of the mAb. The DARC peptide on these engineered mAbs is predicted to bind to PvDBP and act as a receptor binding inhibitor by preventing the binding of PvDBP to native DARC on RBCs. This could potentially increase both the breadth of inhibition and potency of anti-PvDBPII mAbs.

5.3 Functional interactions between mAbs

5.3.1 Antagonism between mAbs

To assess the functional interaction between mAbs, I selected mAbs of varying GIA potency from each epitope community (**Chapter 3.6**) and screened these at a single concentration in pairwise combinations. The most potent mAb and one to two low potency mAbs from each epitope community were tested. Neutralising mAbs were tested at their GIA EC_{50} concentration and non-neutralising mAbs were tested at 0.25 or 0.5 mg/mL. Each mAb was tested on its own and in pairwise combination with another mAb. The predicted Bliss additivity GIA% was calculated from the GIA of each mAb tested alone and subtracted from the measured GIA% of the two mAbs tested in combination. Pairs of mAbs were categorised as additive if predicted Bliss additivity GIA was within 10% of the measured GIA, synergistic if Bliss additivity GIA was >10% lower than the measured GIA or antagonistic if predicted Bliss additivity was >10% higher than the measured GIA (**Figure 5.1**).

In this single concentration screen, pairs of mAbs were mostly additive or antagonistic in the GIA assay. Antagonism was observed between mAbs from the same epitope communities, which is not surprising as they would compete for binding. More surprisingly, antagonism was also observed between mAbs from different epitope communities, including between mAbs from communities that bind in different subdomains. Synergy was only observed between DB178, a neutralising mAb, and two non-neutralising mAbs from the same community.

A

mAb	SD3 binding	DARC binding inhibitor	Comm-unity	PvDBPII variant binding	GIA EC_{50} (µg/mL)	K_D
DB009	Y	N	1	SaII_P_W1	143	1.63E-10
DB188	Y	N	1	SaII_P_W1	NA	4.38E-11
DB201	Y	N	1	SaII_P_W1	27	4.07E-12
DB084	Y	N	2	SaII_W1	NA	3.60E-10
DB176	Y	N	2	SaII_P_W1	84	3.54E-12
DB071	Y	N	3	SaII_P	NA	1.68E-10
DB093	Y	N	3	SaII_P	NA	4.67E-10
DB178	Y	N	3	SaII_P_W1	29	2.57E-12
DB062	N	N	4	SaII	8	1.74E-12
DB007	N	Y	5	SaII_W1	NA	2.01E-10
DB055	N	N	5	SaII_W1	26	1.68E-09
DB131	N	Y	5	SaII_P	93	6.30E-12

B

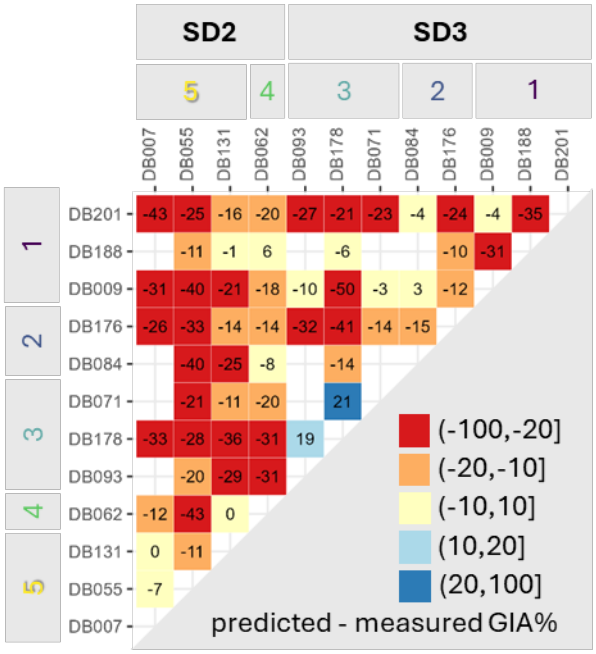

Figure 5.1 GIA of combination of mAbs tested at single concentrations. **(A)** Table of properties of mAbs tested in combination in the GIA assay. **(B)** GIA of mAbs tested alone and in pairwise combination. Neutralising mAbs were tested at their GIA EC_{50} concentration, non-neutralising mAbs at 0.25 or 0.5 mg/mL. The predicted Bliss additivity % GIA was subtracted from measured % GIA of the pair of mAbs and the difference is shown on the heatmap. The epitope communities and subdomain binding of each mAb are shown.

A selection of mAbs were then tested in dilution series on their own and in pairwise combination in a 1:1 ratio. The predicted Bliss additivity at each concentration was calculated from the dilution series GIA of each mAb tested on its own. The GIA EC_{50} of the predicted

Bliss additivity GIA and observed GIA of the test combination of mAbs were estimated by fitting a four-parameter non-linear regression curve. The ratio of GIA EC_{50} of the predicted Bliss additivity to the measured GIA EC_{50} of the test combination of mAbs was calculated. Pairs of mAbs were categorised as additive if the ratio of predicted Bliss additivity GIA EC_{50} to the measured GIA EC_{50} of the test combination was between 0.8 to 1.2, synergistic if the ratio of predicted to measured GIA EC_{50} was >1.2, or antagonistic if the ratio of predicted to measured GIA EC_{50} was <0.8 (**Figure 5.2**).

The majority of mAb combinations were antagonistic when tested in dilution series. Only DB188, a non-neutralising mAb from community 1, was additive with DB62 and synergistic with DB178. The results from these dilution series GIA assays were mostly in agreement with the single concentration GIA results. Two combinations of mAbs were classified differently in the single concentration compared to dilution series GIA assay: DB188 and DB178 were additive at single concentration but synergistic in dilution series and DB201 and DB84 were additive at single concentration but antagonistic in dilution series.

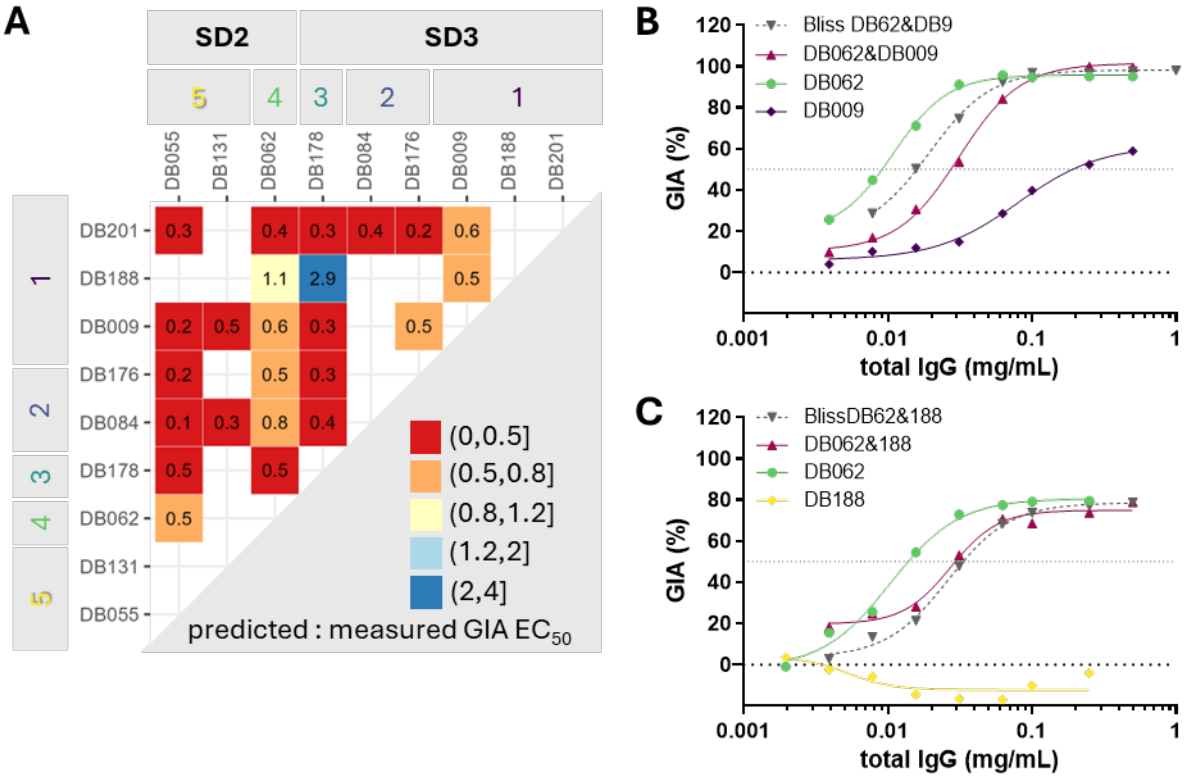

Figure 5.2 GIA of combinations of mAbs tested in dilution series. **(A)** GIA of mAbs tested alone and in pairwise combination in a 1:1 ratio. GIA EC_{50} of predicted Bliss additivity and test combination of mAbs was estimated by fitting a four-parameter non-linear regression curve. The ratio of GIA EC_{50} of the predicted Bliss additivity, calculated from each mAb tested alone, to the GIA EC_{50} of the measured combination of mAbs was calculated and shown on the heatmap. **(B)** Example GIA dilution curves of DB62 and DB9 tested alone at a starting concentration of 0.5 mg/mL each and in pairwise combination of 1:1 mix at a starting concentration of 1 mg/mL total IgG. Predicted Bliss additivity, calculated from each mAb tested alone, is shown as a grey dashed curve. Measured GIA of the combination of two mAbs is shown in pink triangles. **(C)** Example GIA dilution curves as in **(B)** but for DB62 and DB188 tested alone at a starting concentration of 0.25 mg/mL each and in pairwise combination of 1:1 mix at a starting concentration of 0.5 mg/mL total IgG.

5.3.2 Functional interactions between Fabs

To further investigate the antagonism observed between mAb pairs, a representative neutralising mAb from each epitope community was made in Fab form and tested in pairwise combination in the GIA assay. Using the same mAb in Fab form retains the same paratope but removes the Fc region and reduces the binding valency from 2 to 1. Therefore, the contribution of the Fc region and/or binding valency to the antagonism observed between two mAbs can be tested. Initially a pairwise combination of mAb + Fab was tested, along with each mAb and each Fab tested on their own. Combinations of mAb + Fab were tested at the

same concentration each, which equates to a 1:3 molar ratio of mAb:Fab in the pairwise combinations. The predicted Bliss additivity at each molarity was calculated from the dilution series of each mAb or Fab tested on its own. The GIA EC_{50} of predicted Bliss additivity and GIA EC_{50} of the test combination of mAb + Fab were estimated by fitting of a four-parameter non-linear regression curve. The ratio of GIA EC_{50} of the predicted Bliss additivity to the measured GIA EC_{50} of the test combination of mAb + Fab was calculated and used to categorise the interaction as additive (ratio of 0.8-1.2), synergistic (>1.2), or antagonistic (<0.8). Similarly, Fabs were tested in dilution series on their own and in pairwise combination in a 1:1 ratio and the measured GIA compared to the predicted Bliss additivity GIA.

Six mAbs were made in Fab form: DB55, DB62, DB178, DB176, DB9 and DB201 from communities 5, 4, 3, 2, 1 and 1 respectively. Pairwise combinations of these mAbs were all antagonistic in GIA in dilution series (**Figure 5.2**). When testing these in pairwise combination of mAb + Fab, antagonism was no longer observed between SD2-binding mAbs or Fabs (DB55 and DB62) and SD3-binding mAbs or Fabs (DB178, DB176, DB9 and DB201) (**Figure 5.3**). Antagonism was also no longer seen between DB178 Fab and all mAbs. Antagonism mostly remained between SD3-binding mAbs and SD3-binding Fabs. When testing pairs of Fabs, all combinations were additive or synergistic, except DB9 and DB201 Fabs, both from epitope community 1, which continued to show antagonism. The GIA curves of synergistic Fab combinations followed the GIA curve of the potent Fab tested on its own.

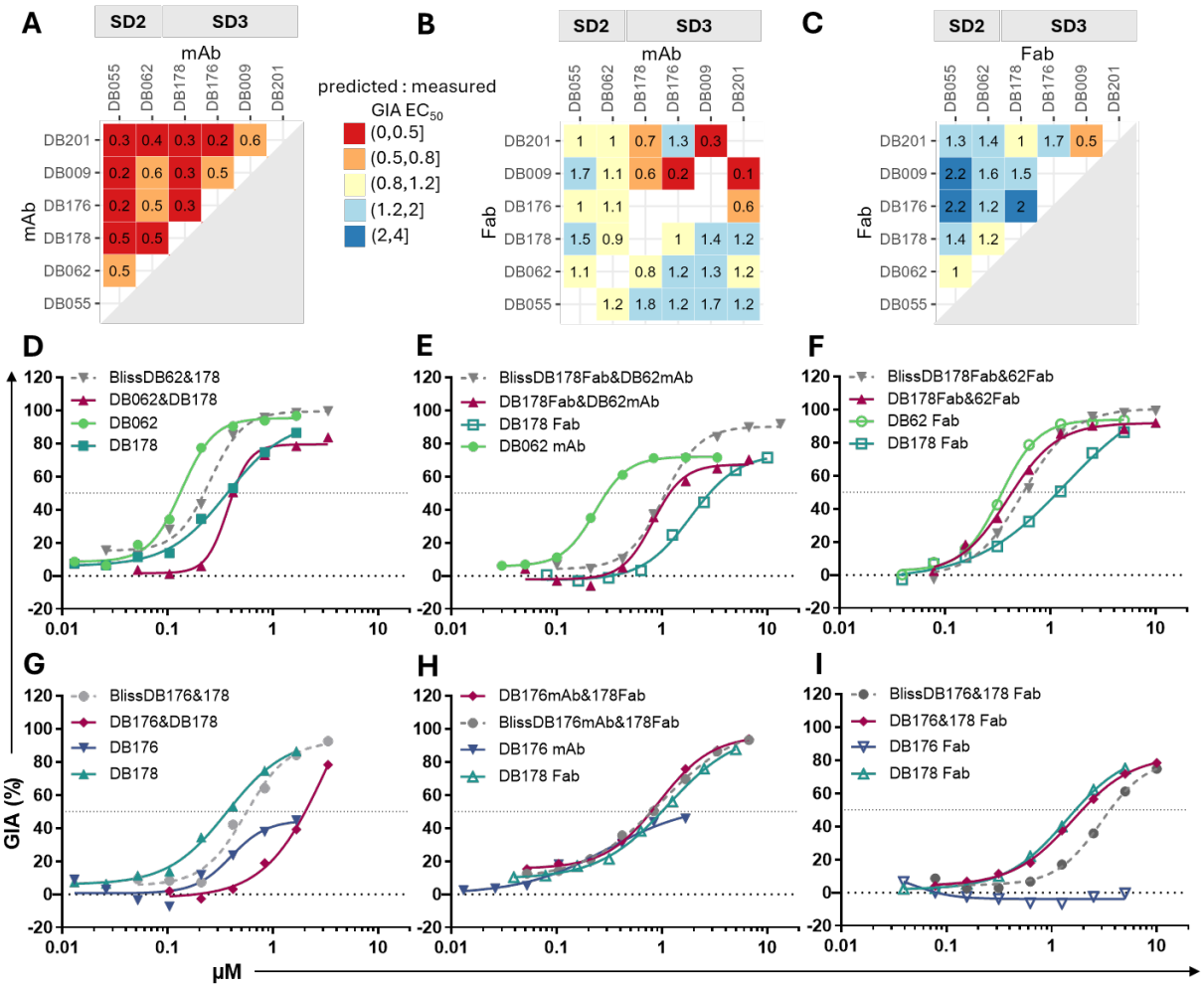

Figure 5.3 GIA of combinations of mAbs and Fabs. **(A-C)** GIA of mAbs or Fabs tested alone and in pairwise combination in dilution series. GIA EC_{50} was estimated by fitting of a four-parameter non-linear regression curve. The ratio of GIA EC_{50} of the predicted Bliss additivity, calculated from each mAb or Fab tested alone, to the of GIA EC_{50} of the measured combination of mAb or Fab was calculated and shown on the heatmap. **(A)** The ratio of predicted to measured GIA EC_{50} of pairs of mAbs tested in a 1:1 ratio; showing the subset of mAbs that were subsequently also tested in Fab form. **(B)** The ratio of predicted to measured GIA EC_{50} of pairs of mAb + Fab tested in a 1:3 molar ratio. **(C)** The ratio of predicted to measured GIA EC_{50} of pairs of Fab + Fab tested in a 1:1 ratio. **(D-I)** Example GIA dilution curves of mAb or Fab tested alone and in pairwise combinations as mAbs (solid symbol) and Fabs (open symbol). Predicted Bliss additivity, calculated from each mAb and/or Fab tested alone, is shown as a grey dashed curve. Measured GIA of the combination of two mAbs or Fabs or mAb+Fab is shown in pink. Total concentration or molarity of antibody is plotted against GIA of **(D)** DB62 and DB178 as mAbs; **(E)** DB62 mAb + DB178 Fab; **(F)** DB62 Fab + DB178 Fab; **(G)** DB176 and DB178 as mAbs; **(H)** DB176 mAb + DB178 Fab; and **(I)** DB176 Fab + DB178 Fab.

5.3.3 Potency of Fabs compared to mAbs

When testing combinations of mAbs with Fabs, single mAbs were run in dilution series in the same GIA assay as their corresponding Fab, which allowed the potency of each mAb to be compared to its Fab form. All Fabs were less potent than the parental mAb form and DB9

(community 1) and DB176 (community 2) in Fab form had no GIA at the highest molarity (5 mM) tested. This difference in potency between mAb and Fab was not solely due to differences in binding valency. After correcting for the 2-fold difference in number of binding sites between mAb and Fab, all mAbs remained more potent than the Fab form, except DB62 which had a similar potency as mAb and Fab, after correcting for number of binding sites available per molecule.

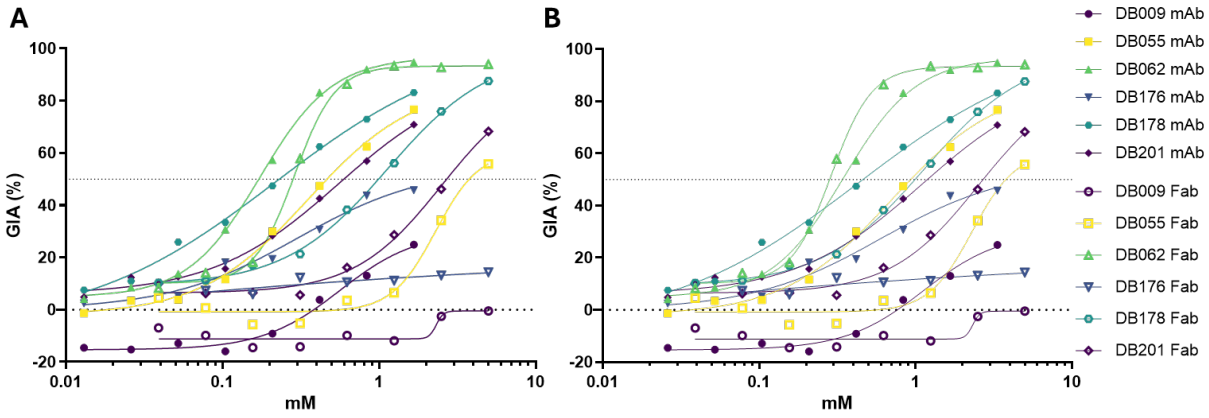

Figure 5.4 GIA of mAb compared to Fab. **(A)** GIA of mAbs and corresponding Fabs tested in dilution series. Molarity of mAb and Fab shown. Open symbol denotes Fab, solid symbol denotes parental mAb. **(B)** Same GIA assay as in **(A)** but with mAbs plotted at double the molarity to adjust for double the number of binding sites compared to Fab.

5.3.4 Functional interaction between multiple mAbs

To determine how multiple antibodies may interact in a polyclonal antibody response in serum, mAbs from different epitope communities were tested in combination in the GIA assay. One neutralising mAb from each epitope community was sequentially added in a 1:1 ratio in combination up to a maximum of 5 mAbs in total. Two sequential combinations were tested: in the first combination DB55 (community 5) was added to DB9 (community 1), followed by DB62 (community 4), DB176 (community 2) and then DB178 (community 3); in the second mixture DB62 was added to DB9, followed by DB176, DB178 and then DB55 (**Figure 5.5**). The combination of DB55 and DB9 was antagonistic and further addition of

DB62 and DB176 to the mixture did not have a significant effect on GIA. The combination of DB62 and DB9 was also antagonistic but more potent than DB55 and DB9. Addition of DB176 to DB62 and DB9 did not change the GIA of the mixture and further addition of DB178 lowered the GIA potency of the mixture. A mixture of all five mAbs was of a similar potency compared to the combination of DB9+62+176+178 but significantly more potent than a combination of DB9+55+62+176.

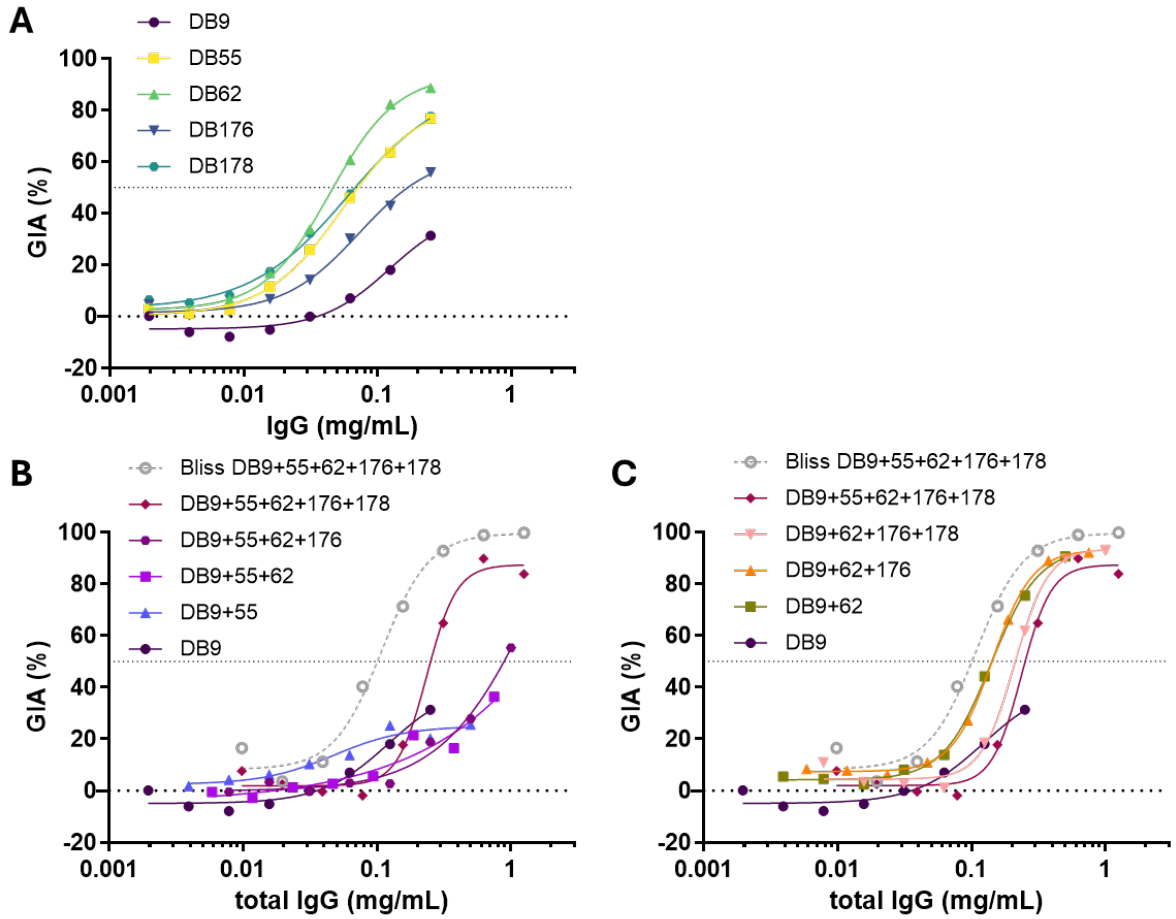

Figure 5.5 GIA of combination of multiple mAbs. GIA of mAbs tested in dilution series. **(A)** mAbs tested on their own at a starting concentration of 0.25 mg/mL. **(B)** GIA of multiple combinations of mAbs in a 1:1 ratio, starting with combination of DB55 and DB9. **(C)** GIA of multiple combinations of mAbs, starting with combination of DB62 and DB9. In **(B-C)** each mAb was tested at a starting concentration of 0.25 mg/mL each and the total IgG concentration of test combinations are plotted (so for the combination of 5 mAbs the total starting concentration was 1.25 mg/mL). Predicted Bliss additivity of the combination of all 5 mAbs was calculated from each mAb tested alone and is shown as a grey dashed curve.

Testing combination of mAbs in the GIA assay has shown significant antagonism between mAbs from all five epitope communities. This observation has implications for vaccine design as antagonism between PvDBPII-specific antibodies in a polyclonal pool may limit the degree of parasite growth inhibition that can be achieved through vaccination. The antagonism between mAbs was no longer observed when the mAbs were tested in Fab form. However, the potency of most of the mAbs was lower as Fabs. Therefore, combining neither mAbs nor Fabs will be a successful strategy to improve the GIA potency beyond that of the most potent single mAb DB62.

5.4 Function of engineered mAbs

5.4.1 GIA of engineered mAbs against parasites expressing PvDBPII SalI strain

A different approach to potentially improve mAb potency and neutralisation breath was by modifying mAbs through addition of a DARC peptide to the Fc region. The idea for this design was derived from a report of an engineered antibody construct against HIV termed eCD4-Ig, a fusion protein of an immunoadhesin CD4-Ig combined with a CCR5-mimetic sulfopeptide (175). eCD4-Ig targets both the CD4 and CCR5 binding sites on the HIV Env protein and showed higher potency and greater breadth of neutralisation than the best HIV broadly-neutralising antibodies. A DARC peptide fused to an anti-PvDBPII mAb, whose epitope does not overlap the DARC binding site, would be hypothesised to bind to PvDBP and (in parallel to the mAb) prevent binding of PvDBP to native DARC on RBCs.

Previous work in the Draper group tested different lengths of peptides of the N-terminal domain of DARC and found that addition of a 35-mer peptide spanning $DARC_{8-42}$ to the C-terminus of the Fc region resulted in the greatest improvement in GIA of engineered DB9 compared to shorter DARC peptides (**Figure 5.6**). Fusion of a DARC peptide to the N-

terminus of the heavy chain, instead of the C-terminus of the mAb, resulted in smaller improvements in mAb potency; and addition of DARC peptides to both the N- and C-termini of the mAb did not further improve GIA compared to constructs with the DARC peptide fused only to the C-terminus. A 35-mer peptide consisting of a scrambled amino acid sequence fused to DB9 (118) and EBL040, an Ebola virus-specific mAb (147), were also tested as controls. The scrambled peptide fused to the GIA negative mAb EBL040 did not show any GIA. In contrast, the scrambled peptide fused to DB9 improved the GIA compared to wild-type DB9 but the improvement in potency was not as great as with engineered DB9 fused to the DARC peptide. EBL040 fused to the 35-mer $DARC_{8-42}$ peptide (eEBL040-35) did show GIA, which suggests that the DARC peptide is functional and able to bind to PvDBP.

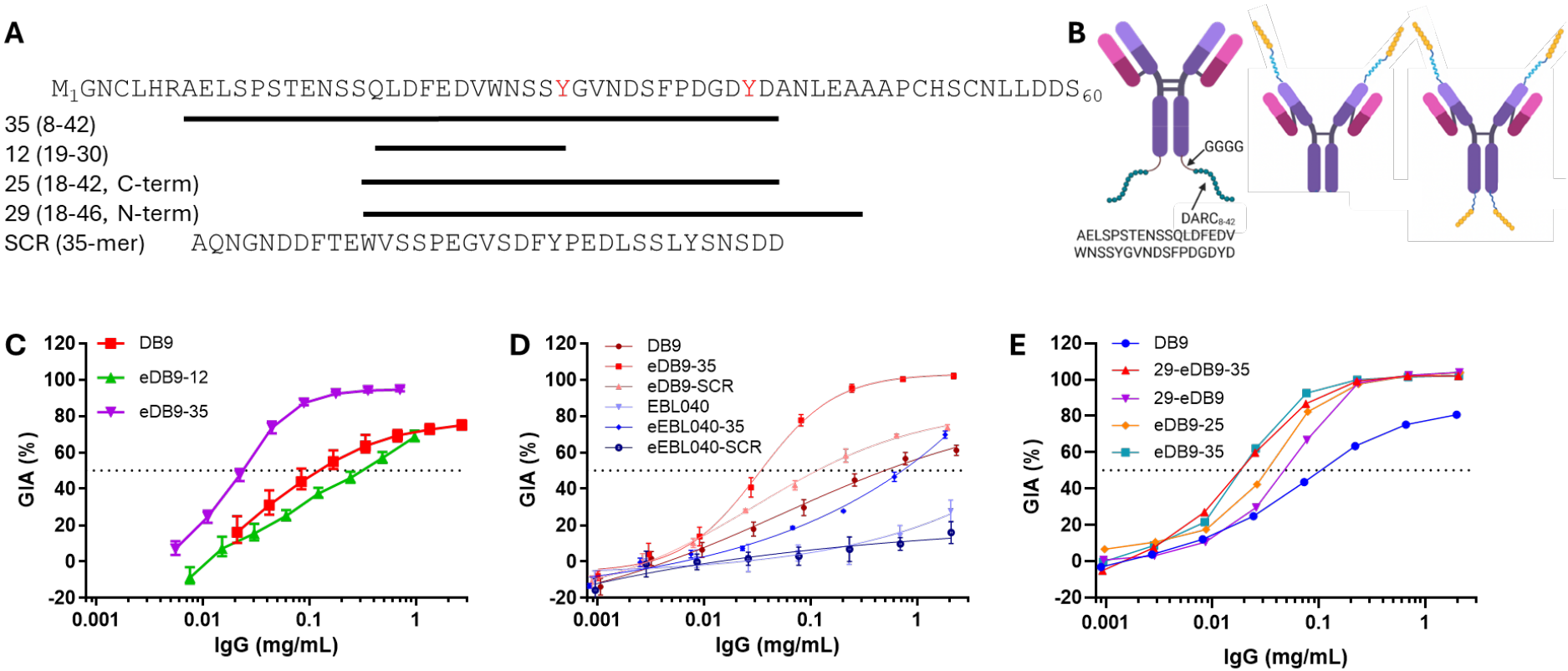

Figure 5.6 Engineered mAb designs and GIA. **(A)** Designs of DARC peptides fused to mAbs. Protein sequence of the 60-amino acid N-terminal domain of DARC, with sulphated tyrosines shown in red. Lengths of different DARC peptides and residues over which the peptides span are shown. DARC peptides were fused to either the C- and/or N-terminus of the mAb heavy chain. SCR = 35-mer peptide with scrambled amino acid sequence. **(B)** Three different designs of engineered mAbs with a DARC peptide fused to: the C-terminus via a GGGG linker; to the N-terminus only or fused to both C- and N-termini of the mAb. **(C)** Dilution series GIA of DB9 and engineered DB9 with a 12-mer (eDB9-12) or 35-mer DARC peptide (eDB9-35) fused to the C-terminal end of wild-type DB9. **(D)** Dilution series GIA of DB9 and engineered DB9 with a 35-mer DARC peptide (eDB9-35) or a scrambled 35-mer peptide (eDB9-SCR) fused to the C-terminal end of DB9. The same peptides were fused to the Ebola mAb EBL040. **(E)** Dilution series GIA of DB9 and engineered DB9 with a 35-mer DARC peptide (eDB9-35) or a 25-mer DARC peptide (eDB9-25) fused to the C-terminal end of DB9. 29-eDB9 has a 29-mer DARC peptide fused to the N-terminus of DB9. 29-eDB9-35 has a 29-mer DARC peptide fused to the N-terminus and a 35-mer DARC peptide fused to the C-terminus of DB9.

The engineered mAb construct consisting of the 35-mer $DARC_{8-42}$ peptide fused to the C-terminal Fc region of the mAb was chosen going forwards because this design improved the GIA potency of DB9 the most. This construct was used to modify a selection of the most potent novel anti-PvDBPII mAbs from each epitope community. These new engineered mAbs were tested in GIA assay dilution series against transgenic *P. knowlesi* expressing PvDBPII SalI strain and compared to wild-type mAb and eEBL040-35 (**Figure 5.7**, **Appendix 7.7.1**).

Addition of the 35-mer $DARC_{8-42}$ peptide improved the GIA potency of mAbs from all epitope communities, except most of the mAbs from community 4. The degree of improvement in potency of engineered mAbs compared to their wild-type form varied between different mAbs. The greatest improvement in GIA EC_{50} was observed for engineered DB103, which was up to 90-fold more potent than wild-type DB103, which is from community 5 and a DARC-binding inhibitor. The most potent engineered mAb was eDB59-35, with a GIA EC_{50} of 5 µg/mL (95% CI 3 to 9), which was about a 10-fold improvement in GIA potency compared to wild-type DB59 (GIA EC_{50} of 45 µg/mL [95% CI 29 to 70]). eDB59-35 was consistently the most potent mAb in each GIA assay and was more potent than all wild-type mAbs tested, including DB62, which had a GIA EC_{50} of 16 µg/mL (95% CI 6 to 46) in these assays. DB59 is a community 5 mAb and one of the few mAbs in this community that showed no DARC-binding inhibition activity in the recombinant assays.

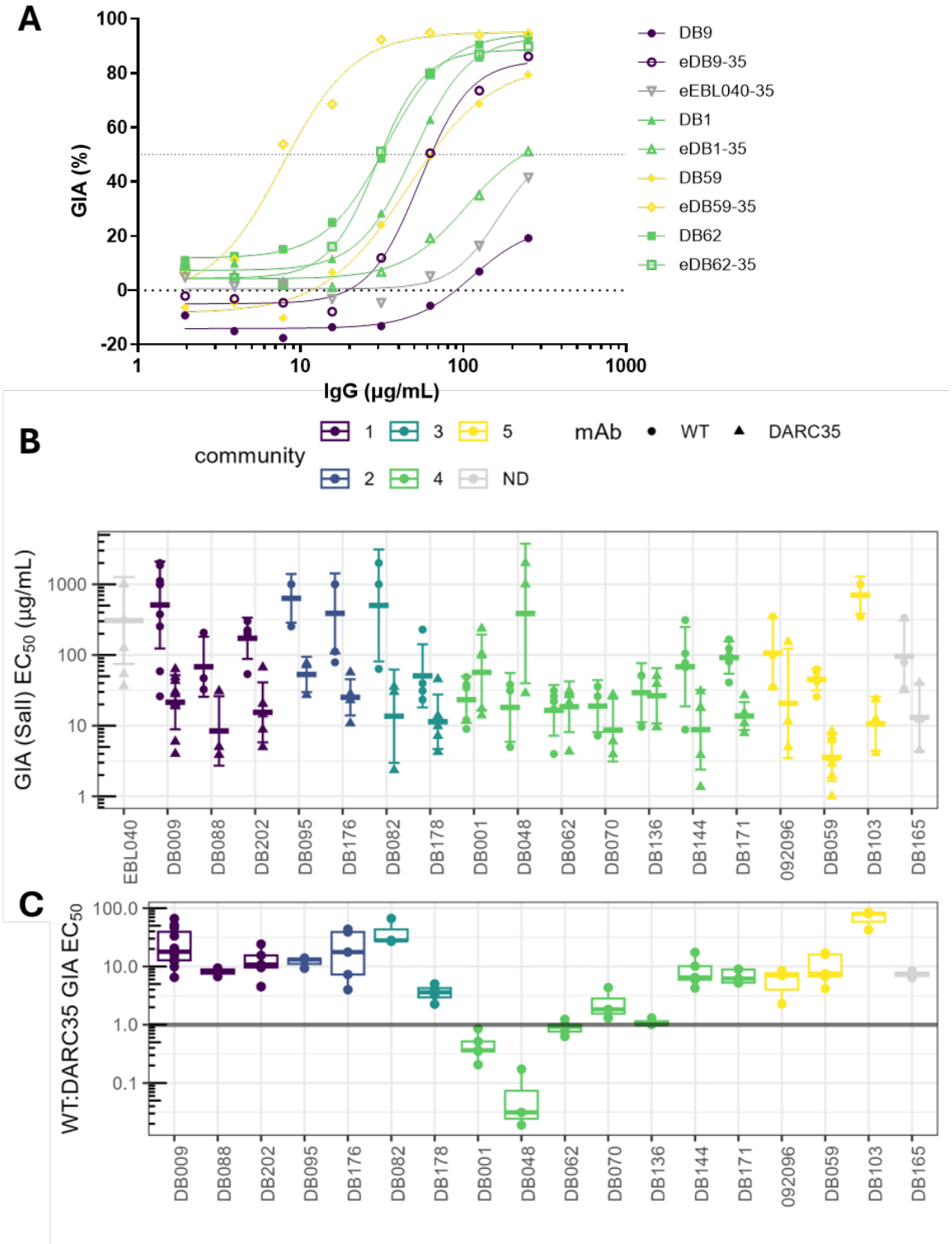

Figure 5.7 GIA of novel anti-PvDBPII mAbs fused to 35-mer DARC peptide. **(A)** Example of dilution series GIA assay of engineered mAbs (open symbols) and wild-type (WT) mAbs (solid symbols). A four-parameter non-linear regression curve was fitted and used to estimate GIA EC_{50} values. **(B)** GIA EC_{50} for each biological replicate are shown with geometric means and error bars indicating 1 standard deviation. WT mAbs are shown as circles, engineered mAbs (DARC35) as triangles. GIA positive mAbs which did not reach 50% GIA were assigned a GIA EC_{50} of 1 or 2 mg/mL, depending on the maximum concentration of mAb tested in the assay. **(C)** The ratio of GIA EC_{50} of WT to engineered mAbs was calculated for each biological replicate. Grey line indicates equal potency of WT and engineered mAb. mAbs are coloured by epitope community, ND = community not determined.

Engineered mAbs from community 4 varied in their potency in comparison to the wild-type mAb. Engineered DB1 and DB48 were less potent than wild-type mAb; engineered DB62, DB70 and DB136 were of similar potency to wild-type mAb and engineered DB144 and DB171 were more potent than wild-type mAb. DB144 and DB171 differ from the other community 4 mAbs in that they both retained GIA to PvDBP P and W1 variants, whereas the other community 4 mAbs lost GIA to at least one of the variants. DB171 also inhibited DARC binding in the recombinant assays. This suggests that DB144 and DB171 have different epitopes to the other community 4 mAbs and are more similar in behaviour to community 5 mAbs, which were consistently more potent in engineered form.

As seen previously, EBL040, which does not bind PvDBP, has GIA in engineered form when fused to the 35-mer DARC peptide. The GIA EC_{50} of eEBL040-35 was 94 μg/mL (95% CI 20 to 441), which was similar in potency to wild-type DB9 but less potent than any other engineered mAb in the panel. To estimate the relative contributions of two components of the engineered mAbs to the improvement in GIA - the DARC peptide in isolation versus the DARC peptide fused to the C-terminus of the mAb, a subset of wild-type mAbs from each epitope community were tested alone and in combination with eEBL040-35 in the GIA assay (**Figure 5.8**). The combination of wild-type mAb + eEBL040-35 were tested in a 1:1 mix and compared to the predicted Bliss additivity calculated from the GIA of the wild-type mAb and a separate DARC peptide (on eEBL040-35) tested on their own. The GIA of the combination of a wild-type mAb + eEBL040-35 was also compared to the engineered mAb, which was run in the same assay.

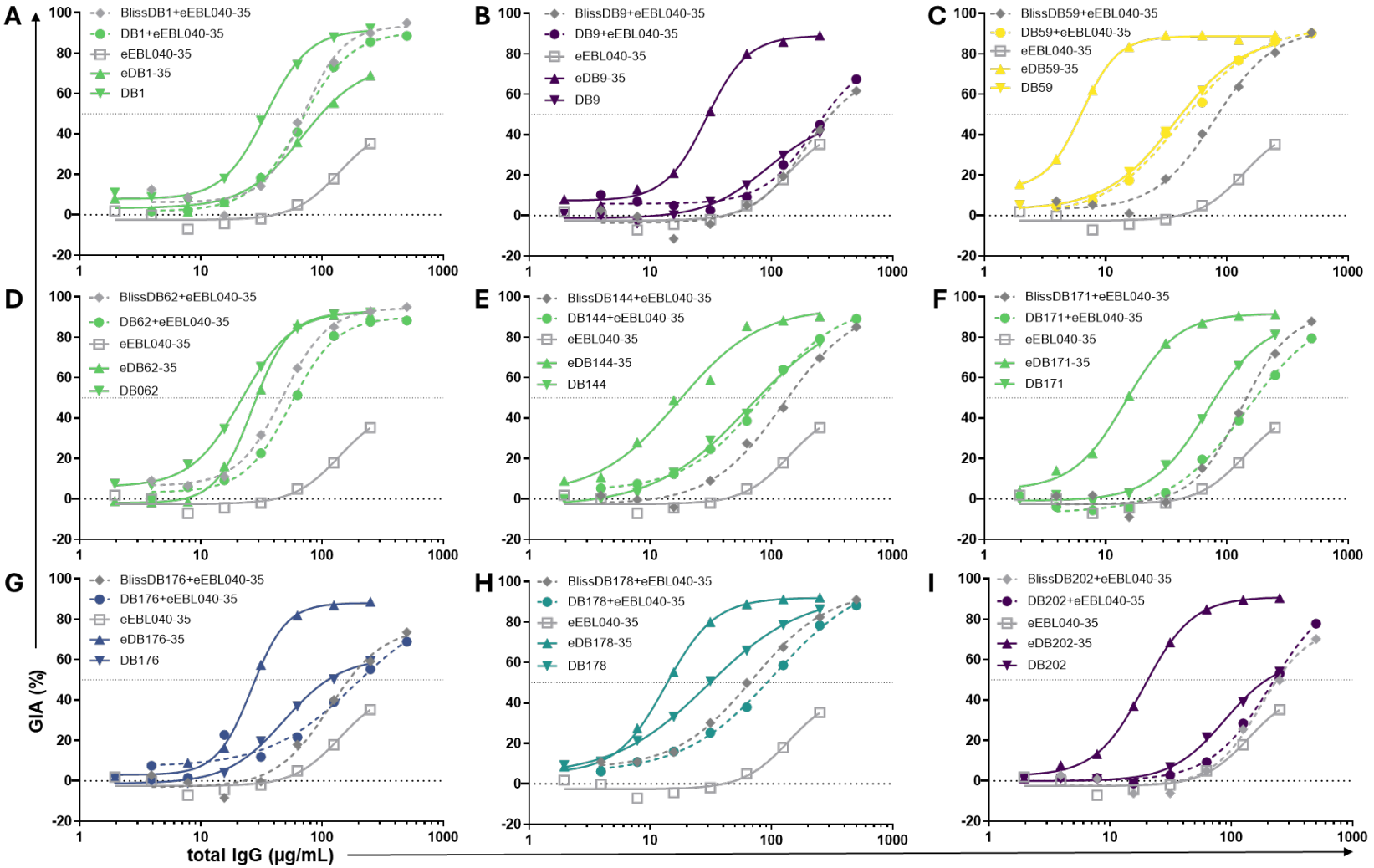

Figure 5.8 GIA of DARC peptide with wild-type mAb. Dilution series GIA assays of wild-type (WT) mAb (DB, down-pointing triangle), engineered mAb (eDB-35, up-pointing triangle) and engineered EBL040 (eEBL040-35, grey square) tested on their own and in a 1:1 combination of WT mAb + eEBL040-35 (circle, dashed line). Predicted Bliss additivity of the combination of WT mAb + eEBL040-35 was calculated from each mAb tested alone (grey diamond, dashed line). The following mAbs were tested **(A)** DB1, **(B)** DB9, **(C)** DB59, **(D)** DB62, **(E)** DB144, **(F)** DB171, **(G)** DB176, **(H)** DB178 and **(I)** DB202.

For DB1 (community 4), DB9 and DB202 (both community 1) a 1:1 combination of eEBL040-35 and the wild-type mAb were additive, which suggests that the 35-mer DARC-peptide does not compete for binding with these mAbs and is able to act independently of the mAb. DB62, DB171 (both community 4), DB176 (community 2) and DB178 (community 3) combined with eEBL040-35 were mildly antagonistic, which suggests that the DARC peptide may be competing for binding to PvDBP with the mAb. For these seven mAbs, the GIA of the combination of eEBL040-35 with the wild-type mAb was less potent than the wild-type mAb on its own, which is explained by the lower potency of the DARC peptide in the mixture. In contrast, DB59 (community 5) and DB144 (community 4) were synergistic with eEBL040-35. The GIA dilution curves of the combination of wild-type DB59 and DB144 with eEBL040-35 overlapped with the dilution curve of the wild-type mAb tested on its own, which suggests that the presence of the DARC peptide may increase the occupancy of the wild-type mAb on PvDBP.

Comparison of the GIA of the combination of wild-type mAb + eEBL040-35 with the engineered mAb showed that for all mAbs except DB1, the engineered mAb was more potent than the combination of wild-type mAb + eEBL040-35. Engineered DB1 was the only mAb that was less potent than the combination of wild-type mAb + eEBL040-35. For all mAbs, the GIA of the engineered mAb does not appear to be simply the additive effect of the wild-type mAb and the DARC peptide acting independently. This indicates that the function of the DARC peptide is affected by its fusion to the Fc region of the mAb, likely due to its physical restriction to the Fc region of a mAb, which could affect the binding of the DARC peptide to PvDBP. The function of the engineered mAb could also be enhanced simply by the additional bulk of the DARC peptide.

5.4.2 GIA of engineered mAbs against parasites expressing PvDBPII P variant

The novel engineered mAbs were also tested in GIA assays against transgenic *P. knowlesi* expressing PvDBPII P variant to determine if the addition of the DARC peptide to a wild-type mAb can increase the breadth of inhibition of the mAb. The 35-mer DARC peptide is predicted to bind the well-conserved residues in the DARC binding site so would be hypothesised to retain GIA against PvDBPII P variant.

Those wild-type mAbs, which retained GIA against parasites expressing PvDBPII P variant, showed similar improvements in GIA in engineered form as against parasites expressing PvDBPII SalI variant (**Figure 5.9**, **Appendix 7.7.2**). Engineered DB103 again showed the greatest improvement in GIA potency against PvDBPII P variant compared to the other mAbs tested. eDB59-35 remained the most potent mAb, with a GIA EC_{50} of 5 μg/mL (95% CI 0.02 to 810), similar to its GIA EC_{50} against PvDBPII SalI variant. DB95 from community 2 and DB1, DB48, DB62 and DB70 from community 4 all lost GIA against PvDBPII P variant as wild-type mAbs (**Chapter 4.5**). In engineered form, these mAbs all regained GIA against PvDBPII P but varied in their potency. eDB1-35 and eDB48-35 were similar in potency to eEBL040-35, which suggests that their GIA was solely from the activity of the DARC peptide. In contrast, eDB62-35, eDB70-35 and eDB95-35 showed higher potency in engineered form than eEBL040-35. This suggests that in addition to the activity of the DARC peptide, the variable region of the mAb may also be contributing to GIA of these engineered mAbs, despite the mAb losing GIA against the P variant as a wild-type mAb.

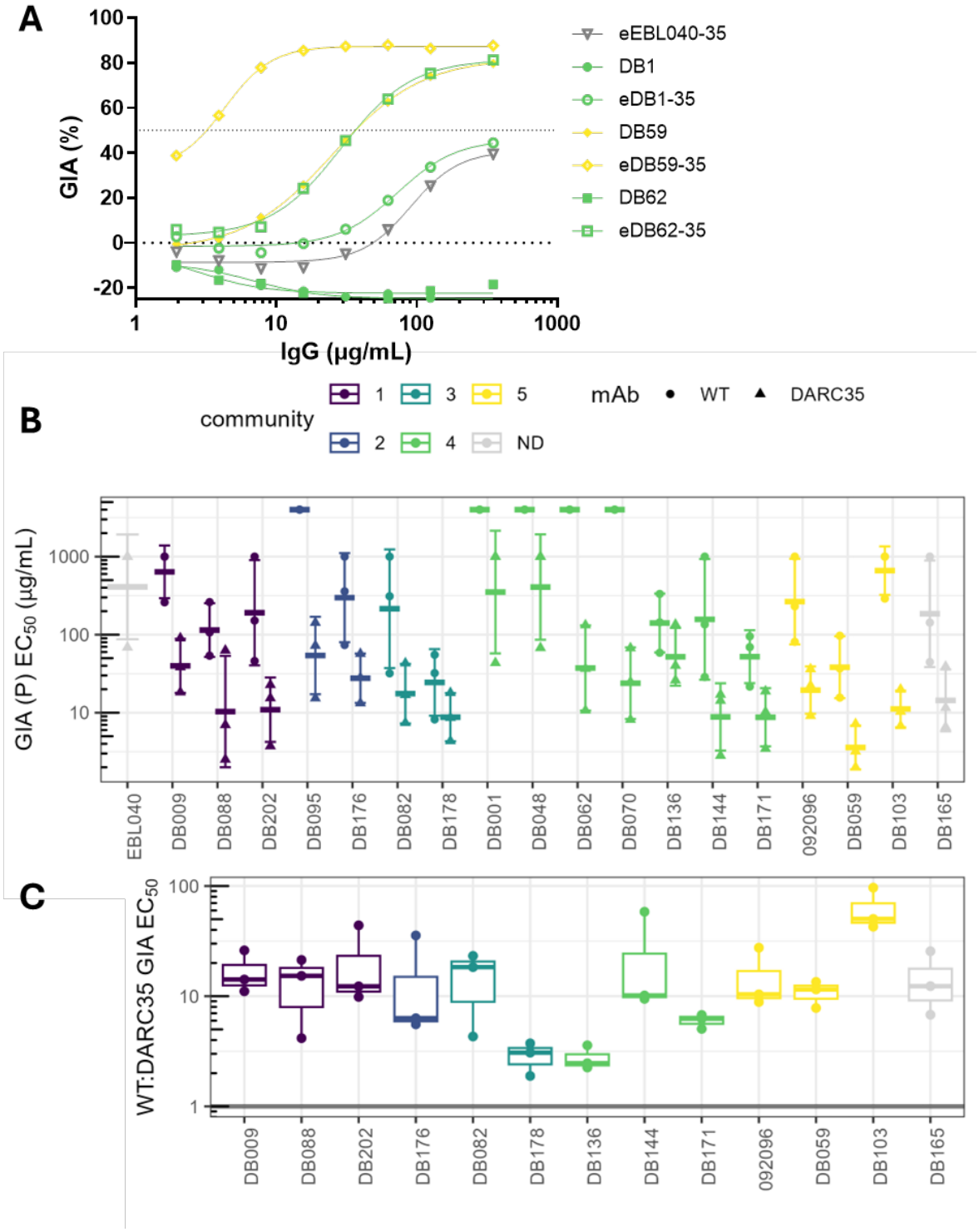

Figure 5.9 GIA of engineered mAbs against PvDBPII P variant. **(A)** Example of dilution series GIA assay of engineered mAbs (open symbols) and wild-type (WT) mAbs (solid symbols). A four-parameter non-linear regression curve was fitted and used to estimate GIA EC_{50} values. **(B)** GIA EC_{50} for each biological replicate are shown with geometric means and error bars indicating 1 standard deviation. WT mAbs are shown as circles, engineered mAbs (DARC35) as triangles. GIA positive mAbs which did not reach 50% GIA were assigned a GIA EC_{50} of 1 mg/mL. GIA negative mAbs were assigned a GIA EC_{50} of 4 mg/mL. **(C)** The ratio of GIA EC_{50} of WT to engineered mAbs was calculated for each biological replicate for mAbs which had GIA as WT mAb. Grey line at ratio of 1 indicates equal potency between WT and engineered mAb. mAbs are coloured by epitope community, ND = community not determined.

5.4.3 GIA of engineered mAbs against *P. knowlesi*

The novel engineered mAbs were also tested in the GIA assay against wild-type *P. knowlesi* A1H1 strain to determine the extent of the breadth of inhibition. Only three wild-type mAbs, DB112, DB133 and DB171, retained GIA against PkA1H1 (**Chapter 4.6**), out of which DB171 was made in engineered form. The other novel mAbs which were made in engineered form all had no GIA as wild-type mAbs against PkA1H1 (**Chapter 4.6**). The majority of engineered mAbs fused to the 35-mer DARC peptide regained some GIA against PkA1H1 and were similar in potency to eEBL040-35 (**Figure 5.10**). Engineered DB9 fused to a scrambled peptide (eDB9-SCR), like wild-type DB9, did not have GIA against PkA1H1. This indicates that the 35-mer $DARC_{8-42}$ peptide was able to bind to PkDBPα and that the GIA of these engineered mAbs was solely from the activity of the DARC peptide. Three of the engineered mAbs were more potent than eEBL040-35 – eDB171-35, eDB144-35 and eDB59-35. DB171 had a similar GIA in wild-type and engineered form. DB144 and DB59 had no GIA as wild-type mAbs (up to 2 mg/mL), which suggests that the addition of the DARC peptide was able to restore some GIA beyond the GIA gained from the DARC peptide on its own. However, eDB59-35 was less potent against PkDBPα (GIA EC_{50} 72 µg/mL [95% CI 56 to 92]) than against PvDBP SalI (GIA EC_{50} 5 µg/mL [95% CI 3 to 9]). Out of this panel of engineered mAbs, DB171 was the most potent mAb against PkA1H1 with a GIA EC_{50} of 23 µg/mL (95% CI 7 to 79).

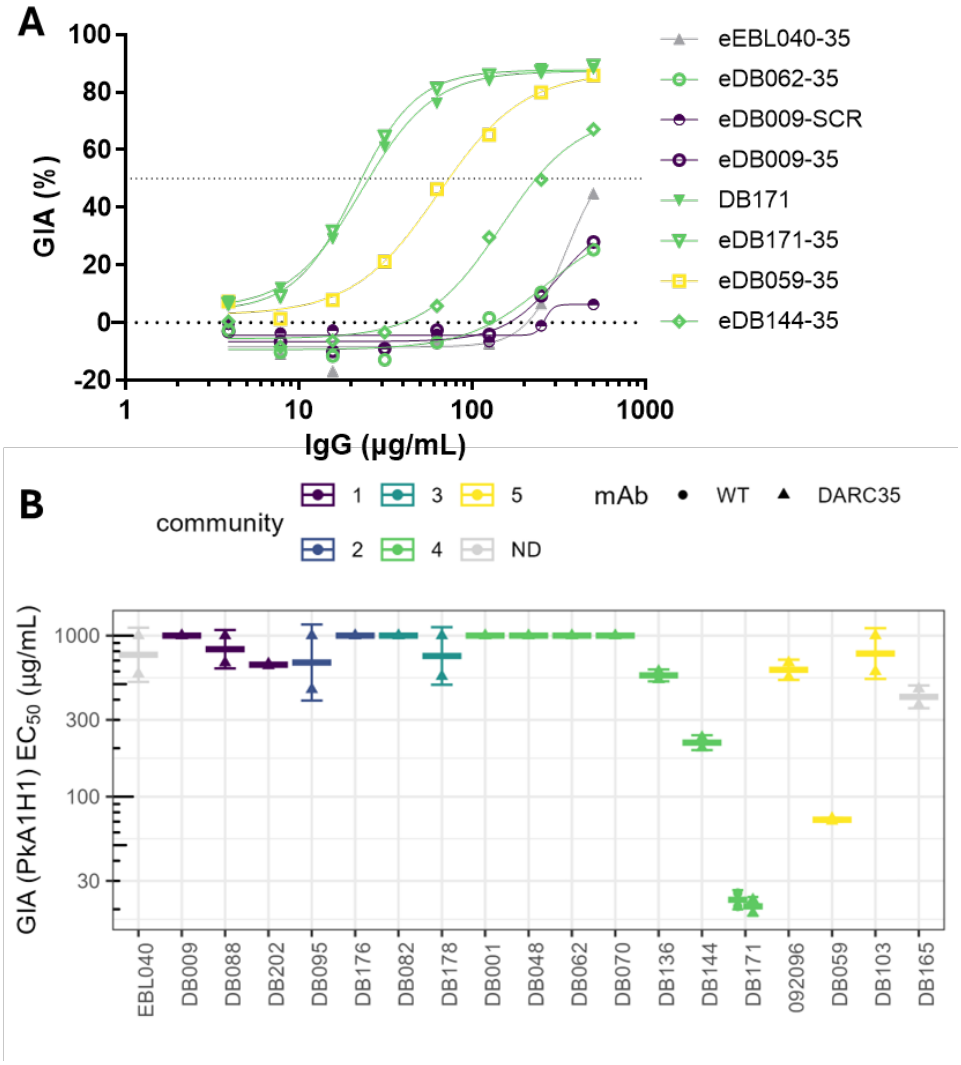

Figure 5.10 GIA of engineered mAbs against wild-type *P. knowlesi*. **(A)** Example dilution series GIA assay of engineered mAbs (open synmbols) and DB171 wild-type (WT) mAb (solid symbols) against PkA1H1. WT DB9, DB59, DB62 and DB144 did not have GIA. A four-parameter non-linear regression curve was fitted and used to estimate GIA EC_{50} values. SCR = 35-mer scrambled peptide. **(B)** GIA EC_{50} for each biological replicate are shown with geometric means and error bars indicating 1 standard deviation. WT mAbs are shown as circles, engineered mAbs (DARC35) as triangles. GIA positive mAbs which did not reach 50% GIA were assigned a GIA EC_{50} of 1 mg/mL.

5.5 Discussion

In this Chapter two different approaches to improve the GIA potency and breadth of inhibition of mAbs were trialled: combining different mAbs and mAb engineering.

5.5.1 Antagonism between anti-PvDBPII mAbs

Antagonism in GIA has previously been observed between anti-PvDBPII mAbs DB1-DB10 and between vaccine-induced and naturally-acquired mAbs which bind different subdomains (118,176). I have now more systematically tested for functional interactions between anti-PvDBPII mAbs from different epitope communities and also observed significant antagonism between mAbs. Antagonism between mAbs from the same epitope communities can be explained by competition for binding to PvDBPII. Two mAbs from the same community are unable to bind simultaneously to PvDBP and therefore cannot act independently of each other and only the bound mAb is functional. The mechanism of antagonism observed between mAbs binding different subdomains in PvDBPII is likely more complex. One mechanism could be steric hindrance between mAbs when bound to native PvDBP as presented on the parasite. Antibodies are large at 150 kDa compared to PvDBPII, which is around 40 kDa, and binding of one mAb could spatially occlude the epitope of a second mAb on PvDBP as presented on the parasite. The mAb epitope binning was performed using recombinant PvDBPII in solution without the rest of the full-length molecule. Different epitopes may be simultaneously accessible on the recombinant protein in solution, that are not accessible on native PvDBP presented on the parasite. Another mechanism of antagonism could be conformational changes that occur when one mAb is bound to native PvDBP, which then disrupt the epitope of another mAb from a different epitope community. SPR could be used to test for this mechanism by sequentially testing pairs of mAbs for binding to PvDBP. Disruption of the binding of one mAb due to the binding of another mAb to PvDBPII may be indicated by a difference in binding affinity between a single mAb binding to PvDBPII, compared to the binding affinity of a mAb binding to an already formed mAb-PvDBPII complex.

Testing a selection of the mAbs as Fabs showed that the antagonism was lost when two Fabs were tested in combination. The paratrope of the Fab and mAb are the same, so the loss of antagonism seen when testing Fabs instead of mAbs suggests that steric hindrance from the Fc region could be contributing to the antagonism observed between two mAbs. Interestingly, when combinations of two Fabs were tested, most combinations were synergistic. DB9 Fab and DB176 Fab did not have GIA up to the highest molarity (5 mM) tested but when either was combined with a different Fab that did have GIA on its own, the combination was synergistic. In contrast, DB9 Fab and DB176 Fab in combination had no GIA. The GIA dilution curve of the combination of DB9 Fab or DB176 Fab with a different inhibitory Fab overlapped with the dilution curve of the inhibitory Fab tested on its own. This could indicate that DB9 Fab and DB176 Fab may be acting by increasing the occupancy of the neutralising Fab on PvDBP but how this might be achieved is unclear. Synergy has been observed previously between mAbs against the blood-stage *P. falciparum* antigen RH5, where a non-inhibitory mAb was able to synergise with inhibitory mAbs by slowing merozoite invasion (38). It is possible that a similar mechanism could explain the synergy observed between anti-PvDBPII Fabs, although the synergy was not observed when the same antibody was tested in mAb form, whereas the anti-RH5 mAb was synergistic as both Fab and mAb.

It is likely that the antagonism observed between pairs of mAbs in the GIA assay also occurs in vaccine-induced polyclonal serum. Antagonism between PvDBPII-specific antibodies could explain the low GIA of polyclonal IgG from the vaccine studies that this panel of anti-PvDBPII mAbs were isolated from, where no serum sample reached more than 50% GIA at 10 mg/mL total polyclonal purified IgG (133). The GIA of a polyclonal IgG response would likely be a balance between additive, antagonistic and synergistic clones within the polyclonal pool, with the overall GIA of the polyclonal response dependent on the functional activity, biophysical properties and percentage composition of antibodies within the pool. In

this Chapter, up to five neutralising mAbs from different (non-competing) epitope communities were tested in combination to mimic what may be observed in a polyclonal response. Combinations of multiple mAbs were antagonistic as expected but the GIA of a mixture of mAbs did not appear to be simply dominated by the mAb with the strongest binding affinity. Problematically, the antagonism between anti-PvDBPII antibodies occurs between mAbs from all epitope communities, thereby making it difficult to rationally engineer a new vaccine immunogen in which antagonism can be removed. The antagonism may also limit the maximal parasite growth inhibition activity that could be achieved through vaccination with only the PvDBPII antigen and alternative strategies are likely required to increase vaccine efficacy. Antagonism between naturally acquired or vaccine-induced antibodies have previously been observed against a variety of other pathogens including *P. falciparum*, hepatitis C and SARS-CoV, which suggests it occurs commonly and may be a mechanism of immune invasion (177–179).

5.5.2 Mechanism of GIA of mAbs and Fabs

Lower potency of Fabs compared to their parental mAb was observed for all antibody clones tested and two mAbs, DB9 and DB176, had no GIA in Fab form up to the highest molarity (5 mM) tested. The difference in potency between mAbs and Fabs suggests that either binding valency and or the Fc region contribute to the GIA of these mAbs. After adjusting for the different number of binding sites available between mAbs and Fabs, for all mAbs except DB62, the corresponding Fab remained significantly less potent than the parental mAb. This suggests that the bulk of the Fc region may contribute to GIA of these mAbs and could be the mechanism of action of SD3-binding mAbs, which do not directly inhibit DARC binding. Another possible, and not exclusive, mechanism of action of these mAbs could be mediated through their bivalency, whereby binding of both arms of a mAb is required for it to be

functionally active. The relative contributions of the binding valency versus the Fc region of mAbs to GIA could be determined by testing Fab2 forms of each mAb, which would retain the bivalent binding but remove the Fc region.

5.5.3 Mechanism of GIA of engineered mAbs

A different approach to improve the potency and neutralisation breath of mAbs was trialled by engineering mAbs with addition of a DARC peptide. Previous work by the Draper group showed that fusion of a DARC peptide to the Fc region of DB9, which binds SD3 of PvDBPII, can increase the potency of the mAb. Testing of different constructs designs showed that the improvement in potency of engineered DB9 is likely through two mechanisms. Firstly, the DARC peptide has GIA activity on its own by binding to PvDBP and thereby preventing it from binding to native DARC on RBCs. Secondly, the peptide adds further bulk of ~4 kDa to the mAb and improves the GIA of DB9 through additional steric hindrance, irrespective of the actual sequence of the peptide that is fused to DB9. This is in concordance with the finding that the GIA of DB9 mAb is much higher than the GIA of DB9 Fab, suggesting that the mechanism of action of DB9 mAb is at least in part through steric hindrance from the Fc region. Out of the different construct designs, the 35-mer $DARC_{8\text{-}42}$ peptide fused to the C-terminal Fc region of the mAb improved the GIA potency of DB9 the most. This is consistent with earlier studies showing that this 35-mer DARC peptide, but not shorter peptides, was able to inhibit PvDBPII binding to RBCs (95). The improvement in GIA potency in the engineered mAbs also required the presence of Y41 in the DARC peptide. Sulfation of Y41, and Y30 to a lesser extent, have been shown in previous studies to be required for DARC binding to PvDBPII (63,97).

The 35-mer DARC$_{8-42}$ peptide construct was used to modify a selection of the more potent novel anti-PvDBPII mAbs from each epitope community. Engineered mAbs from all communities, except mAbs from community 4, were more potent than the wild-type mAb. The degree of improvement in GIA varied between different mAbs, with the greatest improvement seen for engineered DB103, which was up to 90-fold more potent than wild-type DB103, which is a DARC-binding inhibitory mAb from community 5. Eleven out of the 18 engineered mAbs exceeded the GIA potency of the most potent wild-type mAb DB62. The most potent engineered mAb was eDB59-35, which was around 3-fold more potent than wild-type DB62. For all mAbs except DB1, the GIA of the engineered form of each mAb exceeded the GIA of a 1:1 combination of the wild-type mAb and a separate DARC peptide (in the form of engineered EBL040). This suggests that the fusion of the DARC peptide to the C-terminus of a mAb has an additional effect on the GIA of the engineered mAb, which is not simply the additive effect of the GIA of the DARC peptide acting independently from the wild-type mAb. Fusion of a DARC peptide to a mAb could improve its GIA potency through additional steric hindrance, as was seen for DB9, and this may be the mechanism of GIA for SD3-binding mAbs and explain the improved potency of all SD3-binding mAbs in engineered form. This hypothesis could be tested by engineering the same SD3-binding mAbs tested here but fusing the mAb to a 35-mer scrambled peptide, which only adds additional bulk but cannot bind PvDBP and comparing their GIA with the engineered mAb fused to the 35-mer DARC peptide. Fusion of a DARC peptide to the C-terminus of a mAb physically restricts the position of the DARC peptide in relation to the variable region of the mAb. When the variable region of a mAb binds PvDBP, the DARC peptide fused to the Fc region is brought into closer proximity to the parasite membrane, which may also enhance the function of the DARC peptide by increasing its local concentration at the surface of the parasite. For DB9 the GIA of engineered DB9 fused to a scrambled peptide was higher than

the GIA of wild-type DB9, but DB9 fused to the 35-mer DARC peptide had even higher GIA. This suggests that both steric hindrance and direct PvDBP-DARC binding inhibition are likely contributing to the high GIA of eDB9-35. DB9 is not a direct DARC-binding inhibitor and the DARC peptide fused to DB9 should be able to bind to PvDBP at the same time as the variable region of DB9. When wild-type DB9 was tested in combination with a separate DARC peptide (attached to EBL040) the mixture was additive, which supports the hypothesis that both the DARC peptide and the variable region of DB9 can bind PvDBP simultaneously and act independently to inhibit parasite invasion (**Figure 5.8**).

Unexpectedly, the most potent wild-type mAbs from community 4, including DB62, did not improve in potency in engineered form. For two community 4 mAbs, DB1 and DB48, the engineered mAbs were in fact significantly less potent than the wild-type mAb. One possible explanation for why these engineered community 4 mAbs do not improve in potency could be that when these mAbs bind to PvDBP, the DARC peptide fused to the C-terminus of the mAb may become inaccessible to another PvDBP molecule and therefore is not functional. The lack of improvement in GIA potency of most community 4 mAbs also suggests that steric hindrance is not a mechanism of action of these mAbs. The strength of the binding affinity of the variable region of the mAb compared to the binding affinity of the DARC peptide could be the factor that determines if the engineered mAb has the same or lower potency than the wild-type mAb. If the binding affinity of the mAb is greater than the DARC peptide, the mAb preferentially binds to PvDBP and the GIA of the engineered mAb is the same as the parental mAb. If the binding affinity of the mAb is lower than the DARC peptide, then the DARC peptide preferentially binds to PvDBP and the GIA of the engineered mAb is closer to the GIA of the DARC peptide alone (so the GIA is similar to that of engineered EBL040). In support of this, DB48 had the weakest binding affinity (K_D 5 x 10^{-10}) compared to other community 4 mAbs tested, which had K_Ds in the range of 1 to 7 x 10^{-12},

and engineered DB48 had a similar GIA EC_{50} to engineered EBL040. The binding affinity of the 35-mer DARC peptide to PvDBPII has not been measured yet. Differences in the binding affinity of the DARC peptide compared to the binding affinity of wild-type mAbs may explain some of the differences in behaviour of the mAbs in engineered form. In addition, structural studies of an engineered mAb bound to PvDBP may also offer insights into the mechanism of action of engineered mAbs by indicating how the DARC peptide fused to the Fc region of a PvDBPII-specific mAb engages with PvDBP.

5.5.4 GIA of engineered mAbs against parasites expressing the PvDBPII P variant

For those mAbs which as wild-type mAbs retained GIA against parasites expressing the PvDBPII P variant (compared to their activity against PvDBPII SalI expressing parasites (**Chapter 4.5**)), the engineered mAbs showed similar improvements in potency when tested against PvDBPII P variant parasites as compared to the SalI variant parasites. Out of the panel of mAbs tested, eDB59-35 remained the most potent mAb against PvDBPII P variant parasites. Addition of the 35-mer $DARC_{8-42}$ peptide was able to restore GIA to those mAbs from community 2 and 4, which had lost GIA to PvDBPII P variant parasites as wild-type mAbs. The GIA of eDB1-35 and eDB48-35 was relatively low and similar to the GIA of eEBL040-35, which suggests that the GIA of eDB1-35 and eDB48-35 was from the activity of the DARC peptide only and the variable region of these mAbs did not lead to functional GIA (likely through loss of binding due to polymorphisms). In contrast, eDB62-35, eDB70-35 and eDB95-35, were more potent than eEBL040-35, despite losing GIA against PvDBPII P variant parasites as wild-type mAbs. This suggests that in addition to the activity of the DARC peptide, these three engineered mAbs regained some GIA of the wild-type mAb. One potential explanation for this observation could be that binding of the DARC peptide on the engineered mAb to PvDBP brings the variable region of the mAb closer to PvDBP and this

could allow the variable region of the mAb to bind to PvDBP and overcome its much lower binding affinity (in the case of DB95) or loss of binding to the PvDBPII P variant (DB62 and DB70) (**Chapter 3.9**). The GIA EC_{50} of eEBL040-35 was similar against both PvDBPII SalI and P variant parasites, which suggests that the DARC peptide is able to bind well to both PvDBPII variants. The DARC peptide is thus predicted to bind to all PvDBPII variants and restore at least a moderate level of GIA in engineered mAbs that had lost GIA against any PvDBPII variant in wild-type form.

5.5.5 GIA of engineered mAbs against *P. knowlesi*

The breadth of function of engineered mAbs was next tested against wild-type *P. knowlesi*. Only three wild-type mAbs (DB112, DB133 and DB171) had GIA against PkA1H1 strain (**Chapter 4.6**) and out of these only DB171 was made in engineered form. The majority of the engineered mAbs had a similar level of GIA to eEBL040-35. The GIA EC_{30} of eEBL040-35 was slightly higher against parasites expressing PkDBPα as compared to parasites expressing the PvDBPII SalI and P variants, which suggests that the 35-mer $DARC_{8-42}$ peptide is able to bind PkDBPα but potentially with lower affinity than to PvDBP. This is in concordance with a previous study which showed that this 35-mer DARC peptide was able to inhibit the binding of human RBCs to region II of both PvDBP and PkDBPα (95). Only three of the engineered mAbs eDB171-35, eDB144-35 and eDB59-35 were more potent than eEBL040-35 against PkA1H1. DB171 had a similar GIA in wild-type and engineered form, which is in contrast to the improved GIA potency of engineered DB171 against PvDBP. Engineered DB144 and DB59 regained GIA, which was greater than the GIA of the DARC peptide on its own. This behaviour is similar to those engineered mAbs that regained GIA against parasites expressing the PvDBPII P variant, which was above the GIA from the DARC peptide alone, despite losing GIA to the variant parasites as a wild-type mAb.

Nevertheless, the GIA of eDB59-35 against PkA1H1 was lower than that of DB171, which was the most potent mAb against PkA1H1. The difference in behaviour of engineered mAbs against PvDBP and PkDBPα is likely due to differences in their binding to DARC. Six conserved residues (Y295, N296, K297, R304, L369 and I376) have previously been identified to be essential for DARC to bind to both PvDBP and PkDBPα (132). However, additional residues are involved in DARC binding to PvDBP (63), and these residues are not all identical in PkDBPα. The binding of the 35-mer DARC peptide on the engineered mAbs to PvDBP is likely to differ to its binding to PkDBPα and this could affect the function and GIA potency of the DARC peptide. Similarly, the binding of the variable region of DB171 to PvDBP may also differ slightly compared to PkDBPα and this may explain the lack of improvement in potency of engineered DB171 compared to wild-type DB171 against *P. knowlesi*, which is in contrast to the improved potency of engineered DB171 against *P. vivax*.

The previous structural study of PvDBPII bound to N-terminal DARC showed that DARC residues 20 to 47 are involved in binding to PvDBPII (63). The 35-mer $DARC_{8-42}$ peptide includes the sulphated tyrosine which is essential for binding to PvDBPII but does not include an additional five residues which were seen to interact with PvDBPII (63). A longer DARC peptide fused to the Fc region of anti-PvDBPII mAbs may potentially improve the binding of the DARC peptide and may further improve the GIA potency of engineered mAbs beyond the current most potent mAb eDB59-35.

5.5.6 Conclusion

In this Chapter two different approaches to improve the potency and neutralisation breath of anti-PvDBPII mAbs were tested. Combinations of anti-PvDBPII mAbs did not, in nearly all cases, improve GIA potency and were in fact mostly antagonistic in the GIA assay. The

antagonism between mAbs could be reversed when they were tested in Fab form, which suggests that the mechanism of antagonism could be through steric hindrance between the Fc regions of mAbs that are binding to a relatively small molecule on the parasite. However, the Fabs themselves were in turn less potent than the parental mAbs, thereby not providing an obvious route to improving GIA potency overall. Engineering of mAbs was a more successful method to improve the potency and functional breadth of mAbs. Fusion of a 35-mer DARC peptide to the Fc region of wild-type mAbs was able to significantly improve the GIA potency of mAbs from most epitope communities. The most potent engineered mAb, eDB59-35, was about 3-fold more potent than the most potent wild-type mAb DB62 (which was also strain-specific). The fusion of a DARC peptide also resulted in the engineered mAb regaining GIA that was lost to parasites expressing a PvDBPII variant when the antibody clone was in wild-type mAb format, thereby increasing the inhibitory breadth of the engineered mAbs. However, the GIA of the DARC peptide alone was relatively low. The most potent, strain-transcending engineered mAb, will likely be a mAb that is strain-transcending as a wild-type mAb. Approaches to further improve the design of prophylactic mAbs and *in vivo* experiments to confirm these findings from the *in vitro* GIA assays are discussed in the next Chapter.

6 Conclusions and future directions

6.1 Thesis summary

PvDBP is the leading vaccine candidate against blood-stage *P. vivax* that targets the essential interaction between PvDBP and its receptor DARC on RBCs. Clinical trials have demonstrated that PvDBPII-based vaccines can effectively inhibit parasite growth during CHMI (133), however improvements in vaccine efficacy are required. In this Thesis a large panel of vaccine-induced human mAbs against PvDBPII were characterised to determine what features of the antibody response confer inhibition of *P. vivax* invasion into RBCs. These findings will help to inform the design of the next generation of vaccines and prophylactic antibodies against *P. vivax*.

Chapter 3 describes the isolation of a panel of 163 novel anti-PvDBPII mAbs and analysis of the binding characteristics of these mAbs and their gene sequences. The function of mAbs was assessed in Chapter 4 using *in vitro* assays to test the ability of mAbs to inhibit PvDBPII-DARC binding and their ability to inhibit parasite growth using the transgenic *P. knowlesi* GIA assay (119).

The panel of mAbs were grouped into five epitope communities, with each community showing distinct binding and functional characteristics. Mabs from epitope communities 4 and 5 bind to SD2 of PvDBPII, which contains the DARC binding site (63). Most mAbs in community 5 and a small number of mAbs from community 4 inhibited DARC binding *in vitro*. The majority of these DARC-binding inhibitory mAbs had GIA against the vaccine-homologous PvDBP SalI strain and were able to retain GIA against vaccine-heterologous PvDBP variants. Three DARC-binding inhibitory mAbs were also able to inhibit wild-type *P. knowlesi*, which binds to DARC using PkDBPα, which is highly homologous to PvDBP (132). The ten most potent mAbs in the panel were all from community 4, with DB62 having

the lowest GIA EC_{50} of ~8 µg/mL. However, these potent mAbs were strain-specific and lost GIA against parasites expressing both the PvDBPII P and W1 variants. These community 4 mAbs did not inhibit DARC binding *in vitro*, which is in concordance with them binding within the proposed PvDBP dimerisation site, but not the DARC-binding site (63), and their mechanism of action may be by preventing the formation of a PvDBP-DARC heterotetramer complex during parasite invasion (168). Communities 1, 2 and 3 include mAbs that bind to SD3 and all three communities contained mAbs that inhibit parasite growth. None of these SD3-binding mAbs inhibit DARC binding and their mechanism of GIA is probably through steric hindrance, whereby binding of a mAb to PvDBP prevents it from approaching DARC on the RBC membrane. Community 1 mAbs were notable for their ability to inhibit parasite invasion of both vaccine-heterologous PvDBPII strains that were tested and also include the sentinel mAb DB9, which was previously shown to be broadly inhibitory (118).

Analysis of the full mAb panel showed that faster association rate of binding to PvDBPII was correlated with higher GIA potency. This suggests that PvDBP is only accessible for a short time during merozoite invasion and the potency of mAbs is predominantly determined by how quickly they can bind to their target, as was also seen for *P. falciparum* blood-stage anti-RH5 mAbs (157).

In Chapter 5, two different approaches to improve mAb potency and neutralisation breadth were tested: combining different mAbs and mAb engineering. Combination of mAbs from different epitope communities were predominantly antagonistic in GIA assays. This antagonism likely occurs in the polyclonal antibody response to PvDBPII and could limit the potency of the vaccine-induced antibody response that is achievable against PvDBPII. The mechanism of this antagonism is likely partly mediated through steric hindrance between the Fc regions of the mAbs, which prevents multiple mAbs from being able to simultaneously access PvDBPII, despite binding to non-competing epitope communities *in vitro*.

Using mAb engineering, a selection of the more potent anti-PvDBPII mAbs from different epitope communities were modified by fusion of a 35-mer $DARC_{8-42}$ peptide to the Fc region of the mAb. The most potent community 4 mAbs did not improve in potency in engineered form. In contrast, the GIA potency of mAbs from all other communities improved in engineered form, with many engineered mAbs exceeding the potency of the most potent wild-type mAb DB62. The most potent engineered mAb was eDB59-35 which was about 3-fold more potent than DB62. Addition of the DARC peptide to wild-type mAbs was able to restore GIA to those mAbs that had lost GIA against parasites expressing the PvDBPII P variant but the level of GIA from the DARC peptide was relatively low. This suggests that engineering of a strain-transcending wild-type mAb is more likely to achieve consistently high GIA potency against all PvDBPII variants.

6.2 Future directions

6.2.1 Defining epitopes of mAbs

Defining the epitope of mAbs of interest can identify epitopes that induce more potent parasite growth inhibition or well conserved epitopes that induce strain-transcending antibodies. Epitope information can also inform hypotheses on the mechanism of action of antibodies.

Epitope binning performed on the full panel of anti-PvDBPII mAbs defined five epitope communities (**Chapter 3.6**). The epitope binning method only allowed for grouping of mAbs based on competitive binding for overlapping epitopes, but it did not provide any information on which residues make up the epitopes. Four published anti-PvDBPII mAbs with structurally defined epitopes were included in the epitope binning experiments and one mAb was each binned into communities 1, 3, 4 and 5. This left only the epitope of community 2

experimentally unresolved. Data from SD3-binding ELISAs and from the loss of binding to different PvDBPII variants (**Chapters 3.5, 3.8, 3.9**) allow potential epitopes to be inferred at a low-resolution level. In addition, predictions of Fab-PvDBPII complexes using AlphaFold3 was successful for some mAbs, in particular for mAbs from communities 1 and 2 (**Chapter 3.10**). However, at least half of the mAbs from communities 3, 4 and 5 and mAbs of particular interest such as DB59 were not successfully predicted by AlphaFold3. There were also discrepancies for a small number of mAbs between the epitope binning and binding data and AlphaFold3 predicted binding. AlphaFold3 has been shown to be less accurate in predicting the CDRs of antibodies, which could translate to errors in predicting the epitopes of mAbs (144).

Structural studies are limited in their cost and throughput so only a small number of mAbs can be tested. It would be of particular interest to determine the epitope of DB59, the most potent engineered mAb in the panel; DB171, which is able to inhibit both *P. vivax* and *P. knowlesi* and a potent mAb from community 2. These mAbs of interest have been sent to Dr Greg Martin's group at Iowa State University, USA, who are using cryo-electron microscopy to determine the structure of these Fabs bound to PvDBPII.

To date only structures of PvDBPII with the N-terminal domain of DARC have been published and the remainder of full-length PvDBP has not been resolved. This focus on PvDBPII has been due to it being easier to produce recombinantly and because this region contains the receptor binding domain. It would be of interest to determine the structure of full-length PvDBP bound to DARC as this might reveal additional interactions that could explain the mechanism of action of mAbs or the differences in their potency. Structural studies to date also do not indicate how the two DARC alleles Fya and Fyb, which differ only at residue 42, affect PvDBP binding.

6.2.2 Breadth of GIA against polymorphic PvDBPII variants

The panel of mAbs was tested against three PvDBPII variants in the transgenic *P. knowlesi* GIA assay: the vaccine-homologous PvDBP SalI strain and two vaccine-heterologous variants PvDBPII P and W1. The PvDBPII P and W1 variants cover 15 polymorphisms between them, including an insertion at position 430 in the W1 variant. However, many more polymorphisms have been reported from field isolates worldwide and are not covered by testing only these two PvDBPII variants. A study by Mittal *et al.* reported 31 polymorphic residue positions in PvDBPII (69), 7 of which were found in at least 2% of field isolates globally but are not present in either the PvDBPII P or W1 variants tested in GIA. The study also noted that 24% of interface residues between DB9, a community 1 mAb, and PvDBPII are polymorphic.

The high frequency of polymorphic residues within PvDBPII may mean that there are no truly strain-transcending mAbs, however epitope 1 mAbs are likely to have broader inhibitory activity than SD2-binding mAbs, as most polymorphic residues are found in SD2. The presence of a polymorphic residue will not necessarily result in loss of binding and functional activity of a mAb, but this will require experimental testing to verify. Transgenic *P. knowlesi* parasites with other PvDBPII variants have been made by Prof Moon's group at LSHTM but testing the panel of mAbs against a single strain of transgenic *P. knowlesi* in the GIA assay would be time and labour intensive. A higher throughput method is being developed by Prof Moon's group to allow multiple strains of *P. knowlesi* to be tested simultaneously in a modified GIA assay. These transgenic *P. knowlesi* expressing different PvDBPII variants are barcoded with a short genetic sequence to identify each variant. This allows multiple strains of parasites to be pooled together and tested in the same assay. At assay harvest, the growth of each parasite strain is then determined by sequencing the pool of parasites to determine the number of copies of each variant present. A subset of mAbs that

retained GIA to both PvDBPII P and W1 variants have been sent to Prof Moon's group for them to test using this barcoded sequencing parasite growth inhibition assay. Testing the panel of mAbs systematically against a larger number of PvDBPII variants that cover all commonly found polymorphisms will more accurately determine the true breadth of GIA of these mAbs.

6.2.3 GIA against PvDBP high copy number variants

In addition to polymorphisms within PvDBPII, PvDBP gene amplification has been observed in *P. vivax* isolates from different endemic regions (71,73). High CNV ranging up to 5 copies in some isolates have been found at high frequency in some regions (72,180). The functional significance of PvDBP gene amplification is not yet clear. One hypothesis is that gene amplification may be an immune evasion mechanism, which is supported by a study which showed that a small number of naturally-acquired DARC-binding inhibitory mAbs were less effective against *P. vivax* isolates with PvDBP gene amplification (74). Testing a selection of the novel anti-PvDBPII mAbs against *P. vivax* isolates with different numbers of PvDBP gene copies would confirm these previous findings for mAbs from different epitope communities. It would also be important to measure the magnitude of loss of mAb potency against PvDBP high CNV. These experiments are limited by the availability of *P. vivax* isolates with different number of PvDBP gene copies. To circumvent the use of *P. vivax*, transgenic *P. knowlesi* parasites with multiple copies of PvDBP have been generated by Prof Moon's group. However, additional PvDBP genes may not be functional in transgenic *P. knowlesi* and verification is required that the transgenic *P. knowlesi* with multiple copies of PvDBP express higher levels of PvDBP.

6.2.4 *P. vivax* invasion assays

P. vivax cannot be cultured long-term *in vitro*, which limits the *in vitro* study of *P. vivax* to facilities with access to parasites from infected patients and also limits the scalability of *P. vivax* invasion assays. The transgenic *P. knowlesi* GIA assay has therefore been an invaluable tool for testing the functional activity of the panel of mAbs in this Thesis using parasites that can be cultured long-term *in vitro* (119). The *P. knowlesi* GIA assay has been adapted from the more established *P. falciparum* GIA assay (162) and was shown to correlate with *in vivo P. vivax* parasite growth during CHMI (133). However, there are limitations in using transgenic *P. knowlesi* as a model for *P. vivax*, as the differences in biology between the species mean that transgenic *P. knowlesi* are unlikely to fully recapitulate *P. vivax* invasion of RBCs. The major difference is the tropism of *P. vivax* for reticulocytes, whereas *P. knowlesi* can infect mature human RBCs. This means that there are fewer RBCs *in vivo* that can be infected by *P. vivax* than by *P. knowlesi*. In addition to PvDBP, many other *P. vivax* ligands are involved in reticulocyte invasion (45,48,49) and these may interact with PvDBP in the invasion process but are not found in *P. knowlesi*. Lab-adapted *Plasmodium* strains that have been cultured long-term *in vitro* are also phenotypically different from field isolates (181). Testing a subset of the anti-PvDBPII mAbs in *ex vivo P. vivax* invasion assays would corroborate the findings from the transgenic *P. knowlesi* GIA assays and allow comparison of the potency of mAbs between *P. vivax* and transgenic *P. knowlesi*. A subset of the potent wild-type mAbs from each epitope community and the most potent engineered mAbs have been sent to Prof Jean Popovici's group at Institut Pasteur, Cambodia, to be tested using their *ex vivo P. vivax* invasion assay.

P. vivax ex vivo invasion assays use cryopreserved or fresh clinical isolates of *P. vivax* from infected patients and culture these short-term in blood. Patient isolates are often of low parasitaemia, consist of asynchronous parasites, have polyclonal infections and do not

survive well during *ex vivo* culture. Methods to enrich for *P. vivax* infected reticulocytes are used to increase the parasitaemia of the test samples, using for example Percoll density gradient enrichment or magnetic-activated cell sorting (48,182). Reticulocytes are also added to the culture in some protocols. Different methods to measure parasite growth in these assays are used, including standard microscopy, metabolic labelling or using flow cytometry to measure reticulocyte invasion events (74,182). The method used by Prof Popovici's group consists of Percoll gradient enrichment, addition of reticulocytes and flow cytometry to measure new reticulocyte invasion events in dye-labelled RBCs. Given the strain-specificity of some of the anti-PvDBPII mAbs, it will be useful to obtain the gene sequence(s) of PvDBPII of the *P. vivax* isolate(s) used in the assays and determine the PvDBP gene copy number. The need to use multiple different isolates for larger numbers of experiments is a limitation of *ex vivo P. vivax* invasion assays and can make direct comparisons between mAbs difficult, if different isolates vary in their sensitivity to growth-inhibitory mAbs.

6.2.5 *In vivo* mAb efficacy

Animal models for *P. vivax* have been developed to complement short-term *ex vivo* cultures and clinical studies in humans. Progress has been made in recent years to develop humanised mouse models that can be infected with *P. vivax*. Human liver-chimeric mice were first established by transplanting severely immunodeficient FRG mice with primary human hepatocytes (FRG KO huHep) (183). These mice are susceptible to infection with *P. vivax* sporozoites, that are then able to complete the liver-stage of development (184). To establish *P. vivax* blood-stage infection, the mice must additionally be repopulated with human reticulocytes. This requires further immunosuppression of the mice, which was achieved by backcrossing FRG mice with non-obese diabetic mice (FRGN KO). This FRGN KO mouse

model supported the development of the liver-stage and all blood-stage forms of *P. vivax* and can be used to test the efficacy of blood-stage interventions (185).

The FRGN KO mouse model cannot sustain *P. vivax* blood-stage infection for long periods so efforts have been made to develop mouse models that can support human erythropoiesis and maintain sustained *P. vivax* replication in blood. In the Human Immune System Human Erythrocyte (HIS-HEry) mouse model, immunodeficient mice were engrafted with human haematopoietic stem cells and an additional mutation was introduced that reduces murine haematopoietic cell fitness, which resulted in increased human RBC production (186). This HIS-HEry mouse model was able to maintain blood-stage *P. vivax* growth and supported sexual differentiation and onward transmission to *Anopheles* mosquitoes (186). The level of human RBCs in peripheral blood and peripheral parasitaemia were low, with most of the parasite biomass found in the bone marrow. However, this might actually be more representative of natural *P. vivax* infection in humans, where the spleen and bone marrow are major reservoirs of *P. vivax* (28), so the low parasitaemia may not be an impediment for using this model to test blood-stage interventions.

Prior to development of these humanised mouse models, the only *in vivo* model system available for studying *P. vivax* were non-human primates (NHPs). *P. vivax* strains have been adapted to grow in *Aotus* and *Saimiri* monkeys and used as a model system to test blood-stage interventions including vaccines (33,130). Apart from the ethical considerations of using NHPs, the other limitation of these models is that *P. vivax* field isolates cannot infect these NHPs and the extensively NHP-adapted isolates may significantly differ biologically from field isolates. Comparison of a *de novo* assembly of a *P. vivax* field isolate genome with the NHP-adapted SalI strain showed that many genes were absent from the SalI strain, including a gene encoding an erythrocyte binding protein PvEBP (187), which may be involved in RBC invasion (50).

Given the costs and ethical considerations of the animal models available, initial *in vivo* testing is planned with the most potent engineered mAb eDB59-35 in the FRGN KO humanised mouse model. This will be a proof-of-concept study to confirm that this engineered anti-PvDBPII mAb has *in vivo* efficacy.

Looking further ahead, after selecting the best candidate anti-PvDBPII mAb for clinical development, clinical testing in humans can make use of *P. vivax* CHMI studies, as has been used in the development of *P. falciparum* mAbs (188). The Draper/Minassian group have established a blood-stage *P. vivax* CHMI model using a field isolate from Thailand (W1 variant) (134). This was used to test the efficacy of PvDBPII-based vaccines (133) and any future blood-stage *P. vivax* mAbs can similarly be tested for efficacy by CHMI using the same cryopreserved *P. vivax* isolate.

6.2.6 Antibody engineering

The Draper group have previously tested different construct designs of engineered anti-PvDBPII mAbs fused to a DARC peptide. The different designs included peptides of different lengths and spanning different residues within the 60-amino acid N-terminal domain of DARC. Out of the different designs, the longest peptide, 35-mer $DARC_{8\text{-}42}$ fused to the Fc region of the mAb improved the potency of DB9 the most. This design was therefore used to modify some of the more potent mAbs isolated in this Thesis and led to the identification of a novel highly potent engineered mAb eDB59-35.

Insights gained from testing different designs of engineered mAbs suggest that the fused DARC peptide improved the potency of the mAb through two possible mechanisms. Firstly, the DARC peptide binds to PvDBP and inhibits its binding to native DARC (so acts as a receptor binding inhibitor). Secondly, the DARC peptide adds further bulk to a mAb and this

enhances the steric hindrance, which is likely at least a contributing mechanism of action for many of the mAbs that are not DARC binding inhibitors. This suggests that fusion of a longer DARC peptide may further enhance GIA potency by increased steric hindrance. Additionally, if other contacts outside of $DARC_{8-42}$ are involved in PvDBP binding, then using a longer DARC peptide may also enhance its binding affinity to PvDBP. As a first step, the full 60-mer N-terminal domain of $DARC_{1-60}$ could be fused to DB59 and other potent novel mAbs and their GIA compared to the 35-mer DARC peptide.

Protein design strategies have been used to create a DARC mimetic, that was shown to bind PvDBPII and inhibited its binding to RBCs (189). This or similar DARC mimetics could be fused to anti-PvDBPII mAbs instead of the native sequence of DARC. The synthetic mimetic was designed to increase protein stability and could also be engineered to bind to PvDBP with greater affinity than the native sequence.

Other mAb engineering strategies could be employed to try to enhance anti-PvDBPII mAb efficacy and optimise its production for clinical use (190). Engineering of the Fc region can increase the serum half-life of mAbs, which could help reduce the dose and frequency of administration required for clinical use. The most common approach uses the LS mutation (M428L/N434S), which enhances the binding of the Fc region to the neonatal Fc receptor, prevents lysosomal degradation of the bound IgG and releases it back into circulation (191).

Fc effector functions have not been tested in this mAb panel but previous analysis of vaccine-induced anti-PvDBPII antibodies from the clinical trial found that antibody binding to FcγRs was a significant predictor of parasite growth inhibition during CHMI (146). If any specific Fc effector functions were found to enhance the parasite inhibition activity of anti-PvDBPII mAbs, engineering of the Fc region could also be used to enhance specific Fc effector functions.

Protein engineering could also be used to optimise the lead candidate mAb for clinical use by reducing immunogenicity, improving protein production yields and improving protein stability. Improving the ease of production of mAbs would help keep manufacturing costs down and lower the cost of the clinical product.

Another mAb engineering strategy to potentially explore is the generation of bispecific antibodies, which contain two different antigen binding sites within one antibody. A bispecific design to increase the breadth of function could combine two Fabs with high potency against different PvDBPII variants or different species, for example by combining DB171 Fab for inhibition against *P. knowlesi* with eDB59-35 for high potency against *P. vivax*. Another bispecific mAb design that is being explored by the Draper group for *P. falciparum* RH5 mAbs combines a RH5-specific binding site with a second binding site against a different merozoite surface protein on the same antibody. This could be adapted for anti-PvDBPII mAbs by creating a bispecific mAb that binds to PvDBPII with one arm and to for example PvMSP1 on the second arm. PvMSP1 is an abundant protein on the surface of merozoites, which has also been a target for vaccine development (192). In a bispecific mAb, the Fab binding to PvMSP1 could increase the local concentration of the anti-PvDBPII Fab at the merozoite surface, which could allow the PvDBPII-specific arm to bind with faster association rate when PvDBP is briefly exposed during RBC invasion, thereby potentially improving the potency of the engineered mAb.

6.2.7 Next generation PvDBP vaccines

The clinical trials of vaccines targeting PvDBPII conducted by the Draper group have shown that PvDBPII can induce immunity that inhibits the growth of blood-stage *P. vivax* during CHMI. However, only the protein/adjuvant vaccine, given in a delayed 0-1-14-month dosing

regimen inhibited parasite growth by around 50% (133). Improvements in vaccine efficacy, with shorter dosing regimens, are therefore required. The major challenges to overcome in a PvDBPII-based vaccine are the relatively low potency and strain-specificity of the vaccine-induced antibody response.

One suggestion to improve the efficacy of PvDBPII-based vaccines is to focus on SD2 or specifically on the PvDBP-DARC binding domain (158). This is partly due to many previous studies using the recombinant PvDBPII-DARC binding inhibition assay to measure functional activity of antibodies (115,167). However, analysis of the anti-PvDBPII mAbs in this Thesis showed that direct binding inhibition is not the only mechanism of GIA. In fact, mAbs which were not DARC-binding inhibitors were on average more potent than binding inhibitors in the GIA assay. This difference was mainly driven by the potent mAbs in community 4, which potentially act by preventing PvDBP dimerisation, which is a mechanism that is not detected by the recombinant binding inhibition assay. Although epitope community 4 mAbs were more potent than mAbs from other communities, these potent mAbs were also strain specific. Focussing the immune response only on SD2 would remove epitope communities 1 to 3, which were on average of similar GIA potency to community 5 mAbs, which were mostly DARC-binding inhibitors. Community 1 mAbs were also mostly broadly inhibitory and retained GIA against parasites expressing two vaccine-heterologous PvDBPII variants.

The major advantage of focussing the immune response on the PvDBP-DARC binding site is that these residues are well conserved. Because the interaction is essential for RBC invasion, escape mutations are less likely to occur as they may render the parasite unable to infect RBCs. Focussing the immune response to a smaller epitope area could also be a strategy to remove the antagonism between mAbs from different epitope communities that was observed in this thesis (**Chapter 5.3**).

Another strategy to try to induce more a strain-transcending response is a multi-allele vaccine, which may direct the immune response away from polymorphic residues and towards shared epitopes across the different variants. In one study testing this approach, three PvDBPII variants were tested in combination or on their own and found that although high antibody responses were generated against each variant included in the vaccines, the binding-inhibitory activity was similar between the combined and single allele vaccines (193).

Some polymorphic epitopes within PvDBPII may be more immunodominant and prevent generation of antibodies to epitopes within the well conserved DARC-binding site. An engineered PvDBPII immunogen that removed the immunodominant epitope $DEK_{339\text{-}341}$ was designed and tested in mice (194). The latest iteration of this immunogen called DEKnull-2 improved upon the immunogenicity of earlier versions and induced antibodies that could inhibit parasite invasion *in vitro* (195). DEKnull-2 was able to elicit antibodies that inhibited DARC-binding at a similar level against four vaccine-heterologous PvDBPII variants tested but the potency of the antibodies against the vaccine-homologous strain did not exceed those raised against the PvDBPII SalI strain.

Another engineered immunogen that has been tested in pre-clinical studies consists only of SD1 and SD2 and lacks SD3 (196). This S1S2 immunogen elicited significantly lower antibody titres compared to PvDBPII but slightly higher SD1/SD2-specific titres, suggesting that SD3 within PvDBPII is immunodominant. The function of antibodies induced by the S1S2 immunogen was only compared to PvDBPII using the recombinant PvDBPII-DARC ELISA-based assay. As this assay does not measure parasite inhibitory activity, especially of any SD3-binding antibodies induced by the PvDBPII vaccine, direct comparison of the functional potency of S1S2 to PvDBPII cannot be made.

An immunogen that only consists of SD3 has also been tested, based on the rationale that this subdomain contained the epitope of the broadly-inhibitory mAb DB9 (197). A soluble version of SD3 (called interface) was compared to SD3 and PvDBPII in vaccinations in rabbits and the functional activity of vaccine-induced antibodies was measured using the transgenic *P. knowlesi* GIA assay. Unexpectedly PvDBPII appeared to elicit predominantly SD3-binding antibodies and at lower titres compared to the two SD3-based immunogens but the GIA activity of anti-PvDBPII specific antibodies was similar in potency between the three immunogens tested.

An alternative strategy to immunofocussing could be to increase the size of the immunogen to full-length PvDBP, which may induce antibodies to regions outside of region II that may also have GIA. Ultimately, it may be that a PvDBPII-based vaccine will be remain most effective at inhibiting parasite growth. Antibody concentrations induced by the protein/adjuvant vaccine in the recent clinical trial were high and may not be easily exceeded (133). Improving the efficacy of a PvDBPII vaccine may therefore require the induction of antibodies with higher GIA potency. The main factor that was associated with higher GIA potency of anti-PvDBPII mAbs was a higher association rate of binding to PvDBPII (**Chapter 4.4**). Higher levels of SHM in the antibody variable genes correlated with higher association rate and higher SHM was seen in mAbs isolated from the delayed dosing protein/adjuvant vaccinees compared to the viral-vectored vaccinees. Investigating the effects of modulating vaccine dose, vaccination regimens, vaccine platforms and adjuvants may lead to identification of factors that induce antibodies with faster binding rates, which could increase the GIA potency of PvDBPII-based vaccines.

Achieving a highly efficacious *P. vivax* vaccine will likely require a combination of multiple antigens to be targeted simultaneously. Apart from PvDBP, multiple parasite ligands have been identified to be involved in RBC invasion including the family of PvRBPs (44,45,198),

PvEBP (50) and PvAMA1 (199). In addition, the PTRAMP-CSS-RIPR complex is hypothesised to form an essential invasion scaffold in all *Plasmodium* species, which binds with species-specific invasion proteins (200). In *P. falciparum* this complex includes RH5, the vaccine candidate that has shown clinical efficacy in a Phase 2 clinical trial (135). The RBC-binding proteins of this complex in *P. vivax* remain to be identified. Systematic screening for example using *P. knowlesi* as a model could also help identify new blood-stage vaccine targets (201,202). There is likely redundancy in many of the *P. vivax* invasion pathways but targeting multiple pathways simultaneously may improve vaccine efficacy if sequential critical steps in RBC invasion are inhibited. In addition to targeting the blood-stage, a vaccine combining targets in the pre-erythrocytic and transmission stage of the parasite life-cycle may also be a strategy required to achieve a highly efficacious vaccine against *P. vivax* (203).

6.3 Concluding remarks

Proof of concept for blood-stage malaria vaccines has recently been demonstrated for the *P. falciparum* RH5 vaccine, which showed protective efficacy in a Phase 2 clinical trial. PvDBP remains the only known essential parasite ligand that *P. vivax* requires for invasion into red blood cells. I therefore believe it is worthwhile to pursue PvDBP-based vaccines to target *P. vivax* and hope that the data generated in this Thesis will be built upon to improve the efficacy of future PvDBP-based vaccines. In parallel, recent advances in developing mAbs against *P. falciparum* indicate the potential of using antimalarial mAbs as therapeutic or prophylactic agents. The identification of some of the characteristics that define potent mAbs against PvDBPII in this Thesis will hopefully also contribute to the development of antimalarial mAbs for *P. vivax* in the future.

7 Appendix

7.1 Supplementary Materials and Methods

7.1.1 Buffers

Buffer	Components
ELISA development buffer	16 mL dH_2O 4 mL 5x diethanolamine buffer 20 mg 4-nitrophenylphosphate tablet
C-tag elution buffer	dH_2O 2 M $MgCl_2$ 20 mM Tris-HCl pH 7.4
Plasmodium knowlesi culture medium	500 mL RPMI-1640 2.97 g of HEPES 0.025 g of Hypoxanthine 0.15 g Sodium bicarbonate 1 g D-glucose 10 mL L-glutamine (200 nM) 10 µg/mL gentamicin 20% (vol/vol) heat-inactivated human serum
LDH development buffer	45 mL dH_2O ml 5 mL 1M Tris HCl pH 8.0 0.28 g sodium L-lactate 0.125 mL Triton X-100 10 mg nitro blue tetrazolium tablet 10 µg/mL 3-acetylpyridine adenine dinucleotide 0.2 units/mL diaphorase

7.1.2 PCR Primers

VH-Ext Fwd Mix (heavy chain external forward primer mix, PCR1)		
v4.Vh1a-ext	ATGGACTGGACCTGGAG	53.4
v4.Vh1b-ext	ATGGACTGGATTTGGAGG	51.5
v4.Vh1c-ext	ATGGACTGCACCTGGAG	54.3
v4.Vh2a-ext	ACATACTTTGTTCCACGCTC	52.9
v4.Vh2b-ext	GACACACTTTGCTCCACG	53.9
v4.Vh2c-ext	ATGGACACACTTTGCTACAC	52.9
v4.Vh3a-ext	ATGGAGTTTGGGCTGAG	51.9
v4.Vh3b-ext	ATGGAGTTTTGGCTGAGC	53.0
v4.Vh3c-ext	ATGGAGTTGGGGCTGT	53.5
v4.Vh3d-ext	ATGGAGTTGGGGCTGA	53.2
v4.Vh3e-ext	ATGGAGTTGGGACTGAGC	54.4
v4.Vh3f-ext	ATGGAGTTTGGACTGAGC	52.0
v4.Vh3g-ext	ATGGAGTTTGGGCTTAGC	52.4
v4.Vh3h-ext	CGCTGGGTTTTCCTTG	51.0
v4.Vh3i-ext	GCTGGGTTCTCCTTGTTG	53.5

v4.Vh3j-ext	ATGGAATTGGGGCTGAG	52.0
v4.Vh3k-ext	ATGACGGAGTTTGGGCT	53.9
v4.Vh4a-ext	TGTGGTTCTTCCTCCTCC	53.7
v4.Vh4b-ext	TGTGGTTCTTTCTCCTCC	51.3
v4.Vh4c-ext	CTGTGGTTCTTCCTCCTG	52.3
v4.Vh4d-ext	GTTTTTCCTCCTGCTGGT	52.6
v4.Vh4e-ext	TGTGGTTCTTCCTTCTCC	51.3
v4.Vh4f-ext	TGTGGTTCTTCCTGCTC	51.7
v4.Vh5a-ext	TCAACCGCCATCCTC	51.4
v4.Vh5b-ext	TAAACCCAGGCTCCCCT	52.6
v4.Vh6a-ext	ATGTCTGTCTCCTTCCTCATC	53.6

VH-Ext Rev (heavy chain external reverse primer, PCR1)		
HuIGHG-revO	GTGTTGCTGGGCTTGTG	

VK-Ext Fwd Mix (kappa chain external forward primer mix, PCR1)		
v4.Vk1a-ext	ATGGACATGAGGGTCCC	53.8
v4.Vk1b-ext	ATGGACATGAGGGTGCC	54.8
v4.Vk1c-ext	ATGGACATGATGGTCCCC	54.3
v4.Vk1d-ext	ATGGACATGAGAGTCCTCG	53.6
v4.Vk1e-ext	ATGGACATGAGGGTCCTC	53.6
v4.Vk1f-ext	ATGAGGGTCCCCGCT	56.1
v4.Vk2a-ext	ATGAGGCTCCCTGCTCA	55.9
v4.Vk2b-ext	ATGAGGCTCCTTGCTCAG	54.4
v4.Vk3a-ext	CAGCGCAGCTTCTCTTC	53.7
v4.Vk3b-ext	CCAGCACAGCTTCTTCTTC	53.6
v4.Vk3c-ext	CCAGCTCAGCTTCTCTTC	52.7
v4.Vk4a-ext	ATGGTGTTGCAGACCC	52.3
v4.Vk5a-ext	ATGGGGTCCCAGGTT	52.7
v4.Vk6a-ext	TGCCATCACAACTCATTGG	53.1
v4.Vk6b-ext	CGCCATCACAACTCATTG	51.6

VK-Ext Rev (kappa chain external reverse primer, PCR1)		
IGKCrev-ext	CCTGCTCTGTGACACTCTC	54.9

VL-Ext Fwd Mix (lambda chain external forward primer mix, PCR1)		
v4.Vl1a-ext	ATGGCCTGGTCTCCTC	53.7
v4.Vl1b-ext	CTCTCCTCCTCACCCTC	53.4
v4.Vl2a-ext	CTCTGCTGCTCCTCACTC	54.9
v4.Vl2b-ext	CTGCTGCTCCTCCTCAC	55.3
v4.Vl3a-ext	CTCTCCTTCTGAGCCTCC	54.1
v4.Vl3b-ext	CTCTCCTCCTCAGCCTC	53.8
v4.Vl3c-ext	TTCTCCTCCTCGGCCT	55.2
v4.Vl3d-ext	CCTCTACTTCTCCCCCTC	53.3
v4.Vl3e-ext	CTCCCCCTCCTCACTTTC	54.5
v4.Vl3f-ext	GATCCCTCTCTTCCTCGG	53.9
v4.Vl3g-ext	ATCCCTCTCCTGCTCC	53.0
v4.Vl3h-ext	TCTCTGGCTCACTCTCCTC	55.4
v4.Vl4a-ext	CTGGGTCTCCTTCTACCTACT	54.8
v4.Vl4b-ext	CCACTCCTCCTCCTCTTC	53.8
v4.Vl4c-ext	TTCCTCACCCTCCTCCT	54.5
v4.Vl5a-ext	ACTCCTCTCCTCCTCCTG	54.9
v4.Vl6a-ext	CTGGGCTCCACTACTTCTC	54.4
v4.Vl7a-ext	CCTGGACTCCTCTCTTTCTG	54.2
v4.Vl8a-ext	CTGGATGATGCTTCTCCTC	52.4
v4.Vl9a-ext	CTGCTCCTCACCCTCCT	56.2
v4.Vl10a-ext	TCCTCCTGACCCTCCTC	55.3
v4.Vl10b-ext	GCTCCTCCTGAAATCCTC	52.2

VL-Ext Rev (lambda chain external reverse primer, PCR1)		
IGLCrev-ext	GTCTTCTCCACGGTGCTC	55.4

VH-Int Fwd Mix (heavy chain internal forward primer mix, PCR2)		
v4.Vh1a-int	CTGGAGCATCCTTTTCTTGGTGG	58.2
v4.Vh1b-int	CCTCTTCTTGGTGGCAGCAGC	61.0
v4.Vh1c-int	CTGGAGGGTCTTCTGCTTGCTG	60.0
v4.Vh1d-int	CTCTTTGTGGTGGCAGCAGC	59.4
v4.Vh1e-int	CCTCTTCTTGGTGGGAGCAGC	60.3
v4.Vh1f-int	CCTCTTTTTGGTGGCAGCAGC	59.5
v4.Vh1g-int	CTCCTCTTGGTGGCAGCAGC	61.0

v4.Vh1h-int	CCTTTTCTTGGTGGCAGCAGC	59.5
v4.Vh2a-int	CCTGCTGCTGACCATCCCTTC	60.4
v4.Vh2b-int	CCTGCTACTGACTGTCCCGTC	59.3
v4.Vh2c-int	ACACTCCTGCTGCTGACCACC	59.9
v4.Vh3a-int	GTTGGGACTGAGCTGGATTTTCC	58.1
v4.Vh3b-int	GTTTGGACTGAGCTGGGTTTTCC	58.5
v4.Vh3c-int	GTTTGGGCTGAGCTGGGTTTTC	59.1
v4.Vh3d-int	GTTTTGGCTGAGCTGGGTTTTCC	59.2
v4.Vh3e-int	GGGCTTAGCTGGGTTTTCCTTG	58.5
v4.Vh3f-int	GGGCTGAGCTGGCTTTTTCTTG	59.1
v4.Vh3g-int	GGCTGTGCTGGGTTTTCCTTG	59.3
v4.Vh3h-int	GGCTGAGCTGGGTTTTCCTTG	58.8
v4.Vh3i-int	GTTTGGGCTGAGCTGGATTTTCC	58.8
v4.Vh3j-int	GTTGGGGCTGAGGTGGCTTTTTC	61.0
v4.Vh3k-int	GGCTGAGGTGGGTTTTCCTTG	58.6
v4.Vh3l-int	GGGCTGAGGTGGATTTTCCTTTTG	58.5
v4.Vh4a-int	TTCTTCCTCCTCCTGGTGGC	59.0
v4.Vh4b-int	GGTTCTTTCTCCTCCTGGTGGC	59.9
v4.Vh4c-int	TTCTTCCTCCTGCTGGTGGC	59.8
v4.Vh4d-int	GGTTCTTCCTTCTCCTGGTGGC	59.9
v4.Vh5a-int	TTCTCCAAGGAGTCTGTGCCG	59.1
v4.Vh5b-int	TCCCCTCCACAGTGAGAGTCTG	60.0
v4.Vh6a-int	TCTCCTTCCTCATCTTCCTGCC	58.3

VH-Int Rev (heavy chain internal reverse primer, PCR2)		
HuIGHG-revI	GCTGCTGAGGGAGTAGAGTC	

VK-Int Fwd Mix (kappa chain internal forward primer mix, PCR2)		
v4.Vk1a-int	TGCTGCTCTGGCTCCCA	59.6
v4.Vk1b-int	CTCCTGCTGCTCTGGCTCTC	60.0
v4.Vk1c-int	TCCTGGGGCTCCTGCTACTC	61.0
v4.Vk1d-int	TCCTGCTGCTCTGGTTCCC	59.8
v4.Vk1e-int	TGCAGCTCTGGCTCTCAGGT	61.0
v4.Vk1f-int	CCTGCTGCTCTGTTTCCCAG	58.4
v4.Vk2a-int	CTGGGGCTGCTAATGCTCTG	58.3

v4.Vk2b-int	CTCTTGGGGCTGCTAATGCTC	58.2
v4.Vk3a-int	TCCTGCTACTCTGGCTCCCA	60.1
v4.Vk3d-int	CTCCTGCTACTCTGGCTCACAG	59.0
v4.Vk4a-int	GTTGCTCTGGATCTCTGGTGC	58.0
v4.Vk5a-int	CTTCCTCCTCCTTTGGATCTCTG	56.6
v4.Vk6a-int	GTTTCTGCTGCTCTGGGTTCC	58.5

VK-Int Rev (kappa chain internal reverse primer, PCR2)		
IGKCrev-int	GGAGGGCGTTATCCACCTTCC	59.9

VL-Int Fwd Mix (lambda chain internal forward primer mix, PCR2)		
v4.Vl1a-Int	CACCCTCCTCACTCACTGGTC	59.2
v4.Vl1b-Int	CCTCACTCTCCTCGCTCACTG	59.1
v4.Vl2a-Int	CCTCCTCACTCAGGGCACA	59.2
v4.Vl2b-Int	CACTCTCCTCACTCGGGACAC	59.1
v4.Vl2c-Int	TGCTCCTCACTCTCCTCACTCAG	59.7
v4.Vl3a-Int	CCCTCCTCACTCTCTGCACAG	59.2
v4.Vl3b-Int	CCCTCCTCACTTTCTGCACAG	57.7
v4.Vl3c-Int	GCCTCCTCTCTCACTGCACAG	59.7
v4.Vl3d-Int	AGCCTCCTTGCTCACTTTACAGG	59.0
v4.Vl3e-Int	TCACTCTCCTCACTCTTTGCATAGGT	59.1
v4.Vl3f-Int	CCCCCTCTTCACTCTCTGCA	58.7
v4.Vl3g-Int	TCCCCCTCCTCATTCTCTGC	58.6
v4.Vl3h-Int	CTCGGCGTCCTTGCTTACTG	58.2
v4.Vl3i-Int	CTCAGCCTCCTCGCTCACTG	59.8
v4.Vl4a-Int	CTTCCCTCTCCTCCTCCACTG	58.6
v4.Vl4b-Int	ACTGCCCTTCATTTTCTCCACAG	57.4
v4.Vl5a-Int	TCCTCCTGCTCCTCTCTCACTG	59.8
v4.Vl5b-Int	TCCTCCTGTTCCTCTCTCACTGC	60.0
v4.Vl6a-Int	TTCTCACCCTCCTCGCTCAC	58.8
v4.Vl7a-Int	CTGTTCCTCCTCACTTGCTGC	58.2
v4.Vl8a-Int	CTTCTCCTCGGACTCCTTGCTT	58.6
v4.Vl9a-Int	TCACCCTCCTCAGTCTCCTCAC	59.8
v4.Vl9b-Int	TCCTCCTCCACTGCACAGG	59.2
v4.Vl10a-Int	ACCCTCCTCACTCACTCTGCA	60.0

VK-Int Rev (lambda chain internal reverse primer, PCR2)		
IGLCrev-int	GCTTCTGTGGGACTTCCACTGCTC	61.7

Sequencing Primer	Primer Name	Sequence
IgG VH	3CgCH1	GAAGGTGTGCACGCCGCTG
IgG VH*	IgGRevSeq	GTAGTCCTTGACCAGGCAGC
IgG VK	IGKCrev-intJT1	CTGTACTTTGGCCTCTCTGGG
IgG VL	3Cl	CACCAGTGTGGCCTTGTTGGCTTG

7.1.3 Plasmid maps

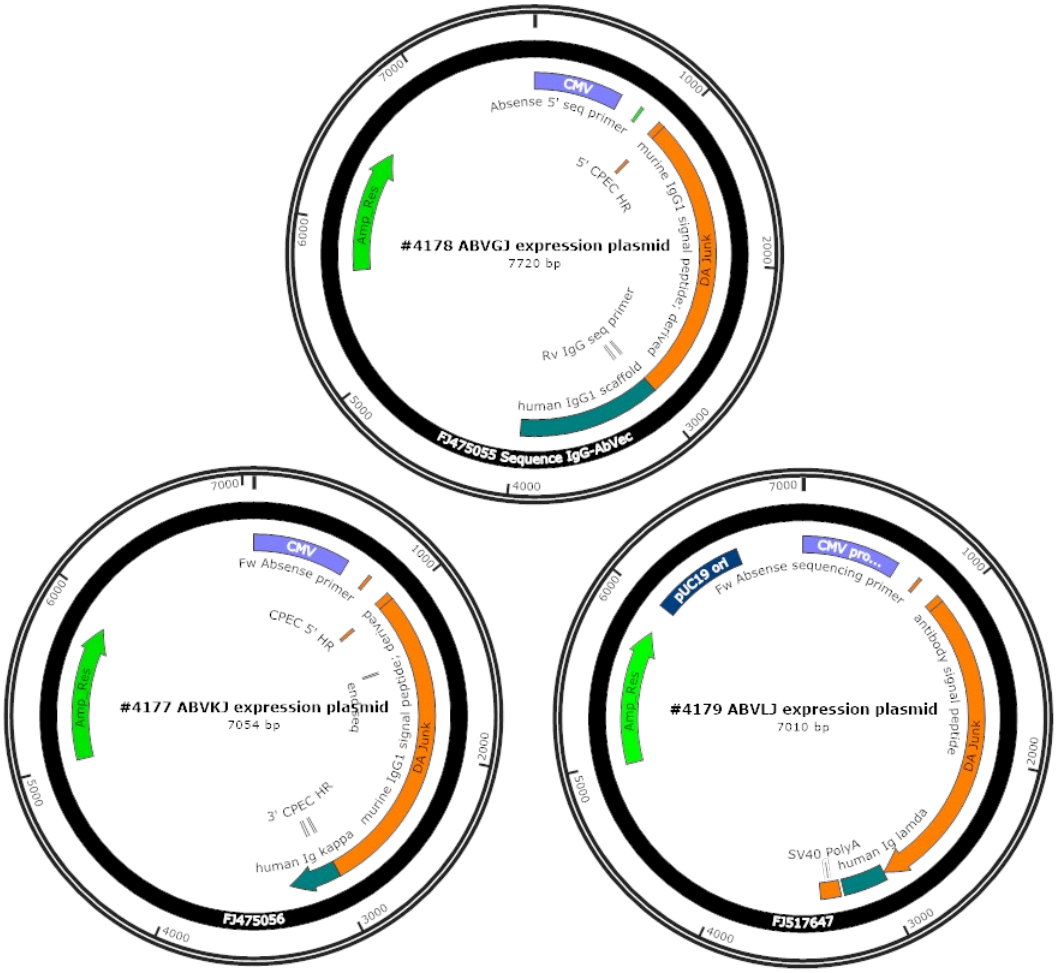

Figure 7.1 AbVec expression plasmids for expression of human IgG1 γ heavy chain (#4178) and κ (#4177) and λ light chains (#4179).

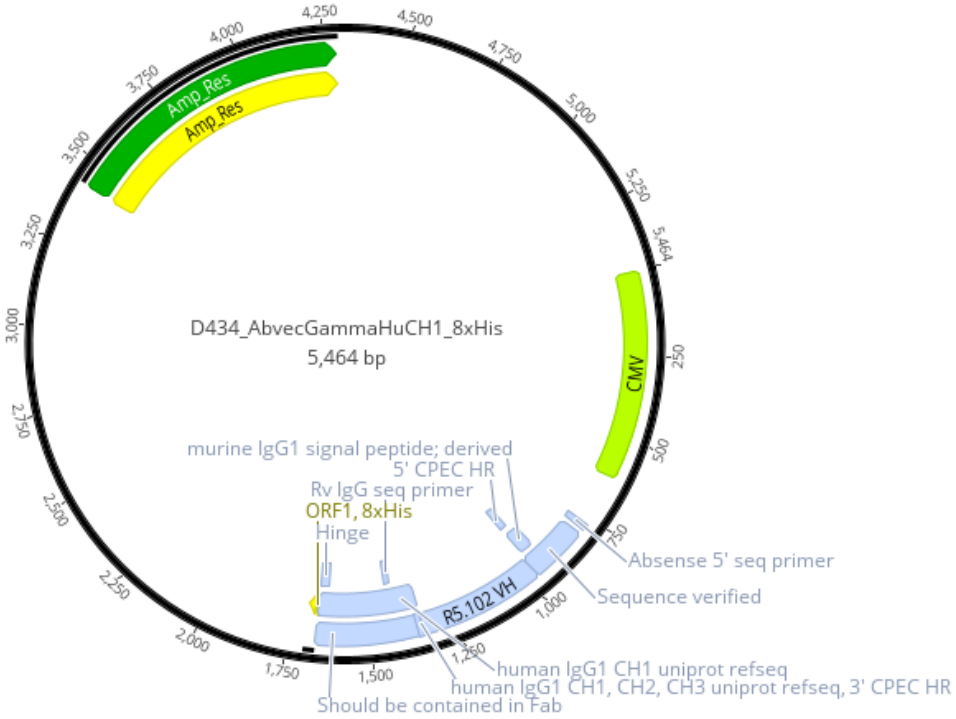

Figure 7.2 Expression plasmid for Fab heavy chain.

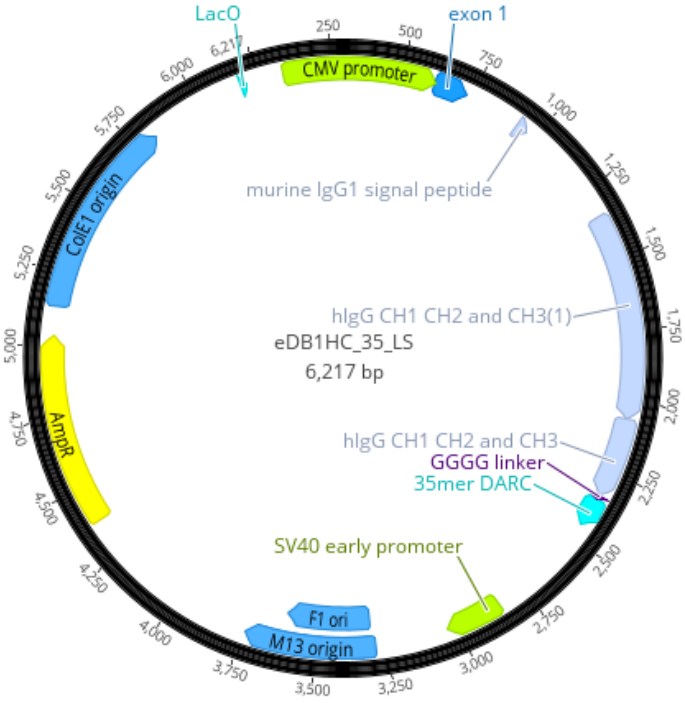

Figure 7.3 Expression plasmid for eDB-35DARC heavy chain.

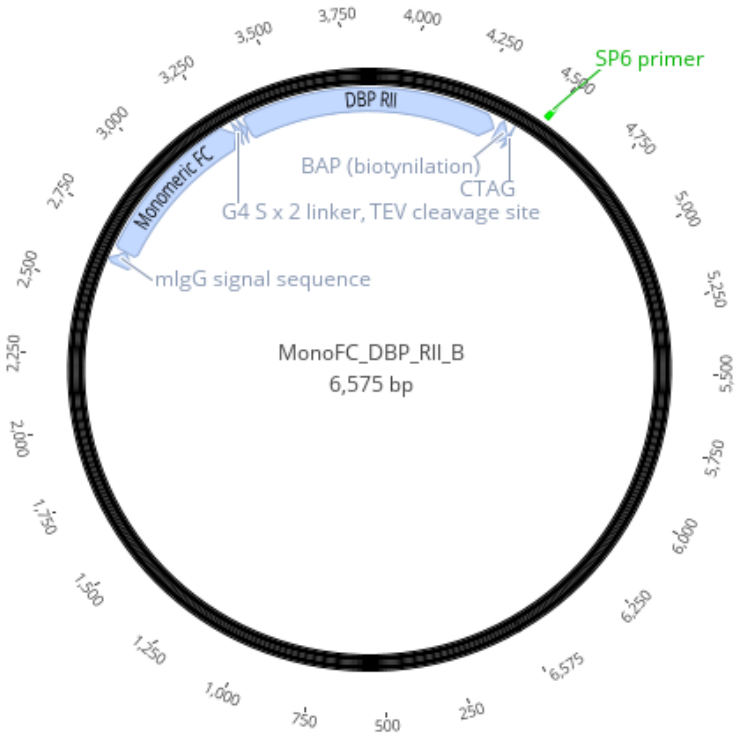

Figure 7.4 Expression plasmid for PvDBPII protein.

7.2 Recombinant proteins

Protein	Amino acid sequence
eDB-DARC	GGGGAELSPSTENSSQLDFEDVWNSSYGVNDSFPDGDYD
nDARC-Fc	MGNCLHRAELSPSTENSSQLDFEDVWNSSYGVNDSFPDGDYDANLEAAAPAHSCNL LDDSGSEPKSCDKTHTCPPCPAPELLGGPSVFLFPPKPKDTLMISRTPEVTCVVVDVS HEDPEVKFNWYVDGVEVHNAKTKPREEQYNSTYRVVSVLTVLHQDWLNGKEYKC KVSNKALPAPIEKTISKAKGQPREPQVYTLPPSREEMTKNQVSLTCLVKGFYPSDIAV EWESNGQPENNYKTTPPVLDSDGSFFLYSKLTVDKSRWQQGNVFSCSVMHEALHNH YTQKSLSLSPGK
PvDBPII SalI subdomain 3	PQIYRWIREWGRDYVSELPTEVQKLKEKCDGKIAYTDKKVCKVPPCQNACKSYDQ WITRKKNQWDVLSNKFISVKNAEKVQTAGIVTPYDILKQELDEFNEVAFENEINKRD GAYIELCVC
PvDBPII SalI variant	DHKKTISSAIINHAFLQNTVMKNCNYKRKRRERDWDCNTKKDVCIPDRRYQLCMKE LTNLVNNTDTNFHRDITFRKLYLKRKLIYDAAVEGDLLLKLNNYRYNKDFCKDIRW SLGDFGDIIMGTDMEGIGYSKVVENNLRSIFGTDEKAQQRRKQWWNESKAQIWTAM MYSVKKRLKGNFIWICKLNVAVNIEPQIYRWIREWGRDYVSELPTEVQKLKEKCDG KINYTDKKVCKVPPCQNACKSYDQWITRKKNQWDVLSNKFISVKNAEKVQTAGIVT PYDILKQELDEFNEVAFENEINKRDGAYIELCVCSVEEAKKNTQEVV
PvDBPII AH variant	DHKKTISSAIINHAFLQNTVMKNCNYKRKRRERDWDCNTKKDVCIPDRRYQLCMKE LTNLVNNTDTNFHSDITFRKLYLKRKLIYDAAVEGDLLLKLNNYRYNKDFCKDIRWS LGDFGDIIMGTDMEGIGYSEVVENNLRSIFGTGEQAQQRRKQWWNESKAQIWTAM MYSVKKRLKGKFIWICKINVAVNIEPQIYRRIREWGRDYVSELPTEVQKLKEKCDGKI NYTDKKVCKVPPCQNACKSYDQWITRKKNQWDVLSNKFKSVKNAEKVQTAGIVTP YDILKQELDEFNEVAFENEINKRDGAYIELCVCSVEEAKKNTQEVV
PvDBPII P variant	DHKKTISSAIINHAFLQNTVMKNCNYKRKRRERDWDCNTKKDVCIPDRRYQLCMKE LTNLVNNTDTNFHSDITFRKLYLKRKLIYDAAVEGDLLFKLNNYRYNKDFCKDIRWS LGDFGDIIMGTDMEGIGYSKVVEDNLRSIFGTGKNAQQHRKQWWNESKAQIWTAM MYSVKKRLKGKFIWICKINVAVNIEPQIYRRIREWGRDYVSELPTEVQKLKEKCDGKI NYTDKKVCKVPPCQNACKSYDQWITRKKNQWDVLSNKFKSVKNAEKVQTAGIVTP YDILKQELDEFNEVAFENEINKRDGAYIELCVCSVEEAKKNTQEVV
PvDBPII W1 variant	DHKKTISSAIINHAFLQNTVMKNCNYKRKRRERDWDCNTKKDVCIPDRRYQLCMKE LTNLVNNTDTNLHSDITFRKLYLKRKLIYDAAVEGDLLLKLNNYRYNKDFCKDIRWS LGDFGDIIMGTDMEGIGYSKVVENNLRSIFGTGKNAQQHRKQWWNETKAQIWRAM MYSVKKRLKGNFIWICKINVAVNIEPQIYRWIREWGRDYVSELPTEVQKLKEKCDGK INYTDKKVCKVLPPCQNACKSYDQWITRKKNQWDVLSNKFISVKNAEKVQTAGIVT PYDILKQELDEFNEVAFENEINKRDGAYIELCVCSVEEAKKNTQEVV

7.3 Antibody gene sequence analysis

mAb	Trial	Volun-teer	IgG sub-class	SD3 binder (ELISA)	Hc V gene family	Hc V gene	Hc SHM (%)	Hc CDR3 length (AA)	Hc CDR3 sequence	Lc V gene family	Lc V gene	Lc SHM (%)	Lc CDR3 length (AA)	Lc CDR3 sequence	Epitope commu-nity
092096	Urusova	NA	NA	N	NA	NA	NA	NA	NA	NA	NA	NA	NA	NA	5
2D10	Carias	NA	NA	Y	NA	NA	NA	NA	NA	NA	NA	NA	NA	NA	3
DB001	VAC051	NA	NA	N	IGHV5	IGHV5-51	1.7	16	ARLAYDSSGYYYAFDI	IGKV1	IGKV1-39	1.7	10	QQSYSTPLIT	4
DB002	VAC051	NA	NA	Y	IGHV4	IGHV4-59	1.4	14	ARHFHSSTAAAFDI	IGKV3	IGKV3-20	2.1	9	QQYGRSPRT	1
DB003	VAC051	NA	NA	Y	IGHV4	IGHV4-30-4	6.4	21	ARSQGYCSSSSCLLPRGYFDY	IGLV1	IGLV1-51	3.7	11	GTWDSSLSAVV	2
DB004	VAC051	NA	NA	Y	IGHV1	IGHV1-69	3.0	14	ARDGGHHGQLVFDY	IGKV1	IGKV1-16	1.4	9	QQYNSYPLT	3
DB005	VAC051	NA	NA	N	IGHV1	IGHV1-46	0.7	21	ARDNSEGAAYYSYYYYGMDV	IGLV1	IGLV1-44	1.0	11	AAWDDSLNGPR	NA
DB006	VAC051	NA	NA	Y	IGHV1	IGHV1-2	2.7	18	ARGLRYSIAWYSDYGLDV	IGKV3	IGKV3-20	1.4	8	QQFGSSLT	1
DB007	VAC051	NA	NA	N	IGHV4	IGHV4-39	2.7	11	ARRSLGYFFGP	IGLV3	IGLV3-21	2.4	11	QLWDTSSDHPV	5
DB008	VAC051	NA	NA	Y	IGHV1	IGHV1-3	2.0	16	ARSYRSSIGWFWMFDY	IGKV4	IGKV4-1	3.0	9	LQYYSIPYT	1
DB009	VAC051	NA	NA	Y	IGHV4	IGHV4-39	1.7	10	ARDGTGALDL	IGKV1	IGKV1-5	5.7	9	QHYNTYPWT	1
DB010	VAC051	NA	NA	N	IGHV3	IGHV3-21	2.7	17	ARDSVAGPFYYFYAMDV	IGLV2	IGLV2-14	1.7	10	SSYTSSSTVV	4
DB011	VAC071	1	NA	Y	IGHV3	IGHV3-30-3	2.4	20	ARDIQTSDTSGYYWAYSFDY	IGLV2	IGLV2-14	2.7	11	SSYTTSSTLVV	3
DB012	VAC071	1	NA	Y	IGHV5	IGHV5-51	1.4	12	ARHVGDSYGFGI	IGKV2	IGKV2D-29	1.3	9	MQSIQLPLT	3
DB017	VAC071	1	NA	Y	IGHV3	IGHV3-30-3	2.7	20	ARDIQTSDTSGYYWAYYFDY	IGLV2	IGLV2-14	2.0	11	SSYTTSSTLVV	3
DB018	VAC071	1	NA	Y	IGHV3	IGHV3-30-3	2.7	20	ARDIQTSDTSGYYWAYSFDY	IGLV2	IGLV2-14	1.3	11	SSYTTSSTLVV	3
DB019	VAC071	1	NA	Y	IGHV3	IGHV3-30	1.4	20	AKEGWGSGSYYKGYYYGMDV	IGKV1	IGKV1-39	2.4	9	QQTYRTPLT	1
DB021	VAC071	1	NA	Y	IGHV3	IGHV3-30-3	3.4	20	ARDIQTSDSSDYYWAFYFDY	IGLV2	IGLV2-14	1.3	11	SSYTTSTTLVV	3
DB022	VAC071	1	NA	Y	IGHV3	IGHV3-30-3	2.7	20	ARDFQTSDSSDYYWAHYFDY	IGLV3	IGLV3-1	2.5	9	QAWDSSTSL	3
DB024	VAC071	1	NA	Y	IGHV3	IGHV3-30	2.4	20	ARDIQTSDSSGFYWAYYFDY	IGLV2	IGLV2-14	2.0	11	SSYTTSSTLVV	3
DB025	VAC071	1	NA	Y	IGHV3	IGHV3-30-3	0.3	20	ARDFQTSDSSDYYWAFYFDY	IGLV2	IGLV2-14	0.7	11	SSYTSSSTLVV	NA
DB026	VAC071	1	NA	Y	IGHV4	IGHV4-59	2.1	20	ARLVCSSSGCLNNHYYGMDV	IGKV1	IGKV1-5	0.3	9	QQYNSYSRT	1
DB027	VAC071	1	NA	Y	IGHV3	IGHV3-30-3	2.7	17	ARDRYNSGYYWGFYFDY	IGLV2	IGLV2-14	1.3	11	SSYTSSSTLVV	3
DB029	VAC071	1	NA	Y	IGHV4	IGHV4-39	2.7	13	ARSQYYYKNWFDP	IGKV3	IGKV3-11	1.7	9	QQRSNWPPS	2
DB031	VAC071	1	NA	Y	IGHV3	IGHV3-30-3	3.0	20	ARDIQTSDTSGYYWAFYFDY	IGLV2	IGLV2-14	3.0	11	SSYTTSSTLVV	3
DB032	VAC071	2	NA	Y	IGHV1	IGHV1-18	2.0	11	ARGLGDAVFDY	IGKV3	IGKV3-15	2.1	9	QQYNNWPRT	2
DB033	VAC071	2	NA	Y	IGHV3	IGHV3-23	2.4	19	AKGGFCSSTSCILTFGFDP	IGLV3	IGLV3-21	1.4	12	QVRDSSSDHLWV	2
DB034	VAC071	2	NA	Y	IGHV4	IGHV4-39	2.0	15	ASHSSGYQYLAGVDY	IGLV1	IGLV1-51	0.3	11	GTWDSSLSAVV	1
DB035	VAC071	2	NA	N	IGHV3	IGHV3-23	1.7	24	AKDLNPRYYDFWSGYYYYYGMDV	IGLV3	IGLV3-1	2.8	9	QAWDSSTSL	NA
DB036	VAC071	2	NA	Y	IGHV1	IGHV1-3	2.7	19	ARGGFSTTANSYFASPLDY	IGLV3	IGLV3-21	2.4	11	QVWDSSSDQWV	2
DB037	VAC071	2	NA	Y	IGHV1	IGHV1-3	2.4	19	ARGGFSTTANSYFASPLDH	IGLV3	IGLV3-21	1.0	11	QVWDRSSDQWV	2

DB041	VAC071	2	NA	Y	IGHV1	IGHV1-18	2.0	21	ARDLRMGDFWSGKYYYYGLDV	IGKV1	IGKV1-39	1.8	9	QQSNSTPWT	NA
DB042	VAC071	2	NA	Y	IGHV3	IGHV3-23	1.7	15	AKDQGQEESQLLFGY	IGLV1	IGLV1-47	0.7	11	AAWDDSLSGVV	1
DB043	VAC071	2	NA	Y	IGHV4	IGHV4-39	1.7	17	ARLLAVAGTVVRMGYDY	IGKV2	IGKV2-28	1.4	8	MQALQGWT	1
DB048	VAC079	4	NA	N	IGHV5	IGHV5-51	2.7	13	ARPGIIGTTDFAY	IGKV2	IGKV2-28	1.0	9	MHTLQILYT	4
DB049	VAC079	4	NA	N	IGHV3	IGHV3-43	1.7	14	AKEYREYYYYGMDV	IGKV3	IGKV3-20	2.1	8	QQYGITPD	5
DB050	VAC079	4	NA	Y	IGHV4	IGHV4-61	6.7	16	ARGPLYSFGPLSGMDV	IGKV3	IGKV3-20	4.2	10	QQYGRSLLFT	1
DB052	VAC079	4	NA	Y	IGHV5	IGHV5-51	7.4	17	ARHFGPGSYRVGGWFDP	IGKV1	IGKV1-39	3.9	9	QQSYSTLYT	1
DB054	VAC079	7	IgG1	N	IGHV3	IGHV3-23	3.0	23	AKDYGEGDYDYVWGSYQNDAFDI	IGLV2	IGLV2-14	1.4	13	CSYTSSSTSRRWV	4
DB055	VAC079	7	IgG1	N	IGHV3	IGHV3-23	6.1	18	AKSDGLLLVGVITGSVDY	IGLV3	IGLV3-21	4.8	11	QVWDSTTDHQV	5
DB056	VAC079	7	IgG1	N	IGHV3	IGHV3-30	5.8	14	ARLRDYVWGSYLDY	IGLV3	IGLV3-19	5.9	13	DSRDIGGDHLGHV	4
DB057	VAC079	7	IgG1	N	IGHV1	IGHV1-24	4.7	12	STETSYASGSYV	IGKV2	IGKV2-28	1.3	9	MQALQTPYT	5
DB058	VAC079	7	IgG1	Y	IGHV3	IGHV3-30	9.5	19	AKDFLQGWSHFFDYYGMDV	IGKV3	IGKV3-11	5.9	9	QQRTNGQPT	2
DB059	VAC079	7	IgG1	N	IGHV3	IGHV3-30	5.5	20	AKVGGISIFEVVPHYNALDV	IGLV3	IGLV3-21	4.2	11	QVWDSSSDRGV	5
DB060	VAC079	7	IgG1	N	IGHV5	IGHV5-10-1	4.1	21	ARKGRLMMFGVVIDHYFGMDV	IGKV1	IGKV1-33	3.9	9	QQYLDLPLA	4
DB061	VAC079	7	IgG1	N	IGHV3	IGHV3-33	3.4	27	ARNYDFWSGYYPDLDLSSEDFDYYMDV	IGLV2	IGLV2-8	0.7	10	SSYAGSNSVV	5
DB062	VAC079	7	IgG1	N	IGHV1	IGHV1-69-2	8.5	14	ATLAGLCRGGSCTI	IGKV2	IGKV2-28	2.0	9	MQVLQTPWT	4
DB070	VAC079	NA	IgG1	N	IGHV1	IGHV1-24	5.8	13	ATTVEVPVYYFDN	IGKV1	IGKV1-39	4.9	9	QQSYSTRLT	4
DB071	VAC079	NA	IgG1	Y	IGHV5	IGHV5-51	3.4	19	ARVMAYSSGRSEDYYSLDV	IGKV1	IGKV1-9	6.0	9	QQLNTYPLT	3
DB072	VAC079	NA	IgG1	Y	IGHV1	IGHV1-69	9.1	14	AKDDPGGATLASAY	IGKV1	IGKV1-9	4.2	9	QQLNSYPLT	3
DB073	VAC079	NA	IgG1	Y	IGHV1	IGHV1-2	9.2	15	ARSIITSSKTRYFDY	IGKV4	IGKV4-1	3.0	9	HHYYSAPYT	1
DB075	VAC079	NA	IgG1	Y	IGHV4	IGHV4-59	2.7	14	TRSQAHYYGSGFDY	IGLV2	IGLV2-8	5.8	10	CSYVGGNHYV	NA
DB076	VAC079	NA	IgG1	Y	IGHV4	IGHV4-59	4.4	17	ARDTRGSSLYSYYGMDV	IGKV2	IGKV2-28	1.7	9	MQGLQTPRT	1
DB077	VAC079	NA	IgG1	Y	IGHV4	IGHV4-59	4.8	17	ARDTRGSSLYSYYGMDV	IGKV2	IGKV2-28	1.0	9	MQGLQTPRT	1
DB079	VAC079	NA	IgG1	Y	IGHV4	IGHV4-4	6.8	16	ARGGYGGNSGFHALDI	IGKV4	IGKV4-1	3.6	9	QQYHSAPRT	1
DB081	VAC079	3	IgG1	Y	IGHV2	IGHV2-70	4.7	22	ARARHSYYYDSSAYYNLYYFDH	IGLV3	IGLV3-19	10.9	10	SSRDSKHNVI	3
DB082	VAC079	3	IgG1	Y	IGHV1	IGHV1-69	9.2	11	ARDRVNQWLFY	IGKV1	IGKV1-13	4.6	9	QQYNSYPFT	3
DB083	VAC079	3	IgG1	Y	IGHV4	IGHV4-59	6.1	16	ARDGYSGSYRGYPFDI	IGKV4	IGKV4-1	2.6	9	QQYYSTPRT	1
DB084	VAC079	5	IgG3	Y	IGHV4	IGHV4-59	5.1	22	ARDRERGYCTTTSCYNSGWFDP	IGKV4	IGKV4-1	0.7	9	QQYYSTPRT	2
DB086	VAC079	5	IgG1	N	IGHV1	IGHV1-69	8.8	22	ARDLSLPPDIVVAAAVDYYFDS	IGKV1	IGKV1-27	2.5	9	QKYNSAPWT	4
DB087	VAC079	5	IgG1	Y	IGHV1	IGHV1-3	2.7	17	ARAGPSGSYNYYYGLDV	IGKV2	IGKV2-28	0.7	9	MQALQTPHT	1
DB088	VAC079	5	IgG3	Y	IGHV1	IGHV1-3	9.5	19	GRGGWESSTPKAGYYGMDV	IGKV1	IGKV1-5	7.1	9	QQYNTYPWT	1
DB089	VAC079	5	IgG1	N	IGHV5	IGHV5-51	2.7	21	ARMLHQVDLDYSVSYDYAFDM	IGKV3	IGKV3-11	3.5	10	QQRRNRPPGS	4
DB090	VAC079	5	IgG1	Y	IGHV4	IGHV4-59	6.9	15	ARMAGGSSYYLGLDV	IGKV4	IGKV4-1	2.0	9	QQYYRTPWT	1
DB091	VAC079	5	IgG1	Y	IGHV4	IGHV4-39	7.4	11	ARLRSYTFFDF	IGKV1	IGKV1-39	10.2	10	QEGYSTPLFT	2
DB092	VAC079	5	IgG1	N	IGHV3	IGHV3-33	4.1	15	ARGVYIVAPNEYLDY	IGLV3	IGLV3-21	3.5	11	QVWDTNSDLGM	5
DB093	VAC079	5	IgG1	Y	IGHV3	IGHV3-48	1.7	14	ARETPVAEGYTFDI	IGLV2	IGLV2-14	2.4	10	SSSTSNSPWV	3
DB094	VAC079	5	IgG1	N	IGHV3	IGHV3-30	6.1	16	AKVYHGDYDDYSHFDD	IGLV6	IGLV6-57	3.7	10	QSYDTSNLYV	5
DB095	VAC079	5	IgG1	Y	IGHV1	IGHV1-3	8.8	19	ARGGYCGSETCYEGNWFDP	IGKV1	IGKV1-39	5.4	8	LQTYRGYT	2

DB096	VAC079	5	IgG1	N	IGHV3	IGHV3-30-3	0.3	15	ARDPYSSGWYHGMDV	IGLV3	IGLV3-1	1.8	9	QTWDSSTVV	NA
DB097	VAC079	5	IgG1	Y	IGHV3	IGHV3-33	7.8	13	AREAHGDSYFFDY	IGKV2	IGKV2D-29	3.7	9	MQSILLPLT	NA
DB098	VAC079	5	IgG1	Y	IGHV3	IGHV3-30-3	2.7	16	ARGLYSSSSHYYSMDV	IGKV1	IGKV1-33	1.8	9	QQYDKLPIT	1
DB099	VAC079	5	IgG1	Y	IGHV3	IGHV3-33	0.7	15	ARGVYIVATIEYFDY	IGLV3	IGLV3-21	0.7	11	QVWDNNSDLGV	NA
DB100	VAC079	5	IgG1	Y	IGHV1	IGHV1-3	10.5	19	ARGGYCSGGDCYHYYGLDF	IGKV1	IGKV1-16	5.6	9	QQYRTYPWT	2
DB101	VAC079	5	IgG1	Y	IGHV1	IGHV1-3	6.8	19	VRGGYCTTTSCYYRSGMDV	IGKV1	IGKV1-16	3.5	9	QQYYSHPPT	2
DB102	VAC079	5	IgG1	Y	IGHV1	IGHV1-18	5.4	20	ARDMGYCGSTDCYRGGWFDP	IGKV1	IGKV1-27	2.1	9	QKYNSAPKT	2
DB103	VAC079	5	IgG1	N	IGHV3	IGHV3-66	6.6	18	ATEIIEMTGYEYYFAMDV	IGLV2	IGLV2-23	3.8	11	CSYGGTYTNWV	5
DB104	VAC079	5	IgG1	N	IGHV3	IGHV3-15	4.3	22	TTAMGGEAWELLGKYDYYGMDV	IGKV1	IGKV1-33	4.6	9	QQYENLPIT	5
DB105	VAC079	5	IgG1	Y	IGHV4	IGHV4-59	9.9	15	ARLGGSYTGDNWFDP	IGLV3	IGLV3-25	5.9	11	QSSDSSGNFVV	3
DB106	VAC079	5	IgG3	N	IGHV3	IGHV3-33	5.4	15	ARGVYIVAPIEKFDY	IGLV3	IGLV3-21	4.2	11	QLWDSSSDLGV	5
DB107	VAC079	5	IgG1	Y	IGHV4	IGHV4-59	4.4	22	ARDRERGFCTTTSCYNSGWFDP	IGKV4	IGKV4-1	2.3	9	QQYYTTPWT	2
DB108	VAC079	5	IgG1	Y	IGHV3	IGHV3-23	6.1	18	AKGGYCSSTNCLYYPMDV	IGKV1	IGKV1-5	1.8	9	QQYNSYLWS	2
DB109	VAC079	5	IgG1	Y	IGHV4	IGHV4-39	1.0	26	ARRRIVATIGEPLASGVAGTGNDMDV	IGKV1	IGKV1-33	0.4	8	QQYDNLFT	4
DB110	VAC079	5	IgG1	N	IGHV3	IGHV3-30	9.2	20	AKASGDRVEGAGAGPEYFQH	IGLV3	IGLV3-25	11.8	13	QAVENNGGYLSWV	NA
DB111	VAC079	5	IgG1	Y	IGHV4	IGHV4-59	6.8	14	ARHMPLSTVAPFDS	IGKV3	IGKV3-20	4.8	9	QQYGSSPRT	1
DB112	VAC079	5	IgG1	N	IGHV3	IGHV3-15	4.7	22	TTGMGGEAWELIGNYDYYGLDV	IGKV1	IGKV1-33	5.3	9	QQYETIPIT	5
DB113	VAC079	5	IgG1	Y	IGHV4	IGHV4-59	10.2	15	ARETLYSSGLSWLDP	IGKV1	IGKV1-6	3.2	9	LQDYTYPRT	1
DB114	VAC079	5	IgG1	Y	IGHV1	IGHV1-18	10.2	13	ARWGVGATHWFDP	IGKV1	IGKV1-39	8.4	10	QQTYNAPPIT	2
DB115	VAC079	5	IgG1	N	IGHV1	IGHV1-24	1.4	12	ATFRGYYSLFDY	IGKV1	IGKV1-33	0.7	9	QQYNNLVCT	4
DB116	VAC079	5	IgG1	Y	IGHV3	IGHV3-23	7.2	19	VKCLGYCSSTTCYVVGMDV	IGKV3	IGKV3-15	2.4	11	QQYNKWPPIFT	2
DB117	VAC079	5	IgG1	Y	IGHV1	IGHV1-18	7.5	15	ARNRSPFSGSYYPSY	IGLV1	IGLV1-40	5.8	11	QSFDASLTDVV	2
DB118	VAC079	6	IgG1	Y	IGHV4	IGHV4-59	6.5	18	ARRIFFPYNNGWYDAFDL	IGKV1	IGKV1-39	5.4	8	QQSYTNAA	3
DB119	VAC079	6	IgG1	N	IGHV2	IGHV2-26	3.0	17	ARIYYDNSGFGDWYFDL	IGLV3	IGLV3-1	4.2	9	QAWDSTTVV	NA
DB121	VAC079	6	IgG1	N	IGHV3	IGHV3-7	5.1	13	ARDSAGISADFDY	IGLV3	IGLV3-1	4.6	9	QAWDSNTFV	5
DB122	VAC079	6	IgG3	Y	IGHV4	IGHV4-59	10.0	16	ARGWRYSGGWFYPFGI	IGKV4	IGKV4-1	2.7	9	QEYYSSQWT	1
DB123	VAC079	6	IgG1	Y	IGHV1	IGHV1-18	13.3	14	ASPTLTIYYYGLNV	IGLV3	IGLV3-19	11.0	11	YSRDSSGHPLV	2
DB124	VAC079	6	IgG1	Y	IGHV4	IGHV4-39	1.3	23	ARRGLGYCSSTSCYWDHSDAFDV	IGKV3	IGKV3-20	0.4	9	QQYGSPLFT	2
DB125	VAC079	6	IgG1	Y	IGHV4	IGHV4-61	8.9	16	ARAGYGGNSRHWYFDH	IGKV1	IGKV1-5	6.4	9	QQYDSYPWT	1
DB126	VAC079	6	IgG1	Y	IGHV4	IGHV4-59	3.4	16	ARHFGNPWSGHFYFDS	IGKV4	IGKV4-1	4.3	9	QQYYSIPLT	1
DB127	VAC079	6	IgG1	Y	IGHV3	IGHV3-23	9.1	20	TKELGYCSSTNCYTLGAFEI	IGKV1	IGKV1-9	5.7	9	QQLNNNLFT	2
DB128	VAC079	6	IgG1	Y	IGHV1	IGHV1-46	4.1	17	ARGYFAMSIVVRYGMDV	IGKV2	IGKV2-28	1.0	8	MQALQTVT	1
DB129	VAC079	6	IgG1	Y	IGHV1	IGHV1-69	6.8	12	ATDGAAGLSFDY	IGKV2	IGKV2-40	6.3	9	MQRIEYPYT	3
DB130	VAC079	6	IgG1	Y	IGHV3	IGHV3-23	4.4	19	AKHPRGACSGGSCYSPFDY	IGKV3	IGKV3-20	2.8	9	QQYGGSPWT	2
DB131	VAC079	6	IgG1	N	IGHV1	IGHV1-69	6.1	19	AREGLEMGDVDAQYDYFDS	IGKV1	IGKV1-39	3.5	10	QQSYSNPPFT	5
DB132	VAC079	6	IgG1	Y	IGHV3	IGHV3-23	8.8	19	AKAGFCSSTNCYWTMWLDP	IGKV1	IGKV1-27	1.4	10	QKYYSAPPWT	2
DB133	VAC079	6	IgG1	N	IGHV1	IGHV1-24	2.7	17	AIILRGSGTYYSDGFDI	IGLV3	IGLV3-1	3.9	9	QAWDRSTAL	3

DB134	VAC079	6	IgG1	Y	IGHV1	IGHV1-69	5.8	16	ATGYSGSVFFSLAFDF	IGKV3	IGKV3-20	2.8	9	QKYGSSPFT	1
DB135	VAC079	6	IgG1	Y	IGHV3	IGHV3-66	3.8	16	ARDLRGYGIYSYGLDV	IGLV1	IGLV1-51	3.4	11	GTWDSSLNAVV	3
DB136	VAC079	6	IgG1	N	IGHV1	IGHV1-69	6.4	13	ARGRPGGYYHFDY	IGLV3	IGLV3-21	5.9	11	QVWDSTSAHWV	4
DB137	VAC079	6	IgG1	N	IGHV1	IGHV1-69	7.2	16	ASGQTTFGVVLDGFDI	IGKV3	IGKV3D-15	5.9	10	LQYYNWPPAS	4
DB138	VAC079	6	IgG1	Y	IGHV3	IGHV3-33	9.9	15	ARDRADYTGSYYFDH	IGKV2	IGKV2D-29	3.7	9	MQSILLPLT	3
DB139	VAC079	6	IgG1	Y	IGHV2	IGHV2-5	4.0	15	AHRQHYDFWSGYFSD	IGKV1	IGKV1-13	3.5	10	QQFNRYFSIT	1
DB140	VAC079	6	IgG1	N	IGHV1	IGHV1-24	3.4	22	ATMKWDAMVPSASLLEGWYFDL	IGLV1	IGLV1-44	3.7	11	VVWDESLNGWV	5
DB141	VAC079	6	IgG1	N	IGHV2	IGHV2-70	9.0	20	ARIVSHYYGPGKTSYQPFDY	IGLV1	IGLV1-47	6.1	11	AAWDESLSGWV	4
DB142	VAC079	6	IgG1	Y	IGHV4	IGHV4-59	4.8	18	ARLAPPWYSARHWGALDI	IGKV4	IGKV4-1	5.6	9	QQYSSFPYT	1
DB143	VAC079	6	IgG1	Y	IGHV1	IGHV1-46	4.7	17	ARGYFTMSIPVRYGLDV	IGKV2	IGKV2-28	3.1	8	MQSLQAVT	1
DB144	VAC079	6	IgG1	N	IGHV1	IGHV1-18	13.7	11	ARSAEVTGTTE	IGLV3	IGLV3-21	9.1	11	QVWDSGSDRWV	4
DB146	VAC079	6	IgG1	Y	IGHV1	IGHV1-3	4.8	12	ATGGSGTYFEVF	IGKV1	IGKV1-39	3.5	10	QQSYSTPTWT	2
DB147	VAC079	6	IgG1	Y	IGHV1	IGHV1-69	3.7	17	ARLWVGSTSHYYFGMDV	IGKV2	IGKV2-28	1.3	9	MQALQTPHT	1
DB149	VAC079	6	IgG1	Y	IGHV1	IGHV1-69	5.5	24	ARRNCSGGSCFSVHLVWDNYGMDV	IGKV1	IGKV1-9	2.1	9	QQLNTYPRT	2
DB150	VAC079	6	IgG3	Y	IGHV4	IGHV4-59	2.7	15	ARAFRGTGYHFGMDV	IGKV1	IGKV1-9	1.0	9	QQLNSYPRT	1
DB152	VAC079	6	IgG1	Y	IGHV4	IGHV4-59	5.5	15	SRAFRGTGYHFGLDV	IGKV1	IGKV1-9	1.7	9	QQLNGYPRT	1
DB153	VAC079	6	IgG1	Y	IGHV4	IGHV4-59	3.8	16	ARHFGTPWSGHFYFDS	IGKV4	IGKV4-1	5.0	9	QQFYSSPYT	1
DB154	VAC079	6	IgG1	Y	IGHV3	IGHV3-23	3.0	19	AKDGHYDSVGNYYFLAMAY	IGKV1	IGKV1-13	1.7	9	QQFKSHPRT	1
DB155	VAC079	6	IgG1	N	IGHV1	IGHV1-24	4.8	18	ATPVVVTALAFAWDGFDF	IGLV1	IGLV1-44	2.7	11	AAWDDSLNGWV	5
DB156	VAC079	6	IgG1	Y	IGHV4	IGHV4-59	4.1	16	ARHFGSPWSAHFYFDS	IGKV4	IGKV4-1	2.3	9	QQYRRPPLT	1
DB157	VAC079	6	IgG1	N	IGHV3	IGHV3-23	2.4	23	AKGTTEYLERFLEWLPVNDGFDM	IGLV2	IGLV2-23	2.4	12	CSYEDSSTPHWV	5
DB158	VAC079	6	IgG1	N	IGHV1	IGHV1-2	4.8	13	ARQLEDGHDAFGI	IGLV3	IGLV3-1	2.1	9	QAWDSSTWV	NA
DB159	VAC079	6	IgG1	N	IGHV3	IGHV3-53	4.1	22	ARGSPHKYDDSSTYYLHDGFDM	IGLV3	IGLV3-19	2.4	11	NSRDNSGNHWV	4
DB160	VAC079	7	IgG1	Y	IGHV1	IGHV1-69	6.4	14	ARDGPNSAYAAFDY	IGKV2	IGKV2-40	2.3	9	MQRIEFPHT	3
DB161	VAC079	7	IgG1	N	IGHV4	IGHV4-39	4.0	28	ARHVGGRWDYDLWSGDSDPYYYYYAMDV	IGLV2	IGLV2-14	2.4	10	SSYTSSNTRV	NA
DB162	VAC079	7	IgG1	N	IGHV3	IGHV3-74	5.1	16	ARGGDDDYGGYVTFDH	IGKV1	IGKV1-33	2.5	9	QQYRNLPIT	4
DB163	VAC079	7	IgG1	N	IGHV1	IGHV1-24	2.4	25	AIVKLPDTTDYEYVWGSYRQTWFAL	IGKV3	IGKV3-20	2.1	10	QQYGSSPPIT	5
DB164	VAC079	7	IgG1	Y	IGHV1	IGHV1-69	9.8	13	AREFGSGTYVDVY	IGKV1	IGKV1-16	4.6	9	QQYDSFPLT	3
DB165	VAC079	7	IgG1	N	IGHV1	IGHV1-46	4.1	17	SRDDSRGFSYGADPFDF	IGLV3	IGLV3-21	3.5	11	HVWDSSNDHYV	NA
DB166	VAC079	7	IgG1	N	IGHV4	IGHV4-4	11.1	14	ARDSTLPTLIPFDF	IGKV1	IGKV1-39	6.0	9	QQNYRTPYT	4
DB167	VAC079	7	IgG2	Y	IGHV4	IGHV4-59	3.8	16	ARGGKLHSSGWYYFDY	IGKV3	IGKV3-20	2.1	9	QQYGSSPLT	1
DB168	VAC079	7	IgG1	N	IGHV1	IGHV1-69-2	4.8	21	ASPLGWGGLQYCSGGNCWVDF	IGLV2	IGLV2-14	3.4	10	NSYTSRNTRV	4
DB169	VAC079	7	IgG1	Y	IGHV3	IGHV3-30-3	11.5	17	AKEDNGSHSGGVDAFDI	IGKV3	IGKV3-11	4.2	9	QQRSSWPPV	NA
DB170	VAC079	7	IgG1	N	IGHV3	IGHV3-64D	1.7	18	VKEYYYGPGNYRGGAFDI	IGKV1	IGKV1-33	1.8	9	QQYDNLPYT	4
DB171	VAC079	7	IgG1	N	IGHV3	IGHV3-15	5.6	20	TTVGSITMFGVVVTNEDFDY	IGLV2	IGLV2-14	2.0	11	RSYTDSSTLVL	4
DB172	VAC079	7	IgG2	N	IGHV4	IGHV4-4	5.1	24	ARTLLEYCSGVGCPTNYYYYGMDV	IGLV2	IGLV2-14	3.4	10	SSYRSTSTLV	NA
DB173	VAC079	7	IgG1	Y	IGHV1	IGHV1-69	8.4	14	ARDGQFSGYVSFDY	IGKV2	IGKV2-40	4.6	9	MQRIEFPYT	3

DB174	VAC079	7	IgG1	N	IGHV4	IGHV4-59	4.1	18	ARDSSGHYLHDSAHGLDI	IGLV3	IGLV3-1	3.2	9	QAWDSNTVV	5
DB175	VAC079	7	IgG1	N	IGHV1	IGHV1-69	3.5	15	HSFINDDYGDSDHDY	IGKV2	IGKV2-30	1.0	9	MQVTHWPWT	5
DB176	VAC079	8	IgG3	Y	IGHV1	IGHV1-3	13.9	18	ARGGFCASAGCYQIWFDP	IGKV1	IGKV1-27	6.0	8	QTYKSDPL	2
DB177	VAC079	8	IgG1	Y	IGHV4	IGHV4-30-4	6.4	15	ARSWDMYTNMWYFDL	IGLV2	IGLV2-14	5.8	10	TSYRDNRGVV	1
DB178	VAC079	8	IgG1	Y	IGHV3	IGHV3-20	9.5	15	ARDYEGVGAYYGMDV	IGKV1	IGKV1-39	6.0	9	QHSHSSPVT	3
DB180	VAC079	8	IgG1	Y	IGHV3	IGHV3-48	4.4	14	ARGLGWEFLRIFEH	IGKV3	IGKV3-15	1.4	9	QQYNNWPLT	1
DB181	VAC079	8	IgG1	Y	IGHV4	IGHV4-59	10.3	15	ARAAAGTGYYFGLNV	IGKV1	IGKV1-5	2.5	6	QQYNRM	1
DB182	VAC079	8	NA	Y	IGHV2	IGHV2-70	5.6	16	ARILRYSSGWPYYFDS	IGLV8	IGLV8-61	6.1	10	ALYLGRGISV	1
DB183	VAC079	8	IgG1	Y	IGHV1	IGHV1-18	4.4	17	ARRYTLSSGHSPWGFDH	IGKV2	IGKV2-28	2.4	9	MQALQTRAT	1
DB184	VAC079	8	IgG1	Y	IGHV4	IGHV4-59	5.5	15	AREARGTGYSMGLDN	IGKV4	IGKV4-1	4.3	9	QQYYRSPQT	1
DB185	VAC079	8	IgG1	Y	IGHV4	IGHV4-59	4.1	17	ARDYITAAGTRSFGFDY	IGKV1	IGKV1-39	6.7	9	QQSYRAPRT	1
DB186	VAC079	8	IgG1	Y	IGHV4	IGHV4-34	7.3	15	ATRYSSSWYGWPYGN	IGKV4	IGKV4-1	4.0	9	HQYYSLPYT	1
DB188	VAC079	8	IgG1	Y	IGHV4	IGHV4-34	7.8	18	ARGRKWLRSSRPLYYFDF	IGKV4	IGKV4-1	2.3	9	QQYYSAPYT	1
DB189	VAC079	8	IgG2	Y	IGHV3	IGHV3-74	6.8	17	VRGDIVASIVLFGYFDY	IGKV4	IGKV4-1	2.3	10	QQYSSTQLYT	1
DB190	VAC079	8	IgG2	Y	IGHV4	IGHV4-61	8.6	15	ARTWGGSYGTHYFDH	IGKV3	IGKV3-20	3.5	9	QQYGSSPRT	1
DB191	VAC079	8	IgG1	Y	IGHV1	IGHV1-69	8.5	16	ARGGYGGNSGHNYFDY	IGKV4	IGKV4-1	4.3	9	QQYYRTQYT	1
DB192	VAC079	8	IgG1	Y	IGHV3	IGHV3-74	2.4	17	ARAPYSGSYYYHFGMDV	IGKV2	IGKV2-28	3.3	8	MQALQTPT	1
DB193	VAC079	8	IgG2	Y	IGHV4	IGHV4-31	7.0	16	ARETRYSSGWGFGLDV	IGKV2	IGKV2-28	1.3	9	MQARQSPYT	1
DB194	VAC079	8	IgG4	Y	IGHV4	IGHV4-61	5.7	15	ARVPSYGGLRWYIDF	IGKV4	IGKV4-1	5.0	9	QQYFTTPLT	1
DB195	VAC079	8	IgG1	Y	IGHV4	IGHV4-59	8.7	15	ARAQAGTGYYFGMDV	IGKV1	IGKV1-5	4.3	6	QQYNRM	1
DB196	VAC079	8	IgG1	Y	IGHV4	IGHV4-59	4.8	17	ARDAVIAAGTRSLGFDY	IGKV1	IGKV1-39	4.2	9	QQGYSSPRT	1
DB197	VAC079	8	IgG1	Y	IGHV4	IGHV4-59	7.6	14	ARSYNNYPGNWFDP	IGKV1	IGKV1-39	4.9	9	QQSYNSPRT	1
DB198	VAC079	8	IgG1	Y	IGHV1	IGHV1-2	4.4	16	ARSYCSSVGCFWPMDY	IGKV4	IGKV4-1	4.6	9	HQYFSLPWT	1
DB199	VAC079	8	IgG1	Y	IGHV3	IGHV3-23	10.5	19	AKDWWGYGGFARKPEYFDS	IGKV1	IGKV1-27	4.5	9	QSYNSGLLT	1
DB200	VAC079	8	IgG1	Y	IGHV1	IGHV1-2	8.4	19	ARDEALTTSSFVWYHGMGL	IGLV2	IGLV2-14	7.5	10	SSYTSSNSYV	1
DB201	VAC079	8	IgG1	Y	IGHV4	IGHV4-59	5.8	15	AREARGTGYSFGLDR	IGKV4	IGKV4-1	3.0	9	HQYYTTPQT	1
DB202	VAC079	8	IgG1	Y	IGHV3	IGHV3-74	6.8	17	VRGSYSGSVFYHFGMDV	IGKV2	IGKV2-28	6.0	8	MQALQTPT	1
DB203	VAC079	8	IgG1	N	IGHV3	IGHV3-23	3.4	22	AKDQPPYYYDSSDYYMHDGFDM	IGLV3	IGLV3-19	2.1	11	NSRDSSVNHRV	4
DB204	VAC079	8	IgG1	Y	IGHV1	IGHV1-69	10.5	16	AREGYGGHTGMNAFDI	IGKV4	IGKV4-1	4.0	9	QQYHTLPWS	1
DB205	VAC079	8	IgG1	Y	IGHV1	IGHV1-69	8.1	16	AREGYGGHSGMNAFDI	IGKV4	IGKV4-1	2.3	9	QQYHSTPWT	1
DB206	VAC079	8	IgG1	Y	IGHV1	IGHV1-58	7.8	17	AAARHCSSVGCYFAFDI	IGKV4	IGKV4-1	5.0	9	QQYHSIPYS	1
DB207	VAC079	8	IgG1	Y	IGHV5	IGHV5-51	8.6	14	TTTAFGDSDHFFDF	IGKV1	IGKV1-16	6.0	9	LQYYTYPIT	3

7.4 PvDBPII variant binding

mAb	Epitope comm-unity	Final designated variant binding	ELISA variant binding	Kinetic variant binding 04/2025	Sall kon	Sall koff	Sall KD	P kon	P koff	P KD	W1 kon	W1 koff	W1 KD	Kinetic variant binding 09/2024
092096	5	Sall_P_W1	NA	Sall_P_W1	6.12E+06	4.13E-05	6.76E-12	8.84E+06	7.63E-05	8.62E-12	2.83E+07	3.90E-05	1.38E-12	Sall_P
2D10	3	Sall_P_W1	NA	Sall_P_W1	1.37E+06	2.41E-04	1.76E-10	1.83E+06	2.64E-04	1.44E-10	4.07E+06	8.91E-03	2.19E-09	Sall_P_W1
DB001	4	Sall	Sall	NA	NA	NA	NA	NA	NA	NA	NA	NA	NA	NA
DB002	1	Sall_P_W1	Sall_AH_P_W1	Sall_P_W1	4.38E+05	1.17E-05	2.68E-11	7.40E+05	1.50E-04	2.03E-10	2.65E+06	1.28E-04	4.82E-11	Sall_P_W1
DB003	2	Sall_W1	Sall_W1	Sall_W1	2.26E+06	1.07E-03	4.73E-10	NA	NA	NA	1.01E+07	9.60E-04	9.48E-11	Sall_W1
DB004	3	Sall_P	Sall_AH_P	Sall_P	1.03E+06	4.95E-04	4.82E-10	1.23E+06	5.83E-04	4.76E-10	NA	NA	NA	NA
DB005	NA	Sall_W1	Sall_W1	Sall_W1	2.50E+05	5.77E-05	2.31E-10	NA	NA	NA	2.40E+06	4.33E-05	1.80E-11	NA
DB006	1	Sall_P_W1	Sall_AH_P_W1	Sall_P_W1	3.21E+05	1.32E-04	4.13E-10	3.10E+05	1.16E-04	3.76E-10	3.85E+06	1.10E-04	2.86E-11	Sall_P_W1
DB007	5	Sall_W1	Sall_AH_P_W1	Sall_W1	7.22E+05	1.45E-04	2.01E-10	NA	NA	NA	6.18E+06	1.68E-04	2.72E-11	NA
DB008	1	Sall_P_W1	Sall_AH_P_W1	Sall_P_W1	4.32E+05	7.80E-05	1.81E-10	6.33E+05	3.61E-05	5.70E-11	2.00E+06	1.14E-04	5.71E-11	Sall_P_W1
DB009	1	Sall_P_W1	Sall_AH_P_W1	Sall_P_W1	2.17E+06	3.54E-04	1.63E-10	3.41E+06	2.32E-04	6.80E-11	5.05E+06	1.87E-04	3.70E-11	Sall_P_W1
DB010	4	Sall	Sall_AH_P_W1	Sall	2.37E+06	3.49E-04	1.47E-10	NA	NA	NA	NA	NA	NA	Sall
DB011	3	Sall_P	Sall_AH_P	NA	NA	NA	NA	NA	NA	NA	NA	NA	NA	Sall_P
DB012	3	Sall_P	Sall_AH_P	NA	NA	NA	NA	NA	NA	NA	NA	NA	NA	Sall_P
DB017	3	Sall_P	Sall_AH_P	Sall_P	1.27E+06	9.19E-04	7.22E-10	1.64E+06	7.74E-04	4.72E-10	NA	NA	NA	Sall_P
DB018	3	Sall_P	Sall_AH_P	Sall_P	1.51E+06	4.78E-04	3.16E-10	2.03E+06	4.05E-04	2.00E-10	NA	NA	NA	Sall_P
DB019	1	Sall_P_W1	Sall_AH_P_W1	Sall_P_W1	4.90E+05	1.00E-04	2.05E-10	7.82E+05	1.11E-04	1.42E-10	3.20E+06	1.00E-04	3.13E-11	Sall_P_W1
DB021	3	Sall_P	Sall_AH_P_W1	Sall_P	1.63E+06	1.37E-03	8.41E-10	1.23E+06	1.14E-03	9.25E-10	NA	NA	NA	Sall_P
DB022	3	Sall_P	Sall_AH_P	Sall_P	1.91E+06	1.58E-03	8.24E-10	1.07E+06	1.72E-03	1.61E-09	NA	NA	NA	Sall_P
DB024	3	Sall_P	Sall_AH_P	Sall_P	1.02E+06	3.45E-04	3.37E-10	1.35E+06	2.95E-04	2.19E-10	NA	NA	NA	Sall_P
DB025	NA	Sall_P	Sall_AH_P	NA	NA	NA	NA	2.83E+05	1.06E-03	3.75E-09	NA	NA	NA	Sall_P
DB026	1	Sall_P_W1	Sall_AH_P_W1	NA	NA	NA	NA	NA	NA	NA	3.31E+06	2.49E-04	7.54E-11	NA
DB027	3	Sall_P	Sall_AH_P_W1	Sall_P	1.26E+06	6.48E-05	5.16E-11	2.33E+06	1.72E-04	7.37E-11	NA	NA	NA	Sall_P
DB029	2	Sall_W1	Sall_AH_P_W1	Sall_W1	1.72E+06	1.77E-03	1.03E-09	NA	NA	NA	4.25E+06	7.01E-04	1.65E-10	Sall_W1
DB031	3	Sall_P	Sall_AH_P	Sall_P	4.52E+05	3.56E-04	7.88E-10	9.24E+05	3.60E-04	3.89E-10	NA	NA	NA	Sall_P
DB032	2	Sall_W1	Sall_AH_P_W1	NA	NA	NA	NA	NA	NA	NA	4.49E+06	2.05E-02	4.56E-09	Sall_W1
DB033	2	Sall_W1	Sall_W1	Sall_W1	2.69E+06	1.16E-03	4.29E-10	NA	NA	NA	8.37E+06	5.01E-04	5.99E-11	Sall_W1
DB034	1	Sall_P_W1	Sall_AH_P_W1	Sall_P_W1	9.41E+05	5.54E-04	5.88E-10	1.64E+06	5.69E-04	3.47E-10	5.39E+06	3.15E-03	5.84E-10	Sall_P_W1
DB035	NA	Sall	Sall_AH	NA	NA	NA	NA	NA	NA	NA	NA	NA	NA	NA
DB036	2	Sall_W1	Sall_W1	Sall_W1	1.65E+06	1.46E-02	8.85E-09	NA	NA	NA	8.31E+06	1.28E-02	1.54E-09	Sall_W1
DB037	2	Sall_W1	Sall_W1	NA	NA	NA	NA	NA	NA	NA	NA	NA	NA	NA
DB041	NA	Sall_W1	Sall_AH_P_W1	NA	NA	NA	NA	NA	NA	NA	NA	NA	NA	Sall_W1

DB042	1	SalI_P_W1	SalI_AH_P_W1	SalI_P	1.39E+06	2.31E-03	1.65E-09	5.46E+05	2.04E-03	3.73E-09	NA	NA	NA	SalI_P_W1
DB043	1	SalI_P_W1	SalI_AH_P_W1	SalI_P_W1	1.93E+05	3.01E-04	1.56E-09	3.11E+05	6.06E-04	1.95E-09	1.09E+06	6.02E-04	5.54E-10	SalI_P_W1
DB048	4	SalI	NA	SalI	3.44E+06	1.66E-03	4.82E-10	NA	NA	NA	NA	NA	NA	SalI
DB049	5	SalI_P_W1	SalI_AH_P_W1	SalI_P_W1	3.10E+06	2.88E-03	9.29E-10	4.71E+06	1.45E-03	3.07E-10	7.62E+06	4.81E-03	6.31E-10	SalI_P_W1
DB050	1	SalI_P_W1	SalI_AH_P_W1	SalI_P_W1	7.00E+05	1.22E-04	1.74E-10	7.10E+05	2.51E-04	3.53E-10	2.22E+06	2.04E-04	9.21E-11	SalI_P_W1
DB052	1	SalI_P_W1	SalI_AH_P_W1	SalI_P_W1	3.27E+05	1.00E-05	3.06E-11	3.82E+05	3.18E-05	8.34E-11	1.57E+06	6.23E-05	3.98E-11	SalI_P_W1
DB054	4	SalI	SalI	NA	NA	NA	NA	NA	NA	NA	NA	NA	NA	SalI
DB055	5	SalI_W1	SalI_AH_P_W1	SalI_W1	1.95E+06	3.28E-03	1.68E-09	NA	NA	NA	1.28E+07	7.63E-03	5.94E-10	SalI_W1
DB056	4	SalI	SalI_AH_P_W1	SalI	3.32E+06	5.56E-05	1.68E-11	NA	NA	NA	NA	NA	NA	SalI
DB057	5	SalI_P_W1	SalI_AH_P_W1	SalI_P_W1	2.47E+06	5.64E-03	2.28E-09	9.25E+05	4.23E-03	4.57E-09	7.85E+06	1.82E-02	2.32E-09	SalI_P_W1
DB058	2	SalI_P_W1	SalI_AH_P_W1	SalI_P_W1	1.88E+06	6.86E-04	3.65E-10	2.39E+06	1.22E-04	5.09E-11	6.39E+06	5.38E-04	8.42E-11	SalI_P_W1
DB059	5	SalI_P_W1	SalI_AH_P_W1	SalI_P_W1	4.17E+06	1.87E-03	4.48E-10	4.27E+05	1.87E-03	4.37E-09	1.02E+07	8.57E-04	8.38E-11	SalI_P_W1
DB060	4	SalI_P_W1	SalI_AH_P_W1	SalI_P_W1	3.37E+06	8.08E-05	2.40E-11	5.92E+06	4.02E-05	6.78E-12	7.26E+06	6.16E-05	8.49E-12	SalI_P_W1
DB061	5	SalI_W1	SalI_W1	SalI_W1	2.18E+06	4.42E-05	2.03E-11	NA	NA	NA	5.65E+06	1.41E-04	2.49E-11	SalI_W1
DB062	4	SalI	SalI	SalI	5.75E+06	1.00E-05	1.74E-12	NA	NA	NA	NA	NA	NA	SalI
DB070	4	SalI	SalI_AH_P_W1	SalI	4.89E+06	3.34E-05	6.82E-12	NA	NA	NA	NA	NA	NA	SalI
DB071	3	SalI_P	SalI_AH_P_W1	SalI_P	1.09E+06	1.83E-04	1.68E-10	1.35E+06	2.77E-04	2.06E-10	NA	NA	NA	SalI_P
DB072	3	SalI_P_W1	SalI_AH_P_W1	SalI_P	2.02E+06	1.00E-05	4.95E-12	3.10E+06	1.00E-05	3.23E-12	NA	NA	NA	SalI_P_W1
DB073	1	SalI_P_W1	SalI_AH_P_W1	SalI_P_W1	5.17E+05	1.00E-05	1.94E-11	1.92E+06	1.42E-05	7.42E-12	5.10E+06	2.19E-05	4.29E-12	SalI_P_W1
DB075	NA	SalI	SalI_AH_P_W1	NA	NA	NA	NA	NA	NA	NA	NA	NA	NA	SalI
DB076	1	SalI_P_W1	SalI_AH_P_W1	SalI_P_W1	1.15E+06	7.92E-05	6.86E-11	1.19E+06	1.46E-04	1.22E-10	5.03E+06	6.77E-05	1.35E-11	SalI_P_W1
DB077	1	SalI_P_W1	SalI_AH_P_W1	SalI_P_W1	1.97E+06	3.29E-05	1.67E-11	2.74E+06	5.00E-05	1.83E-11	7.88E+06	6.02E-05	7.64E-12	SalI_P_W1
DB079	1	SalI_P_W1	SalI_AH_P_W1	SalI_P_W1	6.21E+05	1.00E-05	1.61E-11	2.40E+06	1.00E-05	4.16E-12	7.18E+06	3.39E-05	4.73E-12	SalI_P_W1
DB081	3	SalI_P_W1	SalI_AH_P_W1	SalI_P_W1	3.94E+05	1.00E-05	2.54E-11	5.02E+05	1.00E-05	1.99E-11	5.60E+06	1.47E-03	2.63E-10	SalI_P_W1
DB082	3	SalI_P_W1	SalI_AH_P_W1	SalI_P_W1	1.08E+05	1.00E-05	9.27E-11	5.53E+06	1.00E-05	1.81E-12	5.92E+06	9.28E-03	1.57E-09	SalI_P_W1
DB083	1	SalI_P_W1	SalI_AH_P_W1	SalI_P_W1	3.72E+05	1.00E-05	2.69E-11	4.60E+05	1.00E-05	2.17E-11	2.57E+06	8.70E-05	3.39E-11	SalI_P_W1
DB084	2	SalI_W1	SalI_AH_P_W1	SalI_W1	2.64E+06	9.49E-04	3.60E-10	NA	NA	NA	7.26E+06	3.75E-04	5.17E-11	SalI_W1
DB086	4	SalI_P_W1	SalI_AH_P_W1	SalI_P_W1	4.57E+06	1.92E-05	4.20E-12	6.60E+06	1.00E-05	1.52E-12	2.42E+06	1.00E-05	4.13E-12	SalI_P_W1
DB087	1	SalI_P_W1	SalI_AH_P_W1	SalI_P_W1	4.24E+05	6.73E-05	1.59E-10	7.32E+05	7.35E-05	1.00E-10	1.76E+06	1.85E-04	1.05E-10	SalI_P_W1
DB088	1	SalI_P_W1	SalI_AH_P_W1	SalI_P_W1	4.90E+05	1.00E-05	2.04E-11	2.25E+06	4.31E-05	1.92E-11	4.53E+06	5.95E-05	1.31E-11	SalI_P_W1
DB089	4	SalI	SalI	SalI	4.27E+06	6.31E-05	1.48E-11	NA	NA	NA	NA	NA	NA	SalI
DB090	1	SalI_P_W1	SalI_AH_P_W1	SalI_P_W1	2.49E+06	1.00E-05	4.02E-12	4.27E+06	1.26E-04	2.96E-11	2.93E+06	1.00E-05	3.41E-12	SalI_P_W1
DB091	2	SalI_P_W1	SalI_AH_P_W1	SalI_P_W1	4.13E+06	1.11E-05	2.68E-12	2.59E+06	1.32E-05	5.10E-12	1.27E+07	3.06E-05	2.41E-12	SalI_P_W1
DB092	5	SalI_P_W1	SalI	SalI_P_W1	2.37E+06	1.68E-04	7.09E-11	4.64E+06	1.61E-04	3.46E-11	1.35E+07	4.42E-04	3.26E-11	SalI_P_W1
DB093	3	SalI_P	SalI_AH_P	SalI_P	3.58E+05	1.68E-04	4.67E-10	4.77E+05	2.65E-04	5.55E-10	NA	NA	NA	SalI_P
DB094	5	SalI_P_W1	NA	SalI_P_W1	2.52E+06	2.68E-04	1.06E-10	5.24E+06	3.35E-04	6.40E-11	7.17E+06	2.89E-04	4.03E-11	SalI_P_W1
DB095	2	SalI_P_W1	SalI_W1	SalI_P_W1	2.02E+06	1.18E-04	5.83E-11	1.94E+04	1.49E-04	7.69E-09	7.60E+06	5.34E-05	7.03E-12	SalI_W1
DB096	NA	SalI_P	SalI_AH_P	NA	NA	NA	NA	8.88E+05	3.50E-03	3.93E-09	NA	NA	NA	SalI_P
DB097	NA	SalI_P	SalI_AH_P_W1	SalI_P	2.06E+06	8.61E-05	4.19E-11	2.76E+06	7.88E-05	2.85E-11	NA	NA	NA	SalI_P

DB098	1	SalI_P_W1	SalI_AH_P_W1	SalI_P_W1	3.06E+05	1.00E-05	3.27E-11	3.30E+05	1.00E-05	3.03E-11	2.89E+06	1.00E-05	3.46E-12	SalI_P_W1
DB099	NA	SalI_P_W1	NA	SalI_P_W1	1.21E+06	2.12E-03	1.76E-09	1.83E+06	3.46E-03	1.89E-09	3.44E+06	2.36E-03	6.84E-10	SalI_P_W1
DB100	2	SalI_W1	SalI_AH_P_W1	NA	NA	NA	NA	NA	NA	NA	NA	NA	NA	SalI_W1
DB101	2	SalI_P_W1	SalI_AH_P_W1	SalI_P_W1	2.41E+06	4.24E-05	1.76E-11	2.11E+04	5.34E-04	2.53E-08	5.57E+06	5.08E-05	9.13E-12	SalI_P_W1
DB102	2	SalI_W1	SalI_AH_P_W1	SalI_W1	1.86E+06	1.08E-04	5.79E-11	NA	NA	NA	6.37E+06	1.02E-04	1.61E-11	SalI_W1
DB103	5	SalI_P_W1	SalI	SalI_P	5.27E+05	1.83E-05	3.46E-11	4.12E+05	5.50E-03	1.33E-08	NA	NA	NA	SalI_P_W1
DB104	5	SalI_P_W1	SalI_AH_P_W1	SalI_P_W1	6.36E+06	2.89E-05	4.55E-12	1.06E+07	1.00E-05	9.44E-13	1.36E+07	1.68E-04	1.24E-11	SalI_P_W1
DB105	3	SalI_P	SalI_AH_P_W1	NA	NA	NA	NA	1.07E+05	7.02E-04	6.59E-09	NA	NA	NA	SalI_P
DB106	5	SalI_P_W1	SalI_AH_P_W1	NA	NA	NA	NA	NA	NA	NA	NA	NA	NA	NA
DB107	2	SalI_W1	SalI_W1	SalI_W1	6.85E+06	2.94E-04	4.29E-11	NA	NA	NA	3.78E+07	2.62E-04	6.93E-12	SalI_W1
DB108	2	SalI_W1	SalI_P_W1	SalI_W1	2.66E+06	3.23E-04	1.21E-10	NA	NA	NA	7.85E+06	2.17E-04	2.76E-11	SalI_W1
DB109	4	SalI	SalI_W1	NA	NA	NA	NA	NA	NA	NA	NA	NA	NA	SalI
DB110	NA	SalI_W1	SalI_AH_P_W1	NA	NA	NA	NA	NA	NA	NA	5.25E+06	2.99E-02	5.70E-09	SalI_W1
DB111	1	SalI_P_W1	SalI_AH_P_W1	SalI_P_W1	2.11E+06	1.00E-05	4.75E-12	2.67E+06	1.68E-05	6.28E-12	8.28E+06	1.00E-05	1.21E-12	NA
DB112	5	SalI_P_W1	SalI_W1	SalI_P_W1	8.63E+06	3.04E-05	3.52E-12	1.73E+07	3.55E-05	2.05E-12	3.82E+07	2.52E-04	6.61E-12	SalI_P_W1
DB113	1	SalI_P_W1	SalI_AH_P_W1	NA	NA	NA	NA	1.65E+06	3.92E-05	2.37E-11	5.60E+04	1.00E-05	1.79E-10	NA
DB114	2	SalI_P_W1	SalI_AH_P_W1	SalI_P_W1	2.08E+06	1.00E-05	4.81E-12	2.74E+06	1.00E-05	3.64E-12	8.05E+06	1.00E-05	1.24E-12	SalI_P_W1
DB115	4	SalI_P_W1	SalI_AH_W1	NA	NA	NA	NA	NA	NA	NA	NA	NA	NA	SalI_P_W1
DB116	2	SalI_W1	SalI_W1	SalI_W1	4.34E+06	9.79E-05	2.26E-11	NA	NA	NA	1.10E+07	5.75E-05	5.24E-12	SalI_W1
DB117	2	SalI_P_W1	SalI_AH_P_W1	SalI_P_W1	2.56E+06	1.29E-05	5.04E-12	7.21E+05	4.94E-05	6.86E-11	7.55E+06	2.48E-05	3.28E-12	SalI_P_W1
DB118	3	SalI_P_W1	SalI_AH_P_W1	SalI_P_W1	8.45E+06	2.89E-05	3.42E-12	1.19E+07	1.00E-05	8.39E-13	2.39E+07	1.56E-04	6.52E-12	NA
DB119	NA	SalI_P_W1	SalI_AH_P_W1	SalI_P_W1	1.33E+06	2.27E-05	1.71E-11	5.39E+05	1.00E-05	1.85E-11	4.72E+06	6.36E-05	1.35E-11	NA
DB121	5	SalI_W1	SalI	SalI_W1	3.79E+05	2.26E-04	5.96E-10	NA	NA	NA	1.54E+06	6.05E-03	3.92E-09	NA
DB122	1	SalI_P_W1	SalI_AH_P_W1	SalI_P_W1	2.00E+06	1.00E-05	5.00E-12	2.28E+06	2.60E-05	1.14E-11	7.10E+06	1.00E-05	1.41E-12	SalI_P_W1
DB123	2	SalI_P_W1	SalI_AH_P_W1	SalI_P_W1	4.17E+06	1.00E-05	2.40E-12	1.17E+06	7.84E-04	6.70E-10	1.10E+07	1.00E-05	9.06E-13	SalI_P_W1
DB124	2	SalI_W1	SalI_W1	SalI_W1	2.29E+06	1.37E-02	5.95E-09	NA	NA	NA	7.94E+06	4.51E-03	5.68E-10	SalI_W1
DB125	1	SalI_P_W1	SalI_AH_P_W1	SalI_P_W1	5.62E+05	2.91E-05	5.17E-11	1.94E+06	4.08E-05	2.10E-11	6.10E+06	2.57E-05	4.20E-12	NA
DB126	1	SalI_P_W1	SalI_AH_P_W1	SalI_P_W1	5.27E+05	1.00E-05	1.90E-11	6.86E+05	5.91E-05	8.62E-11	3.42E+06	4.42E-05	1.29E-11	SalI_P_W1
DB127	2	SalI_W1	SalI_W1	SalI_W1	4.79E+06	4.61E-04	9.61E-11	NA	NA	NA	1.04E+07	2.59E-04	2.50E-11	SalI_W1
DB128	1	SalI_P_W1	SalI_AH_P_W1	SalI_P_W1	2.10E+06	2.91E-05	1.38E-11	3.06E+06	1.00E-05	3.27E-12	1.01E+07	1.25E-04	1.24E-11	SalI_P_W1
DB129	3	SalI_P_W1	SalI_AH_P_W1	SalI_P_W1	3.69E+06	1.00E-05	2.71E-12	7.96E+06	1.00E-05	1.26E-12	7.81E+06	2.94E-03	3.76E-10	NA
DB130	2	SalI_W1	SalI_W1	SalI_W1	2.36E+06	6.87E-05	2.92E-11	NA	NA	NA	8.74E+06	3.95E-05	4.52E-12	SalI_W1
DB131	5	SalI_P	SalI	SalI_P	7.49E+06	4.72E-05	6.30E-12	1.56E+07	1.00E-05	6.41E-13	NA	NA	NA	NA
DB132	2	SalI_W1	SalI_W1	SalI_W1	4.60E+06	2.44E-05	5.31E-12	NA	NA	NA	1.17E+07	5.54E-05	4.73E-12	NA
DB133	3	SalI_P_W1	SalI_AH_P_W1	SalI_P_W1	2.61E+06	1.00E-05	3.83E-12	2.32E+06	4.73E-05	2.04E-11	4.27E+06	4.01E-05	9.37E-12	SalI_P_W1
DB134	1	SalI_P_W1	SalI_AH_P_W1	SalI_P_W1	1.93E+06	1.00E-05	5.17E-12	2.41E+06	1.36E-05	5.66E-12	7.97E+06	1.00E-05	1.25E-12	SalI_P_W1
DB135	3	SalI_P	SalI_AH_P_W1	SalI_P	6.60E+05	1.00E-05	1.52E-11	2.06E+06	1.00E-05	4.85E-12	NA	NA	NA	NA
DB136	4	SalI_P	SalI_AH_P_W1	SalI_P	4.20E+06	1.00E-05	2.38E-12	3.26E+06	1.16E-03	3.55E-10	NA	NA	NA	SalI_P
DB137	4	SalI_P_W1	SalI_AH_P_W1	SalI_P_W1	9.73E+06	1.00E-05	1.03E-12	1.45E+07	1.56E-05	1.08E-12	2.05E+07	1.00E-05	4.89E-13	SalI_P_W1

DB138	3	SalI_P_W1	SalI_AH_P_W1	SalI_P_W1	4.24E+06	1.00E-05	2.36E-12	6.09E+06	1.00E-05	1.64E-12	4.94E+06	1.01E-02	2.05E-09	SalI_P_W1
DB139	1	SalI_P_W1	SalI_AH_P_W1	SalI_P_W1	3.46E+06	1.00E-05	2.89E-12	5.21E+06	1.00E-05	1.92E-12	7.27E+06	1.00E-05	1.38E-12	SalI_P_W1
DB140	5	SalI_W1	SalI_AH_P_W1	SalI_W1	1.17E+07	1.00E-05	8.55E-13	NA	NA	NA	3.06E+07	2.56E-05	8.37E-13	SalI_W1
DB141	4	SalI	SalI	SalI	2.85E+05	7.39E-04	2.59E-09	NA	NA	NA	NA	NA	NA	SalI
DB142	1	SalI_P_W1	SalI_AH_P_W1	SalI_P_W1	7.86E+05	3.33E-05	4.23E-11	2.27E+06	1.75E-05	7.72E-12	8.29E+06	6.71E-05	8.10E-12	SalI_P_W1
DB143	1	SalI_P_W1	SalI_AH_P_W1	NA	NA	NA	NA	NA	NA	NA	NA	NA	NA	SalI_P_W1
DB144	4	SalI_P_W1	SalI	NA	NA	NA	NA	NA	NA	NA	NA	NA	NA	SalI_P_W1
DB146	2	SalI_W1	SalI_W1	SalI_W1	4.28E+06	1.00E-05	2.33E-12	NA	NA	NA	1.07E+07	4.32E-05	4.04E-12	SalI_W1
DB147	1	SalI_P_W1	SalI_AH_P_W1	SalI_P_W1	3.65E+05	1.00E-05	2.74E-11	4.87E+05	1.00E-05	2.05E-11	7.41E+05	1.00E-05	1.35E-11	SalI_P_W1
DB149	2	SalI_P_W1	SalI_AH_W1	SalI_W1	1.15E+06	2.42E-05	2.11E-11	NA	NA	NA	6.95E+06	8.47E-05	1.22E-11	SalI_P_W1
DB150	1	SalI_P_W1	SalI_AH_P_W1	NA	NA	NA	NA	NA	NA	NA	3.01E+06	1.61E-02	5.36E-09	SalI_P_W1
DB152	1	SalI_P_W1	SalI_AH_P_W1	SalI_P_W1	2.94E+06	1.00E-05	3.40E-12	1.85E+06	5.80E-05	3.13E-11	2.23E+06	1.00E-05	4.49E-12	SalI_P_W1
DB153	1	SalI_P_W1	SalI_AH_P_W1	SalI_P_W1	4.60E+05	1.00E-05	2.17E-11	4.64E+05	1.00E-05	2.15E-11	2.38E+05	1.00E-05	4.21E-11	SalI_P_W1
DB154	1	SalI_P_W1	SalI_AH_P_W1	NA	NA	NA	NA	NA	NA	NA	6.60E+06	1.00E-05	1.51E-12	NA
DB155	5	SalI_P_W1	SalI_AH_P_W1	SalI_P_W1	8.94E+06	1.00E-05	1.12E-12	1.30E+07	2.08E-05	1.60E-12	2.48E+07	1.03E-03	4.16E-11	SalI_P_W1
DB156	1	SalI_P_W1	SalI_AH_P_W1	SalI_P_W1	4.78E+05	1.00E-05	2.09E-11	4.92E+05	1.00E-05	2.03E-11	4.60E+06	6.89E-05	1.50E-11	SalI_P_W1
DB157	5	SalI_P	SalI_AH_P	SalI_P	2.49E+06	6.81E-05	2.73E-11	1.92E+06	3.36E-04	1.75E-10	NA	NA	NA	SalI_P
DB158	NA	SalI_P_W1	SalI_AH	NA	NA	NA	NA	NA	NA	NA	NA	NA	NA	NA
DB159	4	SalI	SalI	SalI	2.21E+05	1.00E-05	4.53E-11	NA	NA	NA	NA	NA	NA	SalI
DB160	3	SalI_P_W1	SalI_AH_P_W1	SalI_P_W1	3.66E+06	2.53E-05	6.91E-12	6.51E+06	1.00E-05	1.54E-12	1.93E+06	1.70E-03	8.82E-10	SalI_P_W1
DB161	NA	SalI_P_W1	SalI_AH_P_W1	SalI_P_W1	1.08E+06	1.14E-04	1.06E-10	3.09E+06	2.23E-04	7.23E-11	9.79E+06	2.90E-04	2.96E-11	SalI_P_W1
DB162	4	SalI	SalI_AH	SalI	3.06E+06	1.00E-05	3.27E-12	NA	NA	NA	NA	NA	NA	SalI
DB163	5	SalI_W1	SalI_AH_P_W1	SalI_W1	3.45E+06	3.02E-04	8.77E-11	NA	NA	NA	8.16E+06	4.59E-04	5.62E-11	SalI_W1
DB164	3	SalI_P_W1	SalI_AH_P_W1	SalI_P_W1	1.34E+02	1.00E-05	7.44E-08	2.65E+06	1.00E-05	3.78E-12	4.55E+06	3.73E-03	8.20E-10	SalI_P_W1
DB165	NA	SalI_P_W1	SalI_P_W1	SalI_P_W1	5.20E+05	2.32E-04	4.46E-10	4.57E+05	3.18E-03	6.96E-09	2.93E+06	1.84E-04	6.27E-11	SalI_P_W1
DB166	4	SalI	SalI_AH_P_W1	SalI	2.22E+06	1.00E-05	4.51E-12	NA	NA	NA	NA	NA	NA	SalI
DB167	1	SalI_P_W1	SalI_AH_P_W1	SalI_P_W1	4.84E+05	1.00E-05	2.07E-11	5.12E+05	1.00E-05	1.95E-11	4.04E+06	7.17E-05	1.77E-11	SalI_P_W1
DB168	4	SalI	SalI_AH_W1	SalI	2.79E+06	2.64E-04	9.49E-11	NA	NA	NA	NA	NA	NA	SalI
DB169	NA	SalI_P	SalI_AH_P_W1	SalI_P	2.86E+06	1.72E-05	6.01E-12	4.42E+06	2.33E-05	5.27E-12	NA	NA	NA	SalI_P
DB170	4	SalI	SalI	NA	NA	NA	NA	NA	NA	NA	NA	NA	NA	SalI
DB171	4	SalI_P_W1	SalI_P_W1	SalI_P_W1	8.12E+06	1.00E-05	1.23E-12	1.29E+07	1.00E-05	7.74E-13	1.58E+07	8.90E-05	5.63E-12	SalI_P_W1
DB172	NA	SalI_W1	SalI_W1	SalI_W1	2.87E+05	1.00E-05	3.48E-11	NA	NA	NA	1.84E+06	1.36E-05	7.38E-12	SalI_W1
DB173	3	SalI_P_W1	SalI_AH_P_W1	SalI_P	5.00E+06	1.00E-05	2.00E-12	7.07E+06	1.00E-05	1.41E-12	NA	NA	NA	SalI_P_W1
DB174	5	SalI_P_W1	SalI_AH_P_W1	SalI_P_W1	1.62E+06	1.15E-04	7.11E-11	2.79E+06	2.94E-03	1.05E-09	8.13E+06	4.24E-03	5.22E-10	SalI_P_W1
DB175	5	SalI_W1	SalI_W1	SalI_W1	5.56E+05	1.00E-05	1.80E-11	NA	NA	NA	2.07E+06	4.86E-05	2.35E-11	SalI_W1
DB176	2	SalI_P_W1	SalI_AH_P_W1	SalI_P_W1	2.82E+06	1.00E-05	3.54E-12	1.03E+06	6.05E-04	5.87E-10	8.21E+06	1.16E-05	1.41E-12	SalI_P_W1
DB177	1	SalI_P	SalI_AH_P_W1	NA	NA	NA	NA	NA	NA	NA	NA	NA	NA	SalI_P
DB178	3	SalI_P_W1	SalI_AH_P_W1	SalI_P_W1	3.89E+06	1.00E-05	2.57E-12	5.58E+06	1.00E-05	1.79E-12	3.08E+06	4.06E-05	1.32E-11	SalI_P_W1
DB180	1	SalI_P_W1	SalI_AH_P_W1	SalI_P_W1	2.86E+05	3.29E-04	1.15E-09	2.52E+05	9.23E-04	3.66E-09	1.70E+06	4.33E-04	2.55E-10	SalI_P_W1

DB181	1	Sall_P_W1	Sall_AH_P_W1	Sall_P_W1	2.50E+06	1.00E-05	4.00E-12	3.57E+06	3.80E-05	1.07E-11	8.07E+06	1.72E-05	2.13E-12	Sall_P_W1
DB182	1	Sall_P_W1	Sall_AH_P_W1	Sall_P_W1	9.03E+05	1.00E-05	1.11E-11	1.62E+06	1.00E-05	6.18E-12	4.74E+06	7.05E-05	1.49E-11	Sall_P_W1
DB183	1	Sall_P_W1	Sall_AH_P_W1	Sall_P_W1	1.10E+06	7.97E-05	7.27E-11	2.74E+06	3.49E-05	1.27E-11	5.78E+06	7.97E-05	1.38E-11	Sall_P_W1
DB184	1	Sall_P_W1	Sall_AH_P_W1	Sall_P_W1	1.93E+06	3.84E-05	1.99E-11	3.12E+06	1.00E-05	3.21E-12	8.43E+06	3.51E-05	4.17E-12	Sall_P_W1
DB185	1	Sall_P_W1	Sall_AH_P_W1	Sall_P_W1	9.37E+05	1.00E-05	1.07E-11	6.24E+05	1.00E-05	1.60E-11	4.69E+06	1.00E-05	2.13E-12	Sall_P_W1
DB186	1	Sall_P_W1	Sall_AH_P_W1	Sall_P_W1	4.27E+05	1.00E-05	2.34E-11	5.39E+05	1.00E-05	1.86E-11	3.65E+06	3.23E-05	8.84E-12	Sall_P_W1
DB188	1	Sall_P_W1	Sall_AH_P_W1	Sall_P_W1	2.28E+05	1.00E-05	4.38E-11	2.45E+05	1.00E-05	4.08E-11	1.23E+06	3.16E-04	2.57E-10	Sall_P_W1
DB189	1	Sall_P_W1	Sall_AH_P_W1	Sall_P_W1	1.11E+06	1.00E-05	9.03E-12	1.27E+06	1.00E-05	7.87E-12	5.38E+06	1.00E-05	1.86E-12	Sall_P_W1
DB190	1	Sall_P_W1	Sall_AH_P_W1	Sall_P_W1	1.80E+06	1.00E-05	5.56E-12	2.29E+06	1.00E-05	4.37E-12	5.13E+06	3.90E-05	7.60E-12	Sall_P_W1
DB191	1	Sall_P_W1	Sall_AH_P_W1	Sall_P_W1	1.67E+06	1.00E-05	5.99E-12	5.29E+05	1.00E-05	1.89E-11	5.33E+06	2.36E-05	4.42E-12	Sall_P_W1
DB192	1	Sall_P_W1	Sall_AH_P_W1	Sall_P_W1	3.48E+05	1.00E-05	2.87E-11	8.08E+05	1.00E-05	1.24E-11	3.48E+06	3.48E-05	9.98E-12	Sall_P_W1
DB193	1	Sall_W1	Sall_AH_P_W1	NA	NA	NA	NA	NA	NA	NA	NA	NA	NA	Sall_W1
DB194	1	Sall_P_W1	Sall_AH_P_W1	Sall_P_W1	5.29E+05	1.00E-05	1.89E-11	6.02E+05	1.00E-05	1.66E-11	5.55E+06	4.22E-05	7.61E-12	Sall_P_W1
DB195	1	Sall_P_W1	Sall_AH_P_W1	Sall_P_W1	2.16E+06	1.00E-05	4.62E-12	3.90E+06	1.00E-05	2.56E-12	9.47E+06	2.06E-05	2.18E-12	Sall_P_W1
DB196	1	Sall_P_W1	Sall_AH_P_W1	Sall_P_W1	3.90E+05	1.00E-05	2.56E-11	4.30E+05	1.00E-05	2.33E-11	1.42E+06	1.00E-05	7.04E-12	Sall_P_W1
DB197	1	Sall_P_W1	Sall_AH_P_W1	Sall_P_W1	1.76E+06	2.06E-05	1.17E-11	2.43E+06	3.03E-05	1.25E-11	6.27E+06	1.00E-05	1.59E-12	Sall_P_W1
DB198	1	Sall_P_W1	Sall_AH_P_W1	Sall_P_W1	5.66E+05	1.00E-05	1.77E-11	6.41E+05	6.01E-05	9.38E-11	4.53E+06	6.73E-05	1.49E-11	Sall_P_W1
DB199	1	Sall_P_W1	Sall_AH_P_W1	Sall_P_W1	1.54E+06	2.20E-05	1.42E-11	2.32E+06	1.00E-05	4.30E-12	7.42E+06	1.00E-05	1.35E-12	Sall_P_W1
DB200	1	Sall_P_W1	Sall_AH_P_W1	Sall_P_W1	2.00E+06	1.00E-05	5.01E-12	1.47E+06	1.00E-05	6.81E-12	7.49E+06	1.00E-05	1.34E-12	Sall_P_W1
DB201	1	Sall_P_W1	Sall_AH_P_W1	Sall_P_W1	2.46E+06	1.00E-05	4.07E-12	3.78E+06	1.00E-05	2.65E-12	7.51E+06	4.20E-05	5.59E-12	Sall_P_W1
DB202	1	Sall_P_W1	Sall_AH_P_W1	Sall_P_W1	1.47E+06	1.00E-05	6.81E-12	2.05E+06	1.00E-05	4.89E-12	6.38E+06	1.00E-05	1.57E-12	Sall_P_W1
DB203	4	Sall	Sall	Sall	2.00E+06	1.00E-05	4.99E-12	NA	NA	NA	NA	NA	NA	NA
DB204	1	Sall_P_W1	Sall_AH_P_W1	Sall_P_W1	4.91E+05	1.00E-05	2.04E-11	1.27E+06	1.00E-05	7.89E-12	5.42E+06	1.00E-05	1.84E-12	Sall_P_W1
DB205	1	Sall_P_W1	Sall_AH_P_W1	Sall_P_W1	4.72E+05	1.00E-05	2.12E-11	5.00E+05	1.00E-05	2.00E-11	5.14E+06	1.52E-05	2.95E-12	Sall_P_W1
DB206	1	Sall_P_W1	Sall_AH_P_W1	Sall_P_W1	1.30E+06	1.00E-05	7.71E-12	2.00E+06	1.00E-05	5.01E-12	7.26E+06	1.00E-05	1.38E-12	Sall_P_W1
DB207	3	Sall_P_W1	Sall_AH_P_W1	Sall_P_W1	2.41E+06	5.20E-05	2.16E-11	5.21E+06	1.02E-04	1.95E-11	5.11E+06	1.83E-02	3.58E-09	Sall_P_W1

7.5 PvDBPII-DARC binding inhibition activity

mAb	DARC binding to PvDBPII (HT-SPR)	Binding inhibition (%) (ELISA)	DARC binding inhibition classification	Epitope community
092096	N	97.4	Y	5
2D10	Y	-0.5	N	3
DB001	Y	-25.8	N	4
DB002	Y	0.8	N	1
DB003	Y	2.7	N	2
DB004	Y	-11.4	N	3
DB005	Y	-15.5	N	NA
DB006	Y	-5.3	N	1
DB007	N	70.9	Y	5
DB008	Y	69.9	C	1
DB009	Y	24.5	N	1
DB010	Y	-23.7	N	4
DB011	Y	2.5	N	3
DB012	Y	6.1	N	3
DB017	Y	-2.2	N	3
DB018	Y	39.7	N	3
DB019	Y	11.6	N	1
DB021	Y	17.5	N	3
DB022	Y	-0.1	N	3
DB024	Y	2.9	N	3
DB025	N	-11.9	N	NA
DB026	Y	22.6	N	1
DB027	Y	8.9	N	3
DB029	Y	26.4	N	2
DB031	Y	11.2	N	3
DB032	N	22.2	N	2
DB033	Y	29.9	N	2
DB034	Y	42.2	C	1
DB035	Y	9.0	N	NA
DB036	Y	10.0	N	2
DB037	Y	6.6	N	2
DB041	NA	0.1	N	NA
DB042	Y	4.7	N	1
DB043	Y	7.9	N	1
DB048	Y	-8.9	N	4
DB049	N	37.3	N	5
DB050	N	13.5	N	1
DB052	Y	13.8	N	1
DB054	N	12.4	N	4
DB055	N	4.4	N	5
DB056	N	5.9	N	4
DB057	N	13.0	N	5
DB058	N	37.5	N	2
DB059	N	33.0	N	5
DB060	N	95.6	Y	4
DB061	N	93.5	Y	5
DB062	Y	10.4	N	4
DB070	Y	-2.1	N	4
DB071	Y	1.1	N	3
DB072	Y	8.6	N	3
DB073	Y	8.5	N	1
DB075	N	-4.1	N	NA
DB076	Y	6.7	N	1
DB077	Y	9.0	N	1
DB079	Y	8.7	N	1
DB081	Y	15.6	N	3

DB082	Y	3.6	N	3
DB083	Y	16.7	N	1
DB084	Y	15.4	N	2
DB086	N	98.9	Y	4
DB087	Y	9.3	N	1
DB088	Y	15.0	N	1
DB089	Y	-1.5	N	4
DB090	Y	18.3	N	1
DB091	Y	7.3	N	2
DB092	N	86.8	Y	5
DB093	Y	11.5	N	3
DB094	N	90.4	Y	5
DB095	Y	25.0	N	2
DB096	Y	-2.9	N	NA
DB097	Y	11.2	N	NA
DB098	Y	21.1	N	1
DB099	N	41.8	Y	NA
DB100	Y	12.0	N	2
DB101	Y	12.0	N	2
DB102	Y	15.4	N	2
DB103	N	78.0	Y	5
DB104	N	98.4	Y	5
DB105	Y	-10.1	N	3
DB106	NA	90.1	Y	5
DB107	Y	9.0	N	2
DB108	Y	11.8	N	2
DB109	Y	5.3	N	4
DB110	NA	-9.8	N	NA
DB111	Y	11.5	N	1
DB112	N	97.8	Y	5
DB113	Y	18.5	N	1
DB114	Y	29.5	N	2
DB115	N	6.3	N	4
DB116	Y	14.6	N	2
DB117	Y	10.9	N	2
DB118	Y	20.1	N	3
DB119	Y	93.7	C	NA
DB121	N	41.9	Y	5
DB122	Y	23.0	N	1
DB123	Y	22.2	N	2
DB124	Y	7.0	N	2
DB125	Y	22.0	N	1
DB126	Y	14.6	N	1
DB127	Y	23.3	N	2
DB128	Y	18.7	N	1
DB129	Y	23.9	N	3
DB130	N	22.5	N	2
DB131	N	98.5	Y	5
DB132	Y	21.9	N	2
DB133	Y	92.2	C	3
DB134	Y	9.6	N	1
DB135	Y	23.2	N	3
DB136	Y	-0.9	N	4
DB137	N	99.5	Y	4
DB138	Y	22.0	N	3
DB139	Y	23.5	N	1
DB140	N	98.1	Y	5
DB141	Y	11.9	N	4
DB142	Y	20.0	N	1
DB143	Y	8.5	N	1
DB144	Y	-7.1	N	4
DB146	Y	14.7	N	2

DB147	Y	79.8	C	1
DB149	Y	14.5	N	2
DB150	NA	0.2	N	1
DB152	Y	21.2	N	1
DB153	Y	49.4	C	1
DB154	Y	23.9	N	1
DB155	N	98.5	Y	5
DB156	Y	16.3	N	1
DB157	N	95.8	Y	5
DB158	Y	11.3	N	NA
DB159	N	11.5	N	4
DB160	Y	16.9	N	3
DB161	NA	82.8	Y	NA
DB162	Y	5.7	N	4
DB163	N	98.9	Y	5
DB164	Y	13.7	N	3
DB165	NA	-0.7	N	NA
DB166	Y	5.8	N	4
DB167	Y	19.6	N	1
DB168	Y	-2.6	N	4
DB169	Y	11.9	N	NA
DB170	Y	5.5	N	4
DB171	N	98.9	Y	4
DB172	Y	18.9	N	NA
DB173	Y	18.3	N	3
DB174	NA	58.6	Y	5
DB175	N	95.8	Y	5
DB176	Y	19.4	N	2
DB177	Y	28.5	N	1
DB178	Y	37.3	N	3
DB180	N	52.9	C	1
DB181	Y	23.5	N	1
DB182	Y	28.0	N	1
DB183	Y	7.4	N	1
DB184	Y	10.5	N	1
DB185	Y	9.4	N	1
DB186	Y	9.7	N	1
DB188	Y	18.9	N	1
DB189	Y	26.5	N	1
DB190	Y	11.3	N	1
DB191	Y	19.8	N	1
DB192	NA	19.0	N	1
DB193	Y	-6.6	N	1
DB194	Y	20.2	N	1
DB195	Y	8.9	N	1
DB196	Y	12.2	N	1
DB197	Y	11.9	N	1
DB198	Y	28.2	N	1
DB199	Y	11.0	N	1
DB200	Y	87.4	C	1
DB201	Y	19.5	N	1
DB202	Y	18.3	N	1
DB203	Y	7.4	N	4
DB204	Y	22.7	N	1
DB205	Y	26.7	N	1
DB206	Y	17.1	N	1
DB207	Y	12.3	N	3

7.6 GIA against PvDBP SalI, P and W1 variants

		GIA (%) at 0.5 mg/mL against PvDBPII variant					Dilution series GIA vs PvDBPII SalI				Dilution series GIA vs PvDBPII P				Dilution series GIA vs PvDBPII W1			
mAb	Epitope comm-unity	GIA % vs SalI	GIA % vs P	GIA % vs W1	Retains GIA against PvDBPII variants	GIA % vs Pk at 2 mg/mL	N	GIA EC_{50} geomean	GIA EC_{50} 95% CI lower limit	GIA EC_{50} 95% CI upper limit	N	GIA EC_{50} geomean	GIA EC_{50} 95% CI lower limit	GIA EC_{50} 95% CI upper limit	N	GIA EC_{50} geomean	GIA EC_{50} 95% CI lower limit	GIA EC_{50} 95% CI upper limit
092096	5	NA	100.8	NA	Sal_P_W1	-2.8	4	0.033	0.008	0.128	3	0.150	0.038	0.582	2	0.274	0.005	14.715
2D10	3	NA	60.8	47.3	Sal_P_W1	-6.9	3	0.044	0.014	0.133	NA	NA	NA	NA	2	NA	NA	NA
DB001	4	NA	7.0	-4.0	Sal	NA	10	0.028	0.019	0.042	NA	NA	NA	NA	NA	NA	NA	NA
DB002	1	NA	60.4	47.9	Sal_P_W1	NA	1	0.502	NA	NA	NA	NA	NA	NA	NA	NA	NA	NA
DB003	2	NA	-14.6	42.6	Sal_W1	NA	1	0.399	NA	NA	NA	NA	NA	NA	NA	NA	NA	NA
DB004	3	NA	31.9	-3.1	Sal_P	NA	NA	NA	NA	NA	NA	NA	NA	NA	NA	NA	NA	NA
DB005	NA	NA	87.4	56.9	Sal_P_W1	-5.1	5	0.380	0.057	2.530	NA	NA	NA	NA	NA	NA	NA	NA
DB006	1	NA	64.7	51.9	Sal_P_W1	-7.0	2	0.372	0.045	3.073	NA	NA	NA	NA	NA	NA	NA	NA
DB007	5	NA	87.1	44.7	Sal_P_W1	38.1	2	NA	NA	NA	NA	NA	NA	NA	NA	NA	NA	NA
DB008	1	NA	54.8	50.7	Sal_P_W1	NA	NA	NA	NA	NA	NA	NA	NA	NA	NA	NA	NA	NA
DB009	1	NA	76.9	NA	Sal_P_W1	-2.1	32	0.143	0.094	0.216	9	0.153	0.081	0.288	3	0.531	0.495	0.570
DB010	4	NA	6.8	-4.0	Sal	NA	5	0.026	0.017	0.041	NA	NA	NA	NA	NA	NA	NA	NA
DB011	3	59.6	81.4	24.7	Sal_P	NA	2	0.061	0.000	9.063	NA	NA	NA	NA	NA	NA	NA	NA
DB012	3	34.9	NA	NA	NA	NA	NA	NA	NA	NA	NA	NA	NA	NA	NA	NA	NA	NA
DB017	3	66.8	80.5	-0.3	Sal_P	NA	2	0.292	0.003	31.868	NA	NA	NA	NA	NA	NA	NA	NA
DB018	3	33.3	NA	NA	NA	NA	NA	NA	NA	NA	NA	NA	NA	NA	NA	NA	NA	NA
DB019	1	50.2	NA	NA	NA	NA	2	0.157	0.002	11.788	NA	NA	NA	NA	NA	NA	NA	NA
DB021	3	27.9	NA	NA	NA	NA	NA	NA	NA	NA	NA	NA	NA	NA	NA	NA	NA	NA
DB022	3	36.9	NA	NA	NA	NA	NA	NA	NA	NA	NA	NA	NA	NA	NA	NA	NA	NA
DB024	3	45.2	NA	NA	NA	NA	NA	NA	NA	NA	NA	NA	NA	NA	NA	NA	NA	NA
DB025	NA	41.8	NA	NA	NA	NA	NA	NA	NA	NA	NA	NA	NA	NA	NA	NA	NA	NA
DB026	1	34.4	NA	NA	NA	NA	NA	NA	NA	NA	NA	NA	NA	NA	NA	NA	NA	NA
DB027	3	52.9	NA	NA	NA	NA	2	0.290	0.001	72.286	NA	NA	NA	NA	NA	NA	NA	NA
DB029	2	16.1	NA	NA	NA	NA	NA	NA	NA	NA	NA	NA	NA	NA	NA	NA	NA	NA
DB031	3	52.8	NA	NA	NA	NA	2	0.826	0.023	29.789	NA	NA	NA	NA	NA	NA	NA	NA
DB032	2	19.3	NA	NA	NA	NA	NA	NA	NA	NA	NA	NA	NA	NA	NA	NA	NA	NA
DB033	2	42.7	NA	NA	NA	NA	NA	NA	NA	NA	NA	NA	NA	NA	NA	NA	NA	NA
DB034	1	49.8	NA	NA	NA	NA	2	1.386	0.005	380.400	NA	NA	NA	NA	NA	NA	NA	NA
DB035	NA	39.1	NA	NA	NA	NA	NA	NA	NA	NA	NA	NA	NA	NA	NA	NA	NA	NA

DB036	2	46.5	NA	NA	NA	NA	NA	NA	NA	NA	NA	NA	NA	NA	NA	NA	NA	NA
DB037	2	61.9	-1.2	55.4	Sal_W1	NA	2	0.182	0.129	0.258	NA	NA	NA	NA	NA	NA	NA	NA
DB041	NA	9.2	NA	NA	NA	NA	1	3.077	NA	NA	NA	NA	NA	NA	NA	NA	NA	NA
DB042	1	92.4	97.8	17.6	Sal_P	NA	4	0.236	0.131	0.425	NA	NA	NA	NA	NA	NA	NA	NA
DB043	1	48.1	NA	NA	NA	NA	2	1.976	0.842	4.636	NA	NA	NA	NA	NA	NA	NA	NA
DB048	4	103.9	6.0	1.0	Sal	NA	6	0.014	0.005	0.039	1	1.155	NA	NA	NA	NA	NA	NA
DB049	5	33.8	85.1	19.1	Sal_P_W1	NA	NA	NA	NA	NA	NA	NA	NA	NA	NA	NA	NA	NA
DB050	1	50.7	77.7	63.2	Sal_P_W1	NA	1	0.411	NA	NA	NA	NA	NA	NA	NA	NA	NA	NA
DB052	1	27.5	NA	NA	NA	NA	NA	NA	NA	NA	NA	NA	NA	NA	NA	NA	NA	NA
DB054	4	45.5	2.8	-6.5	Sal	NA	1	0.374	NA	NA	NA	NA	NA	NA	NA	NA	NA	NA
DB055	5	97.0	10.5	86.6	Sal_W1	NA	4	0.026	0.009	0.080	NA	NA	NA	NA	3	0.053	0.024	0.118
DB056	4	103.2	2.8	-2.4	Sal	NA	4	0.016	0.003	0.094	NA	NA	NA	NA	NA	NA	NA	NA
DB057	5	83.7	96.0	86.3	Sal_P_W1	4.8	1	0.087	NA	NA	NA	NA	NA	NA	NA	NA	NA	NA
DB058	2	63.5	90.1	74.1	Sal_P_W1	22.0	1	0.044	NA	NA	NA	NA	NA	NA	NA	NA	NA	NA
DB059	5	98.9	NA	95.1	Sal_P_W1	5.4	8	0.035	0.020	0.063	7	0.020	0.011	0.037	3	0.035	0.012	0.100
DB060	4	37.4	102.5	93.2	Sal_P_W1	NA	1	0.630	NA	NA	NA	NA	NA	NA	NA	NA	NA	NA
DB061	5	63.6	2.2	68.8	Sal_W1	NA	1	0.079	NA	NA	NA	NA	NA	NA	NA	NA	NA	NA
DB062	4	103.1	2.8	-2.1	Sal	1.2	11	0.008	0.004	0.019	NA	NA	NA	NA	NA	NA	NA	NA
DB070	4	111.2	21.5	6.9	Sal	NA	6	0.012	0.004	0.034	NA	NA	NA	NA	NA	NA	NA	NA
DB071	3	39.1	NA	NA	NA	NA	NA	NA	NA	NA	NA	NA	NA	NA	NA	NA	NA	NA
DB072	3	30.3	NA	NA	NA	NA	NA	NA	NA	NA	NA	NA	NA	NA	NA	NA	NA	NA
DB073	1	69.3	93.0	74.1	Sal_P_W1	-10.8	2	0.115	0.000	1.40E+07	NA	NA	NA	NA	NA	NA	NA	NA
DB075	NA	13.2	NA	NA	NA	NA	NA	NA	NA	NA	NA	NA	NA	NA	NA	NA	NA	NA
DB076	1	78.3	100.8	78.8	Sal_P_W1	-9.5	3	0.053	0.002	1.412	NA	NA	NA	NA	NA	NA	NA	NA
DB077	1	76.5	101.8	81.9	Sal_P_W1	-11.7	2	0.056	0.000	2.24E+07	NA	NA	NA	NA	NA	NA	NA	NA
DB079	1	56.8	99.4	80.1	Sal_P_W1	-8.4	1	0.069	NA	NA	NA	NA	NA	NA	NA	NA	NA	NA
DB081	3	57.3	85.9	81.9	Sal_P_W1	-4.4	1	0.371	NA	NA	NA	NA	NA	NA	NA	NA	NA	NA
DB082	3	74.6	79.4	52.6	Sal_P_W1	NA	4	NA	NA	NA	2	0.100	0.000	1.87E+05	NA	NA	NA	NA
DB083	1	64.5	65.3	47.6	Sal_P_W1	NA	1	0.556	NA	NA	NA	NA	NA	NA	NA	NA	NA	NA
DB084	2	37.5	4.4	56.3	Sal_W1	NA	NA	NA	NA	NA	NA	NA	NA	NA	NA	NA	NA	NA
DB086	4	77.5	96.8	37.2	Sal_P	NA	1	0.167	NA	NA	NA	NA	NA	NA	NA	NA	NA	NA
DB087	1	61.8	80.4	71.0	Sal_P_W1	9.5	1	0.268	NA	NA	NA	NA	NA	NA	NA	NA	NA	NA
DB088	1	89.9	105.0	77.6	Sal_P_W1	15.1	5	0.056	0.015	0.210	2	0.076	0.001	5.869	NA	NA	NA	NA
DB089	4	109.0	0.0	-5.3	Sal	NA	3	0.017	0.002	0.163	NA	NA	NA	NA	NA	NA	NA	NA
DB090	1	91.7	103.8	88.2	Sal_P_W1	-3.0	1	0.052	NA	NA	NA	NA	NA	NA	NA	NA	NA	NA
DB091	2	60.2	60.5	58.8	Sal_P_W1	-7.7	1	0.105	NA	NA	NA	NA	NA	NA	NA	NA	NA	NA
DB092	5	57.9	104.8	62.6	Sal_P_W1	7.9	1	0.297	NA	NA	NA	NA	NA	NA	NA	NA	NA	NA
DB093	3	36.8	NA	NA	NA	NA	NA	NA	NA	NA	NA	NA	NA	NA	NA	NA	NA	NA
DB094	5	99.7	105.5	58.8	Sal_P_W1	0.0	1	0.069	NA	NA	NA	NA	NA	NA	NA	NA	NA	NA

DB095	2	80.2	4.8	59.4	Sal_W1	NA	2	0.128	0.000	777.954	NA	NA	NA	NA	NA	NA	NA	NA
DB096	NA	19.7	32.6	NA	NA	NA	NA	NA	NA	NA	NA	NA	NA	NA	NA	NA	NA	NA
DB097	NA	76.7	NA	53.5	Sal_P_W1	-2.1	1	0.041	NA	NA	1	0.049	NA	NA	NA	NA	NA	NA
DB098	1	38.6	55.0	47.9	Sal_P_W1	NA	NA	NA	NA	NA	NA	NA	NA	NA	NA	NA	NA	NA
DB099	NA	41.4	NA	NA	NA	NA	NA	NA	NA	NA	NA	NA	NA	NA	NA	NA	NA	NA
DB100	2	77.5	21.5	70.4	Sal_W1	NA	1	0.097	NA	NA	NA	NA	NA	NA	NA	NA	NA	NA
DB101	2	71.7	60.7	71.3	Sal_P_W1	2.9	1	0.041	NA	NA	1	0.524	NA	NA	NA	NA	NA	NA
DB102	2	70.7	-12.9	65.8	Sal_W1	NA	2	0.102	0.000	3.64E+10	NA	NA	NA	NA	NA	NA	NA	NA
DB103	5	68.3	58.2	68.7	Sal_P_W1	1.6	2	0.116	0.000	1.33E+05	1	0.290	NA	NA	3	NA	NA	NA
DB104	5	89.9	95.2	26.1	Sal_P	NA	1	0.560	NA	NA	NA	NA	NA	NA	NA	NA	NA	NA
DB105	3	91.7	102.9	-4.9	Sal_P	NA	3	0.030	0.012	0.078	4	0.019	0.006	0.058	NA	NA	NA	NA
DB106	5	53.2	102.4	64.1	Sal_P_W1	NA	1	1.209	NA	NA	NA	NA	NA	NA	NA	NA	NA	NA
DB107	2	53.2	3.9	55.0	Sal_W1	NA	1	0.211	NA	NA	NA	NA	NA	NA	NA	NA	NA	NA
DB108	2	75.2	4.5	57.9	Sal_W1	NA	1	0.096	NA	NA	NA	NA	NA	NA	NA	NA	NA	NA
DB109	4	32.2	NA	NA	NA	NA	NA	NA	NA	NA	NA	NA	NA	NA	NA	NA	NA	NA
DB110	NA	7.0	NA	NA	NA	NA	NA	NA	NA	NA	NA	NA	NA	NA	NA	NA	NA	NA
DB111	1	77.0	96.6	83.0	Sal_P_W1	12.6	1	0.103	NA	NA	NA	NA	NA	NA	NA	NA	NA	NA
DB112	5	89.4	94.2	48.0	Sal_P_W1	83.5	3	0.070	0.055	0.089	NA	NA	NA	NA	NA	NA	NA	NA
DB113	1	75.1	93.1	65.5	Sal_P_W1	-8.1	1	0.333	NA	NA	NA	NA	NA	NA	NA	NA	NA	NA
DB114	2	29.9	NA	NA	NA	NA	NA	NA	NA	NA	NA	NA	NA	NA	NA	NA	NA	NA
DB115	4	71.7	65.7	7.4	Sal_P	NA	1	0.494	NA	NA	NA	NA	NA	NA	NA	NA	NA	NA
DB116	2	96.3	0.1	51.8	Sal_W1	NA	1	0.091	NA	NA	NA	NA	NA	NA	NA	NA	NA	NA
DB117	2	45.7	NA	NA	NA	NA	NA	NA	NA	NA	NA	NA	NA	NA	NA	NA	NA	NA
DB118	3	66.9	87.6	70.8	Sal_P_W1	7.4	3	0.043	0.006	0.329	3	0.020	0.005	0.082	NA	NA	NA	NA
DB119	NA	75.7	58.7	71.1	Sal_P_W1	-11.5	1	0.321	NA	NA	NA	NA	NA	NA	NA	NA	NA	NA
DB121	5	51.0	NA	NA	NA	NA	NA	NA	NA	NA	NA	NA	NA	NA	NA	NA	NA	NA
DB122	1	85.7	101.6	79.5	Sal_P_W1	-2.2	1	0.110	NA	NA	NA	NA	NA	NA	NA	NA	NA	NA
DB123	2	54.5	42.9	56.2	Sal_P_W1	NA	1	0.681	NA	NA	NA	NA	NA	NA	NA	NA	NA	NA
DB124	2	47.7	NA	NA	NA	NA	NA	NA	NA	NA	NA	NA	NA	NA	NA	NA	NA	NA
DB125	1	65.1	83.0	63.2	Sal_P_W1	-1.0	1	0.108	NA	NA	NA	NA	NA	NA	NA	NA	NA	NA
DB126	1	72.0	95.5	65.8	Sal_P_W1	3.2	1	0.071	NA	NA	NA	NA	NA	NA	NA	NA	NA	NA
DB127	2	65.4	7.1	50.9	Sal_W1	NA	2	0.042	0.000	5093.383	NA	NA	NA	NA	NA	NA	NA	NA
DB128	1	70.6	93.9	74.9	Sal_P_W1	16.2	1	0.169	NA	NA	NA	NA	NA	NA	NA	NA	NA	NA
DB129	3	44.9	NA	NA	NA	NA	NA	NA	NA	NA	NA	NA	NA	NA	NA	NA	NA	NA
DB130	2	51.4	NA	NA	NA	NA	NA	NA	NA	NA	NA	NA	NA	NA	NA	NA	NA	NA
DB131	5	78.9	98.3	13.5	Sal_P	NA	3	0.093	0.027	0.326	NA	NA	NA	NA	NA	NA	NA	NA
DB132	2	77.1	16.4	58.2	Sal_W1	NA	1	0.095	NA	NA	NA	NA	NA	NA	NA	NA	NA	NA
DB133	3	99.8	98.7	80.1	Sal_P_W1	85.6	3	0.052	0.023	0.119	NA	NA	NA	NA	NA	NA	NA	NA
DB134	1	54.2	NA	NA	NA	NA	NA	NA	NA	NA	NA	NA	NA	NA	NA	NA	NA	NA

DB135	3	46.8	NA	NA	NA	NA	NA	NA	NA	NA	NA	NA	NA	NA	NA	NA	NA	NA
DB136	4	104.4	113.4	8.8	Sal_P	NA	6	0.025	0.012	0.050	5	0.054	0.019	0.152	NA	NA	NA	NA
DB137	4	85.5	90.3	33.4	Sal_P	NA	1	0.386	NA	NA	NA	NA	NA	NA	NA	NA	NA	NA
DB138	3	55.6	NA	NA	NA	NA	NA	NA	NA	NA	NA	NA	NA	NA	NA	NA	NA	NA
DB139	1	80.3	89.4	54.1	Sal_P_W1	-7.5	1	0.261	NA	NA	NA	NA	NA	NA	NA	NA	NA	NA
DB140	5	103.1	81.7	86.8	Sal_P_W1	-4.7	3	0.037	0.013	0.101	4	0.150	0.025	0.892	3	0.038	0.009	0.161
DB141	4	36.5	NA	NA	NA	NA	NA	NA	NA	NA	NA	NA	NA	NA	NA	NA	NA	NA
DB142	1	66.3	90.2	75.2	Sal_P_W1	1.4	1	0.212	NA	NA	NA	NA	NA	NA	NA	NA	NA	NA
DB143	1	64.5	90.2	68.7	Sal_P_W1	-2.2	2	0.100	0.001	17.920	NA	NA	NA	NA	NA	NA	NA	NA
DB144	4	101.6	94.0	61.1	Sal_P_W1	19.7	7	0.037	0.015	0.093	3	0.070	0.010	0.509	3	0.284	0.097	0.838
DB146	2	44.6	NA	NA	NA	NA	NA	NA	NA	NA	NA	NA	NA	NA	NA	NA	NA	NA
DB147	1	21.8	NA	NA	NA	NA	NA	NA	NA	NA	NA	NA	NA	NA	NA	NA	NA	NA
DB149	2	42.8	NA	NA	NA	NA	NA	NA	NA	NA	NA	NA	NA	NA	NA	NA	NA	NA
DB150	1	81.9	40.6	49.4	Sal_P_W1	10.2	3	0.167	0.005	5.597	NA	NA	NA	NA	3	NA	NA	NA
DB152	1	89.2	108.6	85.7	Sal_P_W1	38.1	1	0.047	NA	NA	NA	NA	NA	NA	NA	NA	NA	NA
DB153	1	60.8	70.0	68.4	Sal_P_W1	6.8	1	0.104	NA	NA	NA	NA	NA	NA	NA	NA	NA	NA
DB154	1	74.2	85.9	57.0	Sal_P_W1	20.6	1	0.058	NA	NA	NA	NA	NA	NA	NA	NA	NA	NA
DB155	5	96.3	101.0	75.2	Sal_P_W1	4.8	1	0.043	NA	NA	NA	NA	NA	NA	NA	NA	NA	NA
DB156	1	66.7	74.8	71.7	Sal_P_W1	11.0	1	0.132	NA	NA	NA	NA	NA	NA	NA	NA	NA	NA
DB157	5	26.7	NA	NA	NA	NA	NA	NA	NA	NA	NA	NA	NA	NA	NA	NA	NA	NA
DB158	NA	15.4	NA	NA	NA	NA	NA	NA	NA	NA	NA	NA	NA	NA	NA	NA	NA	NA
DB159	4	106.4	0.0	-2.0	Sal	NA	3	0.026	0.014	0.047	NA	NA	NA	NA	NA	NA	NA	NA
DB160	3	69.6	62.6	66.1	Sal_P_W1	NA	3	NA	NA	NA	NA	NA	NA	NA	NA	NA	NA	NA
DB161	NA	93.2	100.9	81.9	Sal_P_W1	19.8	1	0.040	NA	NA	3	0.094	0.050	0.176	3	0.157	0.098	0.250
DB162	4	105.3	0.0	5.6	Sal	NA	3	0.019	0.003	0.137	NA	NA	NA	NA	NA	NA	NA	NA
DB163	5	32.7	NA	NA	NA	NA	NA	NA	NA	NA	NA	NA	NA	NA	NA	NA	NA	NA
DB164	3	26.9	NA	NA	NA	NA	NA	NA	NA	NA	NA	NA	NA	NA	NA	NA	NA	NA
DB165	NA	101.3	NA	76.9	Sal_P_W1	3.6	6	0.026	0.013	0.055	5	0.064	0.036	0.116	3	0.143	0.106	0.193
DB166	4	104.4	12.7	11.2	Sal	NA	3	0.034	0.007	0.165	NA	NA	NA	NA	NA	NA	NA	NA
DB167	1	59.0	76.4	61.1	Sal_P_W1	14.0	1	0.131	NA	NA	NA	NA	NA	NA	NA	NA	NA	NA
DB168	4	105.3	0.0	1.8	Sal	NA	6	0.022	0.008	0.057	NA	NA	NA	NA	NA	NA	NA	NA
DB169	NA	84.2	NA	10.6	Sal_P	NA	4	0.021	0.010	0.043	3	0.024	0.008	0.067	NA	NA	NA	NA
DB170	4	23.7	NA	NA	NA	NA	NA	NA	NA	NA	NA	NA	NA	NA	NA	NA	NA	NA
DB171	4	93.9	102.0	85.4	Sal_P_W1	99.3	8	0.068	0.031	0.149	2	0.039	0.000	63.307	NA	NA	NA	NA
DB172	NA	31.5	NA	NA	NA	NA	NA	NA	NA	NA	NA	NA	NA	NA	NA	NA	NA	NA
DB173	3	63.2	77.7	45.9	Sal_P_W1	NA	3	NA	NA	NA	NA	NA	NA	NA	NA	NA	NA	NA
DB174	5	18.6	NA	NA	NA	NA	NA	NA	NA	NA	NA	NA	NA	NA	NA	NA	NA	NA
DB175	5	71.8	31.5	72.2	Sal_W1	NA	1	0.122	NA	NA	NA	NA	NA	NA	NA	NA	NA	NA
DB176	2	70.0	NA	71.7	Sal_P_W1	0.1	7	NA	NA	NA	4	0.060	0.025	0.144	NA	NA	NA	NA

DB177	1	44.9	NA	NA	NA	NA	NA	NA	NA	NA	NA	NA	NA	NA	NA	NA	NA	NA
DB178	3	103.1	NA	55.2	Sal_P_W1	0.0	8	0.029	0.020	0.041	5	0.010	0.004	0.025	3	NA	NA	NA
DB180	1	26.2	NA	NA	NA	NA	NA	NA	NA	NA	NA	NA	NA	NA	NA	NA	NA	NA
DB181	1	89.7	98.3	73.5	Sal_P_W1	4.6	1	0.048	NA	NA	NA	NA	NA	NA	NA	NA	NA	NA
DB182	1	56.5	78.2	53.5	Sal_P_W1	1.5	2	0.300	0.000	3.60E+06	NA	NA	NA	NA	NA	NA	NA	NA
DB183	1	65.7	99.6	70.3	Sal_P_W1	5.7	1	0.364	NA	NA	NA	NA	NA	NA	NA	NA	NA	NA
DB184	1	81.4	NA	79.1	Sal_P_W1	5.7	3	0.030	0.017	0.056	3	0.031	0.023	0.041	3	0.065	0.016	0.263
DB185	1	61.8	101.4	68.0	Sal_P_W1	20.3	2	0.051	0.000	115.122	2	0.173	0.090	0.331	NA	NA	NA	NA
DB186	1	53.1	76.4	66.3	Sal_P_W1	21.3	2	0.081	0.000	19.635	NA	NA	NA	NA	NA	NA	NA	NA
DB188	1	15.3	NA	NA	NA	NA	NA	NA	NA	NA	NA	NA	NA	NA	NA	NA	NA	NA
DB189	1	38.1	83.0	65.8	Sal_P_W1	NA	NA	NA	NA	NA	NA	NA	NA	NA	NA	NA	NA	NA
DB190	1	55.5	76.1	41.3	Sal_P_W1	-1.4	1	0.166	NA	NA	NA	NA	NA	NA	NA	NA	NA	NA
DB191	1	50.1	82.2	55.2	Sal_P_W1	-2.1	1	0.197	NA	NA	NA	NA	NA	NA	NA	NA	NA	NA
DB192	1	49.4	77.2	54.9	Sal_P_W1	NA	1	0.940	NA	NA	NA	NA	NA	NA	NA	NA	NA	NA
DB193	1	48.9	NA	NA	NA	NA	NA	NA	NA	NA	NA	NA	NA	NA	NA	NA	NA	NA
DB194	1	94.3	87.0	54.7	Sal_P_W1	4.9	1	0.163	NA	NA	NA	NA	NA	NA	NA	NA	NA	NA
DB195	1	73.6	93.6	70.9	Sal_P_W1	2.4	1	0.108	NA	NA	NA	NA	NA	NA	NA	NA	NA	NA
DB196	1	78.3	80.1	85.1	Sal_P_W1	-0.7	1	0.159	NA	NA	NA	NA	NA	NA	NA	NA	NA	NA
DB197	1	76.0	98.3	88.3	Sal_P_W1	12.1	3	0.032	0.017	0.059	3	0.034	0.003	0.348	3	0.105	0.047	0.238
DB198	1	66.8	56.7	41.9	Sal_P_W1	NA	1	0.742	NA	NA	NA	NA	NA	NA	NA	NA	NA	NA
DB199	1	105.0	100.9	82.3	Sal_P_W1	6.2	3	0.031	0.006	0.147	1	0.043	NA	NA	3	0.100	0.022	0.467
DB200	1	99.2	104.3	86.5	Sal_P_W1	17.4	3	0.034	0.003	0.370	1	0.075	NA	NA	3	0.088	0.018	0.419
DB201	1	84.0	NA	84.0	Sal_P_W1	-2.7	6	0.027	0.010	0.072	3	0.018	0.006	0.056	3	0.052	0.010	0.272
DB202	1	85.1	87.7	78.3	Sal_P_W1	-5.3	7	0.084	0.031	0.228	3	0.096	0.019	0.480	3	0.113	0.008	1.677
DB203	4	92.0	1.7	6.0	Sal	NA	2	0.048	0.000	7.347	NA	NA	NA	NA	NA	NA	NA	NA
DB204	1	72.0	80.1	76.6	Sal_P_W1	NA	1	0.767	NA	NA	NA	NA	NA	NA	NA	NA	NA	NA
DB205	1	38.8	NA	NA	NA	NA	NA	NA	NA	NA	NA	NA	NA	NA	NA	NA	NA	NA
DB206	1	71.8	80.6	67.2	Sal_P_W1	NA	1	0.778	NA	NA	NA	NA	NA	NA	NA	NA	NA	NA
DB207	3	73.2	92.3	54.7	Sal_P_W1	6.2	3	0.119	0.000	35.959	NA	NA	NA	NA	NA	NA	NA	NA

7.7 GIA of engineered mAbs

7.7.1 GIA of engineered mAbs against PvDBPII SalI

				GIA of wild-type mAb vs PvDBPII SalI				GIA of engineered mAb-35 vs PvDBPII SalI			
mAb	DARC binding inhibitor	Epitope comm-unity	Retains GIA against PvDBPII variants	N	GIA EC_{50} geomean	GIA EC_{50} 95% CI lower limit	GIA EC_{50} 95% CI upper limit	N	GIA EC_{50} geomean	GIA EC_{50} 95% CI lower limit	GIA EC_{50} 95% CI upper limit
092096	Y	5	Sal_P_W1	3	0.106	0.006	1.863	3	0.015	0.001	0.347
DB001	N	4	Sal	5	0.023	0.009	0.060	5	0.057	0.012	0.262
DB009	N	1	Sal_P_W1	6	0.259	0.046	1.468	10	0.021	0.011	0.040
DB048	N	4	Sal	3	0.018	0.001	0.293	1	0.029	NA	NA
DB059	N	5	Sal_P_W1	5	0.045	0.029	0.070	5	0.005	0.003	0.009
DB062	N	4	Sal	5	0.016	0.006	0.046	5	0.019	0.007	0.052
DB070	N	4	Sal	3	0.019	0.002	0.155	3	0.009	0.001	0.110
DB082	N	3	Sal_P_W1	1	0.064	NA	NA	3	0.014	0.000	0.596
DB088	N	1	Sal_P_W1	3	0.068	0.006	0.774	3	0.008	0.001	0.139
DB095	N	2	Sal_W1	1	0.254	NA	NA	3	0.053	0.013	0.222
DB103	Y	5	Sal_P_W1	1	0.349	NA	NA	3	0.011	0.001	0.095
DB136	N	4	Sal_P	3	0.029	0.003	0.318	3	0.027	0.003	0.247
DB144	N	4	Sal_P_W1	5	0.056	0.015	0.210	5	0.009	0.002	0.044
DB165	N	NA	Sal_P_W1	3	0.077	0.010	0.597	3	0.011	0.001	0.083
DB171	Y	4	Sal_P_W1	5	0.092	0.048	0.177	5	0.014	0.008	0.024
DB176	N	2	Sal_P_W1	2	0.094	0.010	0.884	5	0.025	0.012	0.052
DB178	N	3	Sal_P_W1	4	0.037	0.018	0.074	5	0.010	0.004	0.023
DB202	N	1	Sal_P_W1	5	0.172	0.075	0.397	5	0.013	0.005	0.033
EBL040	NA	NA	NA	NA	NA	NA	NA	4	0.094	0.020	0.441

7.7.2 GIA of engineered mAbs against PvDBPII P

				GIA of wild-type mAb vs PvDBPII P				GIA of engineered mAb-35 vs PvDBPII P			
mAb	DARC binding inhibitor	Epitope comm-unity	Retains GIA against PvDBPII variants	N	GIA EC_{50} geomean	GIA EC_{50} 95% CI lower limit	GIA EC_{50} 95% CI upper limit	N	GIA EC_{50} geomean	GIA EC_{50} 95% CI lower limit	GIA EC_{50} 95% CI upper limit
092096	Y	5	Sal_P_W1	2	0.137	0.000	107	3	0.019	0.003	0.111
DB001	N	4	Sal	NA	NA	NA	NA	1	0.044	NA	NA
DB009	N	1	Sal_P_W1	1	0.260	NA	NA	3	0.040	0.006	0.289
DB048	N	4	Sal	NA	NA	NA	NA	1	0.068	NA	NA
DB059	N	5	Sal_P_W1	3	0.038	0.004	0.370	2	0.005	0.000	0.810
DB062	N	4	Sal	NA	NA	NA	NA	3	0.037	0.002	0.848
DB070	N	4	Sal	NA	NA	NA	NA	3	0.024	0.002	0.330
DB082	N	3	Sal_P_W1	2	0.100	0.000	1.87E+05	3	0.018	0.002	0.156
DB088	N	1	Sal_P_W1	3	0.115	0.016	0.820	3	0.010	0.000	0.613
DB095	N	2	Sal_W1	NA	NA	NA	NA	3	0.054	0.003	0.925
DB103	Y	5	Sal_P_W1	1	0.290	NA	NA	3	0.011	0.003	0.043
DB136	N	4	Sal_P	3	0.141	0.016	1.22	3	0.052	0.006	0.433
DB144	N	4	Sal_P_W1	2	0.062	0.000	1187	3	0.009	0.001	0.104
DB165	N	NA	Sal_P_W1	2	0.080	0.000	131	3	0.014	0.001	0.138
DB171	Y	4	Sal_P_W1	3	0.052	0.008	0.363	3	0.009	0.001	0.074
DB176	N	2	Sal_P_W1	2	0.163	0.000	3813	3	0.028	0.005	0.169
DB178	N	3	Sal_P_W1	3	0.024	0.002	0.281	3	0.009	0.002	0.051
DB202	N	1	Sal_P_W1	2	0.084	0.000	164	3	0.011	0.001	0.116
EBL040	NA	NA	NA	NA	NA	NA	NA	1	0.069	NA	NA

7.7.3 GIA of engineered mAbs against PkA1H1

				GIA of wild-type mAb vs PkA1H1				GIA of engineered mAb-35 vs PkA1H1			
mAb	DARC binding inhibitor	Epitope comm-unity	Retains GIA against PvDBPII variants	N	GIA EC_{50} geomean	GIA EC_{50} 95% CI lower limit	GIA EC_{50} 95% CI upper limit	N	GIA EC_{50} geomean	GIA EC_{50} 95% CI lower limit	GIA EC_{50} 95% CI upper limit
092096	Y	5	Sal_P_W1	NA	NA	NA	NA	2	0.613	0.166	2.26
DB001	N	4	Sal	NA	NA	NA	NA	NA	NA	NA	NA
DB009	N	1	Sal_P_W1	NA	NA	NA	NA	NA	NA	NA	NA
DB048	N	4	Sal	NA	NA	NA	NA	NA	NA	NA	NA
DB059	N	5	Sal_P_W1	NA	NA	NA	NA	2	0.072	0.056	0.092
DB062	N	4	Sal	NA	NA	NA	NA	NA	NA	NA	NA
DB070	N	4	Sal	NA	NA	NA	NA	NA	NA	NA	NA
DB082	N	3	Sal_P_W1	NA	NA	NA	NA	NA	NA	NA	NA
DB088	N	1	Sal_P_W1	NA	NA	NA	NA	1	0.678	NA	NA
DB095	N	2	Sal_W1	NA	NA	NA	NA	1	0.463	NA	NA
DB103	Y	5	Sal_P_W1	NA	NA	NA	NA	1	0.599	NA	NA
DB136	N	4	Sal_P	NA	NA	NA	NA	2	0.566	0.264	1.22
DB144	N	4	Sal_P_W1	NA	NA	NA	NA	2	0.217	0.083	0.562
DB165	N	NA	Sal_P_W1	NA	NA	NA	NA	2	0.417	0.096	1.80
DB171	Y	4	Sal_P_W1	2	0.023	0.007	0.079	2	0.021	0.006	0.070
DB176	N	2	Sal_P_W1	NA	NA	NA	NA	NA	NA	NA	NA
DB178	N	3	Sal_P_W1	NA	NA	NA	NA	1	0.559	NA	NA
DB202	N	1	Sal_P_W1	NA	NA	NA	NA	2	0.660	0.567	0.767
EBL040	NA	NA	NA	NA	NA	NA	NA	1	0.578	NA	NA

8 References

1. Word Health Organisation. World malaria report 2024: addressing inequity in the global malaria response.

2. CDC - DPDx - Malaria [Internet]. 2024 [cited 2025 Apr 9]. Available from: https://www.cdc.gov/dpdx/malaria/index.html

3. William T, Jelip J, Menon J, Anderios F, Mohammad R, Awang Mohammad TA, et al. Changing epidemiology of malaria in Sabah, Malaysia: increasing incidence of Plasmodium knowlesi. Malaria Journal. 2014 Oct 2;13(1):390.

4. Battle KE, Lucas TCD, Nguyen M, Howes RE, Nandi AK, Twohig KA, et al. Mapping the global endemicity and clinical burden of *Plasmodium vivax*, 2000–17: a spatial and temporal modelling study. The Lancet. 2019 July 27;394(10195):332–43.

5. Miller LH, Mason SJ, Clyde DF, McGinniss MH. The resistance factor to Plasmodium vivax in blacks. The Duffy-blood-group genotype, FyFy. N Engl J Med. 1976 Aug 5;295(6):302–4.

6. Twohig KA, Pfeffer DA, Baird JK, Price RN, Zimmerman PA, Hay SI, et al. Growing evidence of Plasmodium vivax across malaria-endemic Africa. PLOS Neglected Tropical Diseases. 2019 Jan 31;13(1):e0007140.

7. Price RN, Commons RJ, Battle KE, Thriemer K, Mendis K. Plasmodium vivax in the Era of the Shrinking P. falciparum Map. Trends in Parasitology. 2020 June;36(6):560–70.

8. Weiss DJ, Dzianach PA, Saddler A, Lubinda J, Browne A, McPhail M, et al. Mapping the global prevalence, incidence, and mortality of Plasmodium falciparum and Plasmodium vivax malaria, 2000–22: a spatial and temporal modelling study. The Lancet. 2025 Mar 22;405(10483):979–90.

9. Saravu K, Rishikesh K, Kamath A, Shastry AB. Severity in Plasmodium vivax malaria claiming global vigilance and exploration – a tertiary care centre-based cohort study. Malaria Journal. 2014 Aug 8;13(1):304.

10. Baird JK. Evidence and Implications of Mortality Associated with Acute Plasmodium vivax Malaria. Clinical Microbiology Reviews. 2013 Jan;26(1):36–57.

11. Patriani D, Arguni E, Kenangalem E, Dini S, Sugiarto P, Hasanuddin A, et al. Early and late mortality after malaria in young children in Papua, Indonesia. BMC Infectious Diseases. 2019 Oct 30;19(1):922.

12. Dini S, Douglas NM, Poespoprodjo JR, Kenangalem E, Sugiarto P, Plumb ID, et al. The risk of morbidity and mortality following recurrent malaria in Papua, Indonesia: a retrospective cohort study. BMC Medicine. 2020 Feb 20;18(1):28.

13. McGready R, Lee SJ, Wiladphaingern J, Ashley EA, Rijken MJ, Boel M, et al. Adverse effects of falciparum and vivax malaria and the safety of antimalarial treatment in early

pregnancy: a population-based study. The Lancet Infectious Diseases. 2012 May 1;12(5):388–96.

14. Poespoprodjo JR, Fobia W, Kenangalem E, Lampah DA, Hasanuddin A, Warikar N, et al. Vivax Malaria: A Major Cause of Morbidity in Early Infancy. Clinical Infectious Diseases. 2009 June 15;48(12):1704–12.

15. Dombrowski JG, Barateiro A, Peixoto EPM, Barros ABC da S, Souza RM de, Clark TG, et al. Adverse pregnancy outcomes are associated with Plasmodium vivax malaria in a prospective cohort of women from the Brazilian Amazon. PLOS Neglected Tropical Diseases. 2021 Apr 29;15(4):e0009390.

16. Mueller I, Galinski MR, Tsuboi T, Arevalo-Herrera M, Collins WE, King CL. Chapter Three - Natural Acquisition of Immunity to Plasmodium vivax: Epidemiological Observations and Potential Targets. In: Advances in Parasitology [Internet]. Academic Press; 2013 [cited 2023 Dec 4]. p. 77–131. Available from: https://www.sciencedirect.com/science/article/pii/B9780124078260000035

17. Mueller I, Galinski MR, Baird JK, Carlton JM, Kochar DK, Alonso PL, et al. Key gaps in the knowledge of Plasmodium vivax, a neglected human malaria parasite. The Lancet Infectious Diseases. 2009 Sept 1;9(9):555–66.

18. Sturm A, Amino R, van de Sand C, Regen T, Retzlaff S, Rennenberg A, et al. Manipulation of Host Hepatocytes by the Malaria Parasite for Delivery into Liver Sinusoids. Science. 2006 Sept;313(5791):1287–90.

19. Wells TNC, Burrows JN, Baird JK. Targeting the hypnozoite reservoir of Plasmodium vivax: the hidden obstacle to malaria elimination. Trends in Parasitology. 2010 Mar 1;26(3):145–51.

20. White NJ. Determinants of relapse periodicity in Plasmodium vivax malaria. Malaria Journal. 2011 Oct 11;10(1):297.

21. World Health Organisation. WHO guidelines for malaria. 2025 Aug.

22. Ramos Júnior WM, Sardinha JFJ, Costa MRF, Santana MS, Alecrim MGC, Lacerda MVG. Clinical aspects of hemolysis in patients with *P. vivax* malaria treated with primaquine, in the Brazilian Amazon. The Brazilian Journal of Infectious Diseases. 2010 July 1;14(4):410–2.

23. Luzzatto L, Ally M, Notaro R. Glucose-6-phosphate dehydrogenase deficiency. Blood. 2020 Sept 10;136(11):1225–40.

24. Malleret B, Li A, Zhang R, Tan KSW, Suwanarusk R, Claser C, et al. *Plasmodium vivax:* restricted tropism and rapid remodeling of CD71-positive reticulocytes. Blood. 2015 Feb 19;125(8):1314–24.

25. Ovchynnikova E, Aglialoro F, Bentlage AEH, Vidarsson G, Salinas ND, von Lindern M, et al. DARC extracellular domain remodeling in maturating reticulocytes explains Plasmodium vivax tropism. Blood. 2017 Sept 21;130(12):1441–4.

26. World Health Organization. Malaria rapid diagnostic test performance: summary results of WHO product testing of malaria RDTs: round 1-8 (2008–2018) [Internet]. Geneva: World Health Organization; 2018 [cited 2025 July 30]. 33 p. Available from: https://iris.who.int/handle/10665/276193

27. Kho S, Qotrunnada L, Leonardo L, Andries B, Wardani PAI, Fricot A, et al. Hidden Biomass of Intact Malaria Parasites in the Human Spleen. New England Journal of Medicine. 2021 May 26;384(21):2067–9.

28. Obaldia N, Meibalan E, Sa JM, Ma S, Clark MA, Mejia P, et al. Bone Marrow Is a Major Parasite Reservoir in Plasmodium vivax Infection. mBio. 2018 May 8;9(3):10.1128/mbio.00625-18.

29. Kho S, Qotrunnada L, Leonardo L, Andries B, Wardani PAI, Fricot A, et al. Evaluation of splenic accumulation and colocalization of immature reticulocytes and Plasmodium vivax in asymptomatic malaria: A prospective human splenectomy study. PLOS Medicine. 2021 May 26;18(5):e1003632.

30. Baro B, Deroost K, Raiol T, Brito M, Almeida ACG, Menezes-Neto A de, et al. Plasmodium vivax gametocytes in the bone marrow of an acute malaria patient and changes in the erythroid miRNA profile. PLOS Neglected Tropical Diseases. 2017 Apr 6;11(4):e0005365.

31. Brito MAM, Baro B, Raiol TC, Ayllon-Hermida A, Safe IP, Deroost K, et al. Morphological and Transcriptional Changes in Human Bone Marrow During Natural Plasmodium vivax Malaria Infections. J Infect Dis. 2022 Apr 1;225(7):1274–83.

32. Udomsangpetch R, Kaneko O, Chotivanich K, Sattabongkot J. Cultivation of Plasmodium vivax. Trends in Parasitology. 2008 Feb;24(2):85–8.

33. Galinski MR, Meyer EVS, Barnwell JW. Chapter One - Plasmodium vivax: Modern Strategies to Study a Persistent Parasite's Life Cycle. In: Advances in Parasitology [Internet]. Academic Press; 2013 [cited 2025 Aug 10]. p. 1–26. Available from: https://www.sciencedirect.com/science/article/pii/B9780124078260000011

34. Putaporntip C, Kuamsab N, Pattanawong U, Yanmanee S, Seethamchai S, Jongwutiwes S. Plasmodium cynomolgi Co-infections among Symptomatic Malaria Patients, Thailand - Volume 27, Number 2—February 2021 - Emerging Infectious Diseases journal - CDC. [cited 2025 Aug 21]; Available from: https://wwwnc.cdc.gov/eid/article/27/2/19-1660_article

35. Moon RW, Hall J, Rangkuti F, Ho YS, Almond N, Mitchell GH, et al. Adaptation of the genetically tractable malaria pathogen Plasmodium knowlesi to continuous culture in human erythrocytes. Proceedings of the National Academy of Sciences. 2013 Jan 8;110(2):531–6.

36. Bantuchai S, Imad H, Nguitragool W. *Plasmodium vivax* gametocytes and transmission. Parasitology International. 2022 Apr 1;87:102497.

37. Vallejo AF, Read RC, Arevalo-Herrera M, Herrera S, Elliott T, Polak ME. Malaria systems immunology: Plasmodium vivax induces tolerance during primary infection

through dysregulation of neutrophils and dendritic cells. Journal of Infection. 2018 Nov;77(5):440–7.

38. Alanine DGW, Quinkert D, Kumarasingha R, Mehmood S, Donnellan FR, Minkah NK, et al. Human Antibodies that Slow Erythrocyte Invasion Potentiate Malaria-Neutralizing Antibodies. Cell. 2019 June 27;178(1):216-228.e21.

39. Dvorak JA, Miller LH, Whitehouse WC, Shiroishi T. Invasion of Erythrocytes by Malaria Merozoites. Science. 1975 Feb 28;187(4178):748–50.

40. Yahata K, Hart MN, Davies H, Asada M, Wassmer SC, Templeton TJ, et al. Gliding motility of Plasmodium merozoites. Proceedings of the National Academy of Sciences. 2021 Nov 30;118(48):e2114442118.

41. Zimmerman PA, Ferreira MU, Howes RE, Mercereau-Puijalon O. Chapter Two - Red Blood Cell Polymorphism and Susceptibility to Plasmodium vivax. In: Advances in Parasitology [Internet]. Academic Press; 2013 [cited 2023 Dec 4]. p. 27–76. Available from: https://www.sciencedirect.com/science/article/pii/B9780124078260000023

42. Miller LH, Aikawa M, Johnson JG, Shiroishi T. Interaction between cytochalasin B-treated malarial parasites and erythrocytes. Attachment and junction formation. Journal of Experimental Medicine. 1979 Jan 1;149(1):172–84.

43. Galinski MR, Medina CC, Ingravallo P, Barnwell JW. A reticulocyte-binding protein complex of plasmodium vivax merozoites. Cell. 1992 June 26;69(7):1213–26.

44. Gupta S, Singh S, Popovici J, Roesch C, Shakri AR, Guillotte-Blisnick M, et al. Targeting a Reticulocyte Binding Protein and Duffy Binding Protein to Inhibit Reticulocyte Invasion by Plasmodium vivax. Sci Rep. 2018 July 12;8(1):10511.

45. Malleret B, El Sahili A, Tay MZ, Carissimo G, Ong ASM, Novera W, et al. Plasmodium vivax binds host CD98hc (SLC3A2) to enter immature red blood cells. Nat Microbiol. 2021 Aug;6(8):991–9.

46. Gruszczyk J, Huang RK, Chan LJ, Menant S, Hong C, Murphy JM, et al. Cryo-EM structure of an essential Plasmodium vivax invasion complex. Nature. 2018 July;559(7712):135–9.

47. Feufack-Donfack LB, Baldor L, Roesch C, Tat B, Orban A, Seng D, et al. The PvRBP2b-TfR1 interaction is not essential for reticulocytes invasion by Plasmodium vivax isolates from Cambodia. npj Vaccines. 2024 Nov 22;9(1):1–8.

48. Kanjee U, Grüring C, Babar P, Meyers A, Dash R, Pereira L, et al. Plasmodium vivax Strains Use Alternative Pathways for Invasion. The Journal of Infectious Diseases. 2021 May 15;223(10):1817–21.

49. Ntumngia FB, Thomson-Luque R, Torres L de M, Gunalan K, Carvalho LH, Adams JH. A Novel Erythrocyte Binding Protein of Plasmodium vivax Suggests an Alternate Invasion Pathway into Duffy-Positive Reticulocytes. mBio. 2016 Aug 23;7(4):10.1128/mbio.01261-16.

50. Lee SK, Crosnier C, Valenzuela-Leon PC, Dizon BLP, Atkinson JP, Mu J, et al. Complement receptor 1 is the human erythrocyte receptor for Plasmodium vivax erythrocyte binding protein. Proceedings of the National Academy of Sciences. 2024 Jan 30;121(5):e2316304121.

51. Miller LH, Mason SJ, Dvorak JA, McGinniss MH, Rothman IK. Erythrocyte receptors for (Plasmodium knowlesi) malaria: Duffy blood group determinants. Science. 1975 Aug 15;189(4202):561–3.

52. Hart MN, Mohring F, DonVito SM, Thomas JA, Muller-Sienerth N, Wright GJ, et al. Sequential roles for red blood cell binding proteins enable phased commitment to invasion for malaria parasites. Nat Commun. 2023 Aug 1;14(1):4619.

53. Pain A, Böhme U, Berry AE, Mungall K, Finn RD, Jackson AP, et al. The genome of the simian and human malaria parasite Plasmodium knowlesi. Nature. 2008 Oct;455(7214):799–803.

54. Dankwa S, Lim C, Bei AK, Jiang RHY, Abshire JR, Patel SD, et al. Ancient human sialic acid variant restricts an emerging zoonotic malaria parasite. Nat Commun. 2016 Apr 4;7(1):11187.

55. Moon RW, Sharaf H, Hastings CH, Ho YS, Nair MB, Rchiad Z, et al. Normocyte-binding protein required for human erythrocyte invasion by the zoonotic malaria parasite Plasmodium knowlesi. Proceedings of the National Academy of Sciences. 2016 June 28;113(26):7231–6.

56. Snounou G, Pérignon JL. Malariotherapy – Insanity at the Service of Malariology. In: Advances in Parasitology [Internet]. Elsevier; 2013 [cited 2023 Nov 24]. p. 223–55. Available from: https://linkinghub.elsevier.com/retrieve/pii/B9780124078260000060

57. Haynes JD, Dalton JP, Klotz FW, McGinniss MH, Hadley TJ, Hudson DE, et al. Receptor-like specificity of a Plasmodium knowlesi malarial protein that binds to Duffy antigen ligands on erythrocytes. Journal of Experimental Medicine. 1988 June 1;167(6):1873–81.

58. Wertheimer SP, Barnwell JW. Plasmodium vivax interaction with the human Duffy blood group glycoprotein: Identification of a parasite receptor-like protein. Experimental Parasitology. 1989 Oct 1;69(3):340–50.

59. Chitnis CE, Miller LH. Identification of the erythrocyte binding domains of Plasmodium vivax and Plasmodium knowlesi proteins involved in erythrocyte invasion. Journal of Experimental Medicine. 1994 Aug 1;180(2):497–506.

60. Adams JH, Sim BK, Dolan SA, Fang X, Kaslow DC, Miller LH. A family of erythrocyte binding proteins of malaria parasites. Proc Natl Acad Sci USA. 1992 Aug;89(15):7085–9.

61. Ranjan A, Chitnis CE. Mapping regions containing binding residues within functional domains of Plasmodium vivax and Plasmodium knowlesi erythrocyte-binding proteins. Proceedings of the National Academy of Sciences. 1999 Nov 23;96(24):14067–72.

62. Carlton JM, Adams JH, Silva JC, Bidwell SL, Lorenzi H, Caler E, et al. Comparative genomics of the neglected human malaria parasite Plasmodium vivax. Nature. 2008 Oct;455(7214):757–63.

63. Moskovitz R, Pholcharee T, DonVito SM, Guloglu B, Lowe E, Mohring F, et al. Structural basis for DARC binding in reticulocyte invasion by Plasmodium vivax. Nature Communications. 2023;14(1).

64. Tsuboi T, Kappe SH, al-Yaman F, Prickett MD, Alpers M, Adams JH. Natural variation within the principal adhesion domain of the Plasmodium vivax duffy binding protein. Infection and Immunity. 1994 Dec;62(12):5581–6.

65. Premaratne PH, Aravinda BR, Escalante AA, Udagama PV. Genetic diversity of *Plasmodium vivax* Duffy Binding Protein II (PvDBPII) under unstable transmission and low intensity malaria in Sri Lanka. Infection, Genetics and Evolution. 2011 Aug 1;11(6):1327–39.

66. Valizadeh V, Zakeri S, Mehrizi AA, Djadid ND. Population genetics and natural selection in the gene encoding the Duffy binding protein II in Iranian *Plasmodium vivax* wild isolates. Infection, Genetics and Evolution. 2014 Jan 1;21:424–35.

67. Xainli J, Adams JH, King CL. The erythrocyte binding motif of *Plasmodium vivax* Duffy binding protein is highly polymorphic and functionally conserved in isolates from Papua New Guinea. Molecular and Biochemical Parasitology. 2000 Dec 1;111(2):253–60.

68. Guy AJ, Irani V, Richards JS, Ramsland PA. Structural patterns of selection and diversity for Plasmodium vivax antigens DBP and AMA1. Malar J. 2018 Dec;17(1):183.

69. Mittal P, Mishra S, Kar S, Pande V, Sinha A, Sharma A. Global distribution of single amino acid polymorphisms in *Plasmodium vivax* Duffy-binding-like domain and implications for vaccine development efforts. Open Biol. 2020 Sept;10(9):200180.

70. VanBuskirk KM, Tobian JLC, Baisor M, Sevova ES, Bockarie M, King CL, et al. Antigenic Drift in the Ligand Domain of Plasmodium vivax Duffy Binding Protein Confers Resistance to Inhibitory Antibodies. The Journal of Infectious Diseases. 2004 Nov 1;190(9):1556–62.

71. Hostetler JB, Lo E, Kanjee U, Amaratunga C, Suon S, Sreng S, et al. Independent Origin and Global Distribution of Distinct Plasmodium vivax Duffy Binding Protein Gene Duplications. PLOS Neglected Tropical Diseases. 2016 Oct 31;10(10):e0005091.

72. Ford A, Kepple D, Abagero BR, Connors J, Pearson R, Auburn S, et al. Whole genome sequencing of Plasmodium vivax isolates reveals frequent sequence and structural polymorphisms in erythrocyte binding genes. Dinglasan RR, editor. PLoS Negl Trop Dis. 2020 Oct 12;14(10):e0008234.

73. Menard D, Chan ER, Benedet C, Ratsimbasoa A, Kim S, Chim P, et al. Whole Genome Sequencing of Field Isolates Reveals a Common Duplication of the Duffy Binding Protein Gene in Malagasy Plasmodium vivax Strains. PLOS Neglected Tropical Diseases. 2013 Nov 21;7(11):e2489.

74. Popovici J, Roesch C, Carias LL, Khim N, Kim S, Vantaux A, et al. Amplification of Duffy binding protein-encoding gene allows Plasmodium vivax to evade host anti-DBP humoral immunity. Nat Commun. 2020 Feb 19;11(1):953.

75. Crawford KS, Volkman BF. Prospects for targeting ACKR1 in cancer and other diseases. Front Immunol [Internet]. 2023 Mar 15 [cited 2025 Apr 25];14. Available from: https://www.frontiersin.orghttps://www.frontiersin.org/journals/immunology/articles/10.3389/fimmu.2023.1111960/full

76. Cutbush M, Mollison PL. The Duffy blood group system. Heredity. 1950 Dec;4(3):383–9.

77. Tournamille C, Colin Y, Cartron JP, Le Van Kim C. Disruption of a GATA motif in the Duffy gene promoter abolishes erythroid gene expression in Duffy–negative individuals. Nat Genet. 1995 June;10(2):224–8.

78. Peiper SC, Wang ZX, Neote K, Martin AW, Showell HJ, Conklyn MJ, et al. The Duffy antigen/receptor for chemokines (DARC) is expressed in endothelial cells of Duffy negative individuals who lack the erythrocyte receptor. Journal of Experimental Medicine. 1995 Apr 1;181(4):1311–7.

79. Howes RE, Patil AP, Piel FB, Nyangiri OA, Kabaria CW, Gething PW, et al. The global distribution of the Duffy blood group. Nat Commun. 2011 Apr 5;2(1):266.

80. Höher G, Fiegenbaum M, Almeida S. Molecular basis of the Duffy blood group system. Blood Transfusion. 2017 Jan 30;(Blood Transfusion-1 2018 (January-February)):93–100.

81. Woolley I j., Hotmire K a., Sramkoski R m., Zimmerman P a., Kazura J w. Differential expression of the Duffy antigen receptor for chemokines according to RBC age and FY genotype. Transfusion. 2000;40(8):949–53.

82. Duchene J, Novitzky-Basso I, Thiriot A, Casanova-Acebes M, Bianchini M, Etheridge SL, et al. Atypical chemokine receptor 1 on nucleated erythroid cells regulates hematopoiesis. Nat Immunol. 2017 July;18(7):753–61.

83. Reich D, Nalls MA, Kao WHL, Akylbekova EL, Tandon A, Patterson N, et al. Reduced Neutrophil Count in People of African Descent Is Due To a Regulatory Variant in the Duffy Antigen Receptor for Chemokines Gene. PLOS Genetics. 2009 Jan 30;5(1):e1000360.

84. Howes RE, Jr RCR, Battle KE, Longbottom J, Mappin B, Ordanovich D, et al. Plasmodium vivax Transmission in Africa. PLOS Neglected Tropical Diseases. 2015 Nov 20;9(11):e0004222.

85. Bradley L, Yewhalaw D, Hemming-Schroeder E, Jeang B, Lee MC, Zemene E, et al. Epidemiology of Plasmodium vivax in Duffy negatives and Duffy positives from community and health centre collections in Ethiopia. Malaria Journal. 2024 Mar 14;23(1):76.

86. Lo E, Russo G, Pestana K, Kepple D, Abagero BR, Dongho GBD, et al. Contrasting epidemiology and genetic variation of *Plasmodium vivax* infecting Duffy-negative individuals across Africa. International Journal of Infectious Diseases. 2021 July 1;108:63–71.

87. Bouyssou I, El Hoss S, Doderer-Lang C, Schoenhals M, Rasoloharimanana LT, Vigan-Womas I, et al. Unveiling P. vivax invasion pathways in Duffy-negative individuals. Cell Host & Microbe. 2023 Dec;S1931312823004572.

88. Dechavanne C, Dechavanne S, Bosch J, Metral S, Redinger KR, Watson QD, et al. Duffy antigen is expressed during erythropoiesis in Duffy-negative individuals. Cell Host & Microbe. 2023 Dec 13;31(12):2093-2106.e7.

89. Kano FS, de Souza AM, de Menezes Torres L, Costa MA, Souza-Silva FA, Sanchez BAM, et al. Susceptibility to Plasmodium vivax malaria associated with DARC (Duffy antigen) polymorphisms is influenced by the time of exposure to malaria. Sci Rep. 2018 Sept 14;8(1):13851.

90. King CL, Adams JH, Xianli J, Grimberg BT, McHenry AM, Greenberg LJ, et al. Fya/Fyb antigen polymorphism in human erythrocyte Duffy antigen affects susceptibility to Plasmodium vivax malaria. Proceedings of the National Academy of Sciences. 2011 Dec 13;108(50):20113–8.

91. Chittoria A, Mohanty S, Jaiswal YK, Das A. Natural Selection Mediated Association of the Duffy (FY) Gene Polymorphisms with Plasmodium vivax Malaria in India. PLOS ONE. 2012 Sept 21;7(9):e45219.

92. Albuquerque SRL, de Oliveira Cavalcante F, Sanguino EC, Tezza L, Chacon F, Castilho L, et al. FY polymorphisms and vivax malaria in inhabitants of Amazonas State, Brazil. Parasitol Res. 2010 Apr 1;106(5):1049–53.

93. McManus KF, Taravella AM, Henn BM, Bustamante CD, Sikora M, Cornejo OE. Population genetic analysis of the DARC locus (Duffy) reveals adaptation from standing variation associated with malaria resistance in humans. PLOS Genetics. 2017 Mar 10;13(3):e1006560.

94. Horuk R, Chitnis CE, Darbonne WC, Colby TJ, Rybicki A, Hadley TJ, et al. A Receptor for the Malarial Parasite Plasmodium vivax: the Erythrocyte Chemokine Receptor. Science. 1993 Aug 27;261(5125):1182–4.

95. Chitnis CE, Chaudhuri A, Horuk R, Pogo AO, Miller LH. The domain on the Duffy blood group antigen for binding Plasmodium vivax and P. knowlesi malarial parasites to erythrocytes. Journal of Experimental Medicine. 1996 Oct 1;184(4):1531–6.

96. Batchelor JD, Malpede BM, Omattage NS, DeKoster GT, Henzler-Wildman KA, Tolia NH. Red Blood Cell Invasion by Plasmodium vivax: Structural Basis for DBP Engagement of DARC. Smith J, editor. PLoS Pathog. 2014 Jan 9;10(1):e1003869.

97. Choe H, Moore MJ, Owens CM, Wright PL, Vasilieva N, Li W, et al. Sulphated tyrosines mediate association of chemokines and Plasmodium vivax Duffy binding protein with the Duffy antigen/receptor for chemokines (DARC): Tyrosine sulphation of DARC. Molecular Microbiology. 2005 Jan 21;55(5):1413–22.

98. Hans D, Pattnaik P, Bhattacharyya A, Shakri AR, Yazdani SS, Sharma M, et al. Mapping binding residues in the Plasmodium vivax domain that binds Duffy antigen during red cell invasion: Binding residues of P. vivax Duffy binding protein. Molecular Microbiology. 2005 Jan 21;55(5):1423–34.

99. VanBuskirk KM, Sevova E, Adams JH. Conserved residues in the *Plasmodium vivax* Duffy-binding protein ligand domain are critical for erythrocyte receptor recognition. Proc Natl Acad Sci USA. 2004 Nov 2;101(44):15754–9.

100. Saha S, Khanppnavar B, Maharana J, Kim H, Carino CMC, Daly C, et al. Molecular mechanism of distinct chemokine engagement and functional divergence of the human Duffy antigen receptor. Cell. 2024 Aug 22;187(17):4751-4769.e25.

101. Antonelli LR, Junqueira C, Vinetz JM, Golenbock DT, Ferreira MU, Gazzinelli RT. The immunology of Plasmodium vivax malaria. Immunological Reviews. 2020;293(1):163–89.

102. Almeida ACG, Kuehn A, Castro AJM, Vitor-Silva S, Figueiredo EFG, Brasil LW, et al. High proportions of asymptomatic and submicroscopic Plasmodium vivax infections in a peri-urban area of low transmission in the Brazilian Amazon. Parasites & Vectors. 2018 Mar 20;11(1):194.

103. Lin E, Kiniboro B, Gray L, Dobbie S, Robinson L, Laumaea A, et al. Differential Patterns of Infection and Disease with P. falciparum and P. vivax in Young Papua New Guinean Children. Ng LFP, editor. PLoS ONE. 2010 Feb 4;5(2):e9047.

104. Cohen S, McGREGOR IA, Carrington S. Gamma-Globulin and Acquired Immunity to Human Malaria. Nature. 1961 Nov;192(4804):733–7.

105. Cole-Tobian JL, Cortés A, Baisor M, Kastens W, Xainli J, Bockarie M, et al. Age-Acquired Immunity to a Plasmodium vivax Invasion Ligand, the Duffy Binding Protein. The Journal of Infectious Diseases. 2002 Aug 15;186(4):531–9.

106. Nicolete VC, Frischmann S, Barbosa S, King CL, Ferreira MU. Naturally Acquired Binding-Inhibitory Antibodies to *Plasmodium vivax* Duffy Binding Protein and Clinical Immunity to Malaria in Rural Amazonians. J Infect Dis. 2016 Nov 15;214(10):1539–46.

107. Cole-Tobian JL, Michon P, Biasor M, Richards JS, Beeson JG, Mueller I, et al. Strain-Specific Duffy Binding Protein Antibodies Correlate with Protection against Infection with Homologous Compared to Heterologous *Plasmodium vivax* Strains in Papua New Guinean Children. Infect Immun. 2009 Sept;77(9):4009–17.

108. King CL, Michon P, Shakri AR, Marcotty A, Stanisic D, Zimmerman PA, et al. Naturally acquired Duffy-binding protein-specific binding inhibitory antibodies confer protection from blood-stage *Plasmodium vivax* infection. Proc Natl Acad Sci USA. 2008 June 17;105(24):8363–8.

109. Grimberg BT, Udomsangpetch R, Xainli J, McHenry A, Panichakul T, Sattabongkot J, et al. Plasmodium vivax Invasion of Human Erythrocytes Inhibited by Antibodies Directed against the Duffy Binding Protein. Beeson J, editor. PLoS Med. 2007 Dec 18;4(12):e337.

110. He WQ, Shakri AR, Bhardwaj R, França CT, Stanisic DI, Healer J, et al. Antibody responses to Plasmodium vivax Duffy binding and Erythrocyte binding proteins predict risk of infection and are associated with protection from clinical Malaria. Sinnis P, editor. PLoS Negl Trop Dis. 2019 Feb 15;13(2):e0006987.

111. Ntumngia FB, Schloegel J, Barnes SJ, McHenry AM, Singh S, King CL, et al. Conserved and Variant Epitopes of Plasmodium vivax Duffy Binding Protein as Targets of Inhibitory Monoclonal Antibodies. Urban JF, editor. Infect Immun. 2012 Mar;80(3):1203–8.

112. Chen E, Salinas ND, Huang Y, Ntumngia F, Plasencia MD, Gross ML, et al. Broadly neutralizing epitopes in the *Plasmodium vivax* vaccine candidate Duffy Binding Protein. Proc Natl Acad Sci USA. 2016 May 31;113(22):6277–82.

113. George MT, Schloegel JL, Ntumngia FB, Barnes SJ, King CL, Casey JL, et al. Identification of an Immunogenic Broadly Inhibitory Surface Epitope of the Plasmodium vivax Duffy Binding Protein Ligand Domain. Sinnis P, editor. mSphere. 2019 June 26;4(3):e00194-19.

114. Kim SH, Hwang SY, Lee YS, Choi IH, Park SG, Kho WG. Single-Chain Antibody Fragment Specific for Plasmodium vivax Duffy Binding Protein. Clinical and Vaccine Immunology. 2007 June;14(6):726–31.

115. Carias LL, Dechavanne S, Nicolete VC, Sreng S, Suon S, Amaratunga C, et al. Identification and Characterization of Functional Human Monoclonal Antibodies to *Plasmodium vivax* Duffy-Binding Protein. The Journal of Immunology. 2019 May 1;202(9):2648–60.

116. Urusova D, Carias L, Huang Y, Nicolete VC, Popovici J, Roesch C, et al. Structural basis for neutralization of Plasmodium vivax by naturally acquired human antibodies that target DBP. Nat Microbiol. 2019 May 27;4(9):1486–96.

117. Payne RO, Silk SE, Elias SC, Milne KH, Rawlinson TA, Llewellyn D, et al. Human vaccination against Plasmodium vivax Duffy-binding protein induces strain-transcending antibodies. JCI Insight. 2017 June 15;2(12):e93683.

118. Rawlinson ThomasA, Barber NM, Mohring F, Cho JS, Kosaisavee V, Gérard SF, et al. Structural basis for inhibition of Plasmodium vivax invasion by a broadly neutralizing vaccine-induced human antibody. Nat Microbiol. 2019 May 27;4(9):1497–507.

119. Mohring F, Hart MN, Rawlinson TA, Henrici R, Charleston JA, Diez Benavente E, et al. Rapid and iterative genome editing in the malaria parasite Plasmodium knowlesi provides new tools for P. vivax research. Soldati-Favre D, Storz G, Spielmann T, editors. eLife. 2019 June 17;8:e45829.

120. Malaria Vaccine Funders Group. Malaria Vaccine Technology Roadmap [Internet]. 2013 [cited 2025 Apr 13]. Available from: https://www.who.int/publications/m/item/malaria-vaccine-technology-roadmap

121. Bennett JW, Yadava A, Tosh D, Sattabongkot J, Komisar J, Ware LA, et al. Phase 1/2a Trial of Plasmodium vivax Malaria Vaccine Candidate VMP001/AS01B in Malaria-

Naive Adults: Safety, Immunogenicity, and Efficacy. Sinnis P, editor. PLoS Negl Trop Dis. 2016 Feb 26;10(2):e0004423.

122. Arévalo-Herrera M, Gaitán X, Larmat-Delgado M, Caicedo MA, Herrera SM, Henao-Giraldo J, et al. Randomized clinical trial to assess the protective efficacy of a Plasmodium vivax CS synthetic vaccine. Nat Commun. 2022 Mar 25;13(1):1603.

123. Clyde DF, McCarthy VC, Miller RM, Woodward WE. Immunization of Man against Falciparum and Vivax Malaria by Use of Attenuated Sporozoites. The American Journal of Tropical Medicine and Hygiene. 1975 May 1;24(3):397–401.

124. Arévalo-Herrera M, Vásquez-Jiménez JM, Lopez-Perez M, Vallejo AF, Amado-Garavito AB, Céspedes N, et al. Protective Efficacy of Plasmodium vivax Radiation-Attenuated Sporozoites in Colombian Volunteers: A Randomized Controlled Trial. PLoS Negl Trop Dis. 2016 Oct 19;10(10):e0005070.

125. Malkin EM, Durbin AP, Diemert DJ, Sattabongkot J, Wu Y, Miura K, et al. Phase 1 vaccine trial of Pvs25H: a transmission blocking vaccine for *Plasmodium vivax* malaria. Vaccine. 2005 May 2;23(24):3131–8.

126. Wu Y, Ellis RD, Shaffer D, Fontes E, Malkin EM, Mahanty S, et al. Phase 1 Trial of Malaria Transmission Blocking Vaccine Candidates Pfs25 and Pvs25 Formulated with Montanide ISA 51. PLOS ONE. 2008 July 9;3(7):e2636.

127. White M, Amino R, Mueller I. Theoretical Implications of a Pre-Erythrocytic Plasmodium vivax Vaccine for Preventing Relapses. Trends in Parasitology. 2017 Apr 1;33(4):260–3.

128. Moreno A, Caro-Aguilar I, Yazdani SS, Shakri AR, Lapp S, Strobert E, et al. Preclinical assessment of the receptor-binding domain of *Plasmodium vivax* Duffy-binding protein as a vaccine candidate in rhesus macaques. Vaccine. 2008 Aug 12;26(34):4338–44.

129. Yazdani SS, Shakri AR, Mukherjee P, Baniwal SK, Chitnis CE. Evaluation of immune responses elicited in mice against a recombinant malaria vaccine based on Plasmodium vivax Duffy binding protein. Vaccine. 2004 Sept;22(27–28):3727–37.

130. Arévalo-Herrera M, Castellanos A, Yazdani SS, Shakri AR, Chitnis CE, Dominik R, et al. Immunogenicity and protective efficacy of recombinant vaccine based on the receptor-binding domain of the Plasmodium vivax Duffy binding protein in Aotus monkeys. Am J Trop Med Hyg. 2005 Nov;73(5 Suppl):25–31.

131. de Cassan SC, Shakri AR, Llewellyn D, Elias SC, Cho JS, Goodman AL, et al. Preclinical Assessment of Viral Vectored and Protein Vaccines Targeting the Duffy-Binding Protein Region II of Plasmodium Vivax. Front Immunol [Internet]. 2015 July 8 [cited 2025 Apr 25];6. Available from: https://www.frontiersin.orghttps://www.frontiersin.org/journals/immunology/articles/10.3389/fimmu.2015.00348/full

132. Singh SK, Hora R, Belrhali H, Chitnis CE, Sharma A. Structural basis for Duffy recognition by the malaria parasite Duffy-binding-like domain. Nature. 2006 Feb;439(7077):741–4.

133. Hou MM, Barrett JR, Themistocleous Y, Rawlinson TA, Diouf A, Martinez FJ, et al. Vaccination with *Plasmodium vivax* Duffy-binding protein inhibits parasite growth during controlled human malaria infection. Sci Transl Med. 2023 July 12;15(704):eadf1782.

134. Minassian AM, Themistocleous Y, Silk SE, Barrett JR, Kemp A, Quinkert D, et al. Controlled human malaria infection with a clone of *Plasmodium vivax* with high-quality genome assembly. JCI Insight. 2021 Dec 8;6(23).

135. Natama HM, Salkeld J, Somé A, Soremekun S, Diallo S, Traoré O, et al. Safety and efficacy of the blood-stage malaria vaccine RH5.1/Matrix-M in Burkina Faso: interim results of a double-blind, randomised, controlled, phase 2b trial in children. The Lancet Infectious Diseases [Internet]. 2024 Dec 10 [cited 2024 Dec 19];0(0). Available from: https://www.thelancet.com/journals/laninf/article/PIIS1473-3099%2824%2900752-7/fulltext

136. Crosnier C, Bustamante LY, Bartholdson SJ, Bei AK, Theron M, Uchikawa M, et al. Basigin is a receptor essential for erythrocyte invasion by Plasmodium falciparum. Nature. 2011 Dec;480(7378):534–7.

137. Farrell B, Alam N, Hart MN, Jamwal A, Ragotte RJ, Walters-Morgan H, et al. The PfRCR complex bridges malaria parasite and erythrocyte during invasion. Nature. 2024 Jan;625(7995):578–84.

138. Scally SW, Triglia T, Evelyn C, Seager BA, Pasternak M, Lim PS, et al. PCRCR complex is essential for invasion of human erythrocytes by Plasmodium falciparum. Nat Microbiol. 2022 Dec;7(12):2039–53.

139. Knuepfer E, Wright KE, Prajapati SK, Rawlinson TA, Mohring F, Koch M, et al. Divergent roles for the RH5 complex components, CyRPA and RIPR in human-infective malaria parasites. PLOS Pathogens. 2019 June 11;15(6):e1007809.

140. Seager BA, Lim PS, Lai KH, Feufack-Donfack LB, Dass S, Xiao X, et al. PTRAMP, CSS and Ripr form a conserved complex required for merozoite invasion of Plasmodium species into erythrocytes [Internet]. bioRxiv; 2025 [cited 2025 Aug 16]. p. 2025.03.25.644866. Available from: https://www.biorxiv.org/content/10.1101/2025.03.25.644866v1

141. Barrett JR, Pipini D, Wright ND, Cooper AJR, Gorini G, Quinkert D, et al. Analysis of the diverse antigenic landscape of the malaria protein RH5 identifies a potent vaccine-induced human public antibody clonotype. Cell [Internet]. 2024 July 25 [cited 2024 Aug 6]; Available from: https://www.sciencedirect.com/science/article/pii/S009286742400655X

142. Brochet X, Lefranc MP, Giudicelli V. IMGT/V-QUEST: the highly customized and integrated system for IG and TR standardized V-J and V-D-J sequence analysis. Nucleic Acids Research. 2008 July 1;36(suppl_2):W503–8.

143. Meng EC, Goddard TD, Pettersen EF, Couch GS, Pearson ZJ, Morris JH, et al. UCSF ChimeraX: Tools for structure building and analysis. Protein Science. 2023;32(11):e4792.

144. Polonsky K, Pupko T, Freund NT. Evaluation of the Ability of AlphaFold to Predict the Three-Dimensional Structures of Antibodies and Epitopes. The Journal of Immunology. 2023 Nov 15;211(10):1578–88.

145. Shakri AR, Rizvi MMA, Chitnis CE. DEVELOPMENT OF QUANTITATIVE RECEPTOR-LIGAND BINDING ASSAY FOR USE AS A TOOL TO ESTIMATE IMMUNE RESPONSES AGAINST *Plasmodium vivax* DUFFY BINDING PROTEIN REGION II. Journal of Immunoassay and Immunochemistry. 2012 Oct;33(4):403–13.

146. Martinez FJ, White M, Guillotte-Blisnick M, Huon C, Boucharlat A, Agou F, et al. PvDBPII elicits multiple antibody-mediated mechanisms that reduce growth in a Plasmodium vivax challenge trial. npj Vaccines. 2024 Jan 6;9(1):10.

147. Rijal P, Elias SC, Machado SR, Xiao J, Schimanski L, O'Dowd V, et al. Therapeutic Monoclonal Antibodies for Ebola Virus Infection Derived from Vaccinated Humans. Cell Reports. 2019 Apr 2;27(1):172-186.e7.

148. Bliss CI. The Toxicity of Poisons Applied Jointly. Annals of Applied Biology. 1939;26(3):585–615.

149. Gu Z, Gu L, Eils R, Schlesner M, Brors B. circlize implements and enhances circular visualization in R. Bioinformatics. 2014 Oct 1;30(19):2811–2.

150. Xu S, Chen M, Feng T, Zhan L, Zhou L, Yu G. Use ggbreak to Effectively Utilize Plotting Space to Deal With Large Datasets and Outliers. Front Genet [Internet]. 2021 Nov 2 [cited 2025 Aug 19];12. Available from: https://www.frontiersin.org/journals/genetics/articles/10.3389/fgene.2021.774846/full

151. ggplot2 Based Publication Ready Plots [Internet]. [cited 2025 Aug 19]. Available from: https://rpkgs.datanovia.com/ggpubr/

152. Ooms J. The jsonlite Package: A Practical and Consistent Mapping Between JSON Data and R Objects [Internet]. arXiv; 2014 [cited 2025 Aug 19]. Available from: http://arxiv.org/abs/1403.2805

153. The Composer of Plots [Internet]. [cited 2025 Aug 19]. Available from: https://patchwork.data-imaginist.com/

154. Wickham H, Averick M, Bryan J, Chang W, McGowan LD, François R, et al. Welcome to the Tidyverse. Journal of Open Source Software. 2019 Nov 21;4(43):1686.

155. Abramson J, Adler J, Dunger J, Evans R, Green T, Pritzel A, et al. Accurate structure prediction of biomolecular interactions with AlphaFold 3. Nature. 2024 June;630(8016):493–500.

156. Chaudhary N, Wesemann DR. Analyzing Immunoglobulin Repertoires. Front Immunol. 2018 Mar 14;9:462.

157. Barrett JR, Silk SE, Mkindi CG, Kwiatkowska KM, Hou MM, Lias AM, et al. Analyses of human vaccine-specific circulating and bone marrow-resident B cell populations reveal benefit of delayed vaccine booster dosing with blood-stage malaria antigens.

Frontiers in Immunology [Internet]. 2024 [cited 2024 Jan 17];14. Available from: https://www.frontiersin.org/articles/10.3389/fimmu.2023.1193079

158. Dickey TH, Tolia NH. Designing an effective malaria vaccine targeting Plasmodium vivax Duffy-binding protein. Trends in Parasitology. 2023 July;S1471492223001472.

159. Briney B, Inderbitzin A, Joyce C, Burton DR. Commonality despite exceptional diversity in the baseline human antibody repertoire. Nature. 2019 Feb;566(7744):393–7.

160. Jaffe DB, Shahi P, Adams BA, Chrisman AM, Finnegan PM, Raman N, et al. Functional antibodies exhibit light chain coherence. Nature. 2022 Nov;611(7935):352–7.

161. Mesin L, Ersching J, Victora GD. Germinal Center B Cell Dynamics. Immunity. 2016 Sept 20;45(3):471–82.

162. Mohring F, Rawlinson T, Draper S, Moon R. Multiplication and Growth Inhibition Activity Assays for the Zoonotic Malaria Parasite, Plasmodium knowlesi. BIO-PROTOCOL [Internet]. 2020 [cited 2025 July 4];10(17). Available from: https://bio-protocol.org/e3743

163. Douglas AD, Baldeviano GC, Lucas CM, Lugo-Roman LA, Crosnier C, Bartholdson SJ, et al. A PfRH5-Based Vaccine Is Efficacious against Heterologous Strain Blood-Stage Plasmodium falciparum Infection in Aotus Monkeys. Cell Host & Microbe. 2015 Jan;17(1):130–9.

164. Singh S, Miura K, Zhou H, Muratova O, Keegan B, Miles A, et al. Immunity to Recombinant Plasmodium falciparum Merozoite Surface Protein 1 (MSP1): Protection in Aotus nancymai Monkeys Strongly Correlates with Anti-MSP1 Antibody Titer and In Vitro Parasite-Inhibitory Activity. Infection and Immunity. 2006 Aug;74(8):4573–80.

165. Hamid MMA, Remarque EJ, Duivenvoorde LM van, Werff N van der, Walraven V, Faber BW, et al. Vaccination with Plasmodium knowlesi AMA1 Formulated in the Novel Adjuvant Co-Vaccine HT^{TM} Protects against Blood-Stage Challenge in Rhesus Macaques. PLOS ONE. 2011 May 31;6(5):e20547.

166. Miura K, Diouf A, Fay MP, Barrett JR, Payne RO, Olotu AI, et al. Assessment of precision in growth inhibition assay (GIA) using human anti-PfRH5 antibodies. Malar J. 2023 May 19;22(1):159.

167. Singh K, Mukherjee P, Shakri AR, Singh A, Pandey G, Bakshi M, et al. Malaria vaccine candidate based on Duffy-binding protein elicits strain transcending functional antibodies in a Phase I trial. npj Vaccines. 2018 Sept 28;3(1):48.

168. Batchelor JD, Zahm JA, Tolia NH. Dimerization of Plasmodium vivax DBP is induced upon receptor binding and drives recognition of DARC. Nat Struct Mol Biol. 2011 Aug;18(8):908–14.

169. Bates JT, Keefer CJ, Slaughter JC, Kulp DW, Schief WR, Crowe JE. Escape from neutralization by the respiratory syncytial virus-specific neutralizing monoclonal antibody palivizumab is driven by changes in on-rate of binding to the fusion protein. Virology. 2014 Apr 1;454–455:139–44.

170. Saul A. Kinetic constraints on the development of a malaria vaccine. Parasite Immunology. 1987;9(1):1–9.

171. Mertens JE, Rigby CA, Bardelli M, Quinkert D, Hou MM, Diouf A, et al. Evaluation of the precision of the Plasmodium knowlesi growth inhibition assay for Plasmodium vivax Duffy-binding protein-based malaria vaccine development. Vaccine. 2024 June;42(16):3621–9.

172. Kayentao K, Ongoiba A, Preston AC, Healy SA, Doumbo S, Doumtabe D, et al. Safety and Efficacy of a Monoclonal Antibody against Malaria in Mali. N Engl J Med. 2022 Nov 17;387(20):1833–42.

173. Kayentao K, Ongoiba A, Preston AC, Healy SA, Hu Z, Skinner J, et al. Subcutaneous Administration of a Monoclonal Antibody to Prevent Malaria. New England Journal of Medicine. 2024 May 1;390(17):1549–59.

174. Williams KL, Guerrero S, Flores-Garcia Y, Kim D, Williamson KS, Siska C, et al. A candidate antibody drug for prevention of malaria. Nat Med. 2024 Jan 2;1–13.

175. Gardner MR, Kattenhorn LM, Kondur HR, von Schaewen M, Dorfman T, Chiang JJ, et al. AAV-expressed eCD4-Ig provides durable protection from multiple SHIV challenges. Nature. 2015 Mar;519(7541):87–91.

176. Watson QD, Carias LL, Malachin A, Redinger KR, Bosch J, Bardelli M, et al. Human monoclonal antibodies inhibit invasion of transgenic Plasmodium knowlesi expressing Plasmodium vivax Duffy binding protein. Malaria Journal. 2023 Dec 4;22(1):369.

177. Zhang P, Wu CG, Mihalik K, Virata ML, Yu M ying W, Alter HJ, et al. Hepatitis C virus epitope-specific neutralizing antibodies in Igs prepared from human plasma. Proceedings of the National Academy of Sciences. 2007 May 15;104(20):8449–54.

178. Patel PN, Dickey TH, Hopp CS, Diouf A, Tang WK, Long CA, et al. Neutralizing and interfering human antibodies define the structural and mechanistic basis for antigenic diversion. Nat Commun. 2022 Oct 6;13(1):5888.

179. Zhong L, Haynes L, Struble EB, Tamin A, Virata-Theimer ML, Zhang P. Antibody-mediated synergy and interference in the neutralization of SARS-CoV at an epitope cluster on the spike protein. Biochemical and Biophysical Research Communications. 2009 Dec 18;390(3):1056–60.

180. Lo E, Hostetler JB, Yewhalaw D, Pearson RD, Hamid MMA, Gunalan K, et al. Frequent expansion of Plasmodium vivax Duffy Binding Protein in Ethiopia and its epidemiological significance. PLOS Neglected Tropical Diseases. 2019 Sept 11;13(9):e0007222.

181. Lapp SA, Mok S, Zhu L, Wu H, Preiser PR, Bozdech Z, et al. Plasmodium knowlesi gene expression differs in ex vivo compared to in vitro blood-stage cultures. Malaria Journal. 2015 Mar 13;14(1):110.

182. Rangel GW, Clark MA, Kanjee U, Lim C, Shaw-Saliba K, Menezes MJ, et al. Enhanced Ex Vivo Plasmodium vivax Intraerythrocytic Enrichment and Maturation for Rapid and

Sensitive Parasite Growth Assays. Antimicrobial Agents and Chemotherapy. 2018 Mar 27;62(4):10.1128/aac.02519-17.

183. Azuma H, Paulk N, Ranade A, Dorrell C, Al-Dhalimy M, Ellis E, et al. Robust expansion of human hepatocytes in Fah−/−/Rag2−/−/Il2rg−/− mice. Nat Biotechnol. 2007 Aug;25(8):903–10.

184. Mikolajczak SA, Vaughan AM, Kangwanrangsan N, Roobsoong W, Fishbaugher M, Yimamnuaychok N, et al. *Plasmodium vivax* Liver Stage Development and Hypnozoite Persistence in Human Liver-Chimeric Mice. Cell Host & Microbe. 2015 Apr 8;17(4):526–35.

185. Schäfer C, Roobsoong W, Kangwanrangsan N, Bardelli M, Rawlinson TA, Dambrauskas N, et al. A Humanized Mouse Model for Plasmodium vivax to Test Interventions that Block Liver Stage to Blood Stage Transition and Blood Stage Infection. iScience [Internet]. 2020 Aug 21 [cited 2023 Sept 17];23(8). Available from: https://www.cell.com/iscience/abstract/S2589-0042(20)30569-1

186. Luiza-Batista C, Thiberge S, Serra-Hassoun M, Nardella F, Claës A, Nicolete VC, et al. Humanized mice for investigating sustained Plasmodium vivax blood-stage infections and transmission. Nat Commun. 2022 July 15;13(1):4123.

187. Hester J, Chan ER, Menard D, Mercereau-Puijalon O, Barnwell J, Zimmerman PA, et al. De Novo Assembly of a Field Isolate Genome Reveals Novel Plasmodium vivax Erythrocyte Invasion Genes. PLOS Neglected Tropical Diseases. 2013 Dec 5;7(12):e2569.

188. Gaudinski MR, Berkowitz NM, Idris AH, Coates EE, Holman LA, Mendoza F, et al. A Monoclonal Antibody for Malaria Prevention. N Engl J Med. 2021 Aug 26;385(9):803–14.

189. Tobin AR, Crow R, Urusova DV, Klima JC, Tolia NH, Strauch EM. Inhibition of a malaria host–pathogen interaction by a computationally designed inhibitor. Protein Science. 2023;32(1).

190. Kang SH, Lee CH. Development of Therapeutic Antibodies and Modulating the Characteristics of Therapeutic Antibodies to Maximize the Therapeutic Efficacy. Biotechnol Bioproc E. 2021 June;26(3):295–311.

191. Zalevsky J, Chamberlain AK, Horton HM, Karki S, Leung IWL, Sproule TJ, et al. Enhanced antibody half-life improves in vivo activity. Nat Biotechnol. 2010 Feb;28(2):157–9.

192. Dobrescu I, de Camargo TM, Gimenez AM, Murillo O, Amorim KN da S, Marinho CRF, et al. Protective Immunity in Mice Immunized With P. vivax MSP119-Based Formulations and Challenged With P. berghei Expressing PvMSP119. Front Immunol [Internet]. 2020 Feb 19 [cited 2025 Aug 11];11. Available from: https://www.frontiersin.org/journals/immunology/articles/10.3389/fimmu.2020.00028/full

193. Ntumngia FB, Schloegel J, McHenry AM, Barnes SJ, George MT, Kennedy S, et al. Immunogenicity of single *versus* mixed allele vaccines of *Plasmodium vivax* Duffy binding protein region II. Vaccine. 2013 Sept 13;31(40):4382–8.

194. Ntumngia FB, Adams JH. Design and Immunogenicity of a Novel Synthetic Antigen Based on the Ligand Domain of the Plasmodium vivax Duffy Binding Protein. Clin Vaccine Immunol. 2012 Jan;19(1):30–6.

195. Ntumngia FB, Pires CV, Barnes SJ, George MT, Thomson-Luque R, Kano FS, et al. An engineered vaccine of the Plasmodium vivax Duffy binding protein enhances induction of broadly neutralizing antibodies. Sci Rep. 2017 Oct 23;7(1):13779.

196. Dickey TH, McAleese H, Salinas ND, Lambert LE, Tolia NH. Structure-based design of a Plasmodium vivax Duffy-binding protein immunogen focuses the antibody response to functional epitopes. Protein Science. 2024;33(8):e5095.

197. Barber NM, Pholcharee T, Lias AM, Quinkert D, Nugent J, King LDW, et al. Structure-guided design of a *Plasmodium vivax* Duffy binding protein-based vaccine immunogen [Internet]. Immunology; 2024 [cited 2025 Mar 14]. Available from: http://biorxiv.org/lookup/doi/10.1101/2024.06.23.600241

198. Gruszczyk J, Kanjee U, Chan LJ, Menant S, Malleret B, Lim NTY, et al. Transferrin receptor 1 is a reticulocyte-specific receptor for Plasmodium vivax. Science. 2018 Jan 5;359(6371):48–55.

199. Srinivasan P, Beatty WL, Diouf A, Herrera R, Ambroggio X, Moch JK, et al. Binding of Plasmodium merozoite proteins RON2 and AMA1 triggers commitment to invasion. Proceedings of the National Academy of Sciences. 2011 Aug 9;108(32):13275–80.

200. Seager BA, Lim PS, Lai KH, Feufack-Donfack LB, Dass S, Xiao X, et al. PTRAMP, CSS and Ripr form a conserved complex required for merozoite invasion of *Plasmodium* species into erythrocytes [Internet]. Microbiology; 2025 [cited 2025 Aug 16]. Available from: http://biorxiv.org/lookup/doi/10.1101/2025.03.25.644866

201. Ndegwa DN, Kundu P, Hostetler JB, Marin-Menendez A, Sanderson T, Mwikali K, et al. Using Plasmodium knowlesi as a model for screening Plasmodium vivax blood-stage malaria vaccine targets reveals new candidates. Beeson JG, editor. PLoS Pathog. 2021 July 1;17(7):e1008864.

202. Elsworth B, Ye S, Dass S, Tennessen JA, Sultana Q, Thommen BT, et al. The essential genome of Plasmodium knowlesi reveals determinants of antimalarial susceptibility. Science. 2025 Feb 7;387(6734):eadq6241.

203. De SL, Ntumngia FB, Nicholas J, Adams JH. Progress towards the development of a *P. vivax* vaccine. Expert Review of Vaccines. 2021 Feb 1;20(2):97–112.